



# Synthèse et relation structure-propriétés de copolymères alternés $\pi$ -conjugués

Jules Oriou

## ► To cite this version:

Jules Oriou. Synthèse et relation structure-propriétés de copolymères alternés  $\pi$ -conjugués. Other. Université Sciences et Technologies - Bordeaux I, 2013. English. NNT : 2013BOR14962 . tel-01070649

**HAL Id: tel-01070649**

**<https://theses.hal.science/tel-01070649>**

Submitted on 24 Nov 2014

**HAL** is a multi-disciplinary open access archive for the deposit and dissemination of scientific research documents, whether they are published or not. The documents may come from teaching and research institutions in France or abroad, or from public or private research centers.

L'archive ouverte pluridisciplinaire **HAL**, est destinée au dépôt et à la diffusion de documents scientifiques de niveau recherche, publiés ou non, émanant des établissements d'enseignement et de recherche français ou étrangers, des laboratoires publics ou privés.

# THÈSE

*Présentée à*

**L'UNIVERSITÉ BORDEAUX 1**

**ÉCOLE DOCTORALE DES SCIENCES CHIMIQUES**

*Par* **JULES ORIOU**

*Pour obtenir le grade de*

**DOCTEUR**

**SPÉCIALITÉ : POLYMÈRE**

---

**SYNTHESIS AND STRUCTURE-PROPERTIES  
RELATIONSHIP OF ALTERNATED  $\pi$ -CONJUGATED  
COPOLYMERS**

---

Date de soutenance: 10 décembre 2013

Devant la commission d'examen formée de :

Dr. Jean RONCALI, MOLTECH-Anjou, CNRS, Université d'Angers  
Pr. Christoph LAMBERT, IOC, University of Würzburg, Germany  
Dr. Bruno SCHMALTZ, PCM2E, Université François-Rabelais, Tours  
Pr. Thierry TOUPANCE, ISM, Université de Bordeaux  
Dr. Cyril BROCHON, LCPO, Université de Bordeaux  
Dr. Eric CLOUTET, CNRS, LCPO, Université de Bordeaux  
Pr. Georges HADZIIOANNOU, LCPO, Université de Bordeaux

*Rapporteur*  
*Rapporteur*  
*Examineur*  
*Examineur*  
*Directeur de thèse*  
*Directeur de thèse*  
*Invité*



*A mes parents, merci pour tout.*

*Děkuji Zuzanko. Jsi nejlepší.*





## ***Acknowledgement/Remerciements***

---

Je tiens tout d'abord à remercier le Prof. Henri Cramail pour m'avoir permis de réaliser cette thèse au Laboratoire de Chimie des Polymères Organiques, mais qui fut aussi mon premier « encadrant » au LCPO lors d'un précédent stage. Malgré sa fonction de directeur, il tente d'être toujours disponible pour toute personne ayant besoin de ses conseils. Je souhaite ensuite remercier mes directeurs de thèse, le Dr Cyril Brochon et le Dr Eric Cloutet, pour m'avoir permis de réaliser ce travail et pour leur encadrement tout au long de ces trois années. Merci pour leur soutien jusqu'au bout... Merci aussi au Prof. Georges Hadzioannou pour m'avoir accueilli dans son équipe. Je souhaite aussi remercier les membres du jury pour leur travail de correction et leur présence durant la soutenance : le Dr Jean Roncali, le Prof. Dr Christoph Lambert, le Dr Bruno Schmaltz et le Prof. Thierry Toupance. Je remercie l'université Bordeaux 1 pour le financement ce travail de thèse.

Je tiens ensuite à remercier chaleureusement le Dr FeiFei NG. Merci pour ton aide et ton soutien (scientifique et moral). Tu m'as beaucoup aidé et appris, en plus de m'avoir remonté le moral plus d'une fois quand les résultats n'étaient pas là. Merci encore ! Je veux aussi remercier particulièrement mes aînés thésards, avec qui j'ai appris, mais qui se sont aussi révélé être de très bons amis : Maréva, Katerina, Antoine et Jun. Un grand merci à deux thésards plus anciens : Bertrand, pour m'avoir fait découvrir le LCPO et m'avoir permis de participer activement à son travail (ainsi que de m'avoir inclus sur sa publi !) et Célia, qui m'a la première fait réellement découvrir les polymères conjugués. Je me dois aussi de remercier les collègues du LCPO pour leur assistance sur certaines caractérisations : Nico, Anne-Laure, Gérard, Mélanie, Gilles. Arrive ensuite le deuxième laboratoire dans lequel j'ai passé peu de temps mais où je me suis toujours senti accueilli et où l'ambiance a toujours été chaleureuse : l'équipe elorga de l'IMS. Un grand merci tout particulièrement au Dr Laurence Vignau pour son aide sur l'électrochimie. Merci au reste de l'équipe avec qui j'ai passé de très bons moments, et merci à Sylvain pour m'avoir fait découvrir l'asso Vertige ! Je voudrais remercier les Dr Laurent Ducasse, Dr Frédéric Castet, et Prof. Alain Fritsch pour leur aide sur la modélisation, même si les résultats n'ont finalement pas été inclus dans ce manuscrit, une thèse continue sur ce projet. Un grand merci à toute ma promo de thèse LCPO pour le soutien mutuel : Lise, Charlotte, Thomas, Vincent, Camille, Romain, et un merci plus grand encore à mes deux co-thésardes du B8 : Chrystilla et Carine. Plusieurs stagiaires ont aussi participé à ce travail de thèse, aussi je les remercie : Florent, Mohammed et surtout Guillaume (bonne chance pour ta thèse !). Je souhaite vivement remercier tous les collègues et amis que j'ai côtoyé pendant ces trois ans, la liste est longue aussi je ne vais pas l'énumérer, ils se reconnaîtront...

Enfin, un énorme merci à ma famille et à celle qui m'a apporté énormément (et plus...) pendant les deux dernières années : merci Zuzka.

## List of abbreviations

---

A	absorbance / Ampere
BDT	benzodithiophene
BHJ	bulk heterojunction
Boc	<i>tert</i> -butyloxycarbonyl
BT	benzothiadiazole
Bu	butyl
°C	degrees centigrade
CB	conduction band
CP	conjugated polymers
CV	cyclic voltammetry
Cz	carbazole
d	doublet
D-A	donor-acceptor
DMF	dimethylformamide
DPP	diketopyrrolopyrrole
DSC	differential scanning calorimetry
DTBT	dithienylbenzodithiophene
e <sup>-</sup>	electron
E	potential
$E_{\theta}$	contribution of the dihedral angle between units
$E_{BLA}$	contribution of the bond length alternation
$E_G$	band gap
$E_{int}$	contribution of intermolecular interactions
$E_{Res}$	contribution of the aromaticity
$E_{Sub}$	contribution of the substituents
EDOT	3,4-ethylenedioxythiophene
eq	equivalents
Et	ethyl
Et <sub>4</sub> NOH	tetraethylammonium hydroxide
EtOAc	ethyl acetate
eV	electronvolt
Fc / Fc <sup>+</sup>	ferrocene / ferrocenium
g	gram

## List of abbreviations

GRIM	Grignard metathesis
h	hours
HOMO	highest occupied molecular orbital
Hz	hertz
I	current
ICT	intramolecular charge transfer
IR	infrared
ITO	indium tin oxide
J	coupling constant
J <sub>sc</sub>	short-circuit current
LEDs	light emitting diodes
LPPP	ladder-type poly(para-phenylene)
LUMO	lowest unoccupied molecular orbital
M	molar (mol/liter)
Me	methyl
MEH-PPV	poly(1-methoxy-4-(2-ethylhexyloxy)- <i>p</i> -phenylenevinylene)
MHz	megahertz
mL	milliliter
mM	milimolar
mmol	millimole
mol	mole
m.p.	melting point
MS	mass spectrometry
n	number of moles
n-BuLi	n-buthyllithium
n-doped	negatively doped
nm	nanometre
NMR	nuclear magnetic resonance
OFET	organic field effect transistor
OLED	organic light emitting diode
Ox	oxidation
p	para-
P3HT	poly(3-hexylthiophene)
PCBT	poly(carbazole- <i>alt</i> -benzothiadiazole)
PCDTBT	poly(carbazole- <i>alt</i> -dithienylbenzodithiophene)
PCE	power conversion efficiency

## List of abbreviations

PCPDT8	poly(4,4-dioctylcyclopentadithiophene)
p-doped	positively doped
Pd(PPh <sub>3</sub> ) <sub>4</sub>	tetrakis(triphenylphosphine)palladium
PEDOT	poly(3,4-ethylenedioxythiophene)
PF	polyfluorene
PF8	poly(9,9-dioctylfluorene)
PIF	poly(indenofluorene)
PIMI	polyimine
PL	photoluminescence
ppm	parts per million
PPP	poly(para-phenylene)
PPV	poly(para-phenylenevinylene)
PSQ	polysquaraine
PSQBDT	poly(squaraine- <i>alt</i> -benzodithiophene)
PSQBT	poly(squaraine- <i>alt</i> -benzothiadiazole)
PSQDA	poly(squaraine- <i>alt</i> -dianiline)
PSQT	poly(squaraine- <i>alt</i> -thiophene)
PSS	polystyrenesulfonic acid
PT	polythiophenes
PTB7	poly(thieno[3,4- <i>b</i> ]thiophene- <i>alt</i> -benzodithiophene)
PTP	poly(tetraphenylene)
PTV	poly(thienylenevinylene)
Red	reduction
ROMP	ring opening metathesis polymerization
r.t.	room temperature
s	second/singlet
SCE	saturated calomel electrode
T	transmittance / temperature
TBAPF <sub>6</sub>	tetrabutyl ammonium fluoride
TFA	trifluoroacetic acid
TGA	thermogravimetric analysis
THF	tetrahydrofuran
TID	thienoisindole-dione
TPD	thienopyrroledione
UV	ultraviolet
V	volt

### *List of abbreviations*

v.	volumic
VB	valence band
vis	visible
V <sub>OC</sub>	open-circuit voltage
vs.	versus

### **Greek**

$\pi$	pi bonding orbital
$\pi^*$	pi anti-bonding orbital
$\delta$	chemical shift
$\epsilon$	molar extinction coefficient
$\Delta$	heat / difference
$\lambda$	wavelength
$\sigma$	sigma bonding orbital
$\sigma^*$	sigma anti bonding orbital

## General table of contents

---

<b>Acknowledgement/Remerciements .....</b>	<b>V</b>
<b>List of abbreviations .....</b>	<b>VII</b>
<b>General table of contents .....</b>	<b>XI</b>
<b>General Introduction .....</b>	<b>1</b>
<b>Chapter 1 Structure-properties relationship in semiconducting polymers: a literature survey .....</b>	<b>5</b>
<b>1.1 Semiconducting polymers .....</b>	<b>9</b>
1.1.1 Band theory and definition of a semiconductor .....	9
1.1.2 Origin of semiconducting properties in organic materials .....	10
1.1.3 Charges generation in semiconducting polymers .....	12
<b>1.2 Conjugated polymers design: structure-properties relationship .....</b>	<b>15</b>
1.2.1 Aromaticity and planarization effect .....	17
1.2.2 Substituents effect .....	23
1.2.3 Quinoid stabilization effect .....	29
1.2.4 Donor-acceptor alternation effect .....	31
1.2.5 Recent trends in the design of alternated conjugated polymers .....	34
<b>1.3 Synthesis of semiconducting polymers .....</b>	<b>37</b>
1.3.1 Evolution of synthetic routes for conjugated polymers .....	37
1.3.2 Stille polycondensation .....	40
1.3.3 Suzuki polycondensation .....	41
1.3.4 Metal-free reactions applied to conjugated polymer synthesis .....	43
<b>1.4 Aim and strategy of the thesis .....</b>	<b>46</b>
<b>1.5 Bibliography .....</b>	<b>50</b>
<b>Chapter 2 Synthesis and characterization of Poly(carbazole-<i>alt</i>-benzothiadiazole)s .....</b>	<b>53</b>
<b>2.1 Literature overview .....</b>	<b>57</b>
<b>2.2 Synthesis of alternated conjugated polymers of carbazole and benzothiadiazole ....</b>	<b>63</b>
2.2.1 Carbazole monomers .....	63
2.2.2 Poly(carbazole- <i>alt</i> -benzothiadiazole)s .....	67
<b>2.3 Properties of PCBTs .....</b>	<b>70</b>
2.3.1 Thermal properties .....	70
2.3.2 Optical properties .....	71
2.3.3 Electrochemical properties .....	75
2.3.4 Photovoltaic performances .....	76



<b>2.4 Conclusion .....</b>	<b>79</b>
<b>2.5 Bibliography.....</b>	<b>81</b>
<b>2.6 Experimental .....</b>	<b>83</b>
2.6.1 Syntheses and structural characterizations .....	83
2.6.2 Thermogravimetric analyses (TGA) .....	96
2.6.3 Differential Scanning calorimetry.....	97
2.6.4 Electrochemistry.....	98
2.6.5 Optical characterizations of PCBT-PCBM blends.....	100
2.6.6 Photovoltaic characterization .....	101
<b>Chapter 3 Synthesis and characterization of bridged polysquaraines.....</b>	<b>103</b>
<b>3.1 Literature overview.....</b>	<b>107</b>
<b>3.2 Synthesis of bridged polysquaraine .....</b>	<b>110</b>
3.2.1 Squaraine monomer.....	110
3.2.2 Bridged polysquaraines .....	113
<b>3.3 Properties of the bridged polysquaraines .....</b>	<b>117</b>
3.3.1 Thermal properties.....	117
3.3.2 Optical properties.....	118
3.3.3 Electrochemical properties .....	120
3.3.4 Preliminary tests for photovoltaic applications .....	122
<b>3.4 Conclusion .....</b>	<b>125</b>
<b>3.5 Bibliography.....</b>	<b>126</b>
<b>3.6 Experimental .....</b>	<b>127</b>
3.6.1 Syntheses and structural characterizations .....	127
3.6.2 Thermogravimetric analyses (TGA) .....	136
3.6.3 Differential Scanning Calorimetry (DSC) .....	136
3.6.4 Electrochemistry.....	137
3.6.5 Optical characterizations.....	139
<b>Chapter 4 Novel conjugated polymers prepared by metal-free polycondensations .....</b>	<b>143</b>
<b>4.1 Literature overview.....</b>	<b>147</b>
4.1.1 Polycondensation with squaric acid .....	147
4.1.2 Polymerization by arylimino-de-oxo-bisubstitution.....	151
4.1.3 Strategy .....	153
<b>4.2 Synthesis and characterization of polysquaraines .....</b>	<b>155</b>
4.2.1 Synthesis of polysquaraines .....	155
4.2.1.1 Indole-based monomers .....	155
4.2.1.2 Aniline-like monomer .....	159

4.2.1.3	Polymerizations with squaric acid .....	161
4.2.2	Characterization of polysquaraines.....	165
4.2.2.1	Thermal properties .....	165
4.2.2.2	Optical properties .....	166
4.2.2.3	Electrochemical properties.....	168
<b>4.3</b>	<b>Synthesis and characterization of polyimines .....</b>	<b>169</b>
4.3.1	Synthesis of polyimines .....	169
4.3.1.1	Carbazole and edot-based monomers .....	169
4.3.1.2	Polymerizations by arylimino-de-oxo-bisubstitution .....	170
4.3.2	Characterization of polyimines.....	171
4.3.2.1	Thermal properties .....	171
4.3.2.2	Optical properties .....	172
<b>4.4</b>	<b>Conclusion .....</b>	<b>174</b>
<b>4.5</b>	<b>Bibliography.....</b>	<b>177</b>
<b>4.6</b>	<b>Experimental .....</b>	<b>178</b>
4.6.1	Syntheses.....	178
4.6.2	Thermogravimetric analyses (TGA) .....	200
4.6.3	Differential Scanning Calorimetry (DSC) .....	201
4.6.4	Optical .....	203
4.6.5	Electrochemistry.....	204
	<b>Conclusion and future work .....</b>	<b>207</b>
	<b>Experimental (general).....</b>	<b>209</b>
	<b>List of figures.....</b>	<b>211</b>
	<b>Introduction, résumé et conclusion de la thèse (french version) .....</b>	<b>219</b>



## General Introduction

---

Within the last century, electronics became a major technological breakthrough and brought solutions to overcome many limitations in fields such as information processing and telecommunication. The resulting applications are so numerous that it has invaded our every-day life: computers, television, domestic appliance, transport, telephones, and so on... All these advances result from the development of devices able to control electron flows. Such devices are usually made from metals and inorganic semiconductors (e.g. silicon).<sup>[1]</sup> Due to the inherent properties of such materials, some drawbacks are emerging. The production and processing of silicon, for instance, require a huge amount of energy. Indeed, this semiconductor has to be obtained in a really pure form, and the most common technique to achieve the pristine and crystalline material (Czochralski process) requires its melting, which occurs at 1414°C.<sup>[2]</sup> In order to make those technologies even more accessible and, more importantly, to reduce the environmental impact of the electronic industry, the nowadays challenge is to reduce this energetic cost. In that regard, organic semiconductors represent a great alternative for the future of electronics.

Although some evidences of electrical conductivity had already been demonstrated in the past, a real breakthrough was made by Hideki Shirakawa, Alan G. MacDiarmid and Alan J. Heeger in 1977 when they demonstrated high conductivity in an organic material: the polyacetylene, see Figure 1).<sup>[3]</sup> This was the starting point of a huge development in the field of organic electronics, and allowed the three discoverers to be rewarded with the Nobel Prize in chemistry for “the discovery and development of conductive polymers” in 2000.

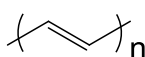
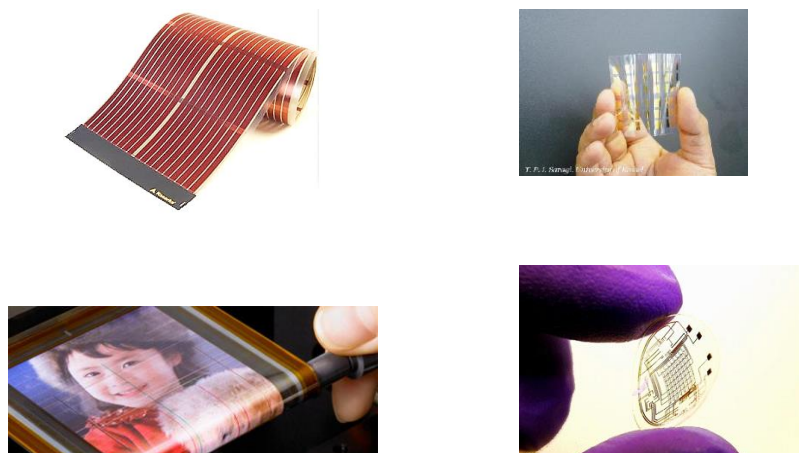


Figure 1: Chemical structure of polyacetylene.

Organic semiconductors consist of  $\pi$ -conjugated organic molecules or macromolecules mainly composed of carbon and hydrogen, but can also contain other elements such as nitrogen, sulfur or oxygen for example. Usually, such compounds are known to be insulators, but selecting the correct chemical structures can lead to organic materials with semiconducting properties.<sup>[4]</sup> A major advantage is the new properties they introduce, such as solubility in common solvents. Indeed, the weak intermolecular interactions allow them to be solubilized, thus the material can be purified with simple and mild techniques such as recrystallization, precipitation or Soxhlet extraction. Moreover, manipulating a solution is easier and less energy consuming: the organic material can be deposited via printing processes, and drying of the solvent will lead to the active semi-conductor.<sup>[5]</sup> Another interesting point is the light weight of organic semiconductors, and in the case of polymers the

possibility to create flexible devices. These novel properties offer applications which can be hardly considered with inorganic materials: flexible displays, textile-integrated light harvesting devices, or biocompatible electronic devices are some examples (see Figure 2).



**Figure 2:** Examples of organic electronics applications taking advantage of flexibility: solar cells (top left), transistors (top right), displays (bottom left) and electronic contact lens (bottom right).

However, the electrical properties (e.g. conductivity) of organic semiconductors can be limited, and the efficiencies of the resulting devices are still not completely competitive against the inorganic-based ones. Although the chemical structure-properties relationship in organic semi-conductors is becoming more and more understood, some investigations remain to be done in order to achieve organic semi-conductors with all the desired opto-electronic properties. Hence, this PhD goal is to synthesize new conjugated polymers and investigate their properties, in order to add novel materials to the already wide catalogue of semiconducting polymers and allow a better comprehension of the relationship between the molecular design and the resulting properties of the material. Furthermore, original and greener synthetic routes towards conjugated polymers will be developed.

- [1] S. M. Sze, M. K. Lee, *Semiconductor Devices: Physics and Technology, 3rd Edition: Physics and Technology*, **2012**.
- [2] O. Madelung, *Semiconductors: Data Handbook*, Springer Verlag, **2004**.
- [3] C. K. Chiang, C. R. Fincher, Jr., Y. W. Park, A. J. Heeger, H. Shirakawa, E. J. Louis, S. C. Gau, A. G. MacDiarmid, *Physical Review Letters* **1977**, 39, 1098-1101.
- [4] A. J. Heeger, N. S. Sariciftci, E. B. Namdas, *Semiconducting and Metallic Polymers*, OUP Oxford, **2010**.
- [5] M. Geoghegan, G. Hadzioannou, *Polymer Electronics*, OUP Oxford, **2013**.





---

Chapter 1    STRUCTURE-PROPERTIES  
RELATIONSHIP IN SEMICONDUCTING  
POLYMERS: A LITERATURE SURVEY





# Table of contents

<b>1.1</b>	<b>Semiconducting polymers .....</b>	<b>9</b>
<b>1.1.1</b>	<b>Band theory and definition of a semiconductor .....</b>	<b>9</b>
<b>1.1.2</b>	<b>Origin of semiconducting properties in organic materials.....</b>	<b>10</b>
<b>1.1.3</b>	<b>Charges generation in semiconducting polymers .....</b>	<b>12</b>
<b>1.2</b>	<b>Conjugated polymers design: structure-properties relationship .....</b>	<b>15</b>
<b>1.2.1</b>	<b>Aromaticity and planarization effect.....</b>	<b>17</b>
<b>1.2.2</b>	<b>Substituents effect .....</b>	<b>23</b>
<b>1.2.3</b>	<b>Quinoid stabilization effect .....</b>	<b>29</b>
<b>1.2.4</b>	<b>Donor-acceptor alternation effect .....</b>	<b>31</b>
<b>1.2.5</b>	<b>Recent trends in the design of alternated conjugated polymers .....</b>	<b>34</b>
<b>1.3</b>	<b>Synthesis of semiconducting polymers .....</b>	<b>37</b>
<b>1.3.1</b>	<b>Evolution of synthetic routes for conjugated polymers .....</b>	<b>37</b>
<b>1.3.2</b>	<b>Stille polycondensation .....</b>	<b>40</b>
<b>1.3.3</b>	<b>Suzuki polycondensation .....</b>	<b>41</b>
<b>1.3.4</b>	<b>Metal-free reactions applied to conjugated polymer synthesis .....</b>	<b>43</b>
<b>1.4</b>	<b>Aim and strategy of the thesis .....</b>	<b>46</b>
<b>1.5</b>	<b>Bibliography .....</b>	<b>50</b>



# 1.1 SEMICONDUCTING POLYMERS

Semiconducting polymers offer a wide range of applications. They can be used as transistors, a fundamental component of electronic devices, as well as active layer in lightning and display technology.<sup>[1]</sup> Light-harvesting devices based on polymers are of great interest, whether they are used as photosensors or as energy power sources. Compared to their inorganic counterparts, another advantage of semiconducting polymers is their better biocompatibility (chemically and mechanically), which makes them suitable candidates for biosensors and other bioelectronics applications<sup>[2]</sup>. This part will give a brief description of the origin of semiconducting behavior in organic polymers.

## 1.1.1 BAND THEORY AND DEFINITION OF A SEMICONDUCTOR

The band theory is the result of a development of the Schrödinger equation and describes the energy of the electrons in a material.<sup>[3]</sup> In organic materials, the electrons are located in defined energetic levels which form bands, and can be promoted towards other vacant levels upon external stimuli.<sup>[1]</sup> The highest occupied molecular orbital (HOMO) and the other occupied levels which are lower in energy are called the valence band because they carry the valence electrons. The lowest unoccupied molecular orbital (LUMO) and the above empty levels are called the conduction band because promoting an electron to that band leads to electrical conductivity of the material. According to the energetic structure, three different kinds of materials can be distinguished: metals, semiconductors and insulators (see Figure 1 - 1).<sup>[3]</sup> In metals, the valence and conduction bands overlap, which allows the electrons to be promoted to the conduction band without an additional source of energy. Insulators, on the other hand, possess an important energetically forbidden gap (typically more than 3 eV) between the valence and conduction band, and the amount of energy required to overcome it is too high and would lead to the degradation of the material. Finally, in semiconductors the energetically forbidden gap is small enough to allow excitation of electrons via thermal or light activation.

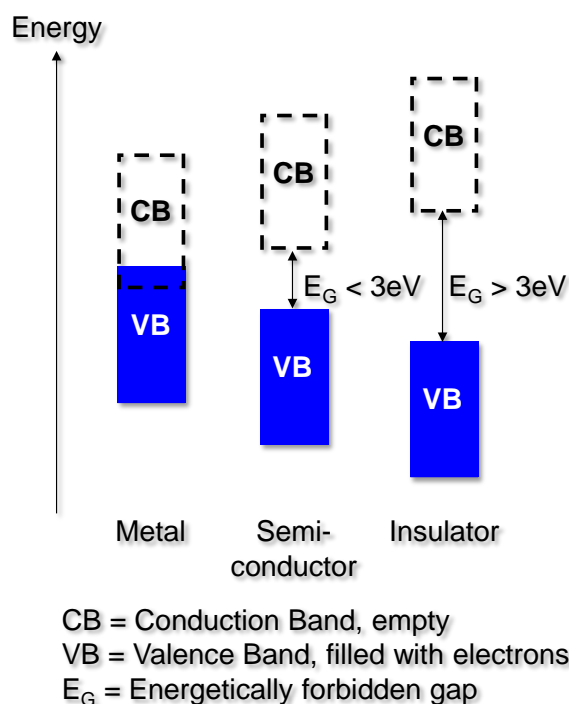


Figure 1 - 1: Representation of the energetic band structure in metals, semiconductors and insulators.

### 1.1.2 ORIGIN OF SEMICONDUCTING PROPERTIES IN ORGANIC MATERIALS

In order to obtain a semiconducting behaviour, a material has to contain electrons which can be moved without destroying its chemical structure.<sup>[4]</sup> In the case of organic materials,  $\pi$ -electrons are the best candidates, since they require less energy to be removed from their bonding state. As the  $\sigma$  single bond between the two atoms remains, the molecule keeps its atoms linked together. Thus only molecules with  $\pi$ -bonds provide semiconducting properties.

The ethylene (or ethene) molecule has an energetic gap between the HOMO and LUMO levels of 7.6 eV,<sup>[1]</sup> which is too large to obtain a semiconducting behaviour. In order to further decrease the energetic gap, a molecule has to contain delocalized  $\pi$ -bonds, so called conjugation effect.

The conjugation effect occurs in a molecule when two or more  $\pi$ -bonds are adjacent and appropriately arranged in space. In that case, the  $\pi$ -electrons are not only located around the source atoms, but are partially delocalized into the whole  $\pi$ -system.<sup>[4]</sup> This delocalization can be illustrated by the different resonance structures as depicted in Figure 1 - 2.

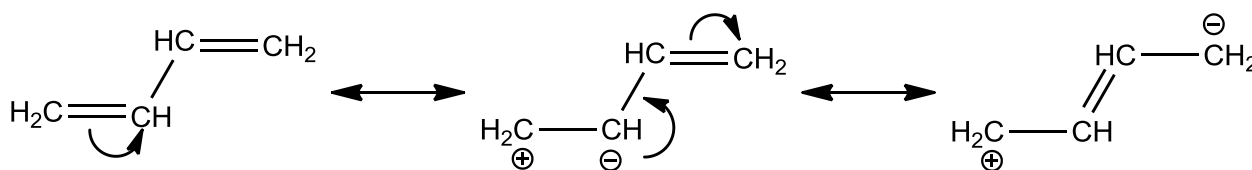


Figure 1 - 2: Resonant forms of the butadiene molecule.

Increasing the number of alternated multiple bonds results in the formation of molecular orbitals which are very close in energy. Therefore the energetic structure of the material is no longer described as discrete levels, but as energetic bands (see Figure 1 - 3).<sup>[4]</sup> Additionally, the gap between the HOMO and LUMO levels is reduced. Therefore conjugated polymers (CPs) show a semiconducting behavior.

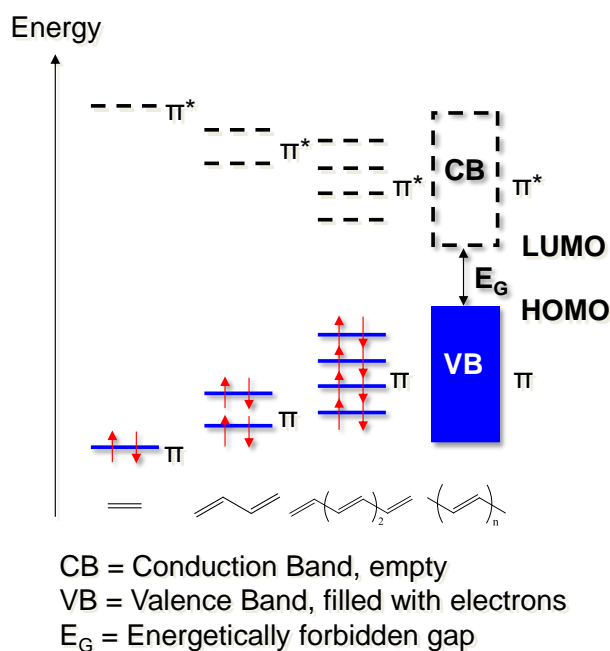


Figure 1 - 3: Representation of molecular orbitals evolution in energy when extending the  $\pi$ -system.

Alternation of single and double bonds in conjugated polymers leads to two possible structures. In the case of polyacetylene, these structures are energetically equivalent and the system is called degenerate (see Figure 1 - 4).<sup>[4]</sup>

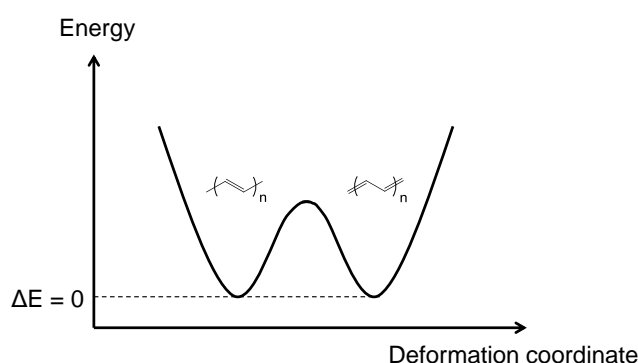


Figure 1 - 4: Sketch of the potential energy curve for a degenerate system (polyacetylene).

Other CPs demonstrate a difference in energy between the two resonance forms, and are therefore described as non-degenerate. The second structure of aromatic-based semiconducting polymer is known as the quinoid form and usually presents higher potential energy (see Figure 1 - 5).<sup>[4]</sup>

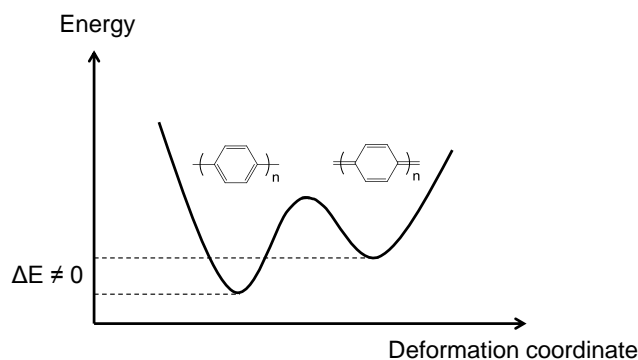


Figure 1 - 5: Sketch of the potential energy curve for a non-degenerate system (polyparaphenylene).

The molecular arrangement of a material can also alter its energetic configuration. Planar molecules with a  $\pi$ -electrons system are known to stack, causing an inter-molecular overlap of the  $\pi$  orbitals. This overlap allows a larger delocalization of the electrons and thus a further decrease of the band gap.<sup>[1]</sup> Other parameters are known to alter the band-gap, such as geometry of the molecule, aromaticity or substituents effect.

### 1.1.3 CHARGES GENERATION IN SEMICONDUCTING POLYMERS

Electrical conductivity induced by a small amount of energy, e.g. ambient temperature, is observed in intrinsic semiconductors,<sup>[5]</sup> where the band-gap is narrow enough to allow promotion of electrons from the valence to the conduction band. Extrinsic semiconductors, on the other hand, have a higher band-gap and require doping to become electrical conductors. Doping can be performed by injecting charges with an electric current sent to the material, or via the inclusion of a dopant, i.e. a material of different nature.<sup>[1]</sup> A semiconductor can be either n-doped or p-doped. N-doping corresponds to the addition of electrons in the conduction band or in newly created energetic levels below the LUMO. P-doping corresponds to the creation of holes (i.e. electron vacancies) in the valence band or in newly created energetic levels above the HOMO. In inorganic materials, doping is usually performed by substituting several atoms with elements of the previous group (creation of a valence electron vacancy, p-doping) or the next group (creation of an extra free valence electron, n-doping).<sup>[3]</sup> In the case of organic materials, a redox process is usually involved to generate charges.<sup>[1]</sup> Most of the semiconductors demonstrate a strong difference in conductivity between their pristine and doped form. Electrical conductivity in conjugated polymers upon doping was demonstrated by the pioneering work of Heeger et al. in 1977.<sup>[6]</sup>

P-doping forms a radical cation, whereas a radical anion is formed by n-doping (see Figure 1 - 6).<sup>[1]</sup> Exciton is the result of an electrostatic interaction between radical cation and anion located in a sufficient proximity (see Figure 1 - 6). It can also be formed by exciting an electron from the HOMO to

a higher energy level upon an external stimulus, which usually corresponds to visible light. This entity is located over several monomeric units in the polymer chain. Recombination of an exciton leads to radiative emission of visible light, whereas absorption of light and dissociation of the formed exciton creates charges in the material.

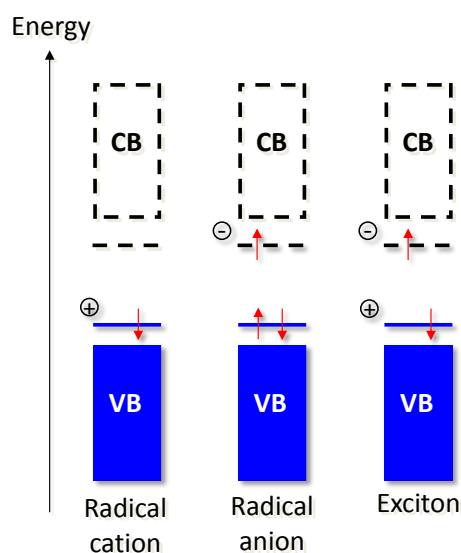


Figure 1 - 6: Representation of radical cation and radical anion in an organic semiconductor.

In a doped CP, the bonds along the backbone rearrange themselves and change the geometry of the macromolecule because of the resulting charges.<sup>[7]</sup> Energetic levels of the material will also be disturbed, and new energetic levels within the forbidden gap can appear. This applies for all polymers with exception of trans-polyacetylene, in which resonant forms are equivalent in energy (see Figure 1 - 7).



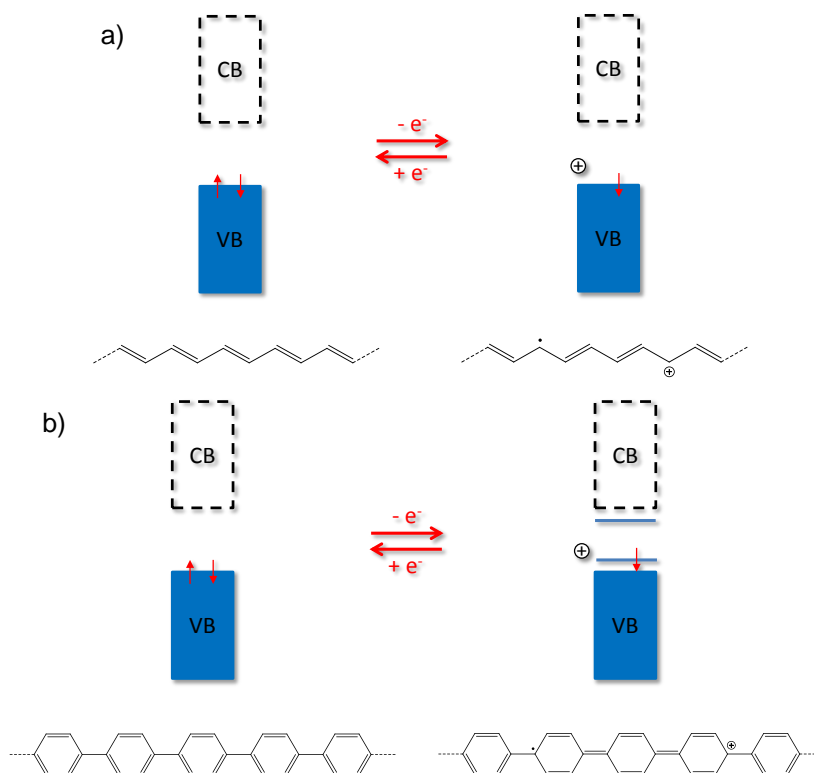


Figure 1 - 7: Creation of a radical cation in degenerated (a) and non-degenerated (b) CP.

The charges can pass through the material via two different processes. Firstly, the  $\pi$ -delocalized system allows them to move along the polymer chain.<sup>[1]</sup> This is illustrated by the resonant structures, also called mesomeric forms (see Figure 1 - 8).

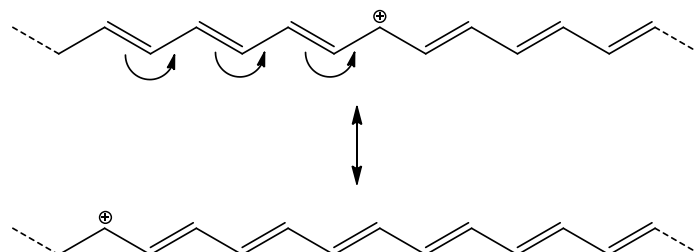


Figure 1 - 8: Charge delocalization in a polyacetylene chain.

The second process is called hopping, in which electrons or holes hop from one chain or chain fragment to another (see Figure 1 - 9). This is considered as the main phenomenon contributing to charge transport in semiconducting polymers.<sup>[1]</sup> Charge transport properties often vary depending on their nature. Most of the semiconducting polymers show a better hole than electron transport.

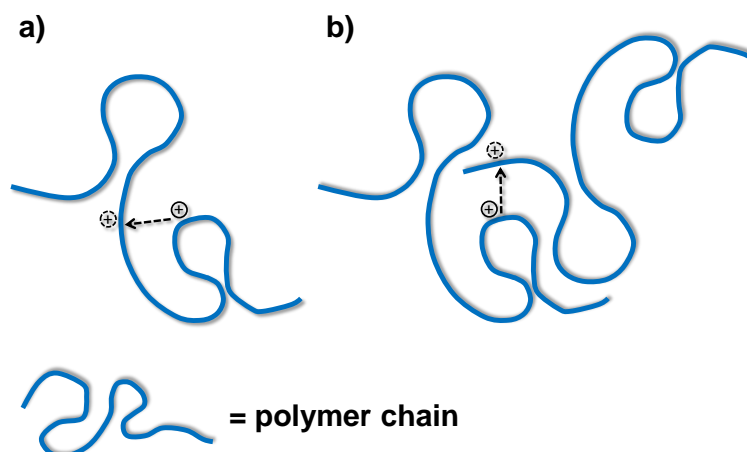
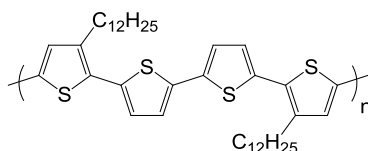


Figure 1 - 9: Hopping transport – a)intramolecular; b)intermolecular.

## 1.2 CONJUGATED POLYMERS DESIGN: STRUCTURE- PROPERTIES RELATIONSHIP

The positions and gap between the HOMO and LUMO levels are important parameters which influence the spectroscopic and electronic properties of the material, since it determines its light absorption/emission range but also its electron donating/accepting behaviour. In the past years, lots of efforts were focusing on the understanding of how the chemical structure of the material influences its final properties, and more particularly the band gap size and position. Nowadays a wide catalogue of conjugated polymers with different spectroscopic and electronic properties is available.<sup>[8-9]</sup>

As mentioned previously, extending the  $\pi$ -electrons system is responsible for the band structure and the decrease of the HOMO-LUMO gap in conjugated polymers. Consequently, increasing the length of the conjugated backbone in an organic semiconductor is a way to reduce its band-gap and bathochromically shift its light absorption. This was illustrated by the work of Briseno and co-workers, who synthesized a series of oligothiophenes with controlled lengths.<sup>[10]</sup> They demonstrated that a red-shift of the light absorption occurred when the number of thiophene rings in the main chain was raised up to 16, after which the absorption spectra showed only slight changes which was consistent with the limited extent of excitons over several repeating units (see Figure 1 - 10). Additionally, increasing the molecular weight can impact the charge transport properties of the material.



Number of repeating unit n (1 r.u. = 4 thiophene rings)	$\lambda_{\max}$ absorption (nm)
1	378
2	436
3	457
4	465
5	468
6	470

Figure 1 - 10: Evolution of the UV-visible absorption with the number of repeating units in oligothiophenes.<sup>[10]</sup>

Similar studies were carried out on different conjugated macromolecules composed of 3,4-ethylenedioxythiophene (EDOT) and thiophene for instance, and they showed an identical trend in terms of spectroscopic properties.<sup>[11]</sup> However, the maximum extent of conjugation may vary according to the employed heteroaromatic units. Hence, oligomers based on diketopyrrolopyrrole (DPP) and thiophene did not demonstrate any remarkable evolution of their properties beyond 2 repeating units.<sup>[12]</sup>

Roncali has given a theoretical definition of an organic semiconductor band-gap according to 5 parameters (see Figure 1 - 11) regardless of the chain length,<sup>[13]</sup> expressed as:

$$E_G = E_{BLA} + E_{Res} + E_{Sub} + E_{\theta} + E_{Int} \quad (2)$$

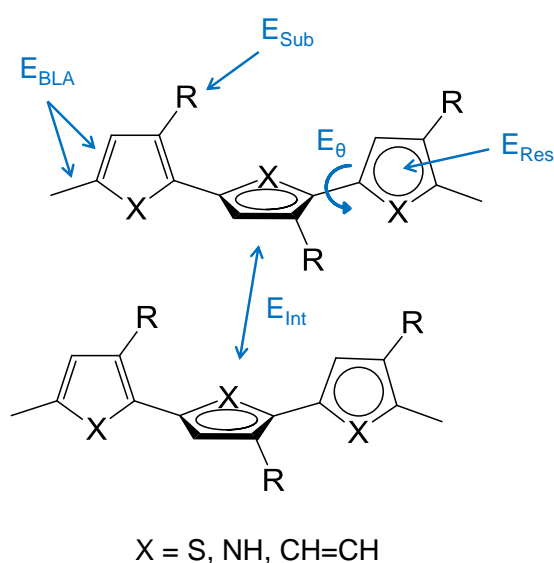


Figure 1 - 11: Structural factors determining the band gap of materials derived from linear  $\pi$ -conjugated systems. Reproduced from Roncali.<sup>[13]</sup>

$E_{BLA}$  represents the contribution of the bond length alternation. Theoretical studies showed that coupling of electrons and phonons with lattice distortions in conjugated materials led to a partial localization of single and double bonds, and thus an alternation of the carbon-carbon bond lengths ( $l_{C-C} > l_{C=C}$ ).<sup>[14-16]</sup> This effect is the major contribution to the band-gap aperture.

$E_{Res}$  is related to the incorporation of aromatic subunits in the backbone. Due to the stabilization effect of aromaticity, electrons tend to be confined in the aromatic units and are thus less available for delocalization.<sup>[17]</sup> A decrease of the degree of aromaticity in the polymer chain therefore leads to a reduced band-gap.

Presence of substituents can also affect the positions of HOMO and LUMO levels by donating or withdrawing electrons through mesomeric or inductive effects, thus represented by  $E_{Sub}$ .<sup>[15]</sup>

Dihedral angle between the subunits, usually due to rotational freedom around  $\sigma$  bonds, breaks the planarity of the backbone. Hence, the p-orbitals overlap is limited as well as the  $\pi$ -electrons delocalization.<sup>[13]</sup> Consequently, increasing the twist angle between units also enlarges the band-gap through the  $E_{\theta}$  contribution.

Finally, intermolecular interactions such as  $\pi$ -stacking can influence the band gap, which is described by the  $E_{Int}$  parameter. It was considered that interchain coupling could dramatically minimize the Peierls instability, thus decreasing the band-gap.<sup>[18]</sup> Each parameter can be tuned through an appropriate design of the monomer subunits.

### 1.2.1 AROMATICITY AND PLANARIZATION EFFECT

An important point to achieve polymeric semiconductors is the incorporation of alternating  $\sigma$  and  $\pi$  bonds along the main chain. The simplest example of such a structure is the polyacetylene, which has a band gap around 1.5 eV.<sup>[19]</sup> This polymer is highly insoluble in organic solvents and quite sensitive to oxidation, due to a high lying HOMO level. Using aromatic units generally helps to lower the HOMO, but a large dihedral angle generally exists between the subunits within the chain, resulting in a higher band-gap as explained above. Therefore, strategies to achieve a more planar backbone were investigated.<sup>[20]</sup>

Planarization has a direct effect on the band-gap by reducing the  $E_{\theta}$  parameter.<sup>[21]</sup> Moreover, a planar structure is favourable to intermolecular interactions ( $E_{Int}$ ).<sup>[1]</sup> The latter is also known to influence the charge carrier mobility in a semiconducting polymer. Additionally, the combination of non-aromatic and aromatic conjugated units decreases the degree of aromaticity and the electrons confinement in the aromatic parts, thus reducing the  $E_{BLA}$  and  $E_{Res}$  contributions.

Poly(*para*-phenylene) (PPP) is one of the most basic structures of aromatic-based CP. Its conductivity upon doping was demonstrated by Baughman et al in 1980.<sup>[22]</sup> The optical properties of PPP are limited by a strong torsion angle between the phenylene units, as well as by a partial localization of  $\pi$ -electrons in the aromatic units. This issue can be addressed by inserting multiple bonds between the phenyl rings. The first effect of double bonds insertion between units is a reduction of steric hindrance between aromatic units leading to a more flatten backbone, thus decreasing the band-gap. In addition, vinylene linkages bring  $\pi$ -electrons which are not involved in aromatic systems. Hence double bonds insertion also decreases the overall degree of aromaticity in a CP, which is beneficial to electronic delocalization and contributes to a narrowing of the HOMO-LUMO gap. Therefore, poly(*p*-phenylenevinylene) (PPV) shows a smaller band-gap than PPP,<sup>[23]</sup> as depicted in Figure 1 - 12. The same effect is observed when comparing poly(thiophene) (PT) to poly(thienylenevinylene) (PTV) resulting in a decrease of the band-gap from 2.0 eV to 1.7 eV.<sup>[24]</sup>

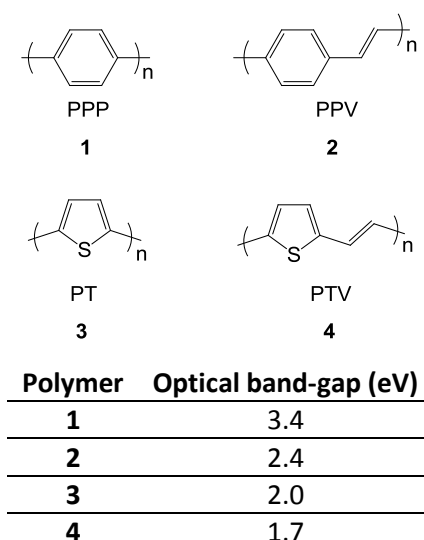
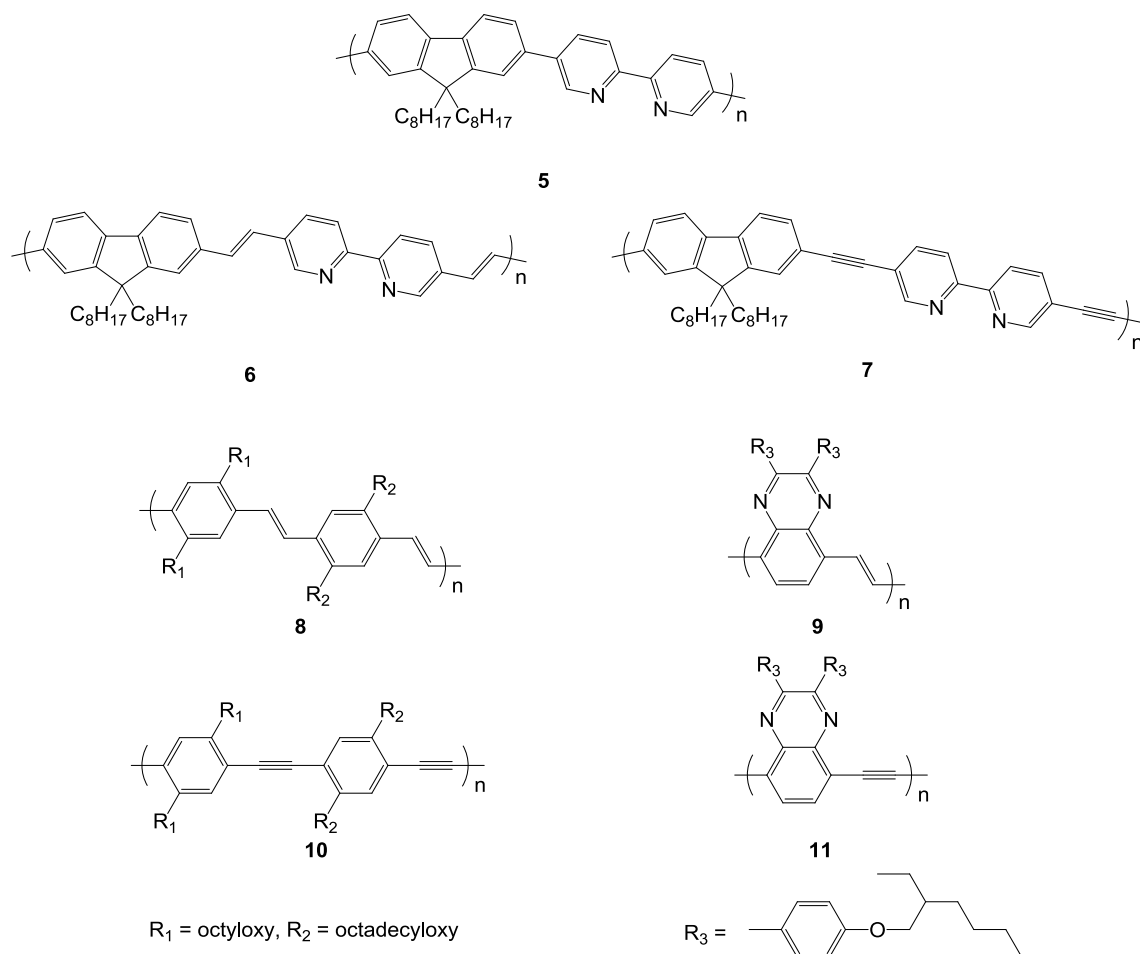


Figure 1 - 12: Effect of double bonds insertion on phenyl and thiophene-based CPs.<sup>[23-24]</sup>

Triple bonds may also be used as spacers, and a great research effort has been focused on the development on poly(arylenethynylene) and related polymers.<sup>[25]</sup> Insertion of ethynylene bonds between the aromatic units allows a decrease of the material's band-gap for the same reasons as vinylene-linked CPs, as depicted in Figure 1 - 13. However, the reduction is generally weaker due to a worse electron delocalization when using triple bonds.<sup>[26]</sup> As an example, incorporation of vinylene links between fluorene and bipyridyl units in a conjugated polymer efficiently reduced the optical band-gap by 0.4 eV (polymer **6**), whereas the reduction was only 0.2 eV when using ethynylene (polymer **7**). This was consistent with other examples of semiconducting polymers in the literature showing smaller band-gaps when linked via double bonds than in the case of triple bonds.<sup>[27-28]</sup> Moreover, it was commonly observed that insertion of *sp* carbons tends to lower the energetic levels

owing to their slight electron-withdrawing nature, making it an potential way to n-type semiconducting polymers.<sup>[29]</sup>

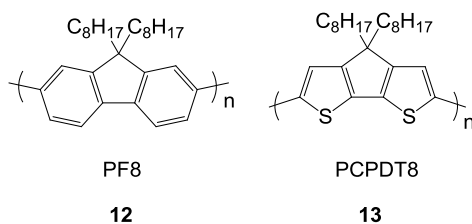


Polymer	Optical band-gap (eV)
5	2.9
6	2.5
7	2.7
8	2.1
9	1.9
10	2.4
11	2.0

**Figure 1 - 13: Examples of poly(arylenevinylene)s and poly(aryleneethynylene)s.** <sup>[26-28]</sup>

Choosing units with a weaker steric hindrance is another approach to achieve planarization. As an example, poly(9,9-dioctylfluorene) (PF8) presents an optical band gap of 3.0 eV.<sup>[8]</sup> Poly(4,4'-dioctylcyclopentadithiophene) (PCPDT8) is an analogous polymer in which the fused benzene rings are replaced by fused thiophene rings. In the latter, the combined effects of the reduced steric hindrance between the subunits and the electronic enrichment of the system due to the presence of sulfur atoms result in a smaller optical band gap of 1.7 eV.<sup>[30]</sup> Thiophene units can be employed as spacers, like double bonds, between more complex and hindered heteroaromatic moieties to reduce

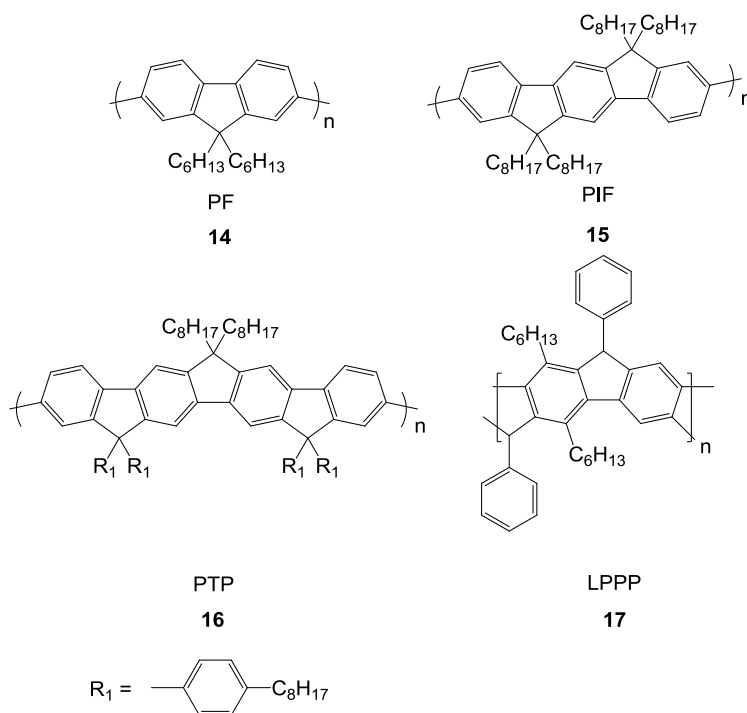
the steric effect. This strategy was widely used in the design of new alternated donor copolymers for photovoltaic applications.<sup>[31]</sup>



Polymer	Optical band-gap (eV)
<b>12</b>	3.0
<b>13</b>	1.7

Figure 1 - 14: Effect of reduced steric hindrance on the optical gap.<sup>[8, 30]</sup>

Another way towards backbone planarization is insertion of covalent bridging between units. Müllen and co-workers have developed a series of methine-bridged poly(*p*-phenylene) in order to investigate the effect of bridging on the optical absorption and emission (see Figure 1 - 15).<sup>[20]</sup> Bathochromical shift of ca. 35 nm was observed when an extra phenylene moiety was bridged to poly(fluorene) **14** (PF), thus yielding poly(indenofluorene) **15** (PIF). This shift is even stronger in the case of poly(tetraphenylene) **16** (PTP). Finally, the fully bridged polymers **17**, also called ladder-type poly(*p*-phenylene) (LPPP), show an absorption maximum at 443 nm. The synthetic route to achieve LPPPs has to be carefully chosen in order to avoid defects and breaks in the bridging along the backbone. It was estimated that the effective conjugation length for absorption in LPPPs corresponds to 11-12 benzene rings, and up to 15 for photoluminescence.<sup>[20]</sup>



Polymer	$\lambda_{\text{max}}$ absorption (nm)
<b>14</b>	380
<b>15</b>	416
<b>16</b>	434
<b>17</b>	443

Figure 1 - 15: Effect of backbone rigidification via methine-bridging.<sup>[32-35]</sup>

LPPPs can be achieved via other kind of covalent bridges, such as ethane and ethene (see Figure 1 - 16).<sup>[36-37]</sup> In the case of ethane a torsion angle between the subunits is expected, thus leading to a decrease in the backbone planarity.<sup>[20]</sup> Nevertheless, both LPPPs showed very similar absorption spectra with maxima of 435 and 437 nm for the ethane-bridged (**18**) and the ethene-bridged (**19**), respectively.

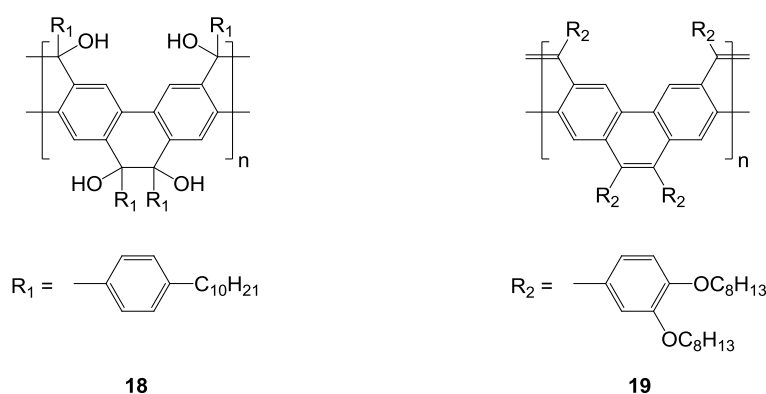
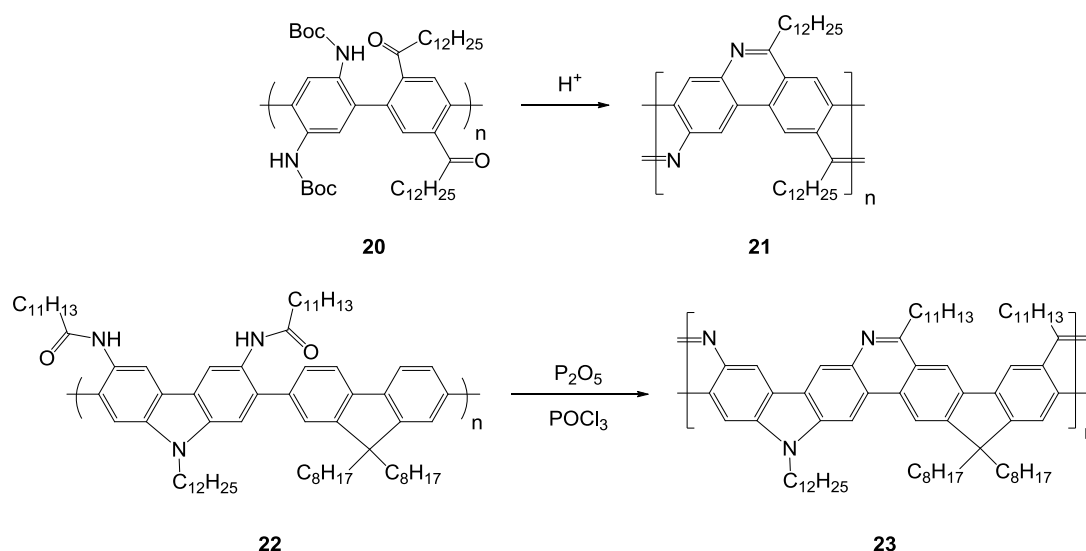


Figure 1 - 16: LPPP with ethane (LPPP1) and ethene (LPPP2) bridges.<sup>[36-37]</sup>

Imine bonds also proved to be an efficient bridge for CPs backbone planarization (see Figure 1 - 17). By treating the polymeric precursor **20** bearing *tert*-butyloxycarbonyl (Boc) and ketone groups in acidic conditions, Tour et al. achieved the soluble imine-bridged LPPP **21**.<sup>[38-39]</sup> LPPP **23** was obtained via the efficient Bischler-Napieralski reaction, which allowed bridging of alternated carbazole and fluorene units the backbone of the precursor **22**.<sup>[40]</sup> In both cases, the resulting ladder-type polymers demonstrated a red-shift in absorption and emission compared to their precursor, which was in good agreement with an extent of conjugation. The method developed by Tour and co-workers was later successfully extended to polymers containing thiophene and pyridine units in the main chain.<sup>[41]</sup>





Polymer	$\lambda_{\text{max}}$ absorption (nm)
<b>20</b>	250
<b>21</b>	463
<b>22</b>	350-360
<b>23</b>	448

Figure 1 - 17: Examples of imine-bridged LPPPs.<sup>[38-40]</sup>

However, the main disadvantage of this strategy is the creation of defects due to the synthetic pathways of LPPPs and their limited absorption in the visible spectrum. For that reason, a preferred way to CPs with smaller band-gaps is the use of bridges on a controlled extent of aromatic units. This type of design resulted in semiconducting polymers such as **24** (see Figure 1 - 18), in which the added effects of bridging, reduced steric hindrance and donor-acceptor effect (described in section 1.2.4) conducted to an optical band-gap of 1.9 eV. BHJ solar cells using this material in the active layer showed high efficiencies, attributed to low-lying energetic levels and good charge-carrier mobility.<sup>[42]</sup>

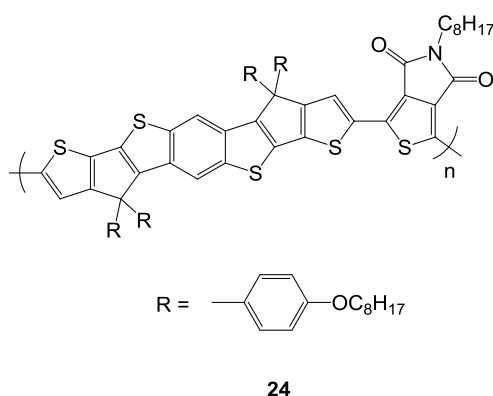


Figure 1 - 18: PBDCPDT-TPD, a semiconducting polymer with enhanced planarity obtained by bridging and reduced steric hindrance.<sup>[42]</sup>

In summary, planarization of the backbone can be achieved by two main strategies. Firstly, one can reduce the steric hindrance by incorporation of spacers or by appropriate geometry of the molecule (thiophene instead of phenylene units for instance). Additionally, the use of non-aromatic spacers

(such as vinylene bonds) effectively delocalizes the  $\pi$ -electrons by decreasing the degree of aromaticity along the backbone, thus reducing the band-gap. Another approach is the rigidification of the polymer chain by covalent bridging of the subunits, which proved to be an efficient way of reducing the band gap.

## 1.2.2 SUBSTITUENTS EFFECT

Unless suitably modified, CPs tend to be insoluble in organic solvents.<sup>[19]</sup> This issue can be overcome by introducing alkyl or alkoxy chains in the backbone, as can for example be done in the phenylene rings of PPP<sup>[43]</sup>. In Figure 1 - 19 is shown a well-known soluble PPV derivative, the poly(1-methoxy-4-(2-ethylhexyloxy)-*p*-phenylenevinylene) (MEH-PPV).<sup>[44]</sup> Such flexible chains, which are easily soluble in common organic solvents, allow the macromolecules to be solvated. Poly(3-alkylthiophene)s and poly(*N*-alkylpyrrole)s are notorious examples of this concept (see Figure 1 - 19).<sup>[45-46]</sup>

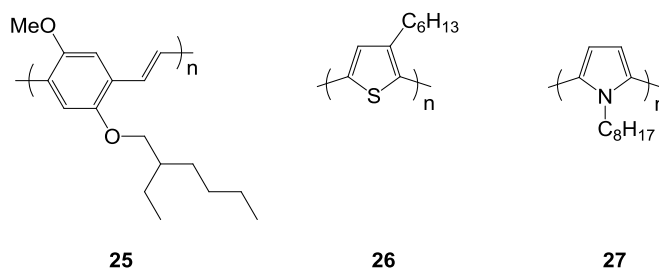


Figure 1 - 19: Examples of soluble CPs. 1: MEH-PPV; 2: poly(3-hexylthiophene) (P3HT); 3: poly(*N*-octylpyrrole).<sup>[44-46]</sup>

Water-soluble semiconducting polymers can be achieved through the use of side-chains functionalized with ionic groups such as sulfonate (**30**)<sup>[47]</sup> or ammonium (**28** and **29**)<sup>[48-49]</sup> (see Figure 1 - 20). Solubility of CPs in water and alcoholic solvents is a great asset in the development of environmental-friendly processes for the fabrication of organic electronic devices for instance.

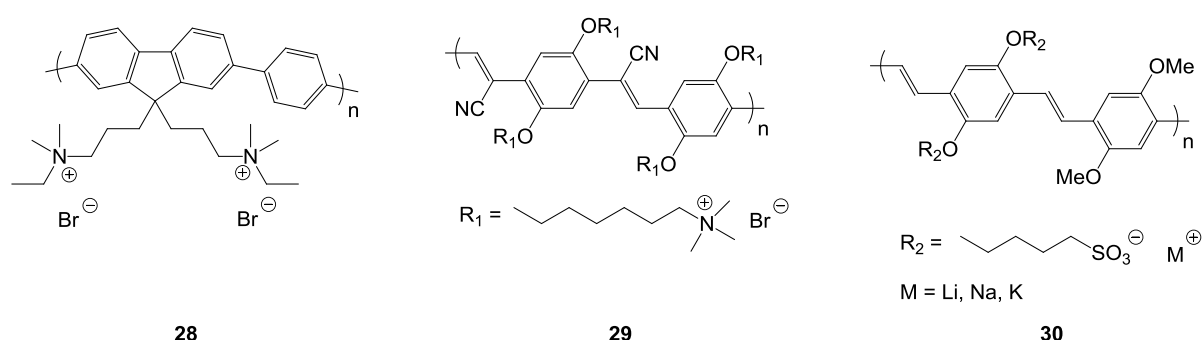
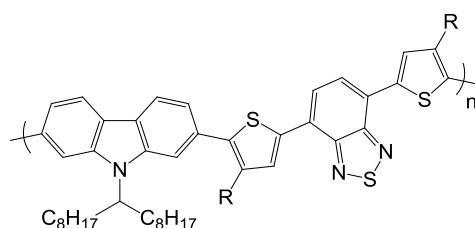


Figure 1 - 20: Examples of CPs soluble in water and alcoholic solvents.<sup>[47-49]</sup>

Additionally, the substituents can induce a higher torsion angle between the subunits via steric hindrance, thus impacting the  $E_g$  contribution (see Figure 1 - 21).<sup>[50-51]</sup> They can also influence the solid-state properties of the material by modifying the inter-molecular arrangement of the polymer

chains, mainly by reducing the stacking between the chains, thus widening the band-gap. A less ordered structure can also have a detrimental impact on the charge carrier mobility.<sup>[52]</sup> Nevertheless, in the case of regioregular polymers, the long-range order of the polymer can be improved by choosing the appropriate substituent, and the band-gap decreased as for poly(3-hexylthiophene) (P3HT).<sup>[53]</sup>

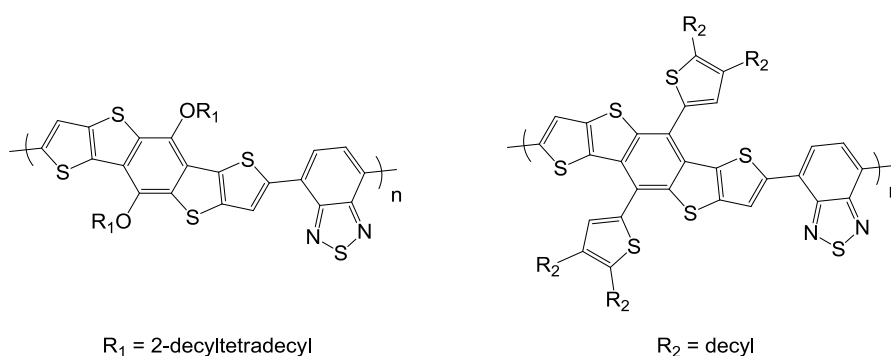


31

Substituent R	Optical band-gap (eV)
-H	1.9
-C <sub>6</sub> H <sub>13</sub>	2.0

Figure 1 - 21: Effect of steric hindrance generated by alkyl substituents on the optical band-gap.<sup>[51]</sup>

It was reported that using conjugated side-chains enhanced the intermolecular interactions.<sup>[54]</sup> Kwon et al. demonstrated that the use of alkyl substituted thiophene side-groups did not affect greatly the optical properties of the materials, but had a drastic influence on the hole mobility of the donor polymer blended with PCBM (see Figure 1 - 22).<sup>[55]</sup>



R<sub>1</sub> = 2-decyltetradecyl

R<sub>2</sub> = decyl

32

33

Polymer	Optical band-gap (eV)	Hole mobility (cm <sup>2</sup> .V <sup>-1</sup> .s <sup>-1</sup> )
32	1.6	0.001
33	1.6	0.55

Figure 1 - 22: Influence of conjugated substituents on hole mobility measured by space-charge-limited current method on polymer:PCBM blends.<sup>[55]</sup>

Furthermore, substituents can affect the  $\pi$ -electrons system through inductive and mesomeric effect ( $E_{sub}$ ). Alkyl side-chains are generally considered as donor due to their inductive effect, though their influence is relatively small. Electron-donating substituents such as amino and alkoxy usually raise

the energetic levels.<sup>[21, 56]</sup> However, this will also destabilize the material since its oxidation potential is lowered. As an example, poly(3,4-ethylenedioxythiophene) (PEDOT) **34** have a smaller band gap<sup>[57]</sup> in comparison with poly(thiophene) **3** due to the incorporation of the electron-donating ethylenedioxy bridge on the thiophene unit, but also thanks to non-covalent sulfur-oxygen interactions which induce a planarization of the backbone (see Figure 1 - 23).<sup>[58]</sup> PEDOT's high lying HOMO level makes it sensitive to oxidation, therefore this polymer is usually employed in its oxidized state. Contrary to its blue coloured neutral non-conductive form, the doped polymer has a reduced band-gap and hence is optically transparent.

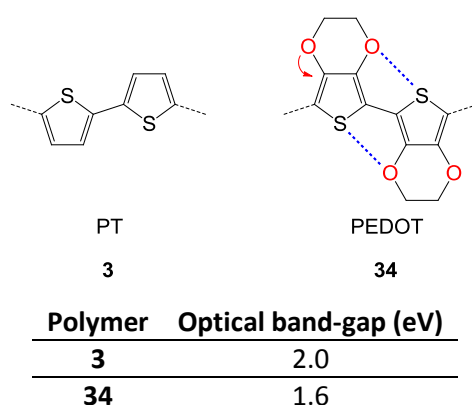


Figure 1 - 23: Ethylenedioxy group insertion on thiophene units and its effect on the polymer band-gap. Red arrow: electron donating effect of the oxygens. Blue dotted lines: sulfur-oxygen interactions.<sup>[57-58]</sup>

In Figure 1 - 24 are shown different examples of polythiophenes substituted with electron-donating groups. As mentioned previously, the donor inductive effect of alkyl chains is negligible, therefore the optical band-gaps of poly(alkylthiophene)s (PATs) such as **35** do not differ from the one of polythiophene. Band-gaps down to 1.7 eV can be obtained with highly regioregular PATs though this is not related to the electron-donating ability of the side-chains.<sup>[53]</sup> Moreover, higher band-gaps can be observed when using alkyl side-chains which are bulky enough to generate a strong steric hindrance and increase the twist between thiophene units. The stronger donor mesomeric effects of alkoxy or amino groups lead to smaller band-gap (see Figure 1 - 24). This narrowing is mainly attributed to a raise of the HOMO level.<sup>[21]</sup>

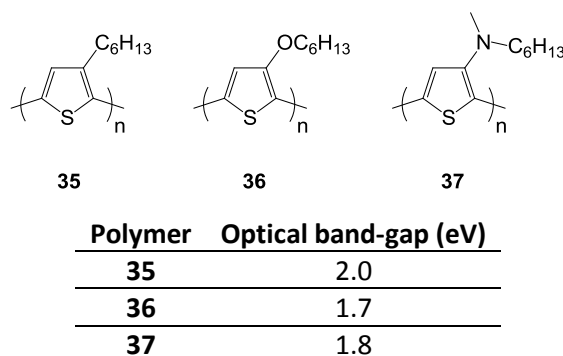
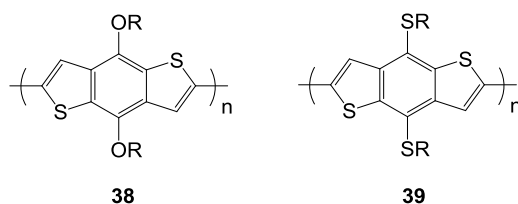


Figure 1 - 24: Examples of electron-donating substituted polythiophenes.<sup>[9, 59-60]</sup>

Thioalkyl groups are potential replacement of the widely employed alkoxy side-chains. Ferraris et al. showed that replacing alkoxy by thioalkyl in poly(benzodithiophene)s led to materials with lower energetic levels, due to the poorer electron-donating property of thioalkyl (see Figure 1 - 24).<sup>[61]</sup> Additionally, enhanced solubility in common organic solvents was observed in the case of **39**.

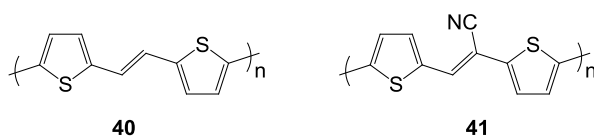


R = 2-ethylhexyl

Polymer	Optical band-gap (eV)	Electrochemical band-gap (eV)	HOMO (eV)	LUMO (eV)
<b>38</b>	2.2	2.4	- 5.3	- 2.9
<b>39</b>	2.1	2.1	- 5.4	- 3.3

Figure 1 - 25: Comparison of thioalkyl and alkoxy substitution on CPs.<sup>[61]</sup>

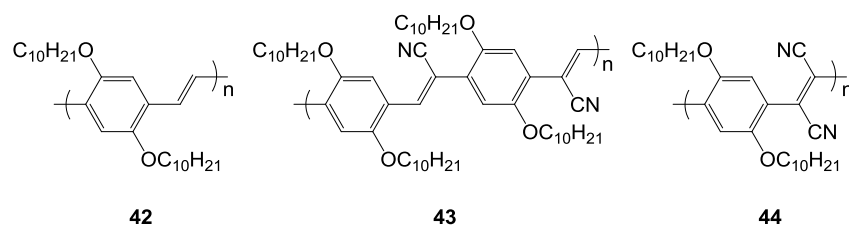
Reversely, the use of electron-withdrawing substituents such as cyano group can lower the energetic levels of the material and reduce the band-gap. Roncali et al. have shown that the band gap of **40** could be reduced by inserting cyano groups on the double bonds between the thiophene units (see Figure 1 - 26).<sup>[62]</sup>



Polymer	Optical band-gap (eV)
<b>40</b>	1.8
<b>41</b>	0.6

Figure 1 - 26: Effect of cyano groups on PTV derivatives.<sup>[62]</sup>

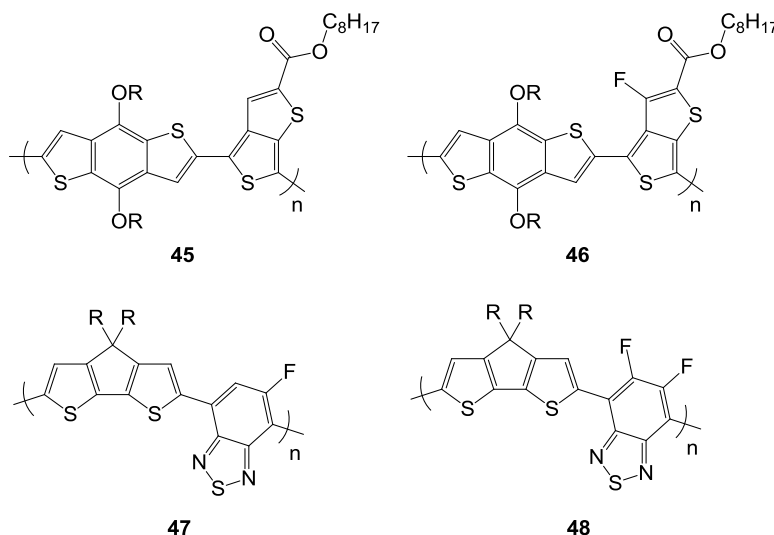
However, if the HOMO level is strongly lowered and the LUMO level only slightly modified, the material can show a higher band gap. It was observed by Zhang et al. on PPV derivatives where the double bond was either mono or di-substituted,<sup>[63]</sup> and led to a higher band gap and a blue-shifted absorption (see Figure 1 - 27). This effect was associated to a disturbed planarity of the structure due to steric hindrance between the cyano groups and the phenylene units.



Polymer	LUMO (eV)	HOMO (eV)	Electrochemical band-gap (eV)
<b>42</b>	-2.9	-5.1	2.2
<b>43</b>	-3.3	-5.8	2.5
<b>44</b>	-3.7	-6.2	2.5

Figure 1 - 27: Effect of cyano groups on the band-gap of PPV derivatives.<sup>[63]</sup>

The strong electronegativity of fluorine makes it a promising candidate as electron-withdrawing substituent. Hence, different research groups successfully employed it to lower the energetic levels of conjugated polymers, as depicted in Figure 1 - 28.<sup>[64-65]</sup> A slight hypsochromic shift of the optical spectrum was observed when inserting a second fluorine atom in polymer **48**, which was attributed to an increase of the steric hindrance of the benzothiadiazole unit.



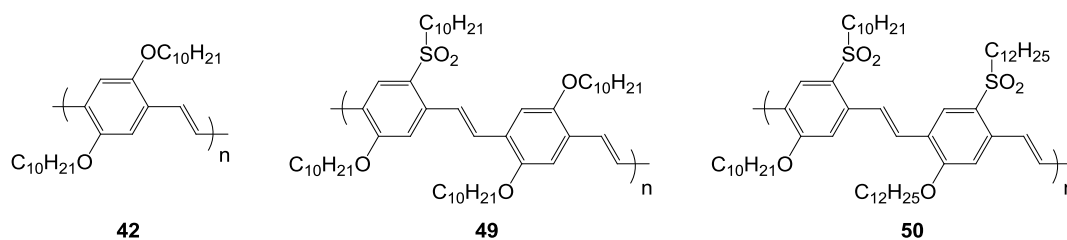
R = 2-ethylhexyl

Polymer	Optical band-gap (eV)	Electrochemical band-gap (eV)	HOMO (eV)	LUMO (eV)
<b>45</b>	1.6	1.8	- 5.0	- 3.2
<b>46</b>	1.6	1.8	- 5.1	- 3.3
<b>47</b>	1.4	1.5	- 5.0	- 3.5
<b>48</b>	1.4	1.6	- 5.2	- 3.6

Figure 1 - 28: Effect of fluorine insertion.<sup>[64-65]</sup>

Sun and co-workers investigated the influence of sulfone functionalization on PPV derivatives (see Figure 1 - 29).<sup>[66]</sup> As expected, the electron-withdrawing character of sulfone groups led to a lowering of the HOMO and LUMO levels. Furthermore, larger band-gaps were obtained when the degree of sulfone functions per repeating unit was increased, which was explained by an intramolecular charge

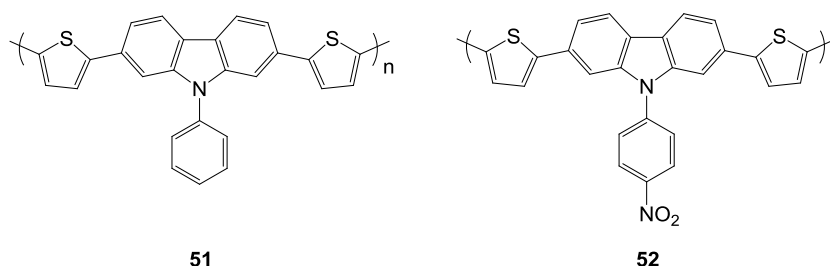
transfer (ICT) between the alkoxy and sulfone groups in *para* positions, therefore creating interruptions in the conjugation along the polymer backbone.



Polymer	Optical band-gap (eV)	Electrochemical band-gap (eV)	HOMO (eV)	LUMO (eV)
<b>42</b>	2.3	2.5	- 5.2	- 2.7
<b>49</b>	2.3	2.5	- 5.4	- 2.9
<b>50</b>	2.6	-	-	- 3.2

Figure 1 - 29: Effect of sulfone-based substitution.<sup>[66]</sup>

The electron-withdrawing ability of nitro groups also proved to be an efficient way to achieve lower lying-energetic levels (see Figure 1 - 30).<sup>[67]</sup> Compared to its analogue **51**, the nitro-substituted polymer **52** demonstrated a lower HOMO level, as well as higher redox stability and multi-electrochromic behavior.



Polymer	Optical band-gap (eV)	Electrochemical band-gap (eV)	HOMO (eV)	LUMO (eV)
<b>51</b>	2.1	-	- 5.1	-
<b>52</b>	2.2	1.6	- 5.3	- 3.7

Figure 1 - 30: Influence of nitro group.<sup>[67]</sup>

To conclude, functionalization of CPs is important for two main reasons. Firstly, flexible substituent such as alkyl chains can enhance the solubility of the material in organic solvents, which is one of the main technological advantages of polymeric semiconductors compared to their inorganic counterparts. Secondly, the electron-withdrawing or electron-donating effect of a substituent can be used to tune the energetic levels (HOMO and LUMO). According to the nature and position of the substituents, steric hindrance or enhanced planarization can occur which can dramatically influence the conjugation length and the band-gap.

### 1.2.3 QUINOID STABILIZATION EFFECT

To achieve semiconducting polymers with a small band-gap, a commonly employed strategy is the use of subunits which can easily adopt the quinoid conformation. As mentioned previously, semiconducting polymers bearing aromatic subunits acquire the quinoid configuration under excitation, oxidation or reduction (see section 1.1.3). This configuration usually presents a lower band-gap. Therefore, enhancing the formation of such a structure in CPs by an appropriate design of the subunit leads to conjugated materials with reduced band-gaps. One of the first example is the poly(isothianaphtene) **53**, which band-gap was estimated to be 1 eV (see Figure 1 - 31).<sup>[68]</sup> Isothianaphtene consists of fused thiophene and benzene rings. When the thiophene ring adopts the quinoid configuration, the benzene ring returns to the aromatic form, which is energetically more favorable due to the resonance energy. In the quinoid structure, the bond-length alternation ( $E_{BLA}$ ) is reduced and the electrons are less confined in the aromatic parts ( $E_{Res}$ ). Furthermore, the new  $\pi$ -bonds between the subunits force planarity of the whole backbone ( $E_{\theta}$ ).

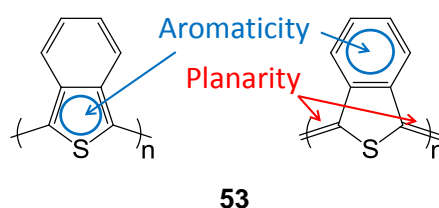


Figure 1 - 31: Aromatic (left) and quinoid (right) forms of poly(isothianaphtene).

Poly(thieno[3,4-*b*]pyrazine) **54** and poly(thieno[3,4-*b*]thiophene) **55**, possessing optical band-gaps of ca. 1 eV and 0.8 eV, respectively, are others examples of homopolymers based on the same concept (see Figure 1 - 32).<sup>[69-70]</sup>

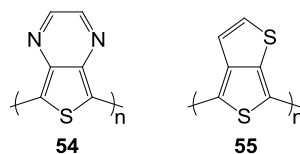
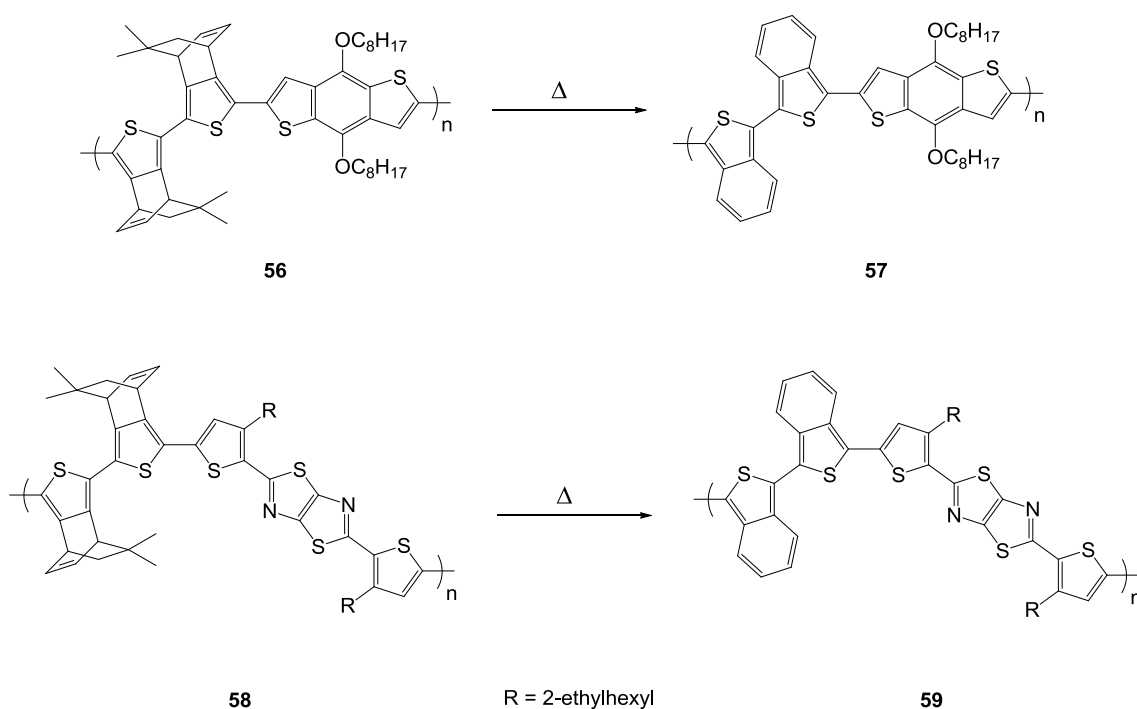


Figure 1 - 32: Poly(thieno[3,4-*b*]pyrazine) and poly(thieno[3,4-*b*]thiophene).<sup>[69-70]</sup>

However, the peculiar structure of monomers like isothianaphtene makes it particularly unstable. To address this problem, Imahori et al. synthesized precursor polymers which were then thermally converted to form the isothianaphtene units in situ (see Figure 1 - 33).<sup>[71-72]</sup> The final polymers showed strongly reduced band-gaps, assessing the formation of units favoring the quinoid structure in the conjugated backbone.

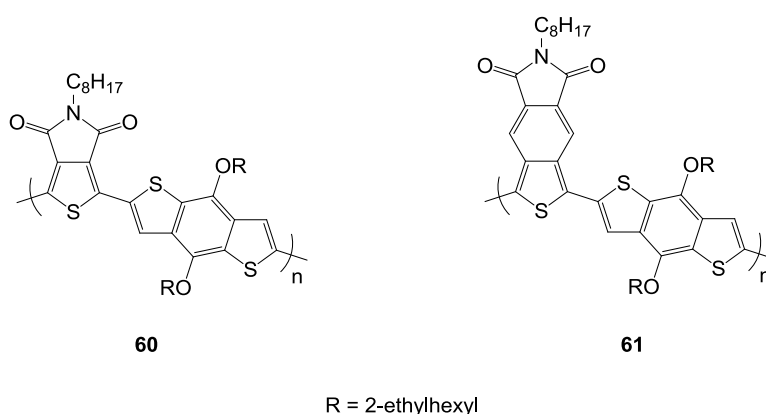




Polymer	Optical band-gap (eV)
<b>56</b>	2.4
<b>57</b>	1.3
<b>58</b>	2.1
<b>59</b>	1.3

Figure 1 - 33: Isothianaphene-based CPs obtained by polymeric precursors.<sup>[71-72]</sup>

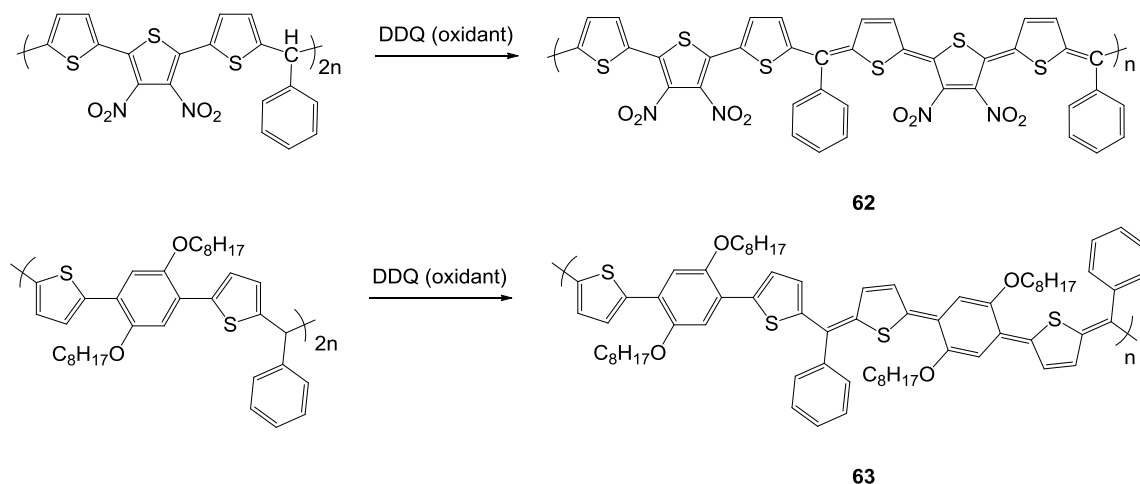
The quinoid stabilization influence is also observed in CPs based on thienopyrroledione (TPD) **60** and thienoisindole-1,1-dione (TID) **61**.<sup>[73]</sup> Although the two units show similarities, the fused benzene ring in the TID moiety acts in the same way as for the isothianaphene unit, therefore leading to a material with smaller band-gap, as depicted in Figure 1 - 34.



Polymer	Optical band-gap (eV)
<b>60</b>	1.8
<b>61</b>	1.4

Figure 1 - 34: TPD (1) and TID (2)-based CPs.<sup>[73]</sup>

Alternatively, quinoid conformation can be forced by dehydrogenation reactions as reported by Zhang et al. (see Figure 1 - 35).<sup>[74-76]</sup> This method is efficient to produce small band-gap polymers, however its limitation lies in creation of defects resulting from incomplete elimination reactions.



Polymer	Optical band-gap (eV)
62	1.5
63	1.1

Figure 1 - 35: Quinoid conformation of CPs obtained by elimination reaction.<sup>[74-76]</sup>

Stabilization of the quinoid conformation has proved to be a very efficient way to reduce the band-gap. The quinoid stabilizing units can also be formed in situ from polymeric precursors. Nevertheless, quinoid character is higher in energy and therefore usually leads to instability of the material.

## 1.2.4 DONOR-ACCEPTOR ALTERNATION EFFECT

Alternation of subunits having electron-withdrawing and -donating features is another efficient way of decreasing the band-gap of CPs. A unit is considered as electron-donating when its HOMO level is high-lying related to its electron-withdrawing counterpart. Reversely, an electron-withdrawing unit has a low-lying LUMO level. If the HOMO level of the donor moiety and the LUMO level of the acceptor moiety are close in energy, then the resulting polymer will have a small band-gap (see Figure 1 - 36).

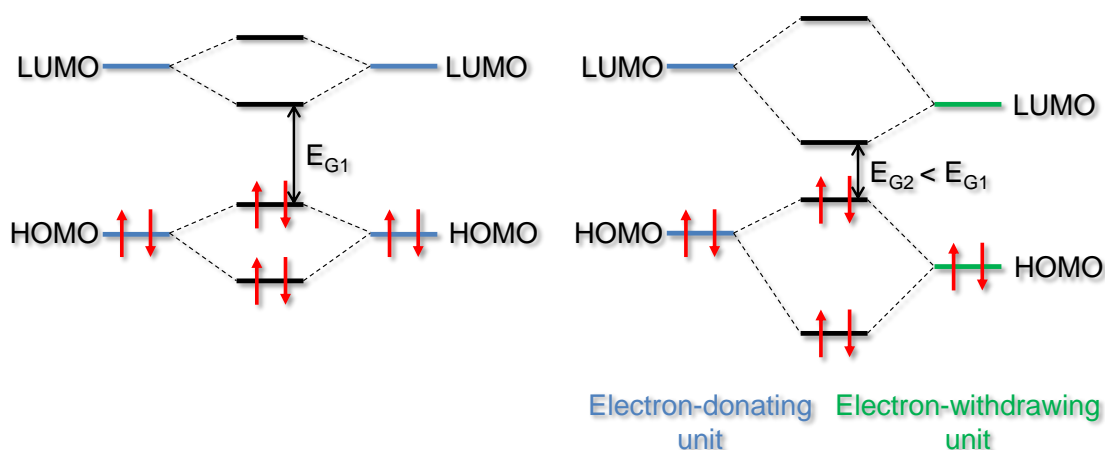


Figure 1 - 36: Orbital interactions in the case of two identical coupled units (left) and two different units (right).

This effect also includes an intramolecular charge transfer (ICT) between the alternating units, and hence the double bond character between the two moieties is increased and the  $E_{BLA}$  contribution affected.<sup>[9]</sup> As depicted in Figure 1 - 37, the enhanced double-bond conformation is responsible for a more planar structure and therefore a smaller band-gap.

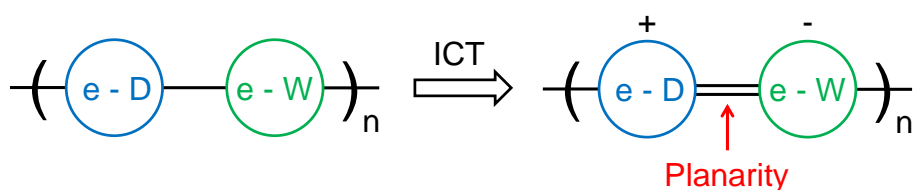


Figure 1 - 37: Geometric influence of the ICT between electron-donating (e-D) and withdrawing (e-W) units.

Such molecular design was firstly reported by Havinga et al. in 1992 who prepared polymers based on squaric **64** and croconic **65** acid (see Figure 1 - 38) with band-gaps down to 0.5 eV.<sup>[77]</sup>

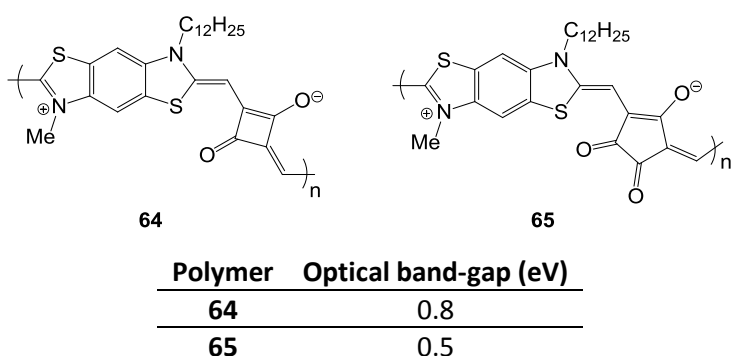


Figure 1 - 38: Small band-gap donor-acceptor polymers based on squaric (left) and croconic (right) acid.<sup>[77]</sup>

Benzothiadiazole (BT) is one of the most frequently used electron-withdrawing building block, and was extensively studied.<sup>[78-80]</sup> In order to avoid an extensive steric hindrance within the backbone, thiophene derivatives are the preferred candidates linked to BT.

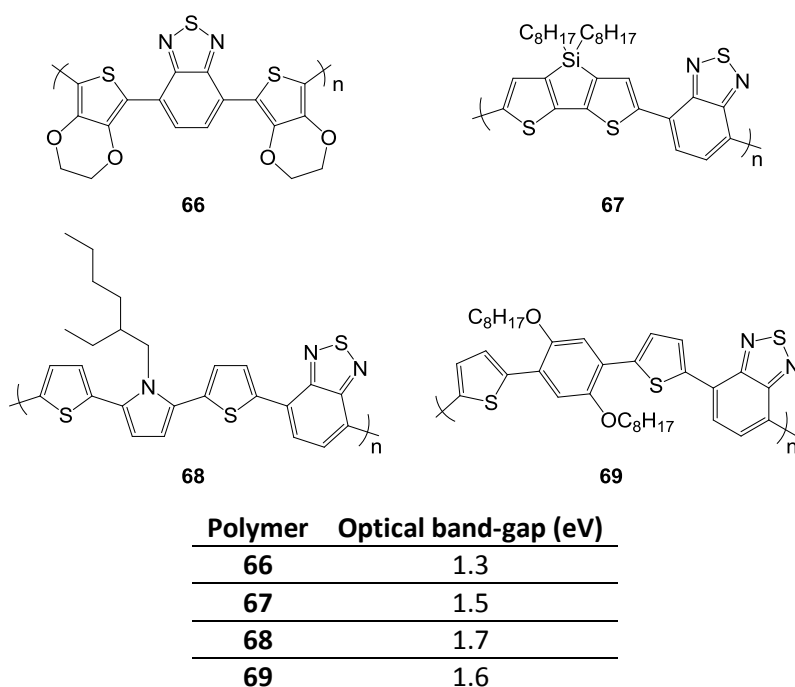


Figure 1 - 39: Alternated copolymers using benzothiadiazole as electron-withdrawing unit.<sup>[78-80]</sup>

The ratio and regular alternation of electron-donating and -withdrawing moieties is an important factor. As an example, Roncali et al developed an alternated copolymer based on 1:1 ratio of EDOT and thienopyrazine units showing a very low band-gap of 0.4 eV.<sup>[81]</sup> However, with ratio of EDOT increased to 2:1, the band-gap of the resulting polymer raised to 1.1 eV (see Figure 1 - 40).<sup>[21]</sup>

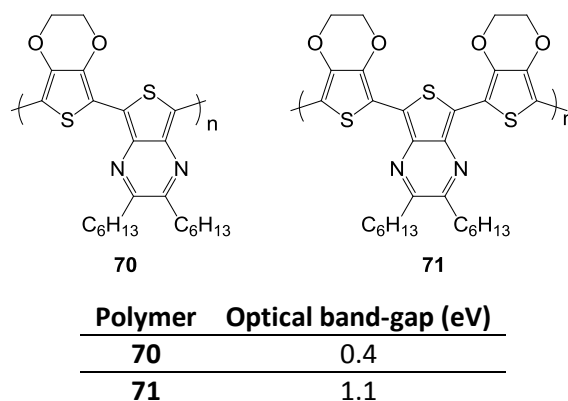
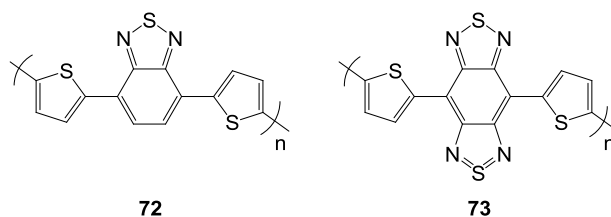


Figure 1 - 40: Effect of the D-A ratio on the band-gap.<sup>[21, 81]</sup>

The strength of the donor-acceptor interaction related to the energetic difference between the associated molecular orbitals strongly influences the band-gap variation. Yamashita et al. investigated the effect of different electron acceptors surrounded by two thiophenes within the polymer chain.<sup>[82]</sup> By replacing the BT with more strongly electron-withdrawing benzobis(1,2,5-thiadiazole) a decrease of 0.6 eV in the band-gap was observed (see Figure 1 - 41). The latter forms more stable quinoidal structure. However, the insolubility of electrochemically prepared polymers 13 and 14 and similar is a major drawback restricting their processing, and thus diminishing the amount of possible applications.



Polymer	Optical band-gap (eV)
<b>72</b>	1.1
<b>73</b>	0.5

Figure 1 - 41: Effect of acceptor strength on the band-gap.<sup>[82]</sup>

Meijer et al. developed an attractive method to decrease the band-gap of a CP containing alternating pyrrole and BT units with enhanced solubility.<sup>[83]</sup> They synthesized a soluble polymer bearing Boc protecting group on the pyrrole cores. A subsequent removal of the Boc groups obtained via heating of the precursor yielded a polymer containing intramolecular hydrogen bonds (**74**), thus forcing planarization and leading to a band-gap of 1.2 eV (see Figure 1 - 42).

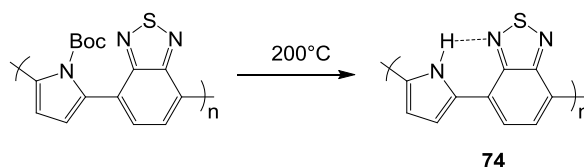


Figure 1 - 42: Generation of hydrogen-bonding in a donor-acceptor CP.<sup>[83]</sup>

## 1.2.5 RECENT TRENDS IN THE DESIGN OF ALTERNATED CONJUGATED POLYMERS

In the past decade, the development of novel polymers for application in photovoltaics has attracted much attention.<sup>[84-85]</sup> The great majority of recently developed materials are based on a donor-acceptor alternated structure. Therefore, a variety of combinations containing different building blocks was investigated.

Amongst the wide variety of subunits considered as donor fluorene,<sup>[8]</sup> thiophene,<sup>[86]</sup> cyclopentadithiophene,<sup>[9]</sup> benzo[1,2-b:4,5-b']dithiophene<sup>[54]</sup> (BDT) and their derivatives are the most commonly employed in alternated semiconducting polymers.

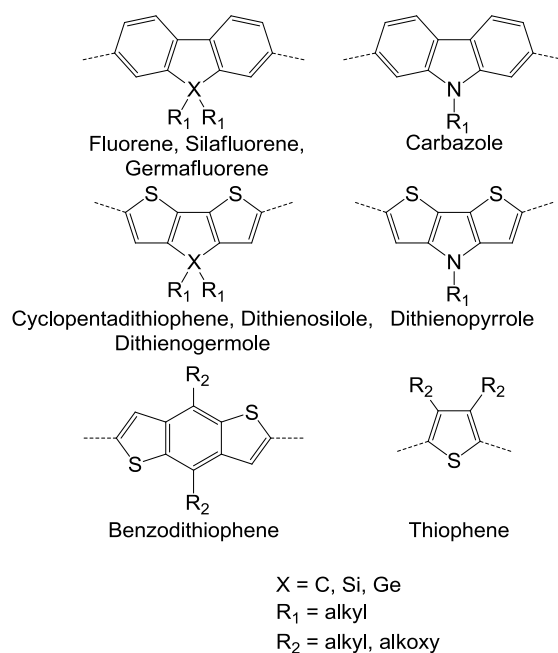


Figure 1 - 43: Commonly used electron-donating units in alternated CPs.<sup>[8-9, 54, 86]</sup>

Similarly, there is also a broad choice of electron-accepting units. Leclerc et al. developed a polymer based on carbazole and DTBT (PCDTBT **75**, see Figure 1 - 44)<sup>[87]</sup> which proved to be very efficient in photovoltaic applications.<sup>[88]</sup> The band-gap of PCDTBT is only 0.1 eV smaller than the one of P3HT, but its energetic levels are suitably modified, hence leading to a higher open-circuit voltage of the device.

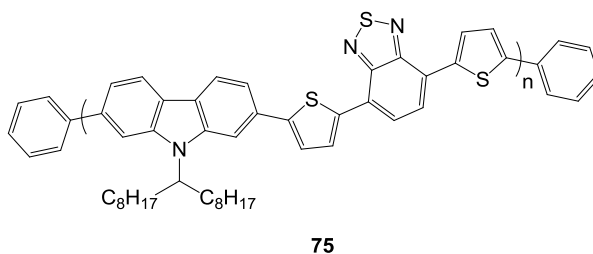
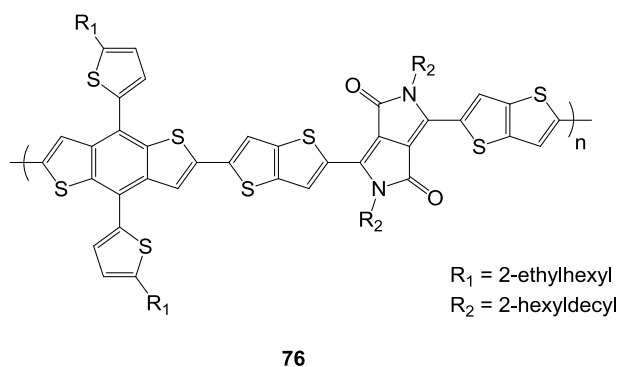


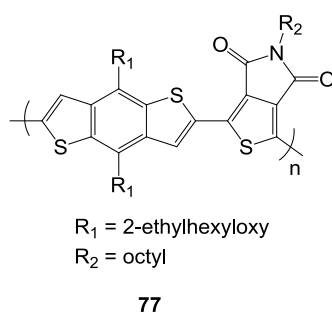
Figure 1 - 44: PCDTBT.<sup>[87]</sup>

Diketopyrrolopyrrole (DPP) represents another suitable example of acceptor. It has low-lying HOMO and LUMO and enhanced planarity, which leads to good charge transport properties.<sup>[89]</sup> Furthermore, the two nitrogen atoms in the pyrrole units offer free positions for functionalization and potential attachment of solubilizing groups. Alternated copolymers containing DPP (**76**, see Figure 1 - 45) were successfully employed as active layers of BHJ solar cells<sup>[90]</sup> and in ambipolar FET.<sup>[91]</sup>



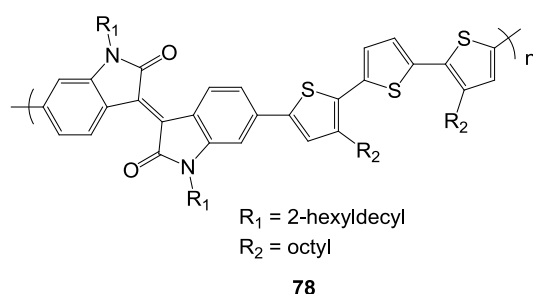
**Figure 1 - 45: PBDPP-3, a DPP-based polymer showing high PCE in BHJ solar cells.<sup>[90]</sup>**

Thienopyrroledione (TPD) was also recently studied in plastic electronics applications. A polymer composed of BDT and TPD units (PBDTPD **77**, see Figure 1 - 46) was simultaneously developed and investigated in photovoltaic devices by the research groups of Fréchet<sup>[92]</sup> and Leclerc.<sup>[93]</sup> Since then, many other materials containing TPD have been applied in solar cell devices reaching PCEs above 7 %.<sup>[94-95]</sup>



**Figure 1 - 46: PBDTPD.<sup>[92-93]</sup>**

Recently, polymers with small band-gap and low-lying energetic levels were achieved via incorporation of the isoindigo unit.<sup>[96]</sup> Similarly as in case of DPP, its planarity enhances short-circuit current and PCE in solar cells (PTI-3 **78**, see Figure 1 - 47).<sup>[97]</sup> Replacement of the benzene rings by thiophene led to improvement of hole mobilities in OFETs.<sup>[98]</sup>



**Figure 1 - 47: PTI-3, an isoindigo-based polymer used in BHJ solar cells with PCE of 6.3%.<sup>[97]</sup>**

Moreover, stronger accepting properties can be obtained by exploiting the substituent effect described earlier. For instance, Yu et al. synthesized a CP based on BDT and thieno[3,4-*b*]thiophene

(PTB7 **79**, see Figure 1 - 48) in which the latter unit bears a fluorine and an ester group with strong electron-withdrawing character.<sup>[99]</sup> In combination with the stabilized quinoid form of thienothiophene, a small band-gap polymer (around 1.7 eV) with good photovoltaic properties (PCE above 7 %) was achieved.

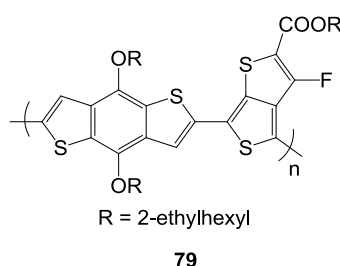


Figure 1 - 48: PTB7.<sup>[99]</sup>

## 1.3 SYNTHESIS OF SEMICONDUCTING POLYMERS

### 1.3.1 EVOLUTION OF SYNTHETIC ROUTES FOR CONJUGATED POLYMERS

Since the discovery of polyacetylene's conductivity, huge interest in other semiconducting polymers has given rise to a large development of new and versatile synthetic methods. The first polyacetylene used in the pioneering work of Heeger<sup>[6]</sup> et al. was synthesized via a Ziegler-Natta polymerization of acetylene, which was previously developed by Shirakawa and co-workers.<sup>[100]</sup> An alternative route is the Durham route<sup>[101]</sup>, in which a polymeric precursor is obtained by ring opening metathesis polymerization (ROMP), and then heated to achieve the desired polyacetylene (see Figure 1 - 49). This method benefits from the ease of processability of the polymeric precursor, although possible incomplete conversion under heating can cause defects in the conjugation.

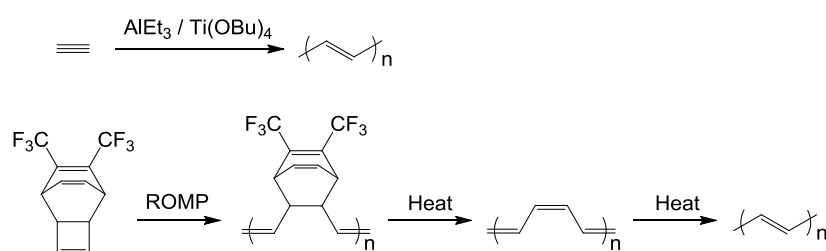


Figure 1 - 49: Ziegler-Natta (top) and Durham (bottom) routes to polyacetylene.<sup>[100-101]</sup>

Oxidative polymerization is a straightforward method for preparation of semiconducting polymers. For instance, PPP can be synthesized from benzene via Friedel-Crafts mechanism (see Figure 1 - 50).<sup>[22]</sup> This kind of polymerization can also be performed electrochemically, which was widely studied most frequently on thiophene derivatives.<sup>[58, 62, 102-103]</sup>



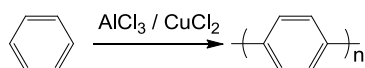


Figure 1 - 50: PPP obtained by oxidative polymerization of benzene.<sup>[22]</sup>

A convenient route for the synthesis of PPV is the Gilch method presented in Figure 1 - 51.<sup>[104]</sup> However, the resulting polymers usually suffer from incomplete conjugation. A significant improvement can be gained by adopting the Wessling-Zimmermann method starting from a sulfonium precursor.<sup>[105]</sup> The reaction is carried out in milder conditions, leading to well defined product with less defects.

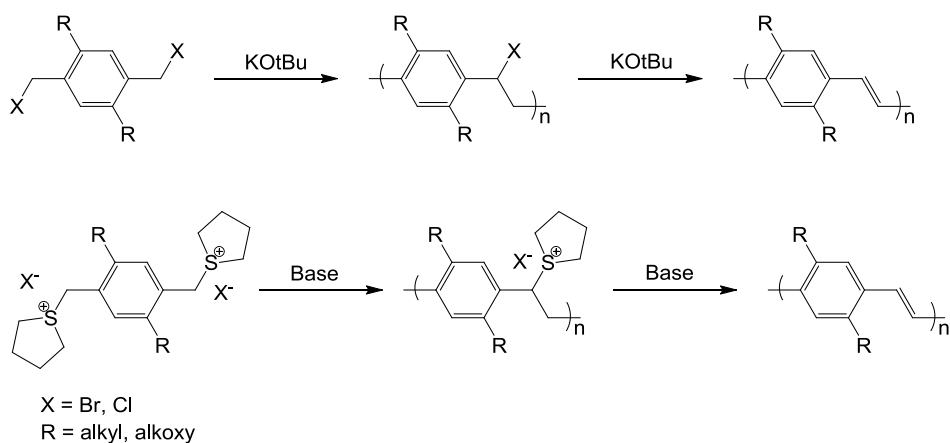
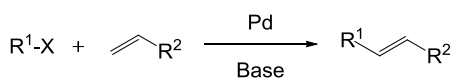
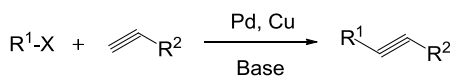


Figure 1 - 51: Gilch (top) and Wessling-Zimmermann (bottom) routes to PPV.<sup>[104-105]</sup>

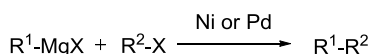
Nowadays, polycondensations involving metal-catalyzed couplings are the most commonly employed reactions (see Figure 1 - 52).

**Heck**

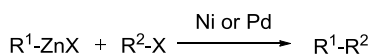
X = halide, triflate

R<sup>1</sup> = aryl, vinylR<sup>2</sup> = alkyl, alkenyl, alkynyl, aryl**Sonogashira**

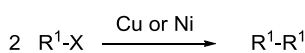
X = halide, triflate

R<sup>1</sup> = aryl, vinylR<sup>2</sup> = alkyl, alkenyl, alkynyl, aryl**Kumada**

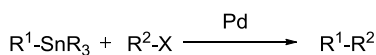
X = halide, triflate

R<sup>1</sup> = alkyl, alkenyl, arylR<sup>2</sup> = alkenyl, aryl**Negishi**

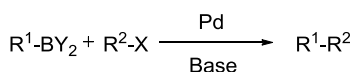
X = halide, triflate

R<sup>1</sup> = alkyl, alkenyl, alkynyl, arylR<sup>2</sup> = alkenyl, aryl**Ullmann (Yamamoto)**

X = halide

R<sup>1</sup> = aryl**Stille**

X = halide, triflate

R<sup>1</sup> = alkyl, alkenyl, alkynyl, arylR<sup>2</sup> = alkenyl, aryl**Suzuki**

X = halide, triflate

Y = -OH, -OR, -R

R<sup>1</sup> = alkyl, alkenyl, alkynyl, arylR<sup>2</sup> = alkyl, alkenyl, alkynyl, aryl**Figure 1 - 52: Examples of metal-catalyzed couplings used in CPs synthesis.**

Polycondensations via the Heck<sup>[106]</sup> or the Sonogashira<sup>[107]</sup> reactions are limited to the synthesis of poly(arylene-vinylene) and poly(arylene-ethynylene), respectively. On the contrary, homocoupling between heteroaromatic units can be achieved via the Ullmann<sup>[108]</sup> reaction. Yamamoto et al. applied that reaction to the nickel-catalyzed coupling of dihalogenated aryl, thus yielding conjugated polymers.<sup>[109]</sup> The main disadvantages are the requirement of a large amount of metal catalyst and the statistical irregularity of the resulting polymer when copolymerizing two different monomers.

A significant improvement was achieved via nickel-catalyzed transformations developed by Kumada<sup>[110]</sup> and Negishi<sup>[111]</sup> using organomagnesium and organozinc as starting materials, respectively. An extensive effort was invested into the development of reliable methods yielding regioregular polymers. The most suitable reaction to achieve highly regioregular poly(3-alkylthiophenes) and its derivatives proved to be Grignard Metathesis (GRIM).<sup>[112]</sup> GRIM polymerization was highlighted by two different research groups in the late 1990s: Yokozawa<sup>[113-114]</sup> et al. and McCullough<sup>[115-116]</sup> et al. McCullough proposed the name "GRIM" for the first time in 2001.<sup>[117]</sup>

The GRIM polymerization is of great interest due to its quasi-living character, and is widely used in macromolecular engineering such as conjugated block copolymers synthesis.<sup>[118-119]</sup> However, a major drawback lies in the inability to obtain a regularly alternated CP. For that purpose the Stille<sup>[120]</sup> and Suzuki<sup>[121]</sup> polycondensations are the preferred choice.

There is a vast amount of synthetic strategies for preparation of CPs and it is out of the scope of this thesis to discuss them all in detail. Only the most relevant and exploited methods for this project are highlighted.

### 1.3.2 STILLE POLYCONDENSATION

The Stille reaction is based on the Pd(0)-mediated cross-coupling of organostannanes with organohalides, triflates or acyl chlorides. This reaction provides an efficient coupling of  $sp^2$  carbons in relatively mild conditions, with a broad choice of solvents, and is tolerant to functional groups. Even though early work showed evidence of such a coupling,<sup>[122-123]</sup> the discovery was attributed to and named after the work of John K. Stille in 1978.<sup>[124]</sup>

The mechanism of Stille coupling includes three main steps, as depicted in Figure 1 - 53. At first, an oxidative addition of the organohalide (or triflate) on the Pd(0) active catalyst forms the Pd(II) intermediate  $[Pd(II)L_nR^1X]$  ( $L$  = ligand). Subsequently, the transmetalation step takes place, in which the Sn-C bond in the organostannane is cleaved and the intermediate is converted to  $[Pd(II)L_nR^1R^2]$ . In the last step, the desired product is achieved via reductive elimination and the Pd(0) catalyst is regenerated.

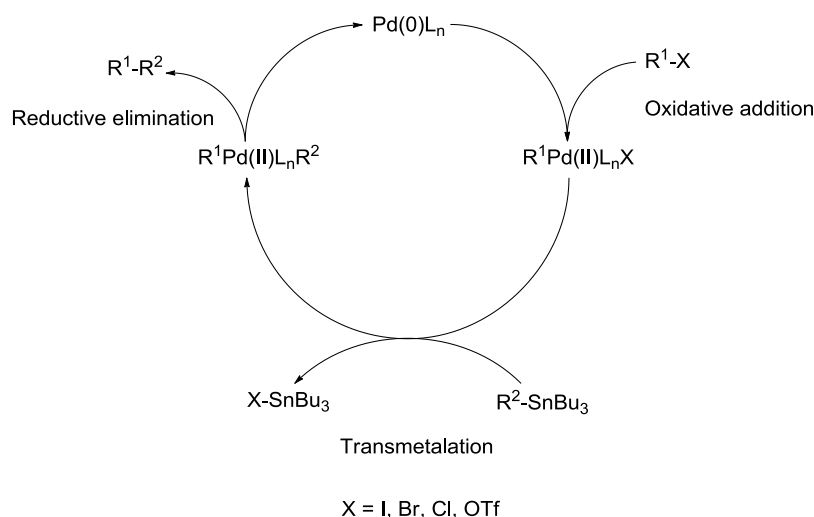


Figure 1 - 53: General mechanism of Stille coupling.<sup>[120]</sup>

Tetrakis(triphenylphosphine)palladium(0)  $Pd(PPh_3)_4$  is the most frequently used catalytic system for the Stille polycondensation, but some other well-known examples of Pd(0) and Pd(II)-based systems

can also be found in the literature.<sup>[125]</sup> If Pd(II) is used, an additional preliminary step takes place where the Pd(II) catalytic system undergoes a reduction to Pd(0) by the organostannane. The choice of the catalytic system and more generally of the reaction conditions depends largely on the nature of the selected monomers and often requires an optimization work.

The use of Stille coupling in CPs synthesis was first reported in the late 1980s<sup>[126]</sup>, and further investigated and optimized few years later by Yu and co-workers.<sup>[127]</sup> Since then, Stille polycondensation has become a reaction of choice for the synthesis of numerous polymeric semiconductors in the field of organic electronics.<sup>[120]</sup> For example, the PBDPP-3 polymer **76** developed by Hou et al. was synthesized by a this method performed in toluene and using Pd(PPh<sub>3</sub>)<sub>4</sub> as a catalyst.<sup>[90]</sup> The resulting polymer showed a number-average molecular weight ( $M_n$ ) of 21 kg/mol, with a dispersity of 2.3, which is a consistent value for polycondensations.

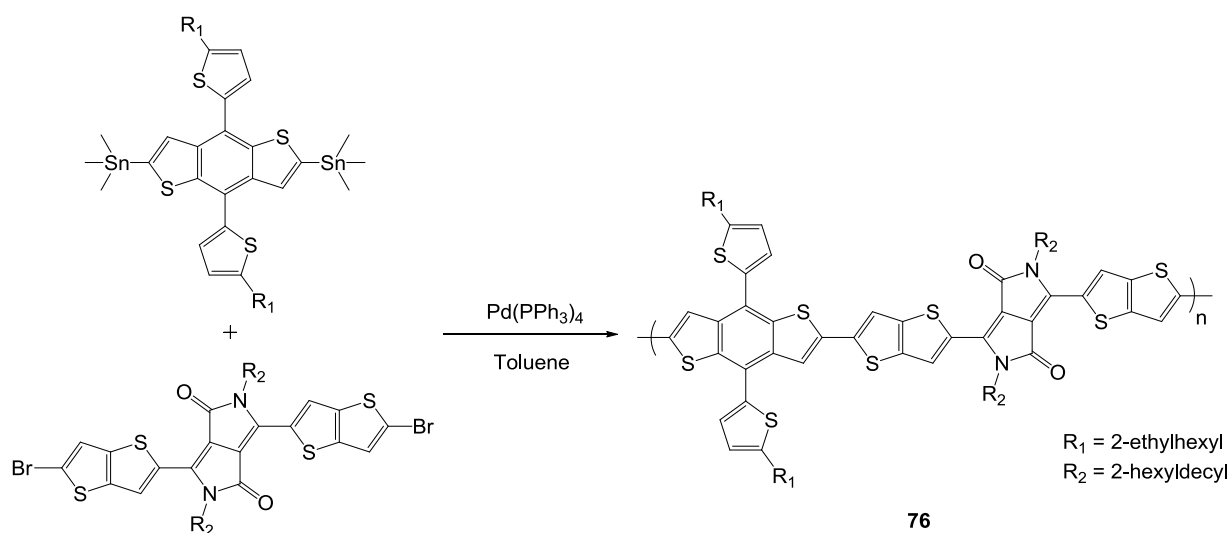


Figure 1 - 54: Synthesis of PBDPP-3 by Stille polycondensation.<sup>[90]</sup>

The main drawback of this synthesis originates from undesirable properties of the organostannane monomers. They can be toxic, difficult to purify and poorly stable over time in ambient conditions. Cross-coupling polycondensations are extremely sensitive to the stoichiometric ratio of monomers, which can be a main issue in the preparation of high molecular weight polymers.

### 1.3.3 SUZUKI POLYCONDENSATION

In 1979, Akira Suzuki and co-workers reported a new palladium-catalyzed cross-coupling between alkenyl organoboranes and aryl or alkenyl halides and triflates in the presence of a base.<sup>[128-129]</sup> This discovery gave rise to a huge development in synthetic chemistry, due to which Suzuki received the 2010 Nobel prize in chemistry,<sup>[130]</sup> jointly with Richard F. Heck and Ei-ichi Negishi. The main

advantage of this reaction compared to the Stille coupling is the better stability of organoboranes, simplifying their synthesis, purification and handling.

Similarly to the Stille coupling, the Suzuki condensation mechanism involves an oxidative addition followed by a transmetalation and the product is obtained via a reductive elimination in the final step. The transmetalation including the organoborane is usually slow, therefore a base is added to accelerate it. Two main mechanisms are proposed for this step (see Figure 1 - 55).<sup>[131-132]</sup> Firstly, the base reacts with the organoborane to form a more reactive boronate which will then transmetalate with the Pd(II) intermediate  $[Pd(II)L_nR^1X]$  (path 1). The second mechanism involves a preliminary exchange of halide or triflate anion in the coordination sphere of the Pd(II) complex with the base ( $[Pd(II)L_nR^1OR]$ ). Thus formed intermediate can subsequently facilitates the transmetalation step with the organoborane (path 2).

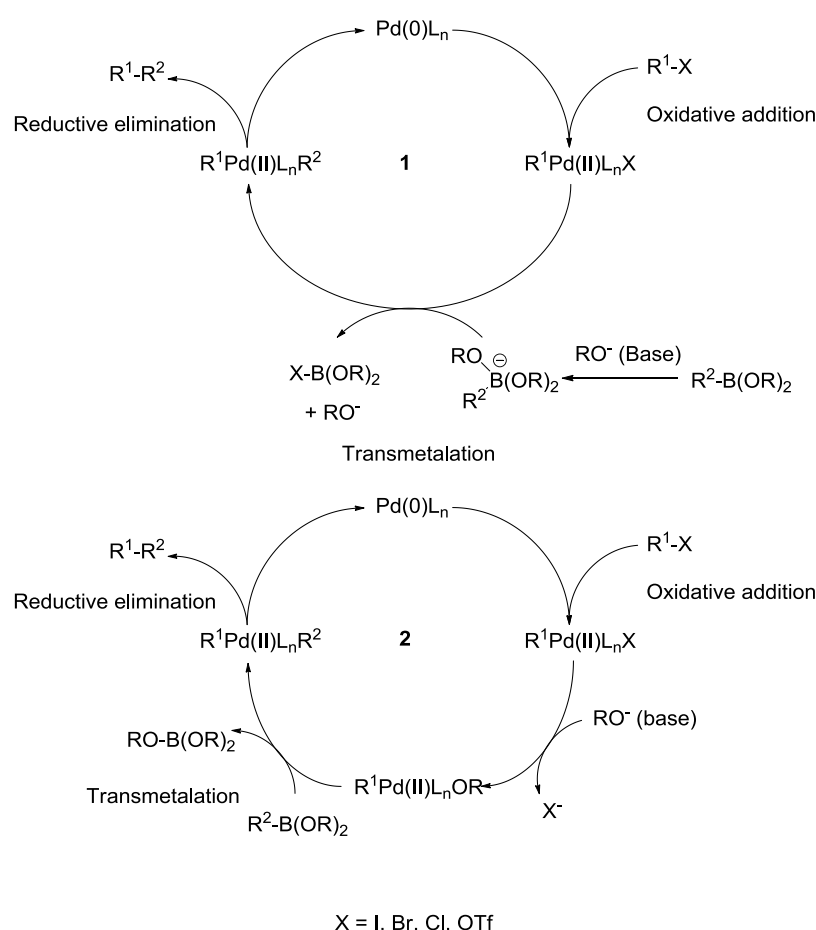


Figure 1 - 55: General mechanisms of Suzuki coupling.<sup>[133]</sup>

Most of the catalytic systems used in Stille coupling are also applicable in Suzuki coupling. However, the widely employed triarylphosphine ligands are too bulky and limit the approach of the reactants towards the catalyst. This is why new efficient ligands such as the dialkylbiarylphosphines developed by Buchwald et al.<sup>[133]</sup> are extensively sought after. The Suzuki coupling is usually performed in a

mixture of organic solvent and water, in order to dissolve the inorganic base. Therefore, phase-transfer agents (e.g. Aliquat 336) are commonly employed to facilitate transfer of the base to the organic phase. Potassium carbonate, sodium hydroxide and potassium fluoride are amongst the most commonly used alkalis. But the use of organosoluble bases such as potassium phosphate, which leads to a one-phase reaction mixture, was also reported.<sup>[133]</sup> The choice of the base for each particular reaction system remains to be rather empirical, since so far, no general rule has been established and further research has to be undertaken.

One of the first examples of Suzuki polycondensation was reported in 1989 by Wegner et al.<sup>[134]</sup> Since then, the ease of synthesis and purification of organoborane compounds have accelerated a further development of suitable monomers and corresponding novel polymers. It is noteworthy to quote a recent work reported by Leclerc et al. on PCDTBT **75**, which was obtained by Suzuki coupling with the  $\text{Pd}_2\text{dba}_3/\text{P}(\text{o-Tol})_3$  catalytic system.<sup>[87]</sup> Tetraethylammonium hydroxide ( $\text{Et}_4\text{NOH}$ ) was used as base and transfer agent. The number-average molecular weight of the resulting polymer was 37 kg/mol with a dispersity of 2.0.

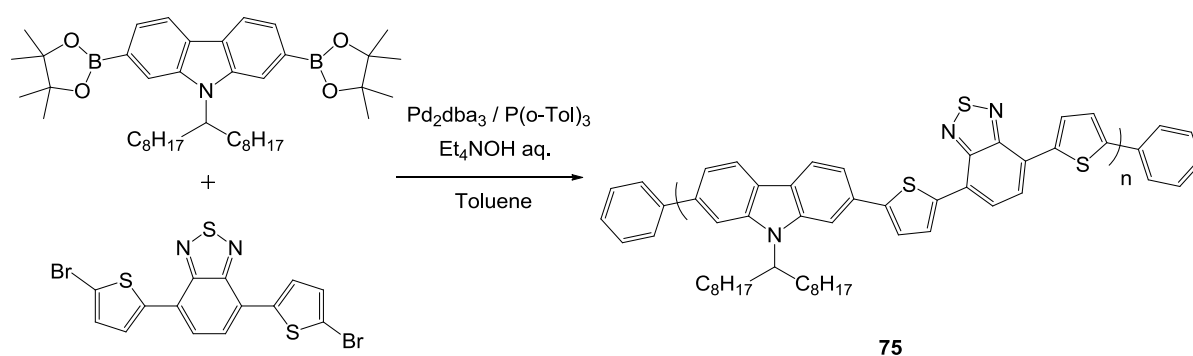


Figure 1 - 56: Synthesis of PCDTBT by Suzuki polycondensation.<sup>[87]</sup>

### 1.3.4 METAL-FREE REACTIONS APPLIED TO CONJUGATED POLYMER SYNTHESIS

The use of metal catalyst is a major drawback of the previously mentioned polycondensations. Presence of impurities in materials dedicated to organic electronics applications is highly undesirable especially when the semiconducting polymer has to remain in its neutral state. Traces of transition metal in the material can dope the semiconductor and also act as charge traps and reduce dramatically the charge carrier mobility. Therefore, synthesis of semiconducting polymers is often followed by long purification techniques, which can have serious economic and environmental impact. A special attention is therefore focused on the development of suitable metal-free reactions.

Knoevenagel condensation is an efficient route towards semiconducting polymers bearing electron-withdrawing substituents. The most common example is the synthesis of poly(arylenevinylene) with

cyano groups, as illustrated in Figure 1 - 57. Holmes et al. synthesized a series of PPV and PTV with number-average molecular weights up to 7.2 kg/mol with a dispersity of 1.6 for the PPV.<sup>[135]</sup> The main advantages of such synthesis include very mild conditions of the reaction, and also fast kinetic (some polymers were obtained in less than 20 minutes). On the other hand, side-reactions like Michael addition between the double bonds of the final product and the nucleophilic reactant can occur, thus creating defects in the backbone. Such materials bearing cyano functions are of interest for applications employing n-type semiconductors.

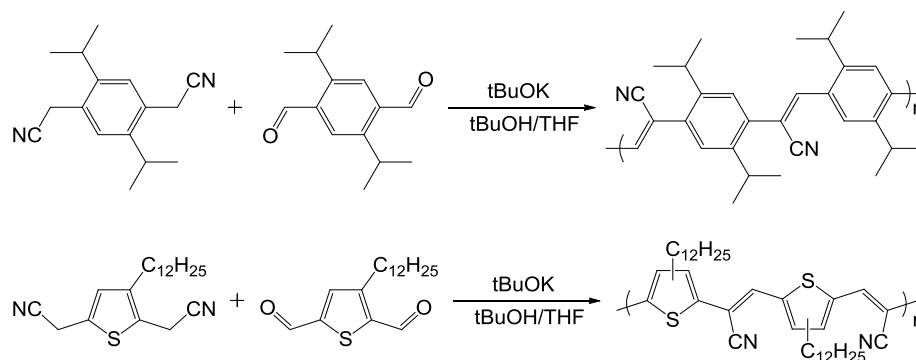


Figure 1 - 57: Examples of CPs synthesized via Knoevenagel condensation.<sup>[135]</sup>

The Siegrist condensation<sup>[136]</sup> is an alternative route towards poly(arylenevinylene). Its use in PPV synthesis was first reported by Meier et al. in 1991.<sup>[137]</sup> A special feature of this synthesis is the monofunctionalization of the polymer chain-end with aldehyde groups, which offer the opportunity for further modifications much desired in macromolecular engineering.<sup>[138]</sup>

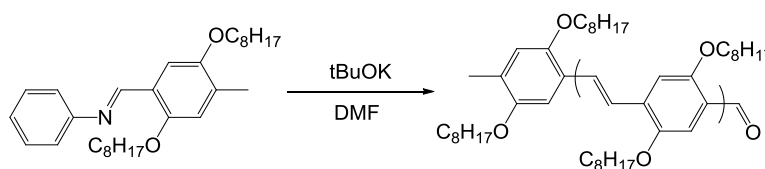


Figure 1 - 58: PPV synthesis by Siegrist polycondensation.<sup>[138]</sup>

Formation of carbon-carbon double bonds via the Wittig reaction was also widely employed in CPs synthesis.<sup>[139-141]</sup> Recently, the aza-Wittig reaction was also applied,<sup>[142]</sup> affording macromolecules containing carbon-nitrogen double bonds (so-called imine). However, broader use of such polymerizations can be limited by the instability of the phosphonium ylides and azide monomers required in Wittig and aza-Wittig polycondensations, respectively.

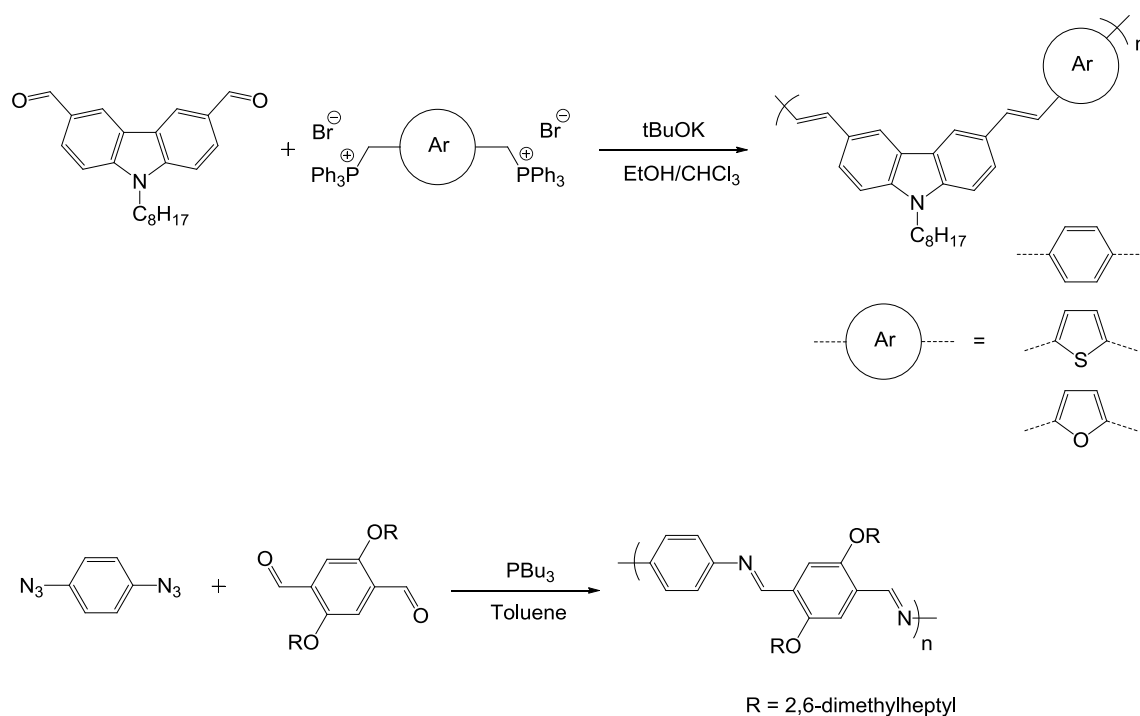


Figure 1 - 59: Examples of Wittig (top) and aza-Wittig (bottom) polycondensations.<sup>[139-142]</sup>

Imine can also be prepared by arylimino-de-oxo-bisubstitution,<sup>[143]</sup> which corresponds to the condensation of primary amines with ketones or aldehydes. Jenekhe et al. reported that this could be exploited in the synthesis of PPV analogues at room temperature, if a drying agent ( $\text{LiCl}$ ) to remove the formed water would be used.<sup>[144]</sup> Other subunits such as fluorene, thiophene,<sup>[145]</sup> selenophene<sup>[146]</sup> and their derivatives were also investigated. As illustrated in Figure 1 - 60, an acid can be used to catalyze the reaction, but it often enhances the formation of undesirable by-products.<sup>[146]</sup>

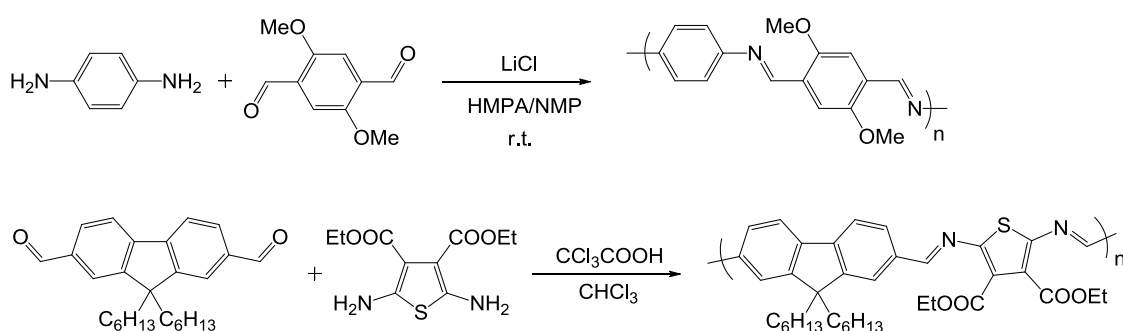


Figure 1 - 60: Examples of semiconducting polymers obtained by arylimino-de-oxo-bisubstitution.<sup>[144-145]</sup>

Squaraine derivatives are compounds of great interest because of their intense and red-shifted absorption and fluorescence.<sup>[147]</sup> They are formed by condensation of electron-rich molecules with squaric acid whilst water being the only by-product. This is a highly beneficial and desirable feature in modern chemical society, because of the growing demand on environmental friendly procedures. The yield of the reaction is usually improved by azeotropic removal of water and in some cases it can



also be base-catalyzed. This condensation can yield two different isomers: the 1,2- and the 1,3-condensation products (see Figure 1 - 61), but only the 1,3-isomer shows the particular light absorption and emission properties.<sup>[147]</sup> In general, the proportion of 1,2-isomer is negligible and can be even avoided by use of an appropriate solvent. Condensing difunctional electron-rich monomers with squaric acid leads to polymers bearing squaraine units in the main chain, as illustrated by the work of Havinga et al.<sup>[77]</sup>

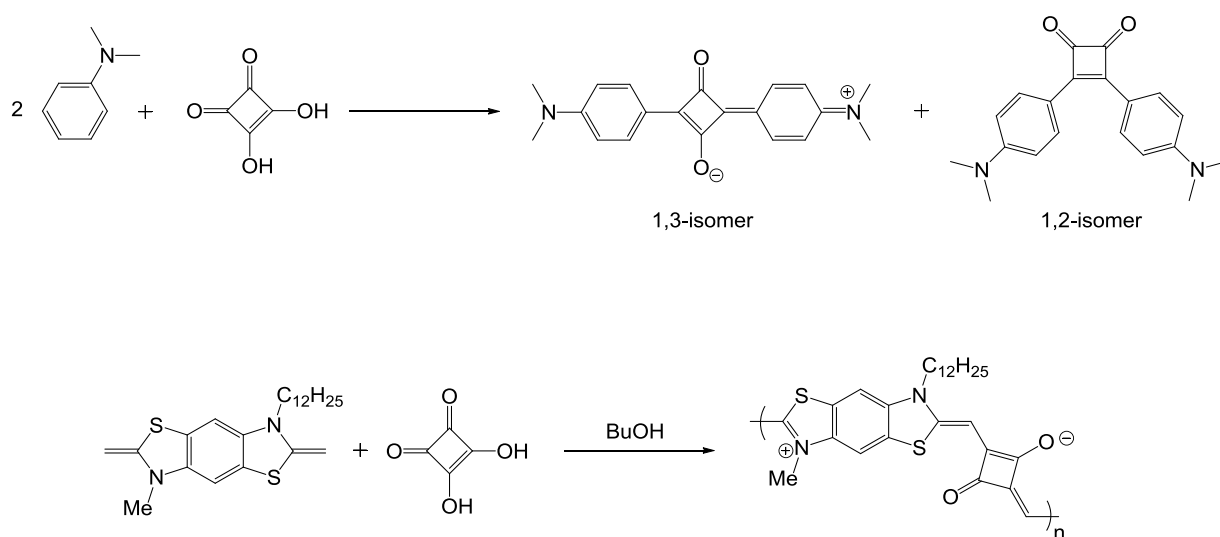


Figure 1 - 61: Synthesis of a well-known squaraine dye (top) and polysquaraine (bottom).<sup>[147]</sup>

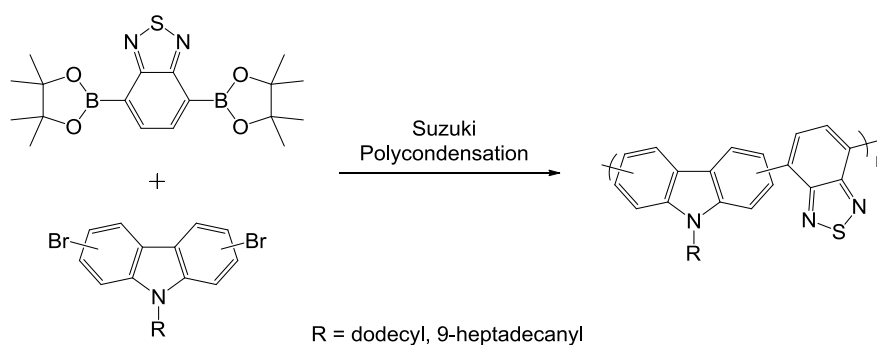
Organic chemistry offers a substantial amount of clever, powerful and metal-free techniques leading towards CPs. The by-products of these reactions are usually easy to remove from the mixture, which offers the possibility to shift the equilibrium towards the desired product and thus accelerate the whole process. In addition, their versatility, in many cases non-toxicity and simplicity of subsequent purification procedures makes them very attractive candidates for green chemistry. Nevertheless, contrary to the metal-based couplings they have been so far only rarely exploited in the synthesis of conjugated macromolecules.

## 1.4 AIM AND STRATEGY OF THE THESIS

The field of conjugated polymers and organic electronics has been studied for three decades, and the literature provides a wide catalogue of available materials with some evidence of how to tune their properties for specific targets. But the exact influence of small structural modifications on the backbone and the morphology of the resulting polymer has not been fully understood yet. Therefore it has to be always examined in each particular case whether their properties are in agreement with the expectations. The aim of this PhD work was to design, synthesize and characterize original

semiconducting polymers via several methodologies, including transition metal-free polycondensations.

The chapter 2 will describe the synthesis and characterizations of different carbazole-based monomers, as well as their polycondensation with functionalized benzothiadiazole monomers by Suzuki cross-coupling. The resulting polymers will bear different alkyl chains and will be linked in 2,7 or 3,6 positions. The relevant properties of the resulting polymers will be examined in order to identify the influence of the alkyl chain size and geometry as well as the position linkage on the carbazole units. A theoretical investigation on the energetic levels position and molecular geometry will be carried out and compared with experimental results.



**Figure 1 - 62: Synthesis of the poly(carbazole-*alt*-benzothiadiazole)s.**

Chapter 3 will report on the use of a functionalized donor-acceptor-donor squaraine dye as monomer in alternated CPs. It will be polymerized with thiophene and benzodithiophene organotin derivatives by Stille cross-coupling and with benzothiadiazole organoborane derivative by Suzuki cross-coupling. The resulting polymers will present an alternation of D-A-D moieties (squaraine) with other electron-donating (thiophene, benzodithiophene) or accepting (benzothiadiazole) units. Effect of this specific structure on the properties of the resulting materials will be investigated.

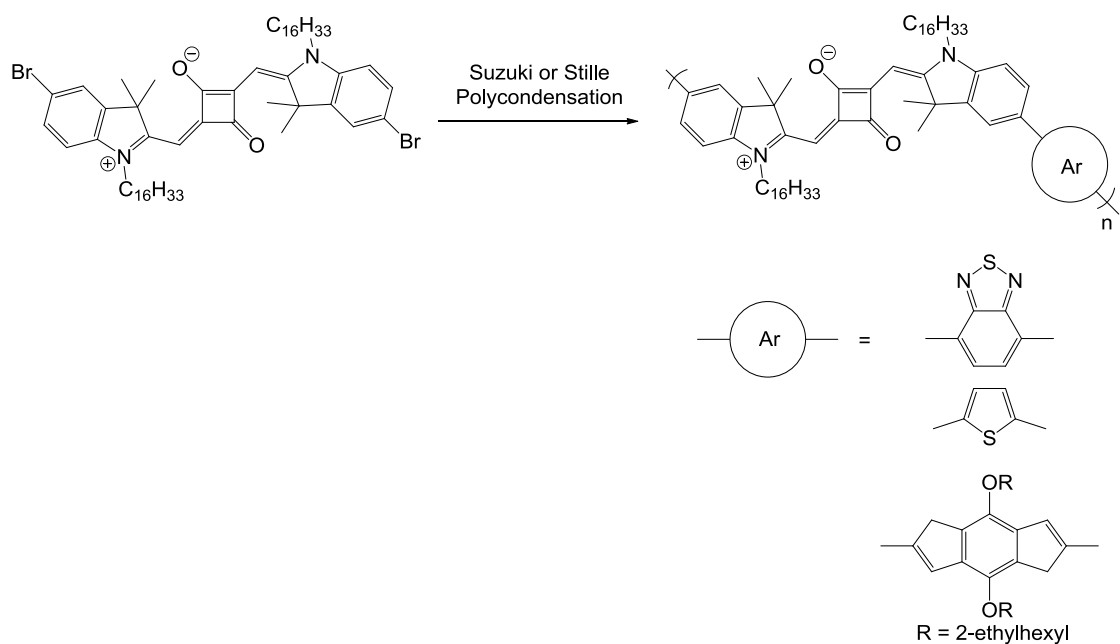
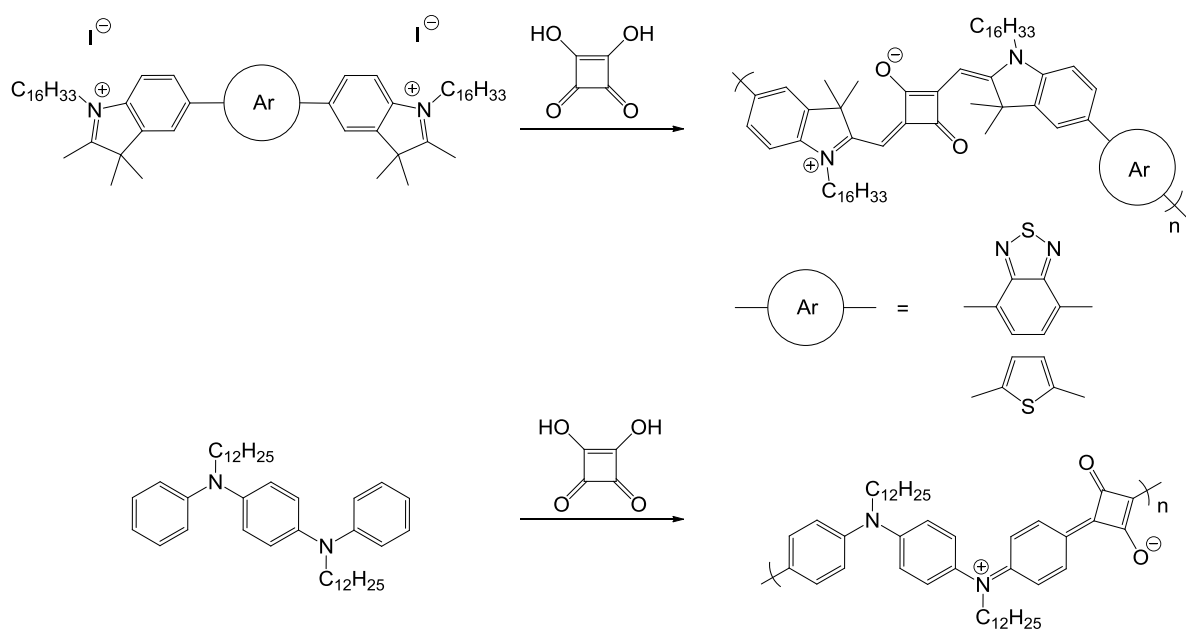


Figure 1 - 63: Synthesis of the different poly(squaraine)s.

Finally, the chapter 4 will describe the design, synthesis and characterization of functionalized monomers subsequently used in metal-free polycondensations. Firstly, difunctional monomers based on thiophene, benzothiadiazole and  $N^1, N^2$ -diphenylbenzene-1,4-diamine will be condensed with squaric acid. Properties of the resulting polymers will be characterized and compared with their analogues obtained by Stille or Suzuki coupling. Secondly, difunctional monomers based on EDOT and carbazole will be connected by arylimino-de-oxo-bisubstitution, and the properties of the resulting polymers will be determined.

### Polymerizations by squaric acid condensation



### Polymerizations by arylimino-de-oxo-bisubstitution

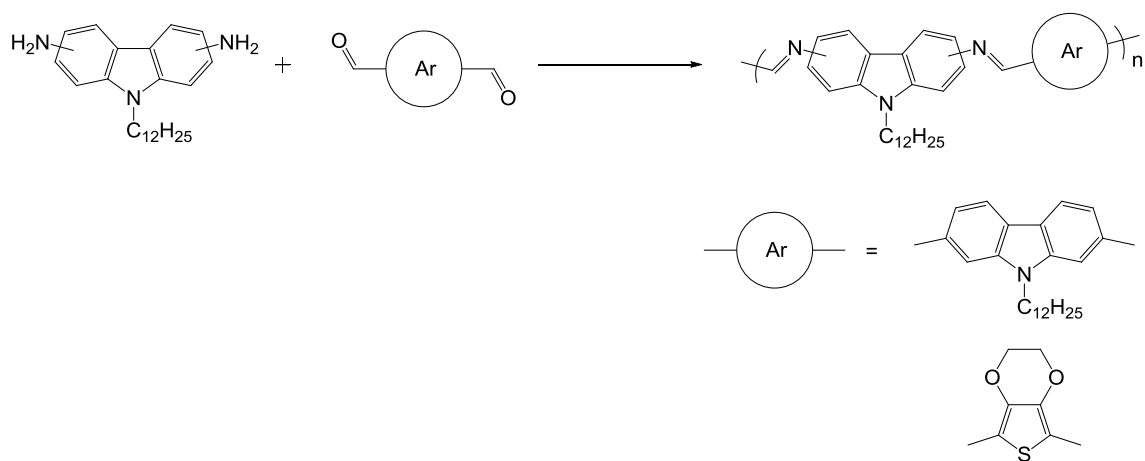


Figure 1 - 64: Metal-free syntheses of the developed CPs.

## 1.5 BIBLIOGRAPHY

- [1] M. Geoghegan, G. Hadzioannou, *Polymer Electronics*, OUP Oxford, **2013**.
- [2] M. Ates, *Materials Science and Engineering: C* **2013**, 33, 1853-1859.
- [3] R. A. Serway, J. W. Jewett, *Principles of Physics, 5th ed*, BROOKS COLE Publishing Company, **2012**.
- [4] A.-J. Attias, *Techniques de l'ingénieur Matériaux pour l'électronique et dispositifs associés* **2002**, base documentaire : TIB271DUO.
- [5] C. Kittel, *Introduction to Solid State Physics*, Wiley, **2005**.
- [6] C. K. Chiang, C. R. Fincher, Jr., Y. W. Park, A. J. Heeger, H. Shirakawa, E. J. Louis, S. C. Gau, A. G. MacDiarmid, *Physical Review Letters* **1977**, 39, 1098-1101.
- [7] A. J. Heeger, N. S. Sariciftci, E. B. Namdas, *Semiconducting and Metallic Polymers*, OUP Oxford, **2010**.
- [8] L.-H. Xie, C.-R. Yin, W.-Y. Lai, Q.-L. Fan, W. Huang, *Progress in Polymer Science* **2012**, 37, 1192-1264.
- [9] C. L. Chochos, S. A. Choulis, *Progress in Polymer Science* **2011**, 36, 1326-1414.
- [10] L. Zhang, N. S. Colella, F. Liu, S. Trahan, J. K. Baral, H. H. Winter, S. C. B. Mannsfeld, A. L. Briseno, *Journal of the American Chemical Society* **2012**, 135, 844-854.
- [11] K. M. N. de Silva, E. Hwang, W. K. Serem, F. R. Fronczek, J. C. Garno, E. E. Nesterov, *ACS Applied Materials & Interfaces* **2012**, 4, 5430-5441.
- [12] B. P. Karsten, R. A. J. Janssen, *Macromolecular Chemistry and Physics* **2011**, 212, 515-520.
- [13] J. Roncali, *Chemical Reviews* **1997**, 97, 173-206.
- [14] W. P. Su, J. R. Schrieffer, A. J. Heeger, *Physical Review Letters* **1979**, 42, 1698-1701.
- [15] J. P. Lowe, S. A. Kafafi, *Journal of the American Chemical Society* **1984**, 106, 5837-5841.
- [16] J. L. Bredas, *The Journal of Chemical Physics* **1985**, 82, 3808-3811.
- [17] V. Hernandez, C. Castiglioni, M. Del Zoppo, G. Zerbi, *Physical Review B* **1994**, 50, 9815-9823.
- [18] P. M. Grant, I. P. Batra, *Solid State Communications* **1979**, 29, 225-229.
- [19] A. J. Heeger, *ChemInform* **2001**, 32, no-no.
- [20] A. C. Grimsdale, K. Müllen, *Macromolecular Rapid Communications* **2007**, 28, 1676-1702.
- [21] J. Roncali, *Macromolecular Rapid Communications* **2007**, 28, 1761-1775.
- [22] L. W. Shacklette, R. R. Chance, D. M. Ivory, G. G. Miller, R. H. Baughman, *Synthetic Metals* **1980**, 1, 307-320.
- [23] H. S. Nalwa, *Handbook of organic electronics and photonics*, American Scientific Pub., Stevenson Ranch, Calif., **2008**.
- [24] K.-Y. Jen, M. Maxfield, L. W. Shacklette, R. L. Elsenbaumer, *Journal of the Chemical Society, Chemical Communications* **1987**, 0, 309-311.
- [25] U. H. F. Bunz, *Chemical Reviews* **2000**, 100, 1605-1644.
- [26] B. Liu, W.-L. Yu, J. Pei, S.-Y. Liu, Y.-H. Lai, W. Huang, *Macromolecules* **2001**, 34, 7932-7940.
- [27] D. A. M. Egbe, C. Bader, E. Klemm, L. Ding, F. E. Karasz, U.-W. Grummt, E. Birkner, *Macromolecules* **2003**, 36, 9303-9312.
- [28] C.-C. Chueh, M.-H. Lai, J.-H. Tsai, C.-F. Wang, W.-C. Chen, *Journal of Polymer Science Part A: Polymer Chemistry* **2010**, 48, 74-81.
- [29] D. A. M. Egbe, B. Carbonnier, E. Birkner, U.-W. Grummt, *Progress in Polymer Science* **2009**, 34, 1023-1067.
- [30] P. Coppo, D. C. Cupertino, S. G. Yeates, M. L. Turner, *Macromolecules* **2003**, 36, 2705-2711.
- [31] P. L. T. Boudreault, A. Najari, M. Leclerc, *Chemistry of Materials* **2011**, 23, 456-469.
- [32] D. Neher, *Macromolecular Rapid Communications* **2001**, 22, 1365-1385.
- [33] S. Setayesh, D. Marsitzky, K. Müllen, *Macromolecules* **2000**, 33, 2016-2020.
- [34] A. K. Mishra, M. Graf, F. Grasse, J. Jacob, E. J. W. List, K. Müllen, *Chemistry of Materials* **2006**, 18, 2879-2885.
- [35] U. Scherf, K. Müllen, *Macromolecules* **1992**, 25, 3546-3548.
- [36] M. Forster, U. Scherf, *Macromolecular Rapid Communications* **2000**, 21, 810-813.
- [37] K. Chmil, U. Scherf, *Acta Polymerica* **1997**, 48, 208-211.
- [38] J. J. S. Lamba, J. M. Tour, *Journal of the American Chemical Society* **1994**, 116, 11723-11736.
- [39] J. M. Tour, J. J. S. Lamba, *Journal of the American Chemical Society* **1993**, 115, 4935-4936.
- [40] Y. Chen, W. Huang, C. Li, Z. Bo, *Macromolecules* **2010**, 43, 10216-10220.
- [41] Y. Yao, Q. T. Zhang, J. M. Tour, *Macromolecules* **1998**, 31, 8600-8606.
- [42] Y.-L. Chen, C.-Y. Chang, Y.-J. Cheng, C.-S. Hsu, *Chemistry of Materials* **2012**, 24, 3964-3971.
- [43] A. D. Schlüter, G. Wegner, *Acta Polymerica* **1993**, 44, 59-69.
- [44] T. A. Skotheim, R. L. Elsenbaumer, J. R. Reynolds, *Handbook of Conducting Polymers*, Marcel Dekker, **1998**.
- [45] K.-Y. Jen, G. G. Miller, R. L. Elsenbaumer, *Journal of the Chemical Society, Chemical Communications* **1986**, 1346-1347.
- [46] A. F. Diaz, J. Castillo, K. K. Kanazawa, J. A. Logan, M. Salmon, O. Fajardo, *Journal of Electroanalytical Chemistry and Interfacial Electrochemistry* **1982**, 133, 233-239.
- [47] B. Xie, M. Bagui, R. Guo, K. Li, Q. Wang, Z. Peng, *Journal of Polymer Science Part A: Polymer Chemistry* **2007**, 45, 5123-5135.
- [48] F. Huang, H. Wu, D. Wang, W. Yang, Y. Cao, *Chemistry of Materials* **2004**, 16, 708-716.

- [49] W. Zhang, L. Xu, J. Qin, C. Yang, *Macromolecular Rapid Communications* **2013**, *34*, 442-446.
- [50] K. C. Park, L. R. Dodd, K. Levon, T. K. Kwei, *Macromolecules* **1996**, *29*, 7149-7154.
- [51] J. Kim, Y. S. Kwon, W. S. Shin, S. J. Moon, T. Park, *Macromolecules* **2011**, *44*, 1909-1919.
- [52] Z. Li, Y. Zhang, S.-W. Tsang, X. Du, J. Zhou, Y. Tao, J. Ding, *The Journal of Physical Chemistry C* **2011**, null-null.
- [53] R. D. McCullough, *Advanced Materials* **1998**, *10*, 93-116.
- [54] P. Sista, M. C. Biewer, M. C. Stefan, *Macromolecular Rapid Communications* **2012**, *33*, 9-20.
- [55] H.-J. Yun, Y.-J. Lee, S.-J. Yoo, D. S. Chung, Y.-H. Kim, S.-K. Kwon, *Chemistry – A European Journal* **2013**, *19*, 13242-13248.
- [56] G. Götz, S. Scheib, R. Klose, J. Heinze, P. Bäuerle, *Advanced Functional Materials* **2002**, *12*, 723-728.
- [57] L. Groenendaal, F. Jonas, D. Freitag, H. Pielartzik, J. R. Reynolds, *Advanced Materials* **2000**, *12*, 481-494.
- [58] J. Roncali, P. Blanchard, P. Frere, *Journal of Materials Chemistry* **2005**, *15*, 1589-1610.
- [59] X. Hu, L. Xu, *Polymer* **2000**, *41*, 9147-9154.
- [60] K. Ogawa, J. A. Stafford, S. D. Rothstein, D. E. Tallman, S. C. Rasmussen, *Synthetic Metals* **2005**, *152*, 137-140.
- [61] D. Lee, E. Hubijar, G. J. D. Kalaw, J. P. Ferraris, *Chemistry of Materials* **2012**.
- [62] H. A. Ho, H. Brisset, P. Frere, J. Roncali, *Journal of the Chemical Society, Chemical Communications* **1995**, 2309-2310.
- [63] J. Sun, L. P. Sanow, S.-S. Sun, C. Zhang, *Macromolecules* **2013**, *46*, 4247-4254.
- [64] Y. Liang, D. Feng, Y. Wu, S.-T. Tsai, G. Li, C. Ray, L. Yu, *Journal of the American Chemical Society* **2009**, *131*, 7792-7799.
- [65] Y. Li, J. Zou, H.-L. Yip, C.-Z. Li, Y. Zhang, C.-C. Chueh, J. Intemann, Y. Xu, P.-W. Liang, Y. Chen, A. K. Y. Jen, *Macromolecules* **2013**, *46*, 5497-5503.
- [66] C. Zhang, J. Sun, R. Li, S. Black, S.-S. Sun, *Synthetic Metals* **2010**, *160*, 16-21.
- [67] F. Baycan Koyuncu, S. Koyuncu, E. Ozdemir, *Organic Electronics* **2011**, *12*, 1701-1710.
- [68] F. Wudl, M. Kobayashi, A. J. Heeger, *The Journal of Organic Chemistry* **1984**, *49*, 3382-3384.
- [69] M. Pomerantz, B. Chaloner-Gill, L. O. Harding, J. J. Tseng, W. J. Pomerantz, *Journal of the Chemical Society, Chemical Communications* **1992**, 1672-1673.
- [70] G. A. Sotzing, K. Lee, *Macromolecules* **2002**, *35*, 7281-7286.
- [71] T. Umeyama, K. Hirose, K. Noda, K. Matsushige, T. Shishido, H. Hayashi, Y. Matano, N. Ono, H. Imahori, *The Journal of Physical Chemistry C* **2011**, *116*, 1256-1264.
- [72] T. Umeyama, K. Hirose, K. Noda, K. Matsushige, T. Shishido, H. Saarenpää, N. V. Tkachenko, H. Lemmetyinen, N. Ono, H. Imahori, *The Journal of Physical Chemistry C* **2012**, *116*, 17414-17423.
- [73] W. A. Braunecker, Z. R. Owczarczyk, A. Garcia, N. Kopidakis, R. E. Larsen, S. R. Hammond, D. S. Ginley, D. C. Olson, *Chemistry of Materials* **2012**, *24*, 1346-1356.
- [74] Q. Zhang, Y. Li, M. Yang, *Synthetic Metals* **2004**, *146*, 69-71.
- [75] Q. Zhang, J. Feng, K. Liu, D. Zhu, M. Yang, H. Ye, X. Liu, *Synthetic Metals* **2006**, *156*, 804-808.
- [76] M. Yang, Q. Zhang, P. Wu, H. Ye, X. Liu, *Polymer* **2005**, *46*, 6266-6273.
- [77] W. t. H. E. E. Havinga, H. Wynberg, *Polymer Bulletin* **1992**, *29*, 119-126.
- [78] S. Akoudad, J. Roncali, *Synthetic Metals* **1999**, *101*, 149.
- [79] M. Jayakannan, P. A. Van Hal, R. A. J. Janssen, *Journal of Polymer Science Part A: Polymer Chemistry* **2002**, *40*, 2360-2372.
- [80] P. M. Beaujuge, W. Pisula, H. N. Tsao, S. Ellinger, K. Müllen, J. R. Reynolds, *Journal of the American Chemical Society* **2009**, *131*, 7514-7515.
- [81] S. Akoudad, J. Roncali, *Chemical Communications* **1998**, 2081-2082.
- [82] M. Karikomi, C. Kitamura, S. Tanaka, Y. Yamashita, *Journal of the American Chemical Society* **1995**, *117*, 6791-6792.
- [83] H. A. M. van Müllekom, J. A. J. M. Venkemans, E. W. Meijer, *Chemical Communications* **1996**, 2163-2164.
- [84] H. Zhou, L. Yang, W. You, *Macromolecules* **2012**, *45*, 607-632.
- [85] A. Facchetti, *Chemistry of Materials* **2010**, *23*, 733-758.
- [86] X. Zhan, D. Zhu, *Polymer Chemistry* **2010**, *1*, 409-419.
- [87] N. Blouin, A. Michaud, M. Leclerc, *Advanced Materials* **2007**, *19*, 2295-2300.
- [88] S. H. Park, A. Roy, S. Beaupre, S. Cho, N. Coates, J. S. Moon, D. Moses, M. Leclerc, K. Lee, A. J. Heeger, *Nat Photon* **2009**, *3*, 297-302.
- [89] D. Chandran, K.-S. Lee, *Macromol. Res.* **2013**, *21*, 272-283.
- [90] S. Zhang, L. Ye, Q. Wang, Z. Li, X. Guo, L. Huo, H. Fan, J. Hou, *The Journal of Physical Chemistry C* **2013**, *117*, 9550-9557.
- [91] S. Cho, J. Lee, M. Tong, J. H. Seo, C. Yang, *Advanced Functional Materials* **2011**, *21*, 1910-1916.
- [92] C. Piliago, T. W. Holcombe, J. D. Douglas, C. H. Woo, P. M. Beaujuge, J. M. J. Fréchet, *Journal of the American Chemical Society* **2010**, *132*, 7595-7597.
- [93] Y. Zou, A. Najari, P. Berrouard, S. Beaupré, B. Réda Aïch, Y. Tao, M. Leclerc, *Journal of the American Chemical Society* **2010**, *132*, 5330-5331.
- [94] T.-Y. Chu, J. Lu, S. Beaupré, Y. Zhang, J.-R. Pouliot, S. Wakim, J. Zhou, M. Leclerc, Z. Li, J. Ding, Y. Tao, *Journal of the American Chemical Society* **2011**, *133*, 4250-4253.

- [95] C. M. Amb, S. Chen, K. R. Graham, J. Subbiah, C. E. Small, F. So, J. R. Reynolds, *Journal of the American Chemical Society* **2011**, *133*, 10062-10065.
- [96] R. Stalder, J. Mei, J. R. Reynolds, *Macromolecules* **2010**, *43*, 8348-8352.
- [97] E. Wang, Z. Ma, Z. Zhang, K. Vandewal, P. Henriksson, O. Inganäs, F. Zhang, M. R. Andersson, *Journal of the American Chemical Society* **2011**, null-null.
- [98] G. K. Dutta, A. R. Han, J. Lee, Y. Kim, J. H. Oh, C. Yang, *Advanced Functional Materials* **2013**, n/a-n/a.
- [99] Y. Liang, Z. Xu, J. Xia, S.-T. Tsai, Y. Wu, G. Li, C. Ray, L. Yu, *Advanced Materials* **2010**, *22*, E135-E138.
- [100] T. Ito, H. Shirakawa, S. Ikeda, *Journal of Polymer Science: Polymer Chemistry Edition* **1974**, *12*, 11-20.
- [101] R. H. Friend, P. D. Townsend, D. D. C. Bradley, W. J. Feast, D. Parker, N. C. Billingham, P. D. Calvert, P. J. S. Foot, D. C. Bott, J. N. Winter, *Synthetic Metals* **1987**, *19*, 989.
- [102] A. S. Abd-El-Aziz, S. Sezgin Dalgakiran, L. Bichler, *European Polymer Journal* **2012**, *48*, 1901-1913.
- [103] J. Aristizabal, J. Soto, L. Ballesteros, E. Muñoz, J. Ahumada, *Polymer Bulletin* **2013**, *70*, 35-46.
- [104] H. G. Gilch, W. L. Wheelwright, *Journal of Polymer Science Part A-1: Polymer Chemistry* **1966**, *4*, 1337-1349.
- [105] R. A. Wessling, 72 ed., **1985**, pp. 55-66.
- [106] Z. Bao, Y. Chen, R. Cai, L. Yu, *Macromolecules* **1993**, *26*, 5281-5286.
- [107] R. Fiesel, U. Scherf, *Macromolecular Rapid Communications* **1998**, *19*, 427-431.
- [108] Q. T. Zhang, J. M. Tour, *Journal of the American Chemical Society* **1998**, *120*, 5355-5362.
- [109] T. Yamamoto, A. Morita, Y. Miyazaki, T. Maruyama, H. Wakayama, Z. H. Zhou, Y. Nakamura, T. Kanbara, S. Sasaki, K. Kubota, *Macromolecules* **1992**, *25*, 1214-1223.
- [110] R. D. McCullough, R. D. Lowe, *Journal of the Chemical Society, Chemical Communications* **1992**, 70-72.
- [111] T.-A. Chen, X. Wu, R. D. Rieke, *Journal of the American Chemical Society* **1995**, *117*, 233-244.
- [112] M. C. Iovu, E. E. Sheina, R. R. Gil, R. D. McCullough, *Macromolecules* **2005**, *38*, 8649-8656.
- [113] R. Miyakoshi, A. Yokoyama, T. Yokozawa, *Journal of the American Chemical Society* **2005**, *127*, 17542-17547.
- [114] A. Yokoyama, R. Miyakoshi, T. Yokozawa, *Macromolecules* **2004**, *37*, 1169-1171.
- [115] P. C. Ewbank, R. S. Loewe, L. Zhai, J. Reddinger, G. Sauvé, R. D. McCullough, *Tetrahedron* **2004**, *60*, 11269-11275.
- [116] R. S. Loewe, S. M. Khersonsky, R. D. McCullough, *Advanced Materials* **1999**, *11*, 250-253.
- [117] R. S. Loewe, P. C. Ewbank, J. Liu, L. Zhai, R. D. McCullough, *Macromolecules* **2001**, *34*, 4324-4333.
- [118] S.-J. Mougner, C. Brochon, E. Cloutet, G. Fleury, H. Cramail, G. Hadzioannou, *Macromolecular Rapid Communications* **2012**, *33*, 703-709.
- [119] S.-J. Mougner, C. Brochon, E. Cloutet, S. Magnet, C. Navarro, G. Hadzioannou, *Journal of Polymer Science Part A: Polymer Chemistry* **2012**, *50*, 2463-2470.
- [120] B. Carsten, F. He, H. J. Son, T. Xu, L. Yu, *Chemical Reviews* **2011**, *111*, 1493-1528.
- [121] J. Sakamoto, M. Rehahn, G. Wegner, A. D. Schlüter, *Macromolecular Rapid Communications* **2009**, *30*, 653-687.
- [122] D. Azarian, S. S. Dua, C. Eaborn, D. R. M. Walton, *Journal of Organometallic Chemistry* **1976**, *117*, C55-C57.
- [123] M. Kosugi, K. Sasazawa, Y. Shimizu, T. Migita, *Chemistry Letters* **1977**, *6*, 301-302.
- [124] D. Milstein, J. K. Stille, *Journal of the American Chemical Society* **1978**, *100*, 3636-3638.
- [125] P. Espinet, A. M. Echavarren, *Angewandte Chemie International Edition* **2004**, *43*, 4704-4734.
- [126] M. Bochmann, K. Kelly, *Journal of the Chemical Society, Chemical Communications* **1989**, 532-534.
- [127] Z. Bao, W. K. Chan, L. Yu, *Journal of the American Chemical Society* **1995**, *117*, 12426-12435.
- [128] N. Miyaura, A. Suzuki, *Journal of the Chemical Society, Chemical Communications* **1979**, 866-867.
- [129] N. Miyaura, K. Yamada, A. Suzuki, *Tetrahedron Letters* **1979**, *20*, 3437-3440.
- [130] A. Suzuki, *Angewandte Chemie International Edition* **2011**, *50*, 6722-6737.
- [131] A. A. C. Braga, N. H. Morgon, G. Ujaque, F. Maseras, *Journal of the American Chemical Society* **2005**, *127*, 9298-9307.
- [132] N. Miyaura, *Journal of Organometallic Chemistry* **2002**, *653*, 54-57.
- [133] R. Martin, S. L. Buchwald, *Accounts of Chemical Research* **2008**, *41*, 1461-1473.
- [134] M. Rehahn, A.-D. Schlüter, G. Wegner, W. J. Feast, *Polymer* **1989**, *30*, 1060-1062.
- [135] S. C. Moratti, R. Cervini, A. B. Holmes, D. R. Baigent, R. H. Friend, N. C. Greenham, J. Grüner, P. J. Hamer, *Synthetic Metals* **1995**, *71*, 2117-2120.
- [136] A. E. Siegrist, P. Liechti, H. R. Meyer, K. Weber, *Helvetica Chimica Acta* **1969**, *52*, 2521-2554.
- [137] H. Kretzschmann, H. Meier, *Tetrahedron Letters* **1991**, *32*, 5059-5062.
- [138] B. de Boer, U. Stalmach, P. F. van Hutten, C. Melzer, V. V. Krasnikov, G. Hadzioannou, *Polymer* **2001**, *42*, 9097-9109.
- [139] A. P. Davey, A. Drury, S. Maier, H. J. Byrne, W. J. Blau, *Synthetic Metals* **1999**, *103*, 2478-2479.
- [140] S. Wang, W. Hua, F. Zhang, Y. Wang, *Synthetic Metals* **1999**, *99*, 249-252.
- [141] Y. Liu, S. Xu, J. Li, Y. Xin, G. Zhao, B. Ye, S. Cao, *Polymers for Advanced Technologies* **2008**, *19*, 793-800.
- [142] J. Miyake, Y. Chujo, *Macromolecules* **2008**, *41*, 5671-5673.
- [143] M. Smith, J. March, Wiley-Interscience, Hoboken, N.J., **2007**.
- [144] C.-J. Yang, S. A. Jenekhe, *Macromolecules* **1995**, *28*, 1180-1196.
- [145] S. Barik, T. Bletzacker, W. G. Skene, *Macromolecules* **2012**, *45*, 1165-1173.
- [146] F. R. Diaz, J. Moreno, L. H. Tagle, G. A. East, D. Radic, *Synthetic Metals* **1999**, *100*, 187-193.
- [147] L. Beverina, P. Salice, *European Journal of Organic Chemistry* **2010**, *2010*, 1207-1225.

---

## Chapter 2    SYNTHESIS AND CHARACTERIZATION OF POLY(CARBAZOLE-*ALT*-BENZOTHIADIAZOLE)S





## Table of contents

<b>2.1</b>	<b>Literature overview .....</b>	<b>57</b>
<b>2.2</b>	<b>Synthesis of alternated conjugated polymers of carbazole and benzothiadiazole .....</b>	<b>63</b>
2.2.1	Carbazole monomers .....	63
2.2.2	Poly(carbazole- <i>alt</i> -benzothiadiazole)s .....	67
<b>2.3</b>	<b>Properties of PCBTs .....</b>	<b>70</b>
2.3.1	Thermal properties .....	70
2.3.2	Optical properties .....	71
2.3.3	Electrochemical properties .....	75
2.3.4	Photovoltaic performances .....	76
<b>2.4</b>	<b>Conclusion.....</b>	<b>79</b>
<b>2.5</b>	<b>Experimental .....</b>	<b>83</b>
2.5.1	Syntheses and structural characterizations .....	83
2.5.2	Thermogravimetric analyses (TGA) .....	96
2.5.3	Differential Scanning calorimetry .....	97
2.5.4	Electrochemistry .....	98
2.5.5	Optical characterizations of PCBT-PCBM blends.....	100
2.5.6	Photovoltaic characterization .....	101
<b>2.6</b>	<b>Bibliography .....</b>	<b>81</b>



## 2.1 LITERATURE OVERVIEW

The carbazole (Cz) moiety offers several advantages. Its derivatives are easy to synthesize from low-cost precursors and can be functionalized with a wide variety of substituents on the nitrogen atom, or in the 2,7- and 3,6-positions of the phenyl rings. Fluorene is an analogous compound known to undergo oxidation at the 9-position (see Figure 2 - 1), which may be an undesirable feature of a CP.<sup>[1]</sup> The presence of the nitrogen atom in carbazole prevents oxidation at this position and also enhances the electron-donating character of the unit.

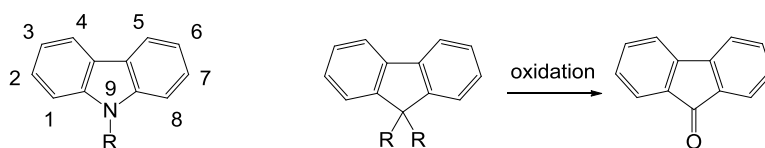
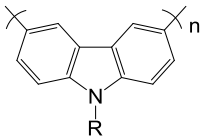
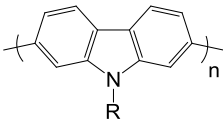
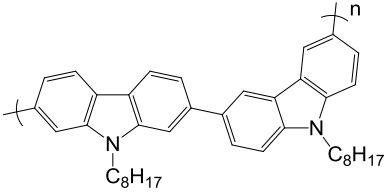


Figure 2 - 1: Representation of the carbazole molecule (left) and oxidation of the fluorene molecule (right).

Homopolymers of 2,7- and 3,6-carbazoles were synthesized by different research groups (see Table 2 - 1) and widely investigated as blue light emitters in OLEDs,<sup>[2-4]</sup> as well as semiconducting layer in OFETs.<sup>[5]</sup> For instance, Iraqi and Wataru used the Kumada coupling for synthesis of a series of 3,6- and 2,7-linked polycarbazoles bearing different alkyl chains.<sup>[6-7]</sup> A poor solubility in THF and chloroform was observed for the poly(2,7-carbazole) possessing the smallest side-chain (2-ethylhexyl), which resulted in lower molecular weights. The longer chains obtained for poly(2,7-carbazole)s compared to poly(3,6-carbazole)s were explained by less numerous termination reactions in the case of 2,7-functionalized monomers.<sup>[6]</sup> Torimitsu et al. produced high molecular weight poly(3,6-carbazole) via Yamamoto coupling, and concluded that the key parameter to obtain long polymeric chains is the addition order of reactants and catalyst.<sup>[8]</sup> When the nickel catalyst was slowly added to the monomer solution, formation of dinickel-substituted complex, which is unstable and leads to termination reaction, was minimized and the chain growth maximized.

It was shown that the poly(3,6-carbazole) have similar light absorption as the dimers.<sup>[4]</sup> This confirms a limited extent of conjugation to two Cz units due to a strongly twisted configuration of the polymer backbone,<sup>[7]</sup> or due to conjugation breaks on the nitrogen atoms.<sup>[9]</sup> On the contrary, the 2,7-linked polymers have extended conjugation along the backbone and hence smaller band-gap. Moreover, their HOMO and LUMO lied ca. 0.3 eV and 0.6 eV below their 3,6 analogues (see Table 2 - 1).

Table 2 - 1: Examples of developed Homopolycarbazoles.

Polymer	Coupling type	M <sub>n</sub> / M <sub>w</sub> (g.mol <sup>-1</sup> ) <sup>a</sup>	HOMO / LUMO (eV) <sup>b</sup>	E <sub>g</sub> <sup>opt</sup> (eV) <sup>c</sup>	Ref
	R = 2-ethylhexyl	2400 / 3900	-5.08 / -1.88 <sup>d</sup>	3.2	[7]
	R = 2-hexyldecyl	4100 / 7200	-5.11 / -1.91 <sup>d</sup>	3.2	
	R = dodecyl	2800 / 4400	-5.10 / -1.90 <sup>d</sup>	3.2	
	R = hexadecyl	3700 / 5800	-5.10 / -1.90 <sup>d</sup>	3.2	
	R = decyl	53400 / 91000	N/A	3.2	[8]
	R = 3,7-dimethyloctyl	84200 / 120000	N/A	3.2	
	R = butyl	3000 / 6000	N/A	3.2	[4]
	R = octyl	3900 / 5200	N/A	N/A	[10]
		3800 / 5800	-5.25 / -2.00	3.18	[11]
	R = 2-ethylhexyl	3000 / 4900	-5.4 / -2.5 <sup>d</sup>	2.89	[6]
	R = 2-hexyldecyl	15100 / 28400	-5.5 / -2.6 <sup>d</sup>	2.88	
	R = dodecyl	6300 / 8600	-5.4 / -2.5 <sup>d</sup>	2.90	
	R = hexadecyl	6800 / 10700	-5.4 / -2.5 <sup>d</sup>	2.90	
	R = octyl	6400 / 9000	N/A	2.8	[10]
	Suzuki	14900 / 25000	-5.33 / -2.43 <sup>d</sup>	2.9	[10]

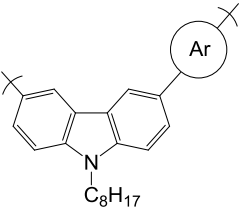
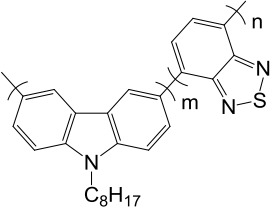
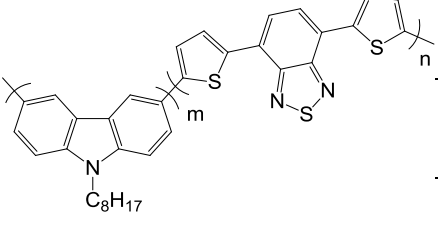
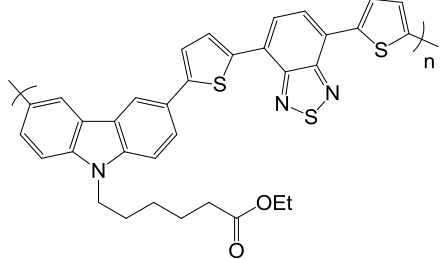
<sup>a</sup> measured by SEC in THF with PS standards; <sup>b</sup> measured by cyclic voltammetry on film; <sup>c</sup> calculated from the absorption spectrum in film; <sup>d</sup> estimated from HOMO and E<sub>g</sub><sup>opt</sup>.

The donor-acceptor strategy was exploited in various semiconducting polymers utilizing Cz as donor unit. Acceptor comonomers such as benzothiadiazole (BT),<sup>[9]</sup> benzoxadiazole<sup>[12]</sup> and quinoxaline<sup>[13]</sup> were used. The previously mentioned PCDTBT (see section 1.4.5 in chapter 1) is a remarkable example of efficient carbazole-based CP which is becoming a reference for newly developed BHJ solar cells.<sup>[14-16]</sup>

Several examples of copolymers based on 3,6-carbazole coupled with variety of heteroaromatic units are presented in Table 2 - 2. The results from the research of Witker and Reynolds confirmed the electron-donating character of the Cz moiety.<sup>[9]</sup> They reported that the alternation with the electron-withdrawing BT allowed a significant decrease of the band-gap in comparison with thiophene, caused by a stronger intramolecular charge transfer (ICT, see chapter 1). Cao and co-workers investigated the influence of the donor-acceptor ratio on the materials properties with two different acceptors.<sup>[11, 17]</sup> Firstly, replacing the BT moiety by the dithienylbenzothiadiazole (DTBT) unit led to a more planar backbone and thus a smaller band-gap. It was observed that increasing the ratio of BT lowered the

HOMO and LUMO levels whereas an opposite effect was found in the case of DTBT. However, the band-gap remained independent on donor-acceptor ratio, which can seem contradictory to the explanation of the importance of a 1:1 ratio in donor-acceptor copolymers mentioned in the previous chapter. The material developed by Chandezon and co-workers showed a low molecular weight, which can be an issue to achieve red-shifted absorption because of a limited conjugation extent. Nevertheless, its optical band-gap was similar to the polymers developed by Cao et al., demonstrating the predominant role of the ICT over  $\pi$ -electrons delocalization in that case.<sup>[18]</sup>

Table 2 - 2: Examples of conjugated copolymers including the 3,6-carbazole unit in the main chain.

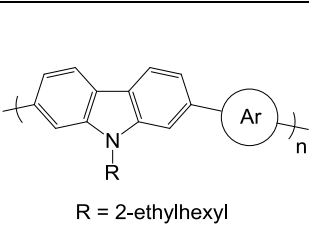
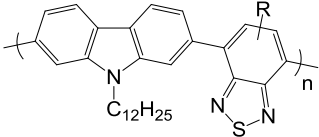
Polymer	Coupling type	Mn / Mw (g.mol <sup>-1</sup> ) <sup>a</sup>	HOMO / LUMO (eV) <sup>b</sup>	E <sub>g</sub> <sup>opt c</sup> / E <sub>g</sub> <sup>cv</sup> (eV)	Ref
	Suzuki	2600 / 4100	N/A	2.8 / -	[9]
		3700 / 5800	N/A	2.5 / -	
		2800 / 3700	N/A	2.3 / -	
	Suzuki	3800 / 5700	-5.30 / -3.00	2.28 / 2.30	[17]
		3600 / 5400	-5.33 / -3.03	2.30 / 2.30	
		2500 / 3800	-5.4 / -3.10	2.28 / 2.30	
	Suzuki	3600 / 4900	-5.30 / -	1.78 / -	[11]
		5600 / 7600	-5.20 / -	1.78 / -	
		4300 / 5400	-5.0 / -	1.78 / -	
	Suzuki	1600 / 2800	-5.34 / -3.52	1.81 / 1.82	[18]

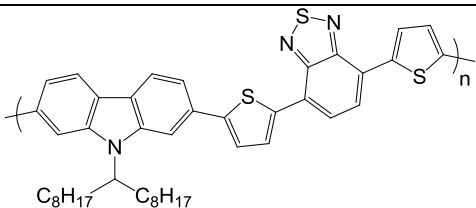
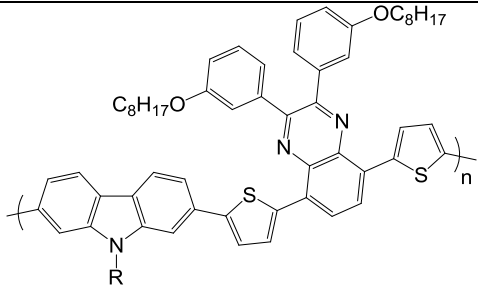
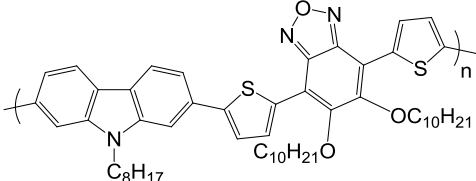
<sup>a</sup> measured by SEC in THF with PS standards; <sup>b</sup> measured by cyclic voltammetry on film; <sup>c</sup> calculated from the absorption spectrum in film.

Table 2 - 3 shows some examples of alternated copolymers including the 2,7-carbazole unit. In general, the band-gaps of these materials are not particularly smaller than their 3,6-Cz analogous, confirming the major effect of the ICT compared to  $\pi$ -electrons delocalization, as mentioned above. Nevertheless, a major difference can be found when comparing alternating Cz-DTBT copolymers.<sup>[18]</sup> The 3,6-derivative demonstrated much smaller hole mobility than the 2,7 which can be attributed to low  $M_n$  and worse morphological properties (packing).

Additionally to the Cz unit, attaching solubilizing groups on the acceptor moiety is a strategy which was successfully employed to improve the solubility and molecular weights of the polymers.<sup>[13, 19-20]</sup> However, it was demonstrated that for some comonomers (BT for instance) this could generate an enhanced steric hindrance and thus a wider band-gap due to an increased twist angle between units.<sup>[19]</sup> The use of alkyl chains with different geometries on the Cz unit also greatly influences the semiconductor properties. As an example, copolymers based on Cz and quinoxaline showed a decrease in the band-gap when linear chains were present on the Cz unit.<sup>[20]</sup> This effect is due to enhanced intermolecular interactions in the solid state.

Table 2 - 3: Examples of conjugated copolymers including the 2,7-carbazole unit in the main chain.

Polymer	Coupling type	Mn / Mw (g.mol <sup>-1</sup> ) <sup>a</sup>	HOMO / LUMO (eV) <sup>b</sup>	E <sub>g</sub> <sup>optc</sup> / E <sub>g</sub> <sup>cv</sup> (eV)	Ref
 <p>R = 2-ethylhexyl</p>	Suzuki	5000 / 11500	N/A	3.02 / -	[13]
		10000 / 28000	N/A	2.59 / -	
	Suzuki	R = H 2500 / 2800	-5.15 / -2.59	2.13 / 2.56	[19]
		R = methyl 3800 / 4900	-5.14 / -2.51	2.47 / 2.63	
		R = heptyl 16000 / 35200	-5.17 / -2.48	2.56 / 2.69	
		R = isopropoxymethyl 11000 / 41800	-5.15 / -2.56	2.41 / 2.59	

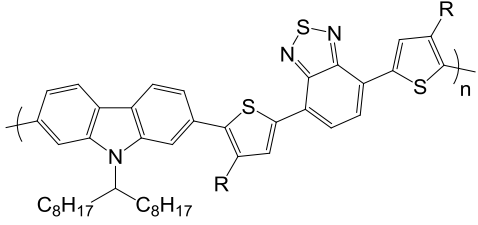
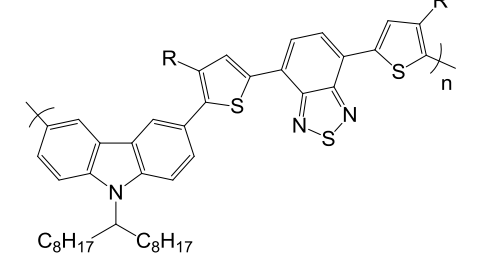
Polymer	Coupling type	Mn / Mw (g.mol <sup>-1</sup> ) <sup>a</sup>	HOMO / LUMO (eV) <sup>b</sup>	E <sub>g</sub> <sup>optc</sup> / E <sub>g</sub> <sup>CV</sup> (eV)	Ref
	Suzuki	37000 / 73000	-5.5 / -3.6	1.88 / 1.87	[14]
 <div style="display: inline-block; vertical-align: middle; margin-left: 10px;"> <p>R = octyl</p> <hr/> <p>R = 9-heptadecanyl</p> </div>	Suzuki	34000 / 98600	-5.56 / -3.29	1.82 / 2.27	[20]
		23000 / 62100	-5.73 / -3.32	1.92 / 2.41	
	Suzuki	4500 / 10400	-5.23 / -3.61	1.71 / 1.62	[12]

<sup>a</sup> measured by SEC in THF with PS standards; <sup>b</sup> measured by cyclic voltammetry on film; <sup>c</sup> calculated from the absorption spectrum in film.

Park and co-workers compared the influence of linkage position (2,7 and 3,6) in alternated copolymers of Cz and DTBT (see Table 2 - 4).<sup>[21]</sup> The optical band-gaps were very similar in both configurations due to an equally effective ICT. Additionally, they investigated the influence of solubilizing groups on the thiophene rings in the DTBT unit. As expected, the introduction of hexyl substituents induced a stronger dihedral angle between units followed by an increase of the band-gap. Surprisingly, the poly(3,6-carbazole)s showed higher hole mobility, as already reported by Leclerc et al.<sup>[22]</sup> In these materials, the created positive charges (from the hole mobility measurement) were assumed to be located on the nitrogen atom due to a better stability, thus the 2,7-configuration did not allow a delocalization of these charges since the nitrogen lone pair is not directly involved in the conjugation.

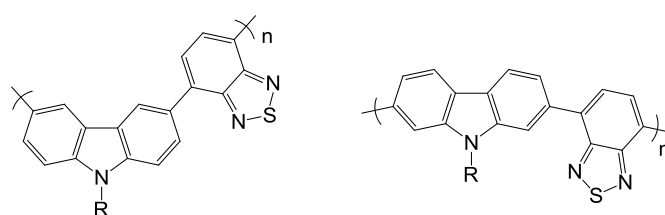


Table 2 - 4: Cz and DTBT-based copolymers developed by Park et al.

Polymer	Synthetic route	Mn / Mw (g.mol <sup>-1</sup> ) <sup>a</sup>	HOMO / LUMO (eV) <sup>b</sup>	E <sub>g</sub> <sup>optc</sup> / E <sub>g</sub> <sup>cv</sup> (eV)
	R = H	21000 / 38500	-5.45 / -3.56	1.88 / 1.89
R = hexyl		4500 / 6100	-5.18 / -3.47	2.01 / 2.12
	R = H	30600 / 55500	-5.63 / -3.51	1.85 / 1.71
R = hexyl		29100 / 42200	-5.66 / -3.50	2.00 / 2.16

<sup>a</sup> measured by SEC in THF with PS standards; <sup>b</sup> measured by cyclic voltammetry on film; <sup>c</sup> calculated from the absorption spectrum in film.

Such a study on polymers based on Cz and BT without thiophene spacers was not reported in the literature. Therefore, carbazole core with either 2,7- or 3,6-configuration was selected for copolymerization with benzothiadiazole as acceptor unit in order to achieve semiconducting polymers with suitable properties for use as donor material in BHJ solar cells (see Figure 2 - 2). Furthermore, the influence of solubilizing groups with two different geometries was studied. This work aims to provide a better understanding of the molecular structure-properties relationship in carbazole-benzothiadiazole alternated CPs.



R = dodecyl, 9-heptadecanyl

Figure 2 - 2: Structures of the developed polymers.

## 2.2 SYNTHESIS OF ALTERNATED CONJUGATED POLYMERS OF CARBAZOLE AND BENZOTHIADIAZOLE

### 2.2.1 CARBAZOLE MONOMERS

Four different carbazole-based monomers were prepared (see Figure 2 - 3) and subsequently polymerized via Suzuki coupling with a commercially available benzothiadiazole functionalized with boronic ester groups in 4 and 7 positions. Suzuki coupling requires that the Cz monomers bear halide or triflate groups. To avoid numerous synthetic steps, halides are the preferred choice, and amongst them bromide and iodide functions are known to be more reactive than chloride.<sup>[23]</sup>

As mentioned previously, the carbazole derivatives are commonly functionalized in 2,7-, 3,6- and rarely in 1,8-positions.<sup>[24]</sup> The latter would induce a strong steric hindrance and a highly kinked conformation of the backbone in the polymer, thus only the 2,7- and 3,6-positions were selected. Moreover, in order to provide solubility of the resulting polymers, suitable alkyl chains have to be incorporated. The nature, length and position of the alkyl chain can have a drastic impact on the properties of the resulting polymer in terms of packing, conformational arrangement, solubility or crystallinity.<sup>[24]</sup> To investigate this dependence, two different alkyl chains were selected and linked to the nitrogen atom – fully linear n-dodecyl and bulkier branched 9-heptadecanyl.

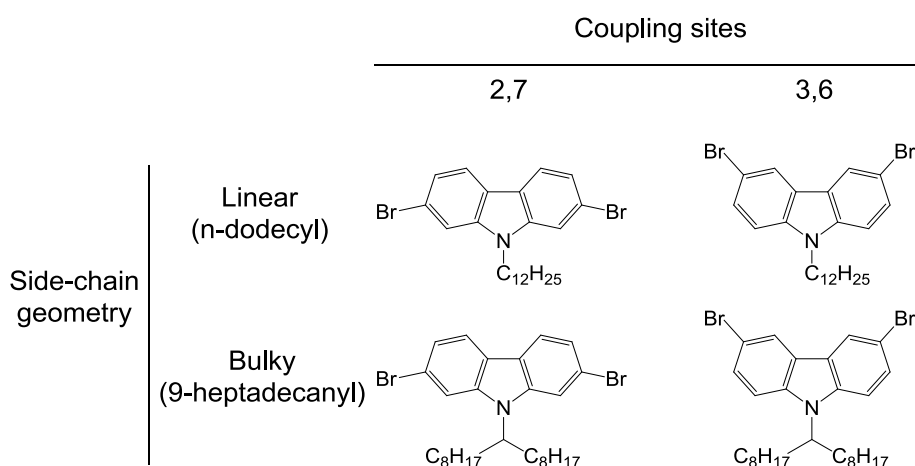


Figure 2 - 3: Structures of the four Cz monomers developed.

Due to the presence of the amino group, the *ortho* and *para* positions are the most reactive towards electrophilic attack.<sup>[25]</sup> Here, the *ortho* position is sterically hindered, causing the reaction to occur solely in *para*, corresponding to 3,6-position of the carbazole. Consequently, 3,6-dibromocarbazole is a low-cost commercially available compound. On the contrary, electrophilic substitution in *meta*,

here corresponding to the 2,7-positions, is highly unfavorable and has to be performed via alternative routes. 2,7-dibromocarbazole was obtained in two steps following a well-known procedure (see Figure 2 - 4).<sup>[26]</sup> Firstly, compound **1** was prepared by nitration of 4,4'-dibromobiphenyl in the presence of fuming nitric/acetic acid, followed by a Cadogan ring-closure reaction using triethylphosphite.<sup>[27]</sup> The desired 2,7-dibromo-9*H*-carbazole **2** was afforded with an overall yield of 63 %.

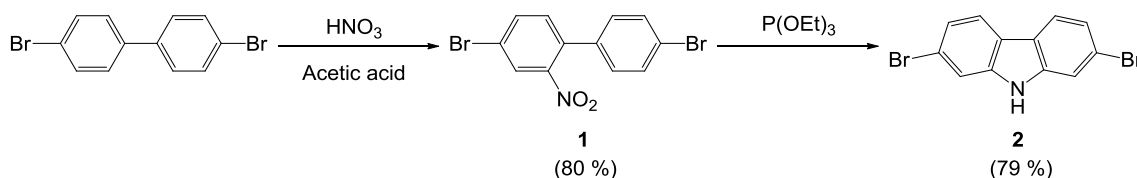


Figure 2 - 4: Synthesis of 2,7-dibromo-9*H*-carbazole **2**.

In order to achieve Cz derivative with a bulky alkyl side-chain, a tosylate derivative of heptadecane had first to be prepared. Therefore, 9-heptadecanyl-4-methylbenzenesulfonate **4** was synthesized in two steps with an overall yield of 74 % (see Figure 2 - 5).<sup>[14]</sup> Ethyl formate was reacted with octylmagnesium chloride to afford heptadecan-9-ol **3**. A subsequent reaction of **3** with *p*-toluenesulfonyl chloride in basic conditions yielded 89 % of tosylated compound **4**.

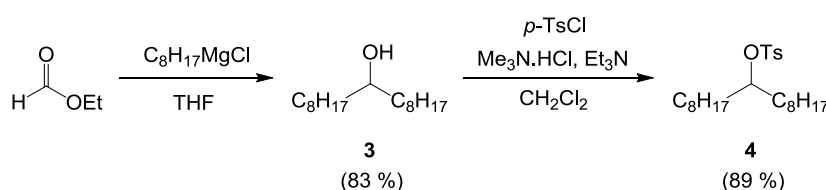


Figure 2 - 5: Synthesis of the 9-heptadecanyl tosylate **4**.

Alkylations of the dibromocarbazole compounds were performed following reported procedures.<sup>[14, 28]</sup> Deprotonation of the secondary amine in the carbazole core was carried out with a base and followed by a nucleophilic substitution with an appropriate alkyl derivative (see Figure 2 - 6). *N*-dodecyl-2,7-dibromocarbazole **5** and *N*-dodecyl-3,6-dibromocarbazole **6** were obtained by reacting 2,7-dibromo-9*H*-carbazole **2** and 3,6-dibromo-9*H*-carbazole with 1-bromododecane in the presence of potassium carbonate. Reaction of the dibromocarbazoles with the tosylate **4** in the presence of potassium hydroxide afforded *N*-9'-heptadecanyl-2,7-dibromocarbazole **7** and *N*-9'-heptadecanyl-3,6-dibromocarbazole **8** in moderate to good yields.

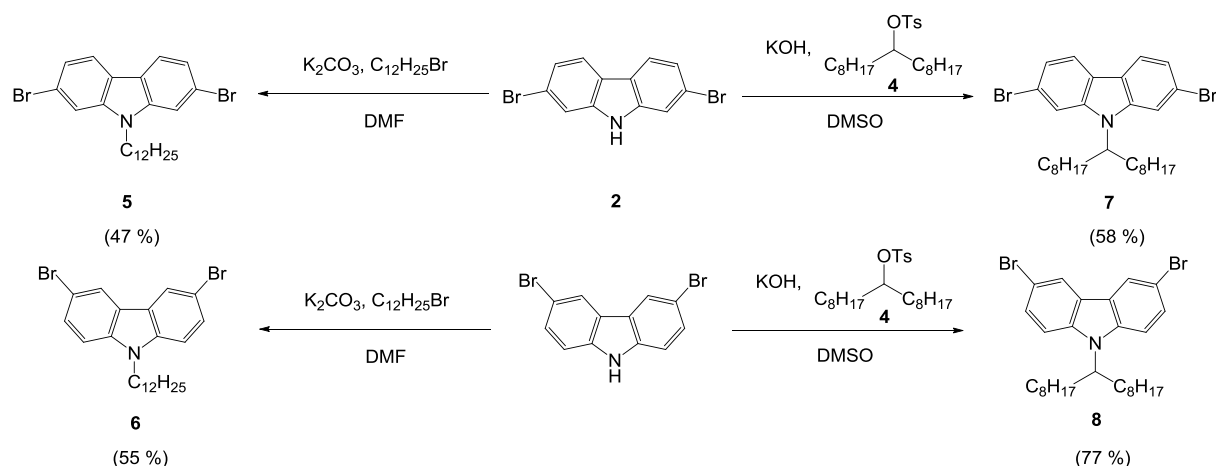
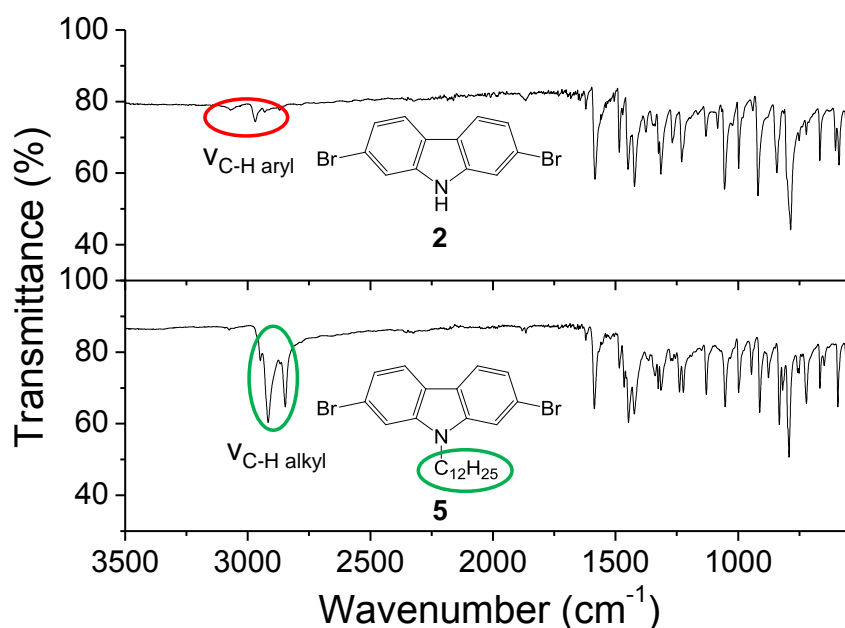


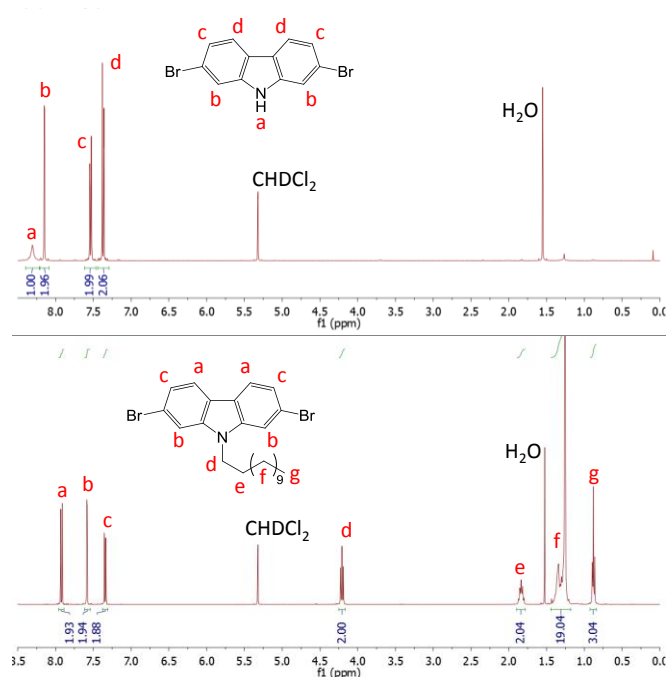
Figure 2 - 6: Synthesis of the alkylated dibromocarbazoles 5-8.

The structures were confirmed by nuclear magnetic resonance spectroscopy ( $^1H$ ,  $^{13}C$  and  $^1H$ - $^{13}C$  HSQC NMR), infrared spectroscopy (IR), high-resolution mass spectroscopy (HRMS), and their melting points were also measured and found to be in good agreement with reported data (see experimental section for details).

IR spectroscopy measured with attenuated total reflectance (ATR) of **5-8** was consistent with the expected chemical structures (see experimental section). Spectra of the non-alkylated dibromocarbazole **2** and N-dodecyl-2,7-dibromocarbazole **5** are shown in Figure 2 - 7 as examples. The intense peaks in the  $2800$ - $3000\text{ cm}^{-1}$  region in the spectrum of **5** correspond to alkyl C-H stretch and provide an evidence of the side chains incorporation in the Cz core. The signals corresponding to aromatic C-H stretch are visible in the  $2900$ - $3100\text{ cm}^{-1}$  region of compound **2** IR spectrum, nevertheless their intensity is too weak to be observable in the spectrum of the alkylated compound **5**.

Figure 2 - 7: IR spectra (ATR) of the carbazole derivatives **2** and **5**.

NMR analyses allowed another confirmation of the desired chemical structures. As an example, Figure 2 - 8 shows the  $^1\text{H}$  NMR spectra of compounds **2** and **5** in  $\text{CD}_2\text{Cl}_2$ . The aromatic protons were assigned with help of peaks multiplicity and coupling values. Disappearance of the peak at 8.30 ppm in the spectrum of **5**, which corresponds to the amine proton in compound **2**, is a clear indication that the alkylated carbazole was obtained without residual reactant or by-product, although the NMR sensitivity only allows to assess a maximum purity of 95 %.

Figure 2 - 8:  $^1\text{H}$  NMR spectra (400 MHz) of compounds **2** and **5** in  $\text{CD}_2\text{Cl}_2$ .

## 2.2.2 POLY(CARBAZOLE-*ALT*-BENZOTHIADIAZOLE)S

In order to produce the desired poly(carbazole-*alt*-benzothiadiazole)s (PCBT), the prepared monomers **5-8** were reacted with 4,7-bis(4,4,5,5-tetramethyl-1,3,2-dioxaborolan-2-yl)benzo[c][1,2,5]thiadiazole under Suzuki cross-coupling conditions (see Figure 2 - 10). First attempts led to small oligomers and low yields, therefore an optimization work was conducted using N-dodecyl-3,6-dibromocarbazole **6** as a model compound (see Figure 2 - 9 and Table 2 - 5).

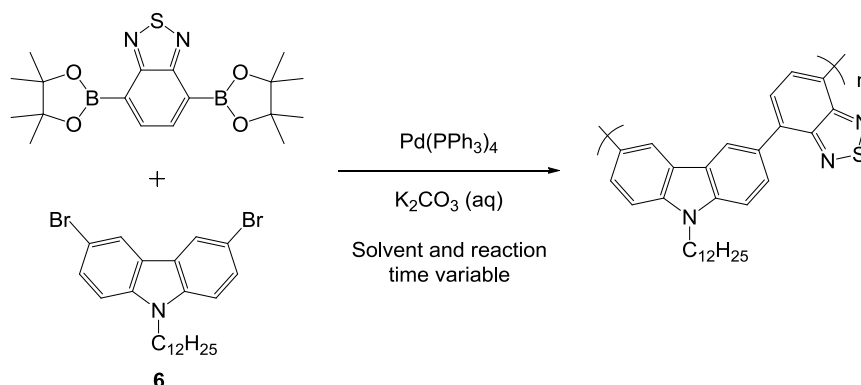


Figure 2 - 9: Reaction carried out to optimize the polymerization conditions of PCBTs.

Table 2 - 5: Optimization of the reaction conditions for the synthesis of PCBT3. Catalyst:  $\text{Pd(PPh}_3)_4$ . Base:  $\text{K}_2\text{CO}_3$ . Reaction medium stirred and heated to reflux (except DMSO: 100°C).

Solvent	Reaction time (h)	Yield (%) <sup>a</sup>	Mn (g.mol <sup>-1</sup> ) <sup>b</sup>
Toluene	40	45	2000
	70	35	2600
THF	22	29	3700
DMSO	22	9	3000
	15	88	5200
Toluene/THF 50:50 vol	22	30	3900
	42	56	3700
Toluene/THF 15:85 vol	15	84	5300

<sup>a</sup> Determined from the resulting mass of product after precipitation and drying; <sup>b</sup> Determined by gel permeation chromatography (GPC) relative to polystyrene standards in THF at 40 °C.

The Suzuki polycondensation was performed in a biphasic mixture. The organic solvent contained the monomers and the catalyst tetrakis(triphenylphosphine)palladium(0) ( $\text{Pd(PPh}_3)_4$ ), and the aqueous phase contained the base. The synthesized polymers were precipitated in diethyl ether and rinsed with acetone for purification. At first, the employed base for the Suzuki polycondensation was sodium bicarbonate, but very low yields and molecular weights were achieved. Hence, a stronger base, potassium carbonate was finally used. All the reactions were carried out at solvent reflux, apart from the one performed in DMSO (heated at 100°C). Solvent and reaction time were then varied to

optimize the polymerization conditions. Firstly, increasing the reaction time when the reaction was carried out in toluene afforded longer chains. However this was not the case when performing the reaction in a 1:1 vol mixture of toluene and THF. Reactions in THF and DMSO allowed higher molecular weights than toluene, but the yields were lower, especially in the case of DMSO which added issues to the recovering and purification of the polymer. Finally, the best yields and highest molecular weights were achieved when employing a mixture of toluene and THF.

Subsequently, the Suzuki polycondensations of **PCBT1-4** were carried out using  $\text{Pd(PPh}_3)_4$  as catalyst and aqueous  $\text{K}_2\text{CO}_3$  as base in a THF/toluene mixture (1:1 vol) for 48h and heating at reflux. The ratio of monomers was 1:1 in order to achieve high molecular weights according to Carothers equation. Prior to the reaction, the BT monomer was purified by sublimation and the reaction solvents degassed with argon to avoid presence of molecular oxygen. An end-capping reaction was performed with benzenboronic acid and bromobenzene, since it was reported that end-capping of CPs allowed a better stability over time of the resulting materials by eliminating the remaining reactive functional end-groups on the polymer chains.<sup>[29]</sup> The synthesized materials were then purified by Soxhlet extraction with methanol (MeOH), pentane and recovered from the THF fraction.

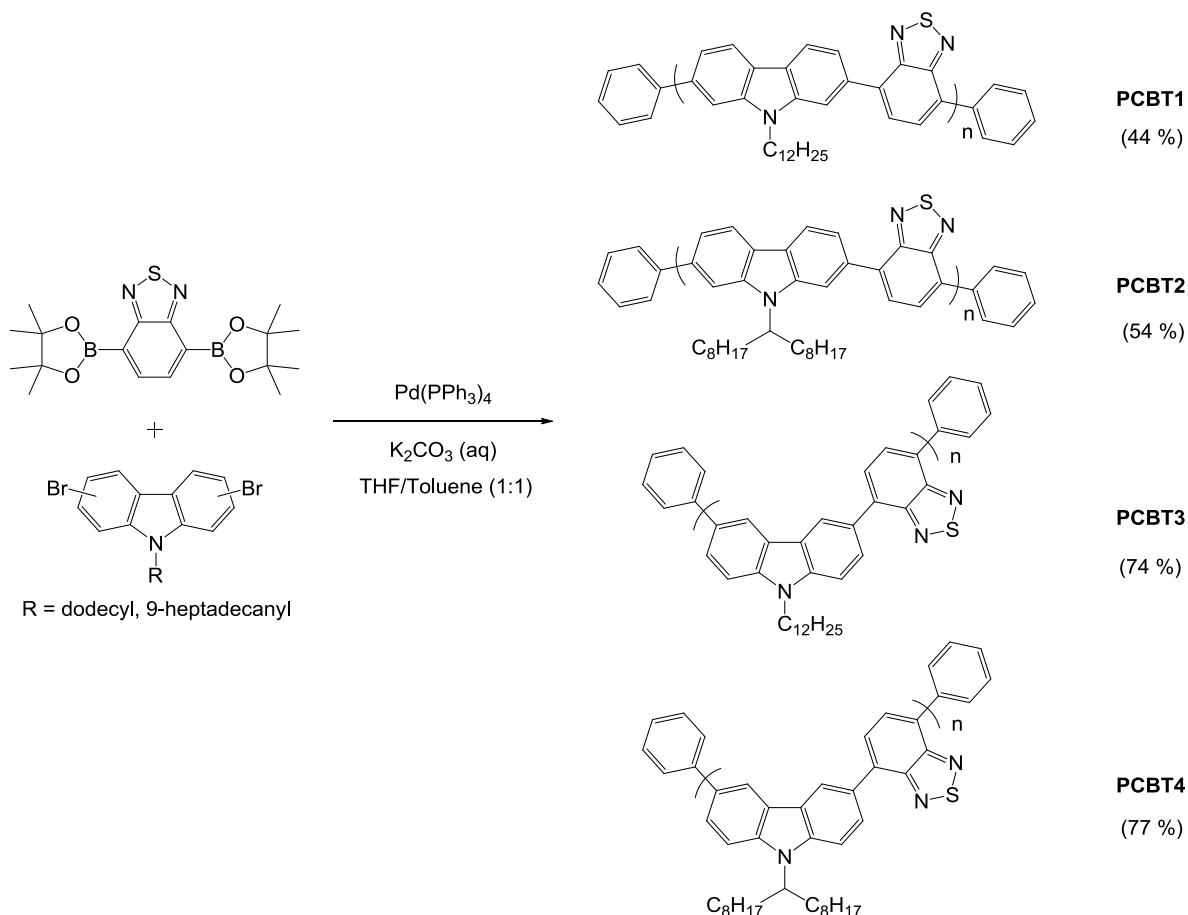


Figure 2 - 10: Synthesis of PCBTs by Suzuki cross-coupling, using  $\text{Pd(PPh}_3)_4$  as catalyst,  $\text{K}_2\text{CO}_3$  as base and toluene/THF mixture (1:1 vol.) as solvent. Reaction medium stirred and heated to reflux.

The products were obtained as strongly colored orange powders soluble in organic solvents such as toluene, THF, dichloromethane, chloroform or *ortho*-dichlorobenzene (ODCB). They demonstrated a strong absorption in solution even at low concentrations, which is a typical feature of conjugated polymers. Their chemical structures were checked by IR and NMR ( $^1\text{H}$ ,  $^{13}\text{C}$  and  $^1\text{H}$ - $^{13}\text{C}$  HSQC). IR spectra of the copolymers were similar to the one of the Cz monomers.

From the  $^1\text{H}$  NMR spectra of the synthesized PCBTs, it can be observed that the  $^1\text{H}$  signals showed a general broadening compared to the monomers, as depicted in the spectrum of **PCBT1** in Figure 2 - 11. The peaks corresponding to the alkyl protons in close vicinity to the nitrogen atom of the Cz units (b) can be clearly identified in the 4-5 ppm region and were thus used as reference for signals integration. No residual peak of boronic pinacol ester functions (sharp singlet at 1.44 ppm) could be observed, assessing that the polymer chains were successfully end-capped. Furthermore, the  $^{13}\text{C}$  and  $^1\text{H}$ - $^{13}\text{C}$  HSQC NMR spectra were consistent with the expected structures (see experimental section).

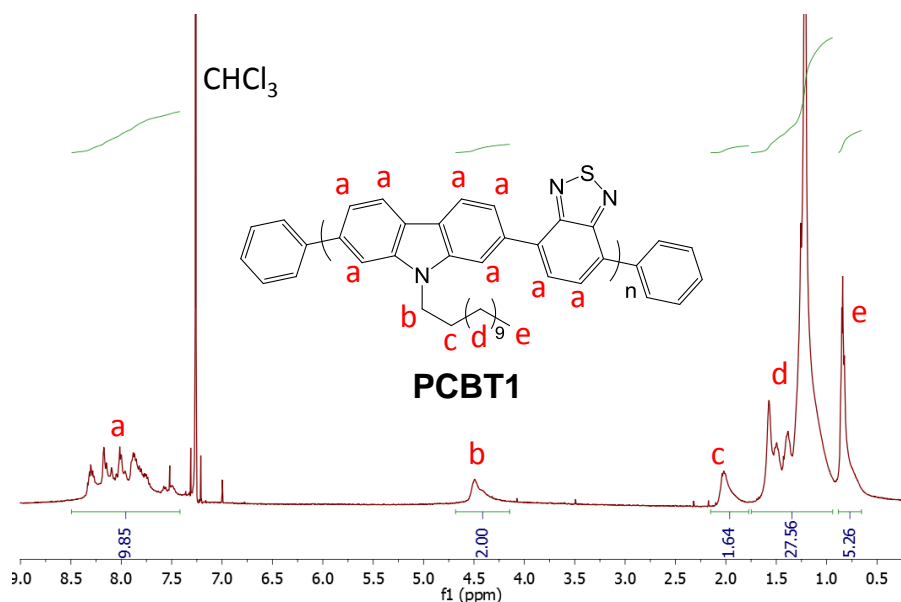


Figure 2 - 11:  $^1\text{H}$  NMR spectra (400 MHz) of PCBT1 in  $\text{CDCl}_3$ .

Molecular weights of the PCBTs were measured by steric exclusion chromatography (SEC) in THF, using polystyrene (PS) as standards (see Table 2 - 6). The number-average molecular weights of the polymers ranged from 1800 to 8100 g/mol. As a comparison, the corresponding degrees of polymerization are also presented, however these values should be only compared between themselves, since the molecular weights are determined with the use of PS standards, which have different Mark-Houwink coefficients, especially when compared to conjugated polymers. Some of the materials (**PCBT1** and **4**) showed short chain lengths. However, these molecular weights could be sufficient to achieve the desired properties, since it was shown in the previous section that even oligomers with a suitable ICT could lead to small enough band-gaps.<sup>[18]</sup>



Table 2 - 6: Molecular weights of PCBTs measured by SEC in THF.

Polymer	$\overline{M}_n$ (g/mol) <sup>a</sup>	$\overline{D}$ <sup>b</sup>	$\overline{DP}_n$ <sup>c</sup>
PCBT1	1 800	1.3	3.8
PCBT2	8 100	2.2	15.1
PCBT3	4 600	1.4	9.8
PCBT4	2 500	1.7	4.6

<sup>a</sup> Determined by steric exclusion chromatography (SEC) relative to polystyrene standards in THF at 40 °C;

<sup>b</sup> Dispersity  $\overline{D} = \frac{\overline{M}_w}{\overline{M}_n}$ ; <sup>c</sup> Number-average degree of polymerization  $\overline{DP}_n = \frac{\overline{M}_n}{M_{rep. unit}}$ .

## 2.3 PROPERTIES OF PCBTs

### 2.3.1 THERMAL PROPERTIES

Thermal properties of the materials were investigated. Differential Scanning Calorimetry (DSC) analyses showed no sign of cristallinity, proving an amorphous structure (see experimental section). Moreover, no clear signal of glass transition was observed between 0°C and 250°C). Thermal stability of the materials was observed by thermogravimetric analysis (TGA) under N<sub>2</sub> atmosphere (see Table 2 - 7).

Table 2 - 7: Thermal decomposition of PCBTs measured by TGA under N<sub>2</sub>.

Polymer	Decomposition temperature (°C) <sup>a</sup>	Weight loss (%)
PCBT1	400	99
PCBT2	329	50
PCBT3	400	33
PCBT4	423	41

<sup>a</sup> Evaluated at 5% weight loss at a heating rate of 10°C/min.

The four materials showed a good thermal stability, with decomposition temperatures ranging from 329 to 423°C. Apart from **PCBT1**, the weight losses at these temperatures corresponded to the weight proportion of the alkyl chains (calculated values of 36 %w and 45 %w for dodecyl and 9-heptadecanyl chains, respectively). This indicated that the first degradation mechanism under inert atmosphere was related to the elimination of side-chains from the backbone, as already reported in the literature.<sup>[21]</sup> The unexpected value for **PCBT1** could be assigned to a stronger influence of the chain ends due to its oligomeric nature.

### 2.3.2 OPTICAL PROPERTIES

The UV-visible absorption spectra of the synthesized materials in ODCB solutions and in solid-state are presented in Figure 2 - 12, and related data are listed in Table 2 - 8. As frequently observed in alternated CPs, all polymers show two absorption maxima, here in the 300-350 nm and 440-490 nm regions.<sup>[30]</sup> The short-wavelength peak is assigned to the carbazole moiety,<sup>[21]</sup> and the long-wavelength peak corresponds to the Intramolecular Charge Transfer (ICT) between the carbazole and benzothiadiazole units. ICT is confirmed by the red-shift in absorption of PCBTs compared to carbazole ( $\lambda_{\text{max}}$  from 310 to 390 nm) or benzothiadiazole ( $\lambda_{\text{max}}$  at 430 nm) homopolymers.<sup>[6-7, 31]</sup>

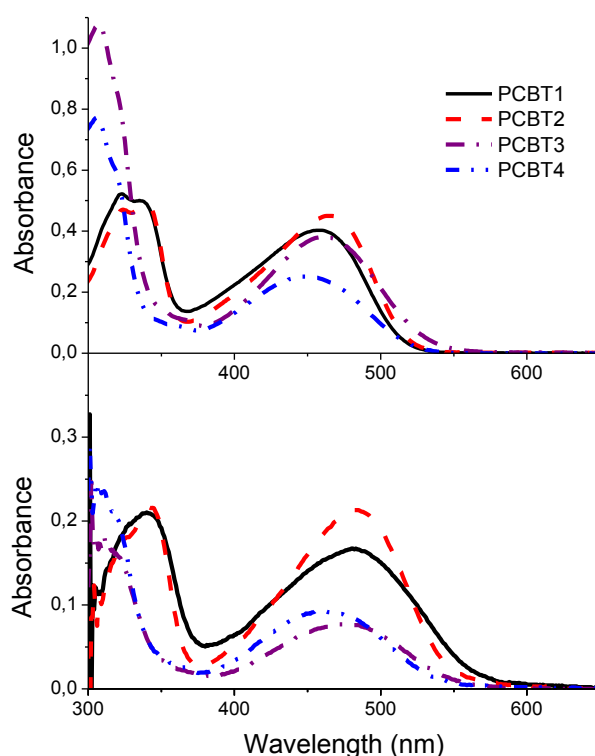


Figure 2 - 12: Absorption spectra of PCBTs in ODCB solutions (top) and as spin-coated films (bottom).

Table 2 - 8: Absorption data of PCBTs.

Polymer	Solution (ODCB)					Film			
	$\lambda_{\text{max 1}}^{\text{sol}}$ (nm) <sup>a</sup>	$\epsilon_1$ (l.mol <sup>-1</sup> .cm <sup>-1</sup> ) <sup>a</sup>	$\lambda_{\text{max 2}}^{\text{sol}}$ (nm) <sup>a</sup>	$\epsilon_2$ (l.mol <sup>-1</sup> .cm <sup>-1</sup> ) <sup>a</sup>	$\lambda_{\text{onset}}^{\text{sol}}$ (nm) <sup>a</sup>	$\lambda_{\text{max 1}}^{\text{film}}$ (nm) <sup>b</sup>	$\lambda_{\text{max 2}}^{\text{film}}$ (nm) <sup>b</sup>	$\lambda_{\text{onset}}^{\text{film}}$ (nm) <sup>b</sup>	$E_g^{\text{opt}}$ (eV) <sup>c</sup>
PCBT1	323	78300	456	60500	514	340	481	564	2.2
PCBT2	324	317300	465	303800	518	342	481	545	2.3
PCBT3	307	412900	462	146100	532	313	477	552	2.2
PCBT4	305	161000	447	52300	522	306	461	540	2.3

<sup>a</sup> Determined in ODCB solution (0.012 g.l<sup>-1</sup>); <sup>b</sup> Determined in film casted on glass from an ODCB solution (12 g.l<sup>-1</sup>); <sup>c</sup> Estimated from the onset point of the absorption edge in a film with the following formula:  $E_g^{\text{opt}} = \frac{1240}{\lambda(\text{nm})}$ .

The calculated extinction coefficients at the two absorption maxima ( $\epsilon_1$  and  $\epsilon_2$ ) were similar in the 2,7-linked polymers (**PCBT1** and **PCBT2**), whereas the 3,6-linked (**PCBT3** and **PCBT4**) demonstrated a much stronger absorption at shorter wavelengths ( $\epsilon_1 \gg \epsilon_2$ ). As the absorption peak at  $\lambda_{\max 2}$  is assigned to the ICT between Cz and BT units, it could be concluded that a stronger ICT takes place in the 2,7-linked polymers.

A red-shift in absorptions of 2,7-linked polymers was expected because of longer conjugation length. Indeed, it was reported that the 3,6-linkage induces conjugation breaks on the nitrogen atom, thus limiting the conjugation length and lowering the wavelength (see Figure 2 - 13).<sup>[21]</sup>

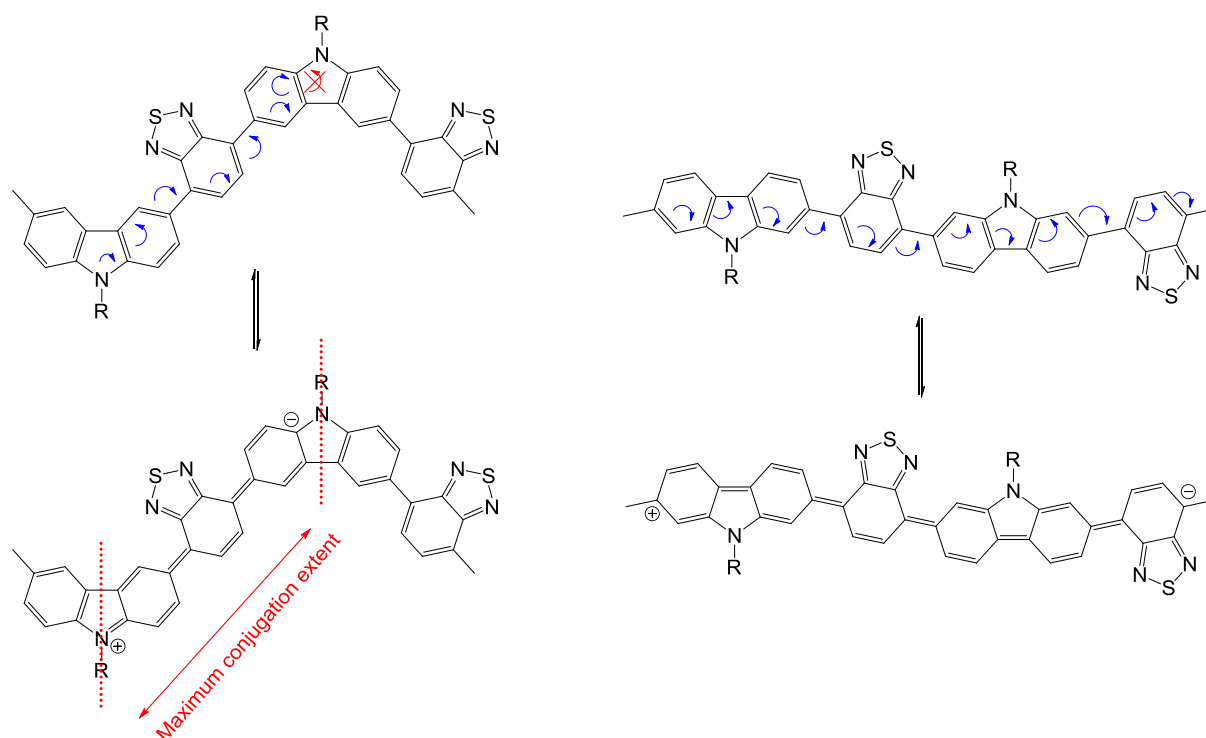


Figure 2 - 13: Representation of conjugation extent in 3,6- (left) and 2,7-linked (right) polymers.

This phenomenon was reported on polycarbazoles<sup>[7]</sup> and alternated copolymers of Cz and DTBT.<sup>[21]</sup> Such a red-shift was observed in case of the polymers with 9-heptadecanyl chains ( $\lambda_{\max 2}$  shifting from 447 nm to 465 nm), however, not in case of the dodecyl chains, where **PCBT1** shows a shorter  $\lambda_{\max 2}$  than **PCBT3**. It was assumed that the conjugation in **PCBT1** was not fully extended due to the oligomeric nature of the material ( $\overline{DP_n} = 3.8$ ).

The absorbance of the materials in solution did not demonstrate a strong dependence of the optical properties on the type of alkyl chain. As they provided a sufficient solubilization, the different geometries of the solubilizing groups had a negligible effect in solution and should influence the solid-state properties only.

Films of the materials were spin-coated from more concentrated ODCB solutions (12 g.l<sup>-1</sup>) onto glass substrates coated with PEDOT-PSS. It was reported that the absorption of conjugated polymers is red-shifted when comparing solid-state to solution due to intermolecular interactions such as  $\pi$ -stacking occurring in the films.<sup>[13, 21]</sup> Each material showed the anticipated red-shift in addition to a slight broadening. **PCBT1** showed the strongest shift ( $\lambda_{\max 2}^{\text{sol}} = 456$  nm and  $\lambda_{\max 2}^{\text{film}} = 481$  nm) due to two factors. Firstly, the 2,7-configuration of the backbone is more linear than the 3,6-, and thus is likely to provide a better arrangement. Secondly, intermolecular interactions are less hindered by the linear dodecyl groups than the bulky 9-heptadecanyl chains. This effect is even more pronounced when comparing the shift of  $\lambda_{\text{onset}}$  in solution and film. The optical band-gaps of the materials were estimated from the  $\lambda_{\text{onset}}$  of the solid-state absorptions according to the following equation:

$$E_g^{\text{opt}} = \frac{1240}{\lambda(\text{nm})}$$

Photoluminescence (PL) spectra of the identical solutions and films of PCBTs are shown in Figure 2 - 14 and data are listed in Table 2 - 9. In solution, it was observed that excitation at either  $\lambda_{\max 1}$  or  $\lambda_{\max 2}$  resulted in the same emission. Therefore, the below PL spectra were obtained from an excitation at  $\lambda_{\max 2}$ . An unexpected observation was the two-peaks emission shown by all materials, which indicated that light emission had two different origins. Firstly, the excited state could be localized on one unit (Cz or BT) and emission could result from this local excited state at short wavelengths ( $\lambda_{\max 1}$ ). Secondly, this local excited state could undergo an ICT, resulting in a structure having a smaller band-gap (see quinoid structure in Figure 2 - 13), thus leading to the long-wavelength emission peak ( $\lambda_{\max 2}$ ).

Structural differences between 2,7- and 3,6-carbazole units led to different energies of excited states, with more stabilized excited state for the 3,6-configuration due to the participation of the nitrogen atom (positive charges are more stabilized when localized on nitrogen). This results in shorter wavelength ( $\lambda_{\max 1}$ ) when comparing **PCBT1** and **PCBT2** (494 and 495 nm, respectively) with **PCBT3** and **PCBT4** (528 and 512 nm, respectively).

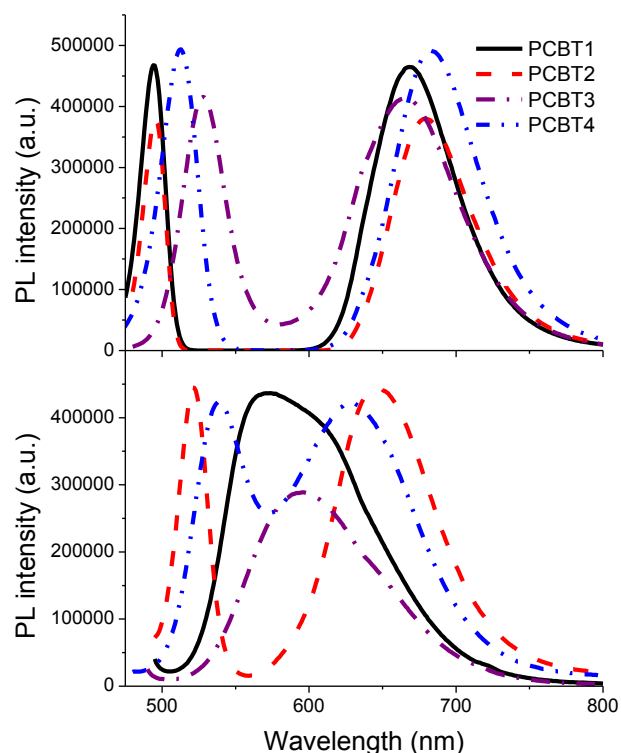


Figure 2 - 14: Photoluminescence (PL) spectra of PCBTs in ODCB solutions (top) and spin-coated films (bottom). Each PCBT was excited at  $\lambda_{\text{max}}$  determined in absorption spectra.

Table 2 - 9: PL data of PCBTs.

Polymer	Solution (ODCB)		Film	
	$\lambda_{\text{max 1}}^{\text{sol}}$ (nm) <sup>a</sup>	$\lambda_{\text{max 2}}^{\text{sol}}$ (nm) <sup>a</sup>	$\lambda_{\text{max 1}}^{\text{film}}$ (nm) <sup>b</sup>	$\lambda_{\text{max 2}}^{\text{film}}$ (nm) <sup>b</sup>
PCBT1	494	669	572	-
PCBT2	495	679	521	647
PCBT3	528	666	596	-
PCBT4	512	682	538	628

<sup>a</sup> Determined in ODCB solution (0.012 g.l<sup>-1</sup>); <sup>b</sup> Determined in film casted on glass from an ODCB solution (12 g.l<sup>-1</sup>).

In the solid-state the two emission peaks shifted towards each other, and they even merged in the case of polymers bearing linear alkyl chains (**PCBT1** and **PCBT3**, see **Error! Reference source not found.**). The intermolecular arrangement is considered to be responsible for this phenomenon. The stronger effect for **PCBT1** and **PCBT3** was consistent with enhanced intermolecular interactions when the carbazole units bear a linear side-chain.

To summarize, the synthesized polymers showed light absorption in the 300-550 nm region, which is suitable for harvesting light in the solar spectrum. Moreover, absorption and emission spectra in solid state highlighted the enhancement of intermolecular interactions by the 2,7-configuration and by the linear dodecyl chains.

### 2.3.3 ELECTROCHEMICAL PROPERTIES

The positions of the HOMO and LUMO energetic levels are important parameters when considering electronic applications. Cyclic voltammetry (CV) is a good way to measure the ionization potential and electron affinity, which are usually associated to the HOMO and LUMO levels, respectively. Therefore CV was performed under inert atmosphere using dichloromethane solutions of **PCBT1-4** (see experimental section), tetrabutylammonium hexafluorophosphate (TBAPF<sub>6</sub>) as electrolyte, silver for the reference electrode and the working and counter-electrode were made of platinum. As an example, the reduction and oxidation cyclic voltammograms of **PCBT3** are presented in Figure 2 - 15.

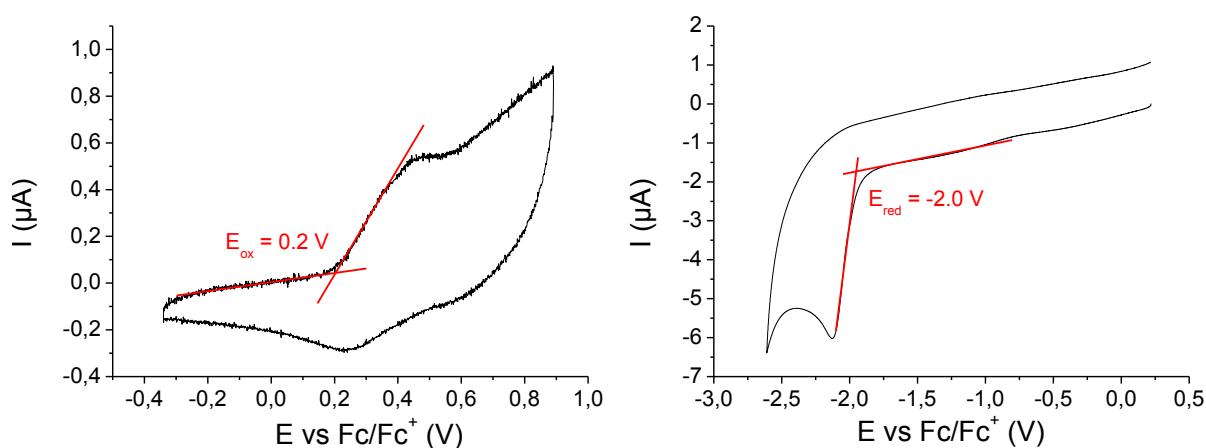


Figure 2 - 15: Cyclic voltammograms (left-oxidation, right-reduction) of PCBT3 in CH<sub>2</sub>Cl<sub>2</sub> solution (0.1 g.l<sup>-1</sup>).

The HOMO and LUMO levels could be determined from the onset of the oxidation and reduction peaks ( $E_{onset\ ox}$  and  $E_{onset\ red}$ ), respectively, using the following equations:

$$E_{HOMO}(eV) = -(E_{ox\ vs\ Fc/Fc^+}(V) + 4.8)$$

$$E_{LUMO}(eV) = -(E_{red\ vs\ Fc/Fc^+}(V) + 4.8)$$

Where 4.8 eV corresponds to the energetic position of the potential  $E_{1/2}$  for the ferrocene/ferrocene<sup>+</sup> (Fc/Fc<sup>+</sup>) redox couple, estimated from a ferrocene solution in dichloromethane using saturated calomel electrode as reference.<sup>[32]</sup> In Table 2 - 10 are shown the calculated values.

Table 2 - 10: CV data of PCBTs.

Polymer	$E_{HOMO}(eV)^a$	$E_{LUMO}(eV)^b$	$E_g^{CV}(eV)^c$	$E_g^{opt}(eV)^d$
PCBT1	-5.5	-3.0	2.5	2.4
PCBT2	-5.3	-3.0	2.3	2.4
PCBT3	-5.0	-2.8	2.2	2.3
PCBT4	-5.3	-3.0	2.3	2.4

<sup>a</sup> Calculated from the onset of the oxidation peak ( $E_{ox}$ ); <sup>b</sup> Calculated from the onset of the reduction peak ( $E_{red}$ );

<sup>c</sup> Calculated as following:  $E_g = E_{onset\ ox} - E_{onset\ red}$ ; <sup>d</sup> Optical band-gaps in solution calculated from  $\lambda_{onset}^{sol}$ .

The electrochemically and optically measured band-gaps in solution were in good agreement. The small differences observed between the electrochemical and optical values can be explained as the redox peaks result from localized sites instead of from the conjugated backbone.<sup>[33]</sup> Figure 2 - 16 shows the energetic repartition of the four materials compared to PCBM. Apart from **PCBT3**, the copolymers show low-lying HOMO compared to P3HT, which is desired to reach high values of open-circuit voltage in BHJ solar cells.<sup>[33]</sup>

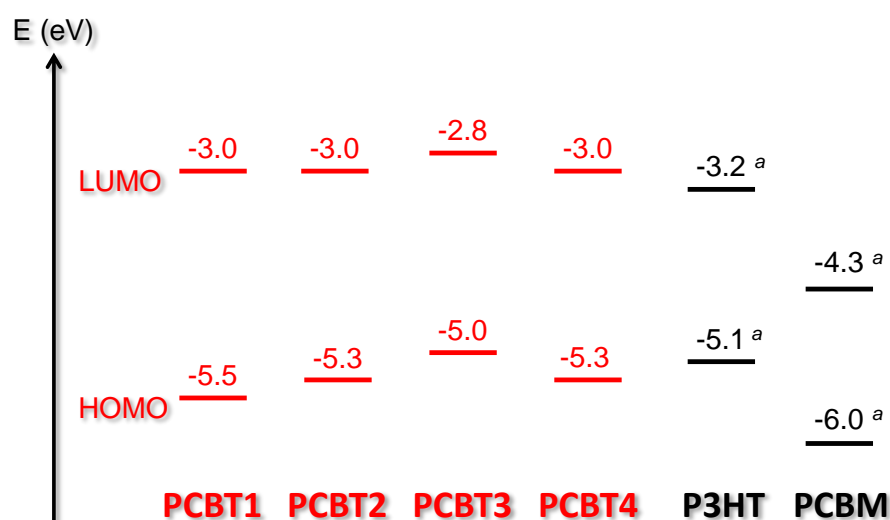


Figure 2 - 16: Energetic representation of the four PCBTs. <sup>a</sup> Values for P3HT and PCBM are from the literature.<sup>[34]</sup>

### 2.3.4 PHOTOVOLTAIC PERFORMANCES

Due to their low-lying HOMO levels, the synthesized PCBTs were considered as donor material in the active layer of bulk heterojunction (BHJ) solar cells with phenyl-C<sub>61</sub>-butyric acid methyl ester (PCBM) as acceptor material. The performance of a BHJ solar cell depends on the physical interaction of the donor and acceptor components. The target is to find the most suitable morphology of the active layer to avoid loss of energy through charge transport and maximize the efficiency of the device. In this sense, phase-separation, solubility and overall processability are among several aspects that must be addressed when fabricating the device. This may well lead to synthetic modifications in order to get the optimal characteristics. Hence, **PCBT1-4** were solubilized with PCBM at different ratios in ODCB, and subsequently spin-casted onto a glass substrate coated with a PEDOT-PSS layer, simulating conditions similar to the active layer in BHJ solar cells.

Optical properties of the blends were measured at first. In Figure 2 - 17 is presented the evolution of **PCBT2** absorption spectrum in solid state when blended with different ratio of PCBM. The quantity of polymer was kept constant in each blend. It can be observed that the addition of PCBM disturbed the arrangement of the polymer chains since a blue shift occurred in the low energy absorption peak

with increased ratio of PCBM. Additionally, the light absorption of PCBM induces an intensity increase of the high energy absorption peak. A similar evolution was found for the three other PCBTs (see experimental section).

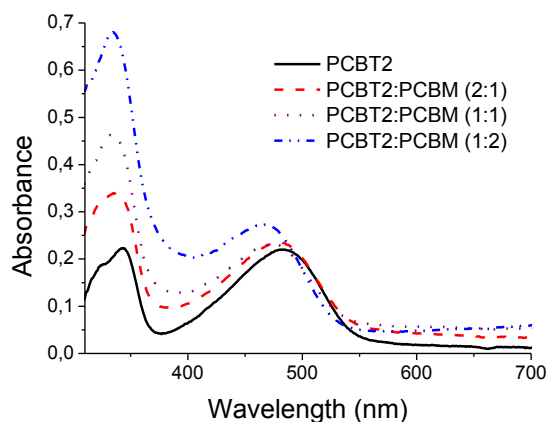


Figure 2 - 17: Solid-state light absorption of PCBT2:PCBM blends at different ratios, spin-coated from ODCB solutions onto PEDOT-PSS coated glass substrates.

Photoluminescence spectra of **PCBT2** and **PCBT2:PCBM** blends are shown in Figure 2 - 18. The blends were excited at the  $\lambda_{\text{max } 2}$  of absorption (461-481 nm, see Table 2 - 8), where PCBM only shows a very weak absorption. Presence of PCBM induced a strong decrease of the polymer fluorescence. This revealed a possible dissociation of photogenerated excitons in the semiconducting polymers by electron transfer to PCBM. Same behavior was observed in case of **PCBT1**, **3** and **4**. Although this is an encouraging result for BHJ solar cells application, this effect could also originate from an energy transfer between the polymer and PCBM.

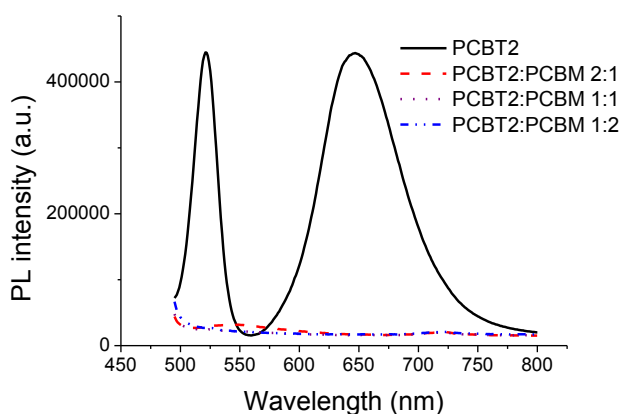


Figure 2 - 18: Solid-state PL of PCBT2:PCBM blends at different ratios, spin-coated from ODCB solutions onto PEDOT-PSS coated glass substrates. Excited at 481 nm.

In order to investigate the surface morphology and appearance of the donor-acceptor blend, images of the **PCBT1-4**/PCBM blends (1:1) were recorded by atomic force microscopy (AFM) and are shown in Figure 2 - 19.



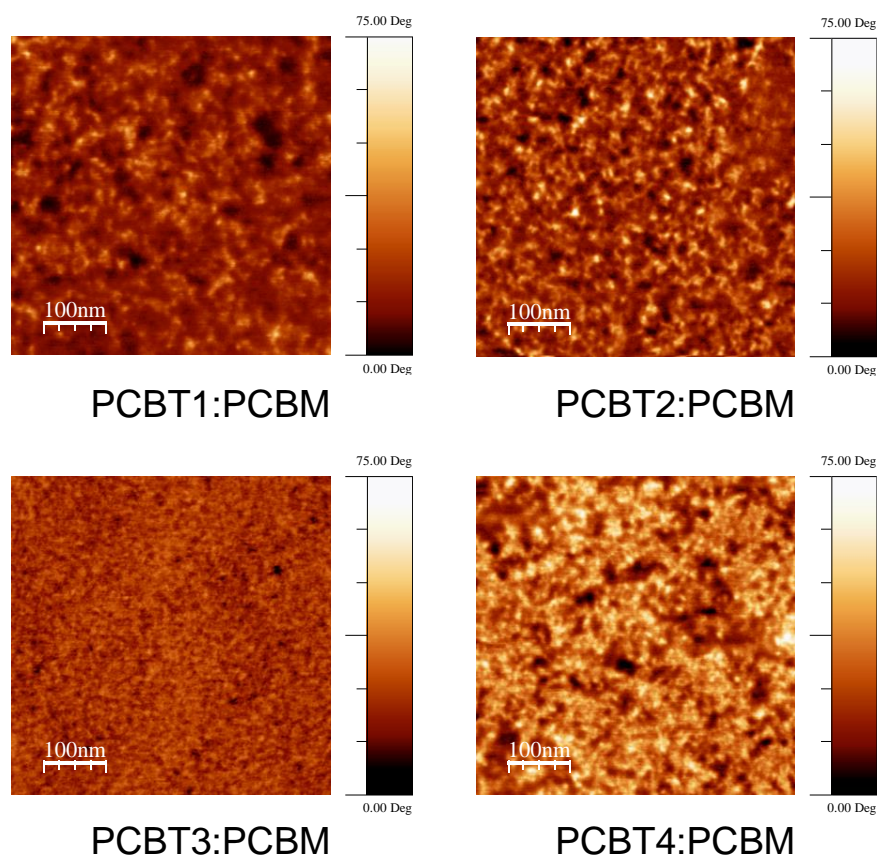


Figure 2 - 19: AFM phase images of the PCBT:PCBM blends with a 1:1 ratio.

A good contrast between two different materials was found, and domains up to 50 nm were observed, which confirmed strongly intermixed blends of the polymers with PCBM. This nanoscale phase separation is favourable for exciton dissociation and supported the findings from PL measurements. However, a weaker contrast as well as smaller domain size was observed in the case of **PCBT3**, which could be caused by a more homogeneous blend hindering the charge transport. Another explanation would be the main segregation of one material at the film surface.

These preliminary studies gave evidences of suitable properties of PCBTs for use as donor material in the active layer of BHJ solar cells. Therefore, photovoltaic devices with a direct architecture were fabricated under inert atmosphere (see experimental section). The polymers bearing linear chains (**PCBT1** and **3**) were selected in order to allow better intermolecular interactions in the blends. Measurements were carried out before and after annealing of the devices, which is known to influence the morphology of the device.

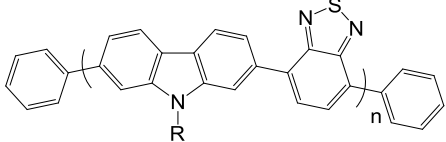
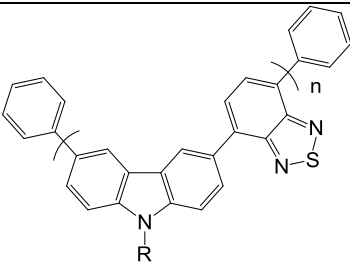
The first results in BHJ solar cells showed low efficiencies, mainly due to surprisingly low short-circuit currents ( $J_{SC}$ ). The hole mobility of the PCBTs could not be measured, but it is assumed that poor mobility are responsible for such values of  $J_{SC}$ . Indeed, evidences of efficient exciton dissociation in the blend were given previously, thus the limiting factor was probably a poor charge carrier mobility

of the materials and/or limited charge transport in the blend. The values observed for the open circuit voltage ( $V_{oc}$ ) were consistent with values obtained in the literature for similar materials.<sup>[18]</sup> However, devices based on **PCBT1** demonstrated lower  $V_{oc}$  than **PCBT3**, which was unexpected from the measured HOMO levels. Thermal annealing allowed in both case an increase of the  $J_{sc}$ , probably due to a better intermolecular arrangement in the donor material domains. Moreover, the previously recorded AFM images of the blends are representative of the surface only, and the observed morphology can differ from the bulk.

## 2.4 CONCLUSION

Four alternated conjugated oligomers of carbazole and benzothiadiazole (PCBT) were successfully synthesized by Suzuki polycondensation, presenting 2,7- or 3,6-linkage of the Cz units, and two different solubilizing groups. Their structures were confirmed by NMR, IR and SEC, and their thermal properties by DSC and TGA.

UV-visible absorbance and photoluminescence of the materials were measured, as well as their HOMO and LUMO level by cyclic voltammetry. Spectroscopic investigations highlighted the existence of a donor-acceptor ICT in the main chain, thus decreasing the band-gap of the material compared to homopolymers based on carbazole. Although their structural differences influenced their optical and electrochemical properties, the light absorptions of the four materials were similar, indicating the predominant role of the ICT over the electrons delocalization along the backbone.

Polymer		$E_{HOMO}$ (eV) <sup>a</sup>	$E_{LUMO}$ (eV) <sup>a</sup>	$E_g^{CV}$ (eV) <sup>a</sup>	$E_g^{opt\ film}$ (eV) <sup>b</sup>
	R = n-dodecyl ( <b>PCBT1</b> )	-5.5	-3.0	2.5	2.2
	R = 9-heptadecanyl ( <b>PCBT2</b> )	-5.3	-3.0	2.3	2.3
	R = n-dodecyl ( <b>PCBT3</b> )	-5.0	-2.8	2.2	2.2
	R = 9-heptadecanyl ( <b>PCBT4</b> )	-5.3	-3.0	2.3	2.3

<sup>a</sup> Determined by cyclic voltammetry in solution; <sup>b</sup> Optical band-gaps in film calculated from  $\lambda_{onset}^{film}$ .

Preliminary studies on blends of PCBTs and PCBM (AFM and fluorescence quenching) showed encouraging results for photovoltaic application. Unfortunately BHJ solar cells based on these materials still require an optimization work to demonstrate good efficiencies.

Despite the ICT, the band-gaps of the materials were not small enough compared to well-known polymers such as P3HT, therefore further design work on the monomer units should be carried out. An important twist angle may exist between the carbazole and benzothiadiazole moieties, hence insertion of spacers should be considered. The study of model oligomers or small molecules with controlled chain-length could also lead to more consistent and reliable data for this kind of system. Additionally, the use of electron-withdrawing and donating substituents (on the 3 and 6 positions of Cz unit in **PCBT1** and **2** for instance) could provide an interesting way to further tune the HOMO and LUMO levels.

## 2.5 BIBLIOGRAPHY

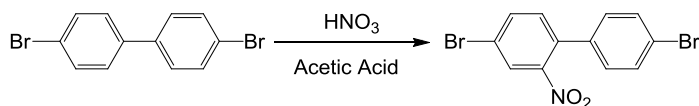
- [1] E. J. W. List, R. Guentner, P. Scanducci de Freitas, U. Scherf, *Advanced Materials* **2002**, *14*, 374-378.
- [2] A. Siove, D. Adès, *Polymer* **2004**, *45*, 4045-4049.
- [3] Q. Pei, Y. Yang, *Chemistry of Materials* **1995**, *7*, 1568-1575.
- [4] D. B. Romero, M. Schaer, M. Leclerc, D. Adès, A. Siove, L. Zuppiroli, *Synthetic Metals* **1996**, *80*, 271-277.
- [5] C. Beginn, J. V. Gražulevičius, P. Strohrriegl, J. Simmerer, D. Haarer, *Macromolecular Chemistry and Physics* **1994**, *195*, 2353-2370.
- [6] A. Iraqi, I. Wataru, *Chemistry of Materials* **2004**, *16*, 442-448.
- [7] A. Iraqi, I. Wataru, *Journal of Polymer Science Part A: Polymer Chemistry* **2004**, *42*, 6041-6051.
- [8] Z.-B. Zhang, M. Fujiki, H.-Z. Tang, M. Motonaga, K. Torimitsu, *Macromolecules* **2002**, *35*, 1988-1990.
- [9] D. Witker, J. R. Reynolds, *Macromolecules* **2005**, *38*, 7636-7644.
- [10] Y. Fu, Z. Bo, *Macromolecular Rapid Communications* **2005**, *26*, 1704-1710.
- [11] J. Huang, Y. Xu, Q. Hou, W. Yang, M. Yuan, Y. Cao, *Macromolecular Rapid Communications* **2002**, *23*, 709-712.
- [12] P. Ding, C. Zhong, Y. Zou, C. Pan, H. Wu, Y. Cao, *The Journal of Physical Chemistry C* **2011**, *115*, 16211-16219.
- [13] J.-F. Morin, M. Leclerc, *Macromolecules* **2002**, *35*, 8413-8417.
- [14] N. Blouin, A. Michaud, M. Leclerc, *Advanced Materials* **2007**, *19*, 2295-2300.
- [15] S. H. Park, M. Leclerc, A. J. Heeger, K. Lee, *Vol. 7416*, **2009**, pp. 74160P-74160P-74110.
- [16] J. S. Moon, J. Jo, A. J. Heeger, *Advanced Energy Materials* **2012**, *2*, 304-308.
- [17] J. Huang, Y. Niu, W. Yang, Y. Mo, M. Yuan, Y. Cao, *Macromolecules* **2002**, *35*, 6080-6082.
- [18] N. Berton, C. Ottone, V. Labet, R. de Bettignies, S. Bailly, A. Grand, C. Morell, S. Sadki, F. Chandezon, *Macromolecular Chemistry and Physics* **2011**, n/a-n/a.
- [19] J. Du, E. Xu, H. Zhong, F. Yu, C. Liu, H. Wu, D. Zeng, S. Ren, J. Sun, Y. Liu, A. Cao, Q. Fang, *Journal of Polymer Science Part A: Polymer Chemistry* **2008**, *46*, 1376-1387.
- [20] E. Wang, L. Hou, Z. Wang, Z. Ma, S. Hellström, W. Zhuang, F. Zhang, O. Inganäs, M. R. Andersson, *Macromolecules* **2011**, *44*, 2067-2073.
- [21] J. Kim, Y. S. Kwon, W. S. Shin, S. J. Moon, T. Park, *Macromolecules* **2011**, *44*, 1909-1919.
- [22] G. Zotti, G. Schiavon, S. Zecchin, J.-F. Morin, M. Leclerc, *Macromolecules* **2002**, *35*, 2122-2128.
- [23] J. Sakamoto, M. Rehahn, G. Wegner, A. D. Schlüter, *Macromolecular Rapid Communications* **2009**, *30*, 653-687.
- [24] H. Fujita, T. Michinobu, *Macromolecular Chemistry and Physics* **2012**, *213*, 447-457.
- [25] J.-F. Morin, M. Leclerc, D. Adès, A. Siove, *Macromolecular Rapid Communications* **2005**, *26*, 761-778.
- [26] E. S. H. Kang, J. D. Yuen, W. Walker, N. E. Coates, S. Cho, E. Kim, F. Wudl, *Journal of Materials Chemistry* **2010**, *20*, 2759-2765.
- [27] J. I. G. Cadogan, M. Cameron-Wood, R. K. Mackie, R. J. G. Searle, *Journal of the Chemical Society (Resumed)* **1965**, 4831-4837.
- [28] J. F. Morin, M. Leclerc, *Macromolecules* **2001**, *34*, 4680-4682.
- [29] J. K. Park, J. Jo, J. H. Seo, J. S. Moon, Y. D. Park, K. Lee, A. J. Heeger, G. C. Bazan, *Advanced Materials* **2011**, *23*, 2430-2435.
- [30] P. M. Beaujuge, C. M. Amb, J. R. Reynolds, *Accounts of Chemical Research* **2010**, *43*, 1396-1407.
- [31] T. Kanbara, T. Yamamoto, *Chemistry Letters* **1993**, *22*, 419-422.
- [32] C. M. Cardona, W. Li, A. E. Kaifer, D. Stockdale, G. C. Bazan, *Advanced Materials* **2011**, *23*, 2367-2371.
- [33] P. L. T. Boudreault, A. Najari, M. Leclerc, *Chemistry of Materials* **2011**, *23*, 456-469.
- [34] M. C. Scharber, D. Mühlbacher, M. Koppe, P. Denk, C. Waldauf, A. J. Heeger, C. J. Brabec, *Advanced Materials* **2006**, *18*, 789-794.



## 2.6 EXPERIMENTAL

### 2.6.1 SYNTHESIS AND STRUCTURAL CHARACTERIZATIONS

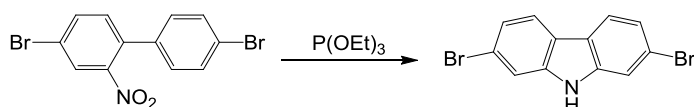
#### 4-4'-Dibromo-2-nitrobiphenyl (**1**)



4-4'-Dibromobiphenyl (5.06 g, 16.2 mmol) and 75 mL of glacial acetic acid were heated up to 100°C. Then a mixture of 25 mL of fuming nitric acid and 5 mL H<sub>2</sub>O was added dropwise and the reaction was allowed to stir for 30 min at reflux, then at room temperature for 16h. The yellow precipitate was collected by filtration, and recrystallized in ethanol to give a yellow solid (4.63 g, 80%).

m.p. 118°C. <sup>1</sup>H NMR (400 MHz, CDCl<sub>3</sub>): δ (ppm) 8.06 (d, *J* = 2.0 Hz, 1H), 7.79 (dd, *J* = 8.3, 2.0 Hz, 1H), 7.58 (m, 2H), 7.32 (d, *J* = 8.3 Hz, 1H), 7.19 (m, 2H). <sup>13</sup>C NMR (101 MHz, CDCl<sub>3</sub>): δ (ppm) 135.70, 135.44, 134.28, 133.17, 132.18, 129.56, 129.07, 127.42, 123.23, 121.99. FT-IR (ATR): ν = 3091, 3073, 2913, 2848, 1694, 1591, 1518, 1463, 1342, 1262, 1151, 1097, 1071, 1000, 885, 872, 846, 810, 761, 706, 599, 542 cm<sup>-1</sup>.

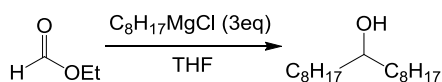
#### 2,7-Dibromocarbazole (**2**)



The previously prepared 4-4'-dibromo-2-nitrobiphenyl **1** (4.16 g, 12 mmol) and 25 mL of triethylphosphite (155 mmol) were refluxed for 24h under argon. Then the excess triethylphosphite was removed by distillation. Flash chromatography of the raw product (cyclohexane first, then cyclohexane/ethyl acetate 19:1) gave white crystals (3.00 g, 79%).

m.p. 229°C. <sup>1</sup>H NMR (400 MHz, CDCl<sub>3</sub>): δ (ppm) 8.04 (br s, 1H), 7.87 (d, *J* = 8.3 Hz, 2H), 7.56 (d, *J* = 1.6 Hz, 2H), 7.36 (dd, *J* = 8.3, 1.7 Hz, 2H). <sup>13</sup>C NMR (101 MHz, CDCl<sub>3</sub>): δ (ppm) 140.41, 123.44, 121.91, 121.61, 119.88, 113.96. FT-IR (ATR): ν = 3071, 2969, 1538, 1449, 1423, 1315, 1230, 1055, 997, 919, 842, 786, 667, 588 cm<sup>-1</sup>.

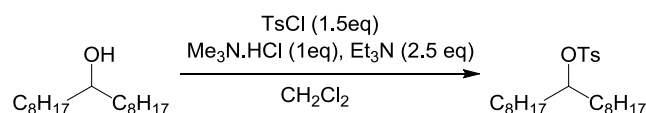
#### Heptadecan-9-ol (**3**)



Ethyl formate (7.40 g, 0.1 mol) and 150 ml of dry THF were added to a flame-dried 500 ml round-bottom flask and stirred under Ar. The solution was cooled down to  $-78^{\circ}\text{C}$  and 150 ml of a 2M octylmagnesium chloride solution in THF (0.3 mol) was added dropwise through a burette for 1h. The reaction mixture was then allowed to come back to room temperature overnight and poured in a mixture of 100 ml of MeOH and 100 ml of saturated aqueous ammonium chloride. The mixture was extracted three times with 100 ml of diethyl ether, washed with brine and dried over  $\text{MgSO}_4$ . After solvent evaporation, the crude product was distilled under vacuum (b.p.  $130^{\circ}\text{C}$  at 0,45 mmHg) to get a white solid (21.33 g, 83%).

m.p.  $62^{\circ}\text{C}$ .  $^1\text{H}$  NMR (400 MHz,  $\text{CDCl}_3$ ):  $\delta$  (ppm) 3.58 (m, 1H), 1.52 – 1.19 (m, 30H), 0.88 (t,  $J = 6.9$  Hz, 6H).  $^{13}\text{C}$  NMR (101 MHz,  $\text{CDCl}_3$ ):  $\delta$  (ppm) 72.18, 37.65, 32.04, 29.87, 29.75, 29.43, 25.81, 22.82, 14.25. FT-IR (ATR):  $\nu = 3307, 2956, 2917, 2872, 2848, 1466, 1376, 1352, 1135, 1089, 1054, 1026, 986, 895, 848, 795, 720, 667, 603\text{ cm}^{-1}$ .

#### **Heptadecan-9-yl-4-methylbenzenesulfonate (4)**



Heptadecan-9-ol **3** (20.00 g, 78 mmol), trimethylamine hydrochloride (7.45 g, 78 mmol), triethylamine (19.73 g, 195 mmol) and 80 ml of  $\text{CH}_2\text{Cl}_2$  were cooled down to  $0^{\circ}\text{C}$ , and *p*-toluenesulfonyl chloride (22.30 g, 117 mmol) in 80 ml of  $\text{CH}_2\text{Cl}_2$  was added dropwise through an addition funnel for 30 min. The mixture was allowed to come back to room temperature for 2h, and then quenched with 200 ml of water. The two phases were separated, the aqueous layer was extracted two times with 50 ml of  $\text{CH}_2\text{Cl}_2$ . Organic phases were combined, dried with  $\text{MgSO}_4$  and solvent was evaporated. The crude product was purified by flash chromatography (cyclohexane/ethyl acetate 19:1) to give an oil which turned into a white solid within few hours (28.60 g, 89%).

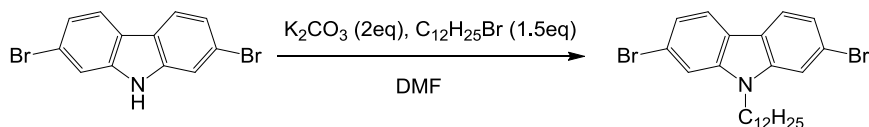
m.p.  $< 50^{\circ}\text{C}$ .  $^1\text{H}$  NMR (400 MHz,  $\text{CDCl}_3$ ):  $\delta$  (ppm) 7.78 (d,  $J = 8.3$  Hz, 2H), 7.31 (d,  $J = 8.0$  Hz, 2H), 4.53 (p,  $J = 6.0$  Hz, 1H), 2.43 (s, 1H), 1.63 – 1.47 (m, 4H), 1.34 – 1.10 (m, 24H), 0.87 (t,  $J = 7.0$  Hz, 6H).  $^{13}\text{C}$  NMR (101 MHz,  $\text{CDCl}_3$ ):  $\delta$  (ppm) 144.38, 134.97, 129.74, 127.85, 84.78, 70.82, 34.26, 31.97, 29.48, 29.42, 29.28, 24.81, 22.78, 21.71, 14.23. FT-IR (ATR):  $\nu = 2954, 2923, 2852, 1598, 1521, 1495, 1465, 1354, 1305, 1173, 1097, 1020, 895, 816, 766, 720, 662, 575, 554\text{ cm}^{-1}$ .

#### **General procedure for dibromocarbazole alkylation with n-dodecyl chain**

Dibromocarbazole (1eq), powdered potassium carbonate (2eq) and DMF were added in a round-bottom flask. The mixture was stirred at  $80^{\circ}\text{C}$  under argon, and 1-bromododecane (1.5eq) was added

dropwise. The mixture was stirred for 16h. The crude product was extracted with diethyl ether. The combined organic phases were washed with water and dried over  $\text{MgSO}_4$ . Solvent was removed under vacuum. The crude compound was finally purified by flash chromatography (eluent: cyclohexane first, then cyclohexane/ethyl acetate 90/10).

### **N-dodecyl-2,7-dibromocarbazole (5)**



Starting from 2,7-dibromocarbazole **2** (1.00 g, 3.1 mmol). The reaction product was obtained as white crystals (0.704 g, 47%).

m.p. 70°C.  $^1\text{H}$  NMR (400 MHz,  $\text{CDCl}_3$ ):  $\delta$  (ppm) 7.88 (d,  $J$  = 8.3 Hz, 2H), 7.52 (d,  $J$  = 1.5 Hz, 2H), 7.34 (dd,  $J$  = 8.3, 1.7 Hz, 2H), 4.18 (t,  $J$  = 7.4 Hz, 2H), 1.89 – 1.77 (m, 2H), 1.42 – 1.17 (m, 18H), 0.88 (t,  $J$  = 6.9 Hz, 3H).  $^{13}\text{C}$  NMR (101 MHz,  $\text{CDCl}_3$ ):  $\delta$  (ppm) 141.51, 122.66, 121.61, 121.42, 119.83, 112.16, 43.50, 32.05, 29.74, 29.70, 29.63, 29.47, 28.91, 27.31, 14.27. FT-IR (ATR):  $\nu$ =2917, 2847, 1586, 1447, 1423, 1314, 1239, 1223, 1129, 1052, 997, 911, 832, 818, 792, 721, 593  $\text{cm}^{-1}$ . HRMS ( $\text{EI}^+$ ,  $m/z$ ) [ $\text{M}$ ] $^+$  calculated for  $\text{C}_{24}\text{H}_{31}\text{Br}_2\text{N}$ : 491.0823, found 491.0815.

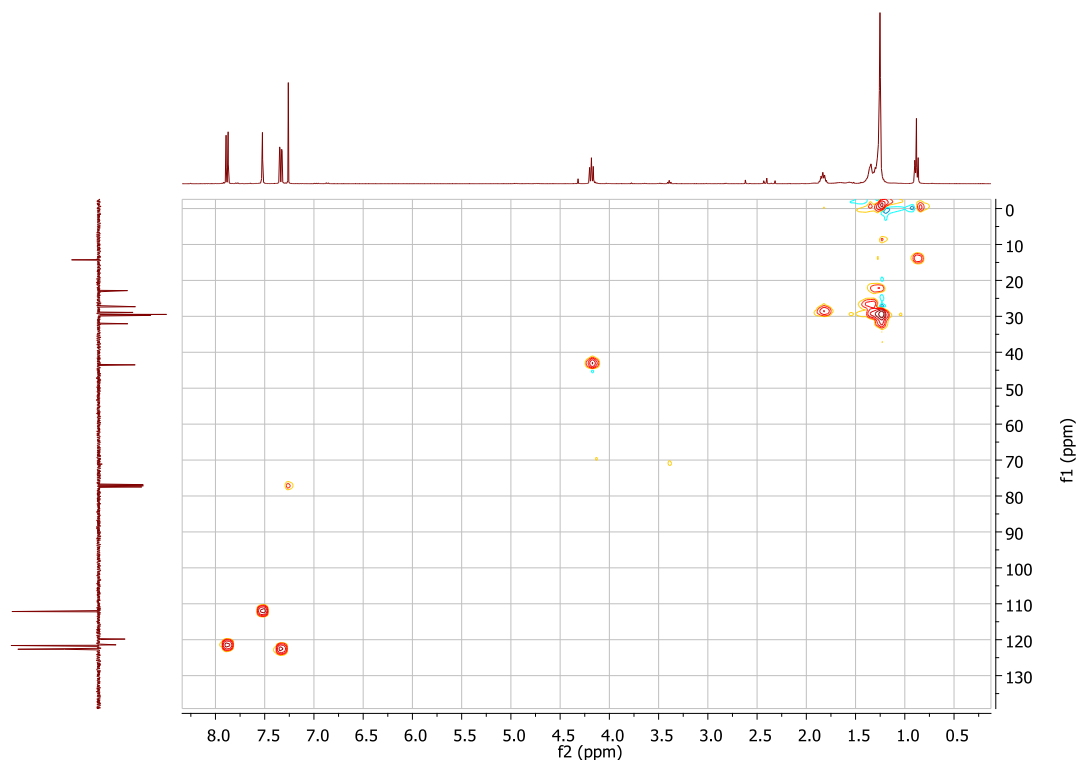


Figure 2 - 20:  $^1\text{H}$ - $^{13}\text{C}$  HSQC NMR spectra (400 MHz) of **5** in  $\text{CDCl}_3$ .



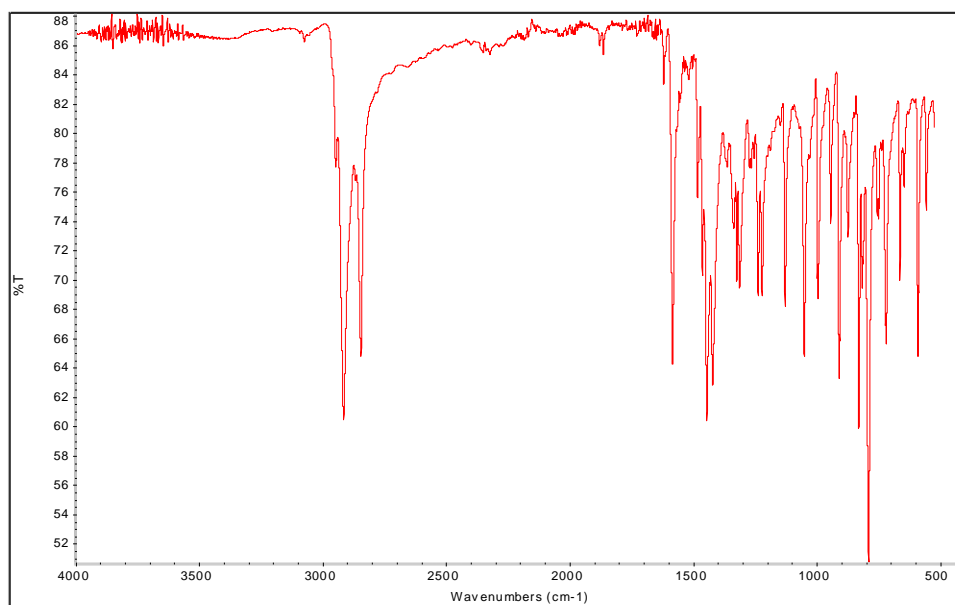
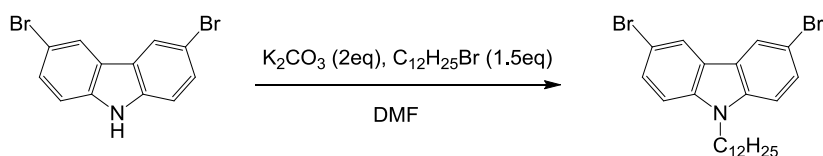


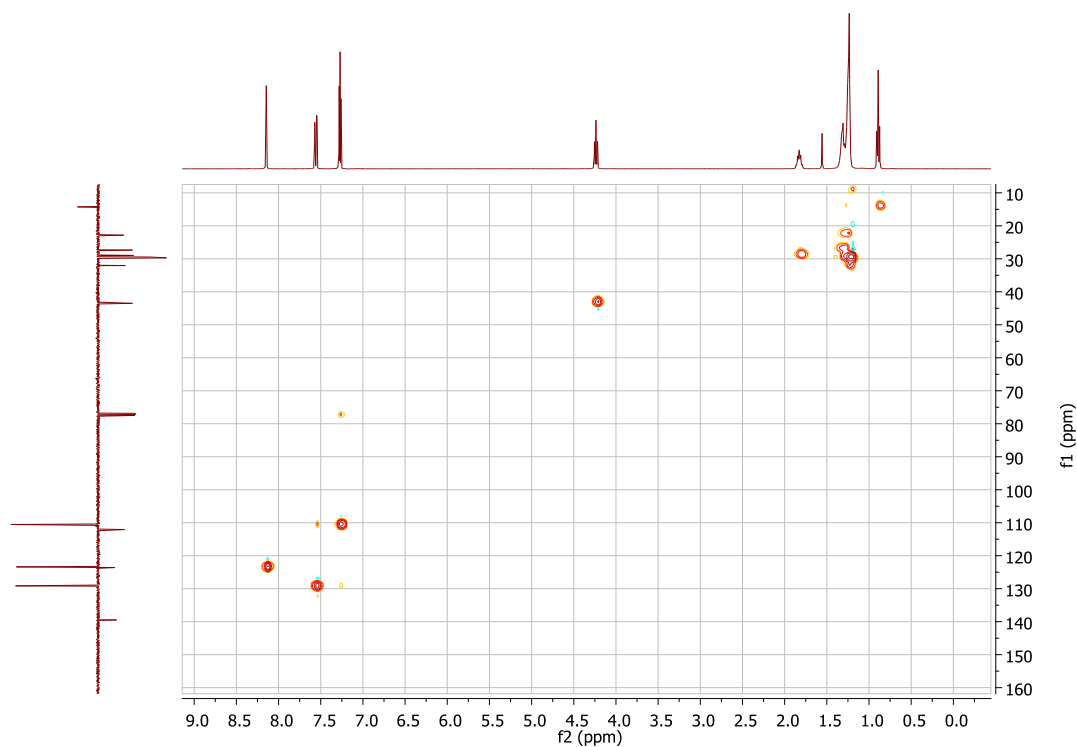
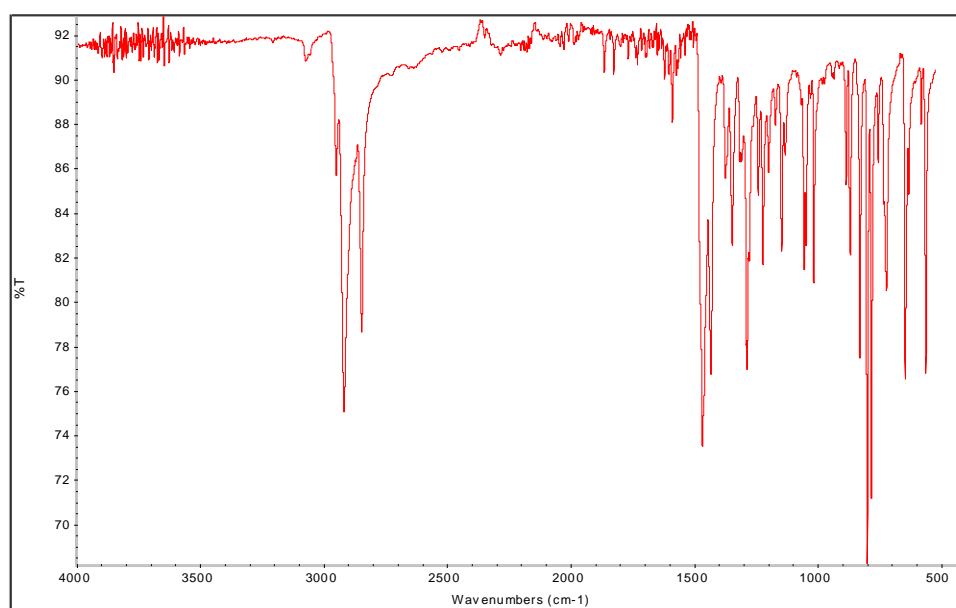
Figure 2 - 21: IR spectrum (ATR) of 5.

**N-dodecyl-3,6-dibromocarbazole (6)**

Starting from commercially available 3,6-dibromocarbazole (6.600 g, 20.3 mmol). The reaction product was obtained as white crystals (5.503 g, 55%).

m.p. 68°C.  $^1\text{H}$  NMR (400 MHz,  $\text{CD}_2\text{Cl}_2$ ):  $\delta$  (ppm) 8.15 (d,  $J = 1.9$  Hz, 2H), 7.57 (dd,  $J = 8.7$  Hz, 2.0 Hz, 2H), 7.32 (d,  $J = 8.7$  Hz, 2H), 4.25 (t,  $J = 7.2$  Hz, 2H), 1.83 (m, 2H), 1.28 (m, 18H), 0.88 (t,  $J = 6.9$  Hz, 3H).

$^{13}\text{C}$  NMR (101 MHz,  $\text{CDCl}_3$ ):  $\delta$  (ppm) 139.46, 129.14, 123.59, 123.40, 112.07, 110.53, 43.50, 32.05, 29.72, 29.66, 29.59, 29.47, 28.98, 22.83, 14.27. FT-IR (ATR):  $\nu = 2919, 2847, 1469, 1434, 1288, 1224, 1148, 1057, 1017, 870, 831, 802, 785, 724, 648, 564$   $\text{cm}^{-1}$ . HRMS (EI+,  $m/z$ )  $[\text{M}]^+$  calculated for  $\text{C}_{24}\text{H}_{31}\text{Br}_2\text{N}$ : 491.0823, found 491.0810.

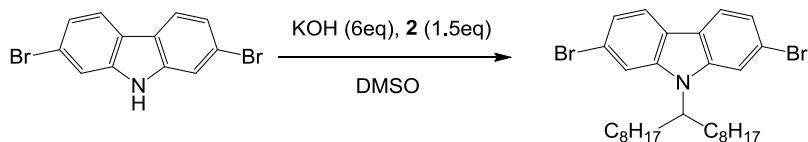
Figure 2 - 22:  $^1\text{H}$ - $^{13}\text{C}$  HSQC NMR spectra (400 MHz) of **6** in  $\text{CDCl}_3$ .Figure 2 - 23: IR spectrum (ATR) of **6**.

### **General procedure for dibromocarbazole alkylation with 9-heptadecanyl chain**

Dibromocarbazole (1eq), powdered potassium hydroxide (6eq) and DMSO were added in a round-bottom flask. The mixture was stirred at room temperature under argon, and a solution of heptadecan-9-yl-4-methylbenzenesulfonate **2** (1.5eq) dissolved in DMSO was added dropwise. The mixture was stirred for 20h at room temperature, and quenched by addition of water. The mixture was extracted with cyclohexane. The combined organic phases were washed with water and dried

over  $\text{MgSO}_4$ . The solvent was removed under vacuum. The crude compound was finally purified by flash chromatography (cyclohexane).

### **N-9-heptadecanyl-2,7-dibromocarbazole (7)**



Starting from 2,7-dibromocarbazole **2** (1.00 g, 3.1 mmol). The reaction product was obtained as a white solid (1.038 g, 58%).

m.p.  $73^\circ\text{C}$ .  $^1\text{H}$  NMR (400 MHz,  $\text{CDCl}_3$ ):  $\delta$  (ppm) 7.90 (t,  $J = 9.4$  Hz, 2H), 7.69 (s, 1H), 7.54 (s, 1H), 7.33 (d,  $J = 3.7$  Hz, 2H), 4.42 (tt,  $J = 10.2, 5.1$  Hz, 1H), 2.26 – 2.13 (m, 1H), 1.96 – 1.84 (m, 1H), 1.31 – 1.07 (m, 11H), 1.04 – 0.91 (m, 1H), 0.83 (t,  $J = 7.0$  Hz, 3H).  $^{13}\text{C}$  NMR (101 MHz,  $\text{CDCl}_3$ ):  $\delta$  (ppm) 143.06, 139.59, 122.47, 121.62, 121.36, 120.98, 119.91, 114.68, 112.31, 57.10, 33.62, 31.88, 29.42, 29.40, 29.25, 26.87, 22.74, 14.20. FT-IR (ATR):  $\nu = 2918, 2850, 1585, 1450, 1421, 1331, 1235, 1218, 1131, 1058, 999, 922, 790, 721, 669, 607\text{ cm}^{-1}$ . HRMS (EI+,  $m/z$ )  $[\text{M}]^+$  calculated for  $\text{C}_{29}\text{H}_{41}\text{Br}_2\text{N}$ : 561.1606, found 561.1601.

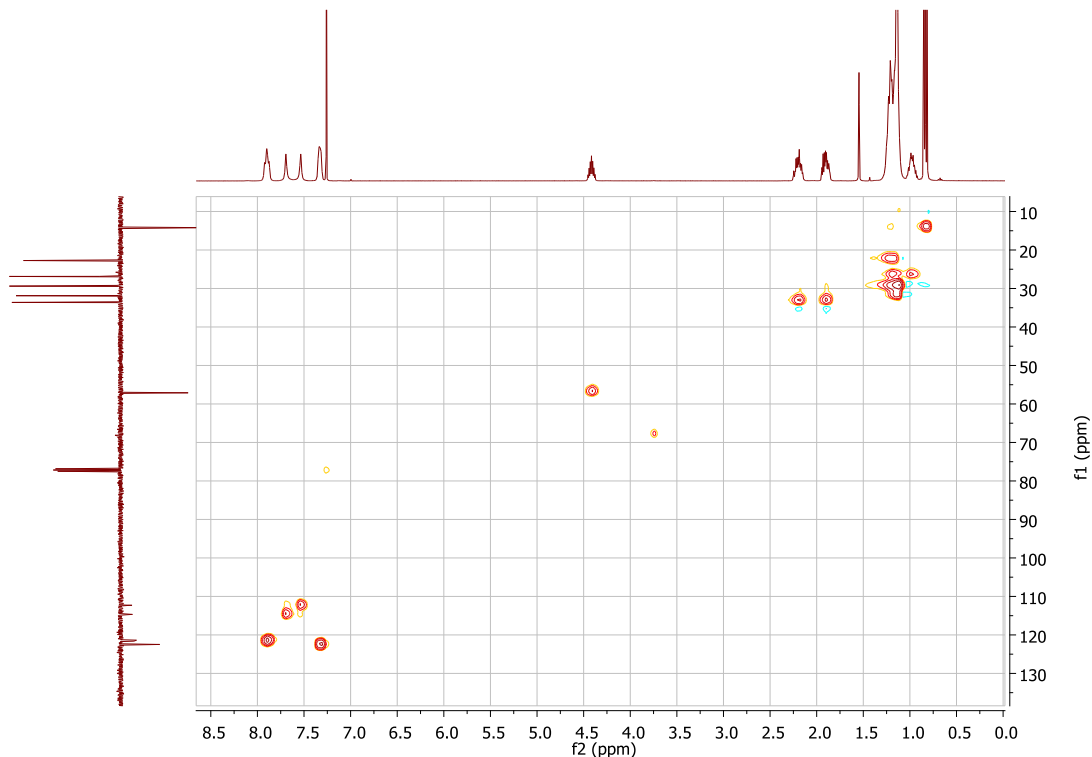


Figure 2 - 24:  $^1\text{H}$ - $^{13}\text{C}$  HSQC NMR spectra (400 MHz) of **7** in  $\text{CDCl}_3$ .

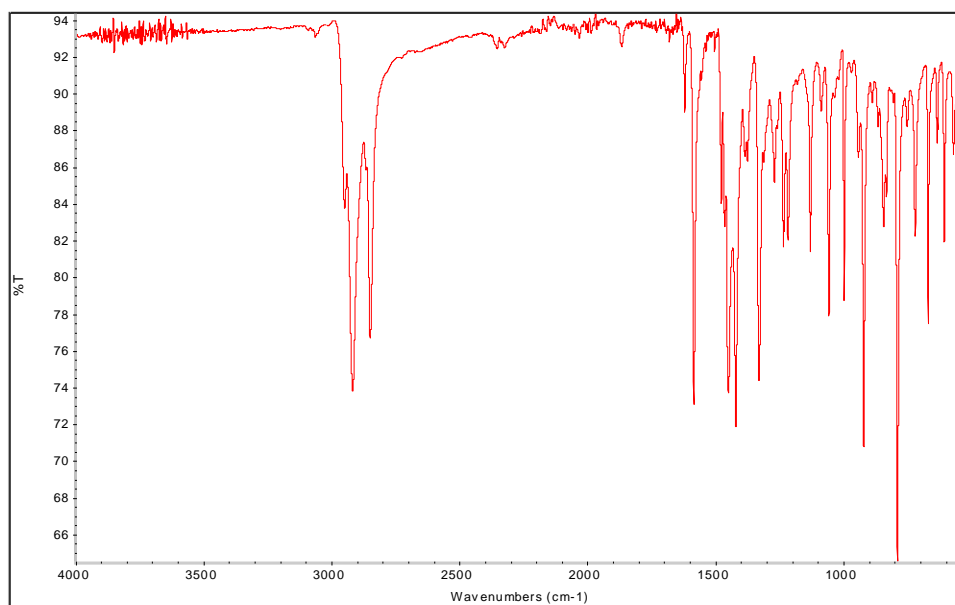


Figure 2 - 25: IR spectrum (ATR) of 7.

**N-9-heptadecanyl-3,6-dibromocarbazole (8)**

Starting from commercially available 3,6-dibromocarbazole (3.00 g, 9.2 mmol). The reaction product was obtained as a white solid (4.00 g, 77%).

m.p. 55°C.  $^1\text{H}$  NMR (400 MHz,  $\text{CDCl}_3$ ):  $\delta$  (ppm) 8.15 (d,  $J$  = 8.6 Hz, 2H), 7.57 – 7.27 (m, 4H), 4.47 (tt,  $J$  = 10.1, 4.9 Hz, 1H), 2.27 – 2.15 (m, 2H), 1.94 – 1.82 (m, 2H), 1.38 – 1.03 (m, 22H), 0.99 – 0.86 (m, 2H), 0.83 (t,  $J$  = 7.1 Hz, 6H).  $^{13}\text{C}$  NMR (101 MHz,  $\text{CDCl}_3$ )  $\delta$  (ppm) 141.07, 137.53, 130.06, 129.14, 128.71, 124.65, 123.48, 123.14, 113.18, 112.05, 111.76, 110.66, 56.97, 33.77, 31.86, 29.41, 29.39, 29.23, 26.80, 22.72, 14.19. FT-IR (ATR):  $\nu$  = 2921, 2849, 1469, 1438, 1284, 1220, 1061, 1016, 863, 824, 801, 794, 723, 635, 552, 538  $\text{cm}^{-1}$ . HRMS (EI+,  $m/z$ )  $[\text{M}]^+$  calculated for  $\text{C}_{29}\text{H}_{41}\text{Br}_2\text{N}$ : 561.1606, found 561.1599.

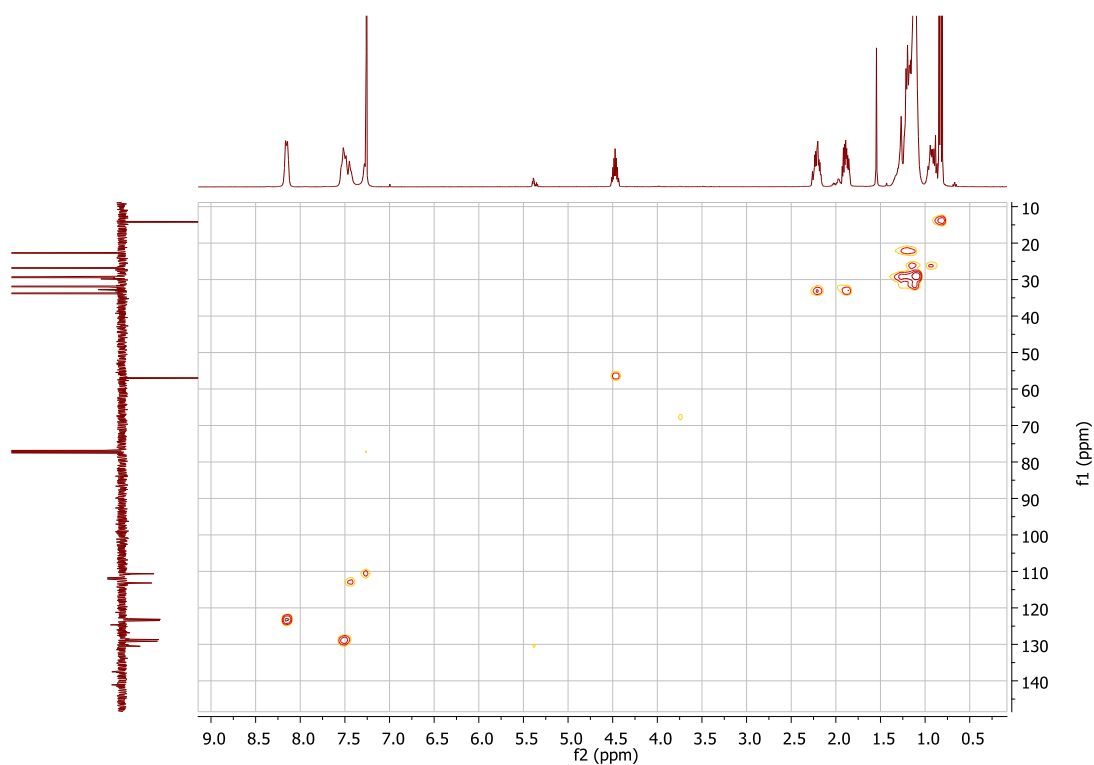
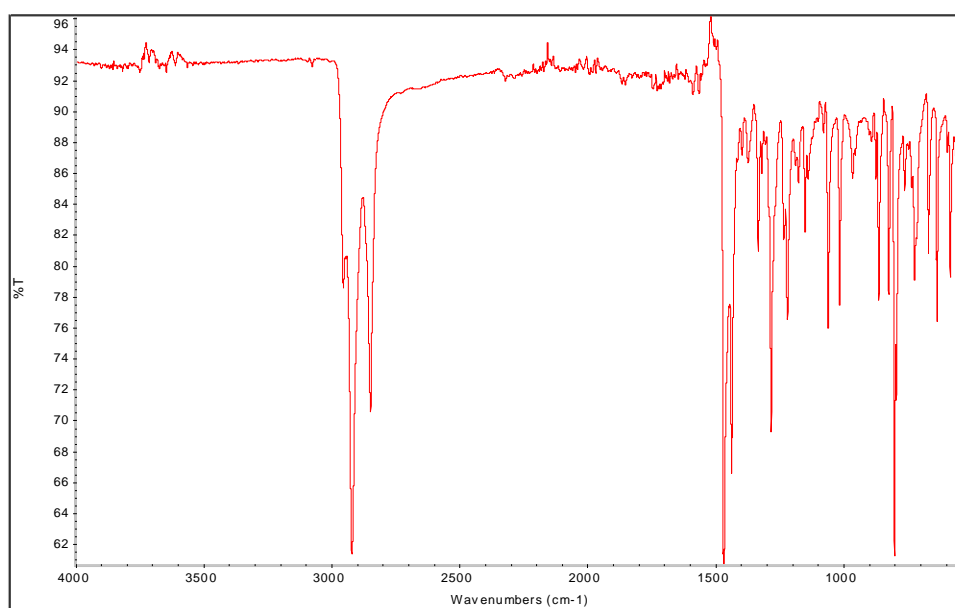
Figure 2 - 26:  $^1\text{H}$ - $^{13}\text{C}$  HSQC NMR spectra (400 MHz) of 8 in  $\text{CDCl}_3$ .

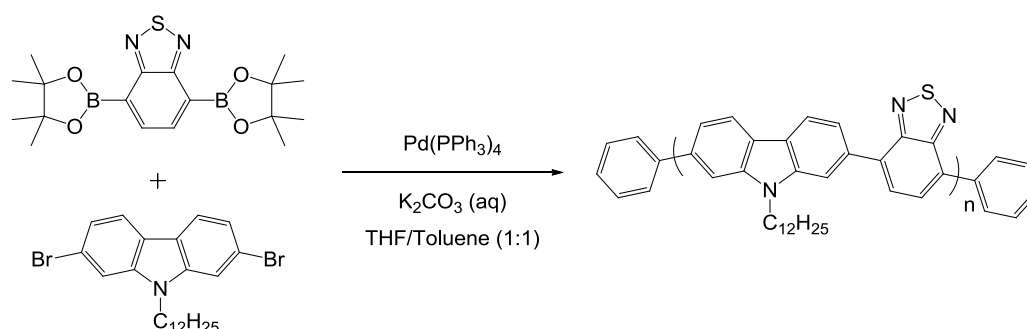
Figure 2 - 27: IR spectrum (ATR) of 8.

### **General procedure for polymerization of carbazole monomers 5-8**

Dibromocarbazole (0.5 mmol), 2,1,3-Benzothiadiazole-4,7-bis(boronic acid pinacol ester) (194 mg, 0.5 mmol) and tetrakis(triphenylphosphine)palladium(0) (15 mg, 0.013 mmol) were dissolved in 10 mL of a degassed THF/toluene mixture (1:1 vol) in a 50 mL round-bottom flask, followed by several cycles vacuum/argon. Then, 10 mL of a degassed 2 M potassium carbonate aqueous solution was added. The reaction was refluxed under argon for 24h. Afterwards, bromobenzene (6  $\mu\text{L}$ , 0.05 mmol)

in 1 mL of a degassed THF/toluene mixture (1:1 vol) was added. The reaction was allowed to stir at reflux for 6h, and benzeneboronic acid (12 mg, 0.1 mmol) in 1 mL of a degassed THF/toluene mixture (1:1 vol) was added, followed by stirring under reflux for 16h. The reaction mixture was then poured into 200 mL of methanol. The orange precipitate was collected by filtration, rinsed with water and methanol, followed by purification on Soxhlet apparatus (methanol, pentane and THF). The THF fraction was precipitated in methanol. The resulting solid was recovered by filtration and dried under vacuum at 40°C overnight.

**Poly(N-dodecyl-2,7-carbazole-*alt*-benzothiadiazole) (PCBT1)**



Starting from N-dodecyl-2,7-dibromocarbazole **5** (247 mg, 0.5 mmol). The final product was obtained as an orange powder (102 mg, 44%).

$^1\text{H}$  NMR (400 MHz,  $\text{CDCl}_3$ ):  $\delta$  (ppm) 8.48 – 7.35 (m, 8H), 4.49 (br, 2H), 2.13 – 1.78 (br, 2H), 1.73 – 0.95 (br, 18H), 0.92 – 0.62 (br, 3H). Due to a too small quantity of material available, a  $^{13}\text{C}$  NMR spectrum could not be obtained. FT-IR (ATR):  $\nu$ = 2920, 2851, 1454, 1434, 1335, 1258, 1094, 1020, 874, 843, 800, 754, 724, 695  $\text{cm}^{-1}$ .

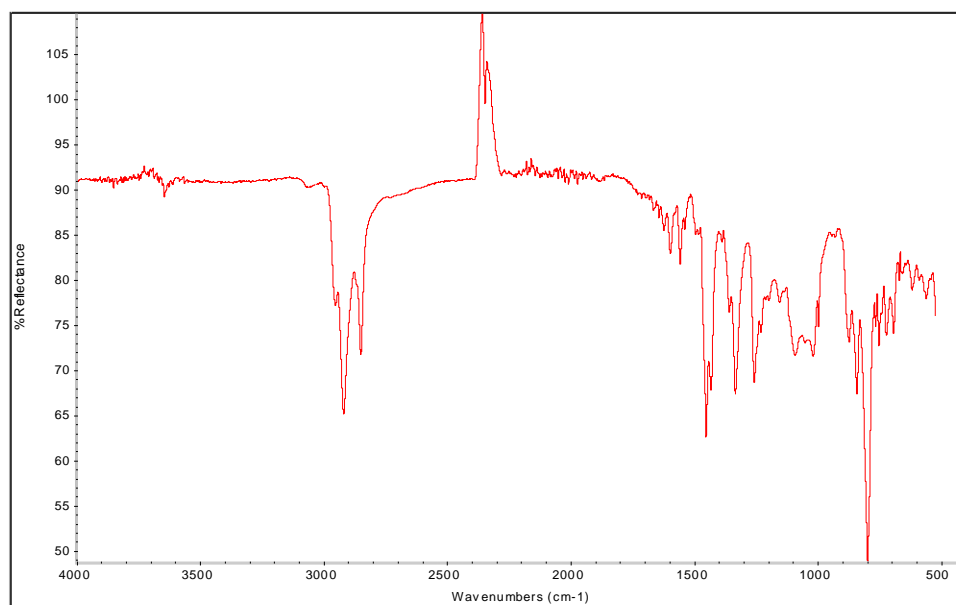
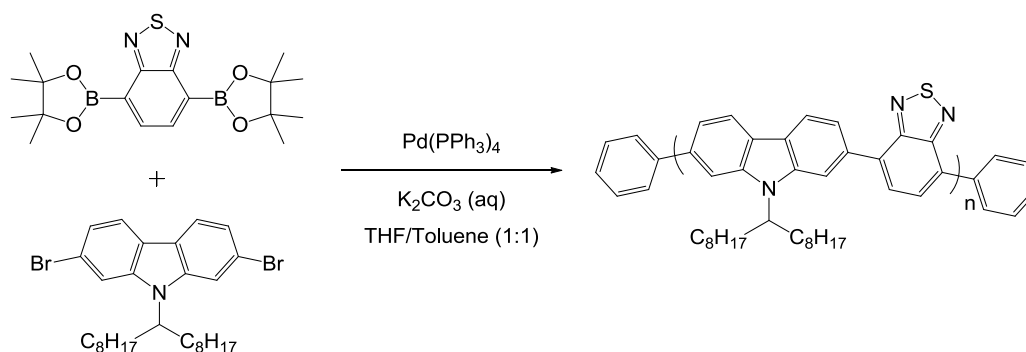


Figure 2 - 28: IR spectrum (ATR) of PCBT1.

**Poly(N-9-heptadecanyl-2,7-carbazole-*alt*-benzothiadiazole) (PCBT2)**



Starting from N-9-heptadecanyl-2,7-dibromocarbazole **7** (283 mg, 0.5 mmol). The final product was obtained as an orange powder (145 mg, 54%).

$^1\text{H}$  NMR (400 MHz,  $\text{CDCl}_3$ ):  $\delta$  (ppm) 8.48 – 7.38 (m, 8H), 4.81 (br s, 1H), 2.45 (br, 2H), 2.12 (br, 2H), 1.47 – 0.95 (m, 24H), 0.81 (t,  $J = 5.6$  Hz, 6H).  $^{13}\text{C}$  NMR (101 MHz,  $\text{CDCl}_3$ ):  $\delta$  (ppm) 154.76, 143.19, 139.87, 135.52, 134.94, 134.38, 132.43, 132.33, 129.43, 128.81, 128.54, 120.85, 120.61, 120.46, 113.44, 110.63, 34.11, 31.95, 29.65, 29.55, 29.41, 27.09, 22.75, 14.20. FT-IR (ATR):  $\nu = 2922, 2851, 1594, 1557, 1455, 1434, 1334, 1220, 1112, 1059, 999, 881, 842, 800, 754, 724, 657, 611, 557\text{ cm}^{-1}$ .

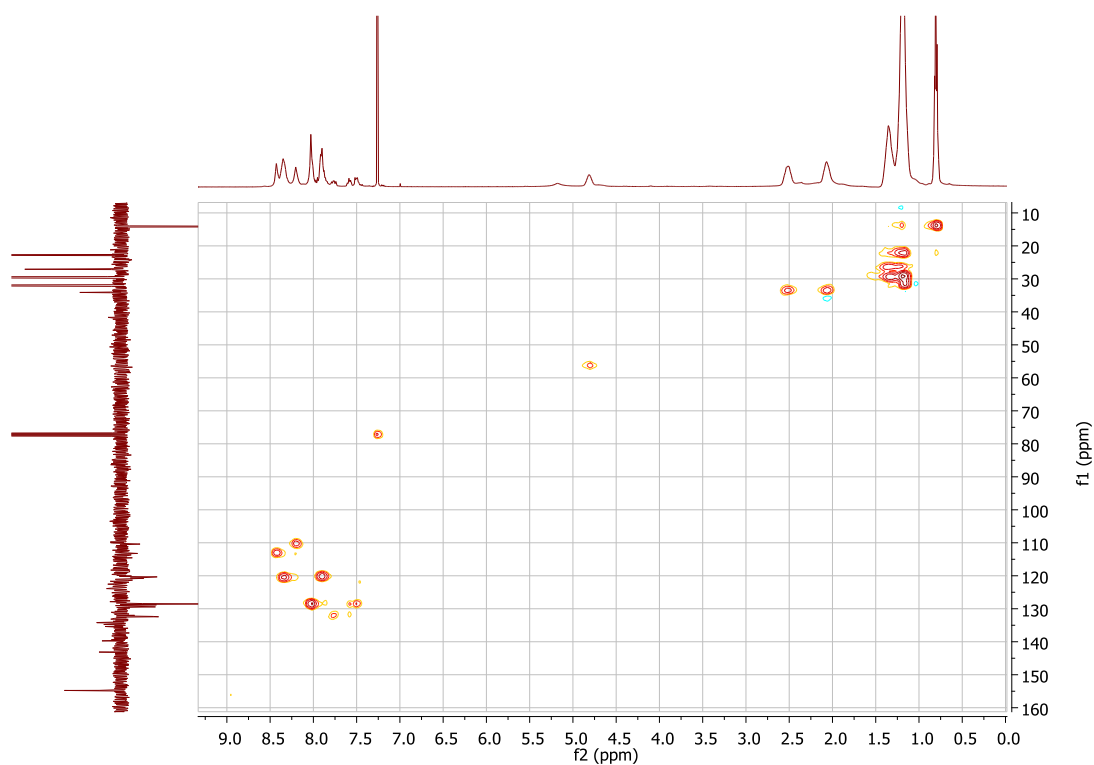


Figure 2 - 29:  $^1\text{H}$ - $^{13}\text{C}$  HSQC NMR spectra (400 MHz) of PCBT2 in  $\text{CDCl}_3$ .

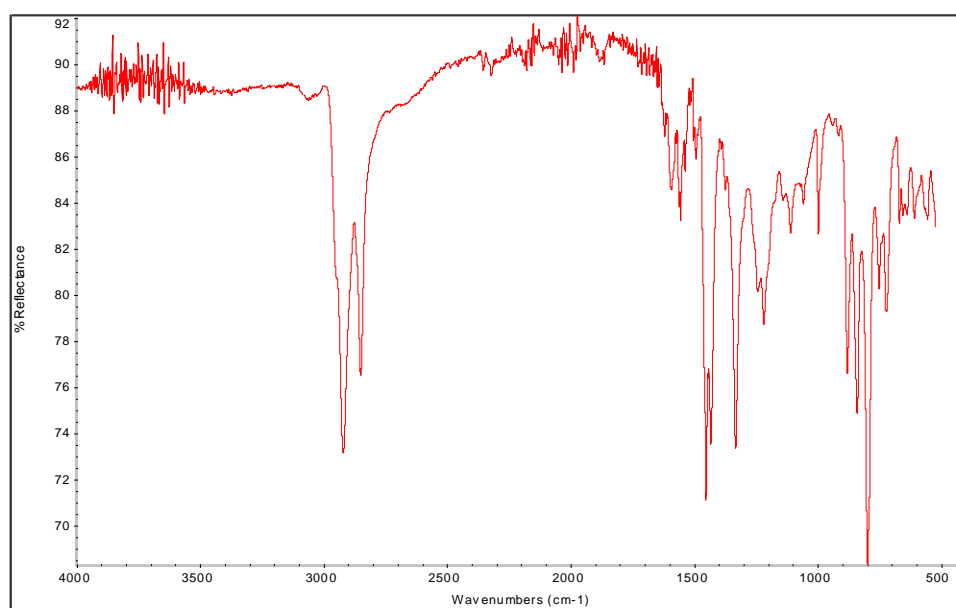
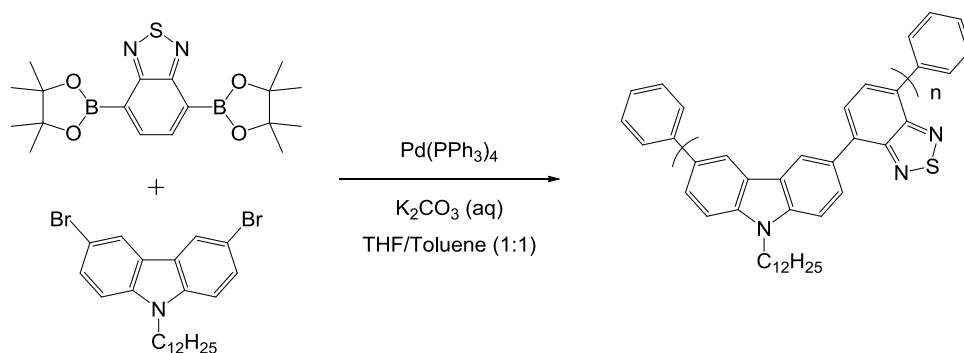


Figure 2 - 30: IR spectrum (ATR) of PCBT2.

**Poly(N-dodecyl-3,6-carbazole-*alt*-benzothiadiazole) (PCBT3)**





Starting from N-dodecyl-3,6-dibromocarbazole **6** (247 mg, 0.5 mmol). The final product was obtained as an orange powder (173 mg, 74%).

$^1\text{H}$  NMR (400 MHz,  $\text{CDCl}_3$ ):  $\delta$  (ppm) 8.92 – 7.29 (m, 8H), 4.50 – 3.72 (m, 2H), 2.07 – 1.57 (m, 2H), 1.55 – 0.99 (m, 2H), 0.87 (br, 3H).  $^{13}\text{C}$  NMR (101 MHz,  $\text{CDCl}_3$ ):  $\delta$  (ppm) 154.95, 141.31, 133.67, 128.38, 127.66, 127.46, 123.76, 123.36, 121.69, 121.39, 109.20, 32.05, 29.76, 29.65, 29.49, 29.24, 27.49, 22.82, 14.26. FT-IR (ATR):  $\nu$  = 2919, 2849, 1627, 1600, 1473, 1384, 1343, 1278, 1231, 1143, 1025, 886, 846, 798, 720, 694, 646, 561  $\text{cm}^{-1}$ .

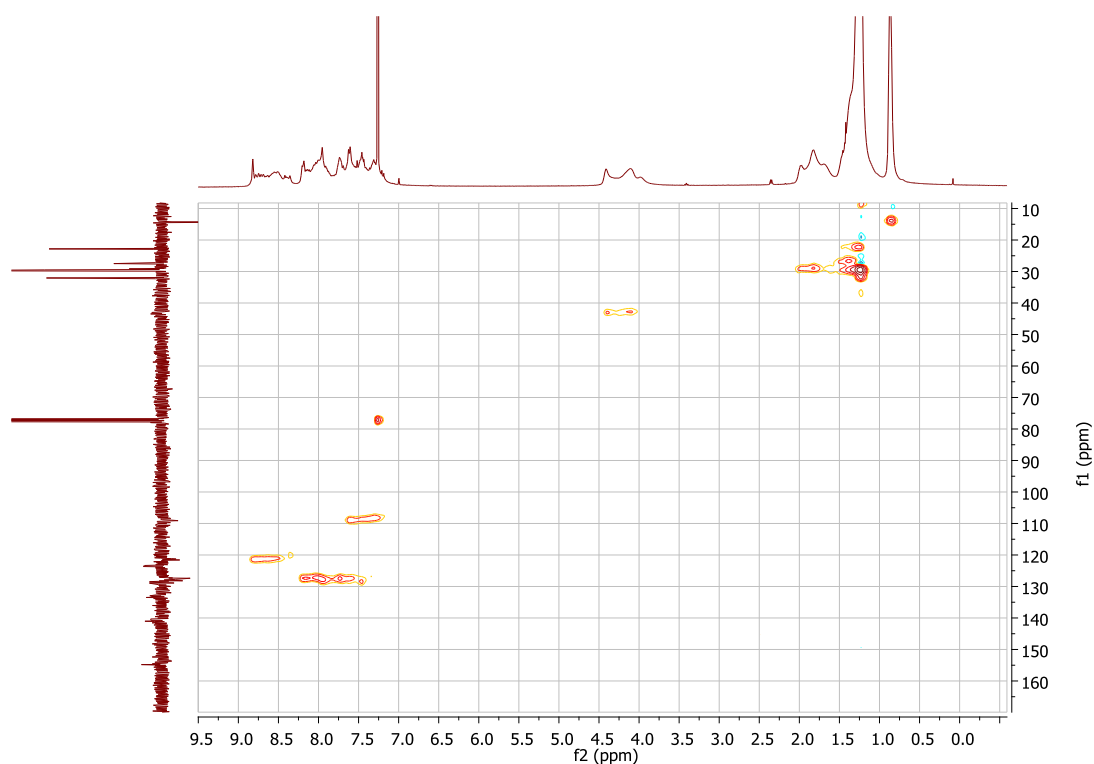


Figure 2 - 31:  $^1\text{H}$ - $^{13}\text{C}$  HSQC NMR spectra (400 MHz) of PCBT3 in  $\text{CDCl}_3$ .

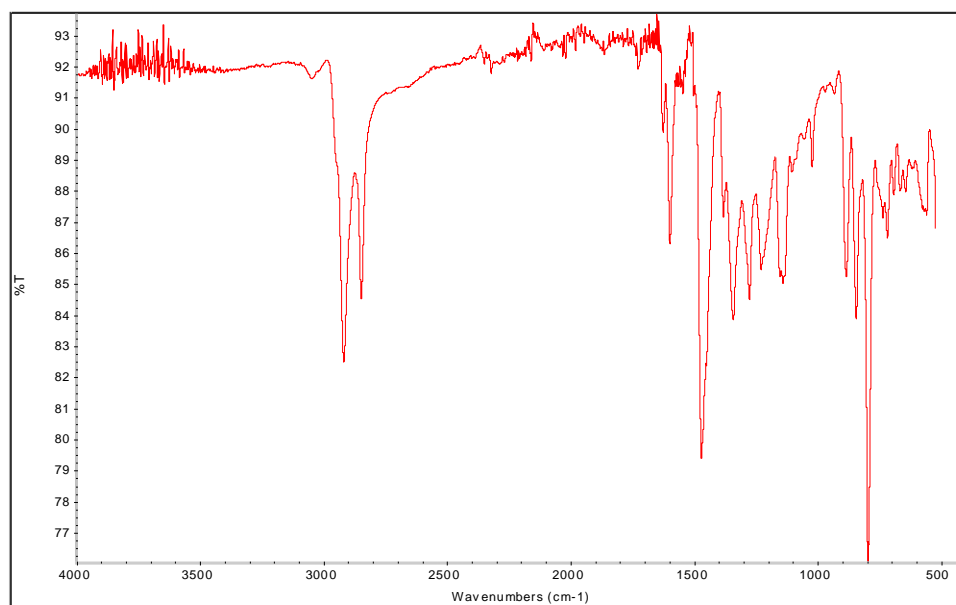
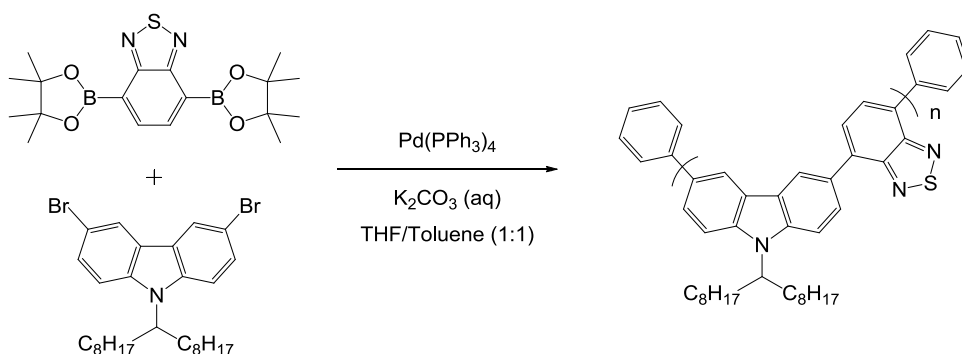


Figure 2 - 32: IR spectrum (ATR) of PCBT3.

**Poly(N-9-heptadecanyl-3,6-carbazole-*alt*-benzothiadiazole) (PCBT 4)**



Starting from N-9-heptadecanyl-3,6-dibromocarbazole **8** (283 mg, 0.5 mmol). The final product was obtained as an orange powder (207 mg, 77%).

$^1\text{H}$  NMR (400 MHz,  $\text{CDCl}_3$ ):  $\delta$  (ppm) 8.97 – 7.37 (m, 8H), 4.68 (br s, 1H), 2.39 (br s, 2H), 2.11 – 1.94 (m, 2H), 1.48 – 0.99 (m, 24H), 0.95 – 0.68 (m, 6H).  $^{13}\text{C}$  NMR (101 MHz,  $\text{CDCl}_3$ ):  $\delta$  (ppm) 155.10, 142.77, 133.57, 130.04, 129.47, 128.80, 128.25, 127.61, 57.13, 34.06, 31.91, 29.62, 29.50, 29.35, 27.09, 25.74, 22.73, 14.20. FT-IR (ATR):  $\nu$  = 2921, 2851, 1626, 1600, 1473, 1403, 1341, 1283, 1224, 1147, 1099, 1027, 885, 848, 799, 754, 721, 694, 670, 605  $\text{cm}^{-1}$ .

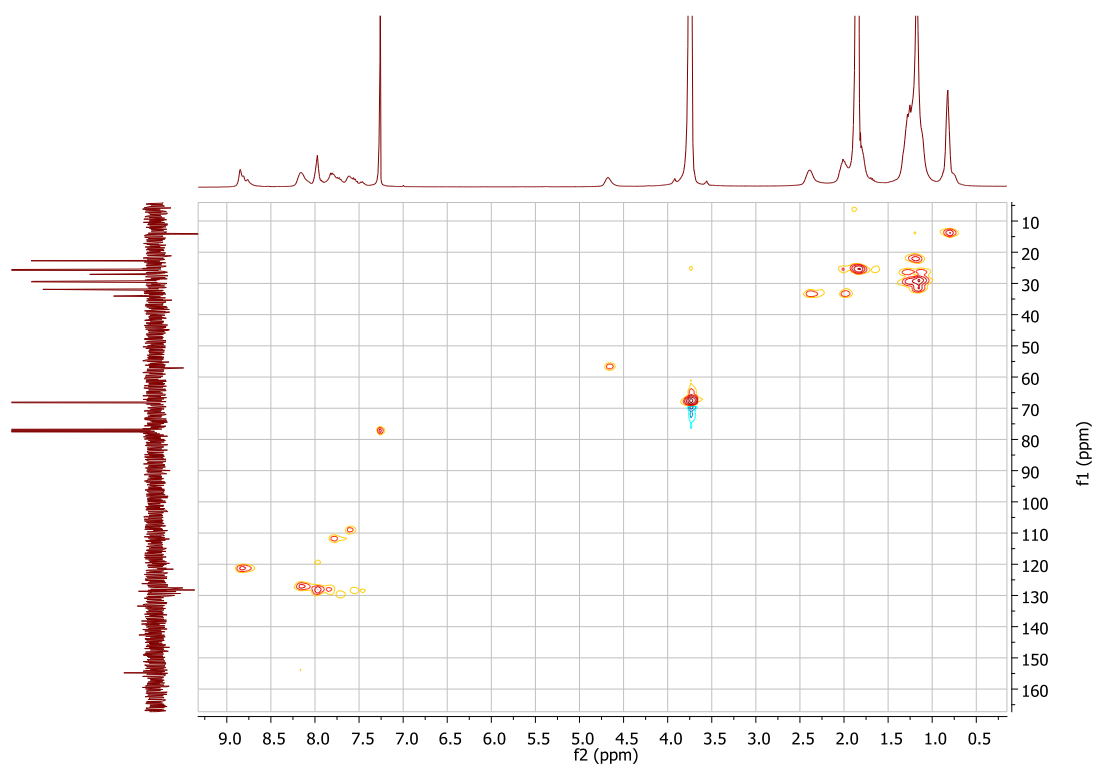


Figure 2 - 33:  $^1\text{H}$ - $^{13}\text{C}$  HSQC NMR spectra (400 MHz) of PCBT4 in  $\text{CDCl}_3$ .

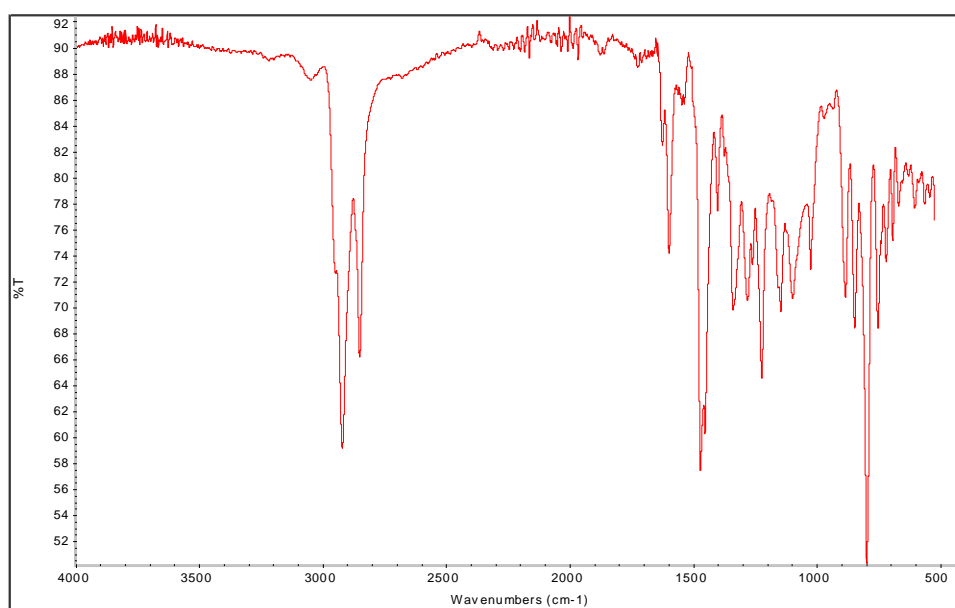


Figure 2 - 34: IR spectrum (ATR) of PCBT4.

## 2.6.2 THERMOGRAVIMETRIC ANALYSES (TGA)

TGA data were recorded under  $\text{N}_2$  atmosphere at a heating rate of  $10^\circ\text{C}/\text{minute}$ .

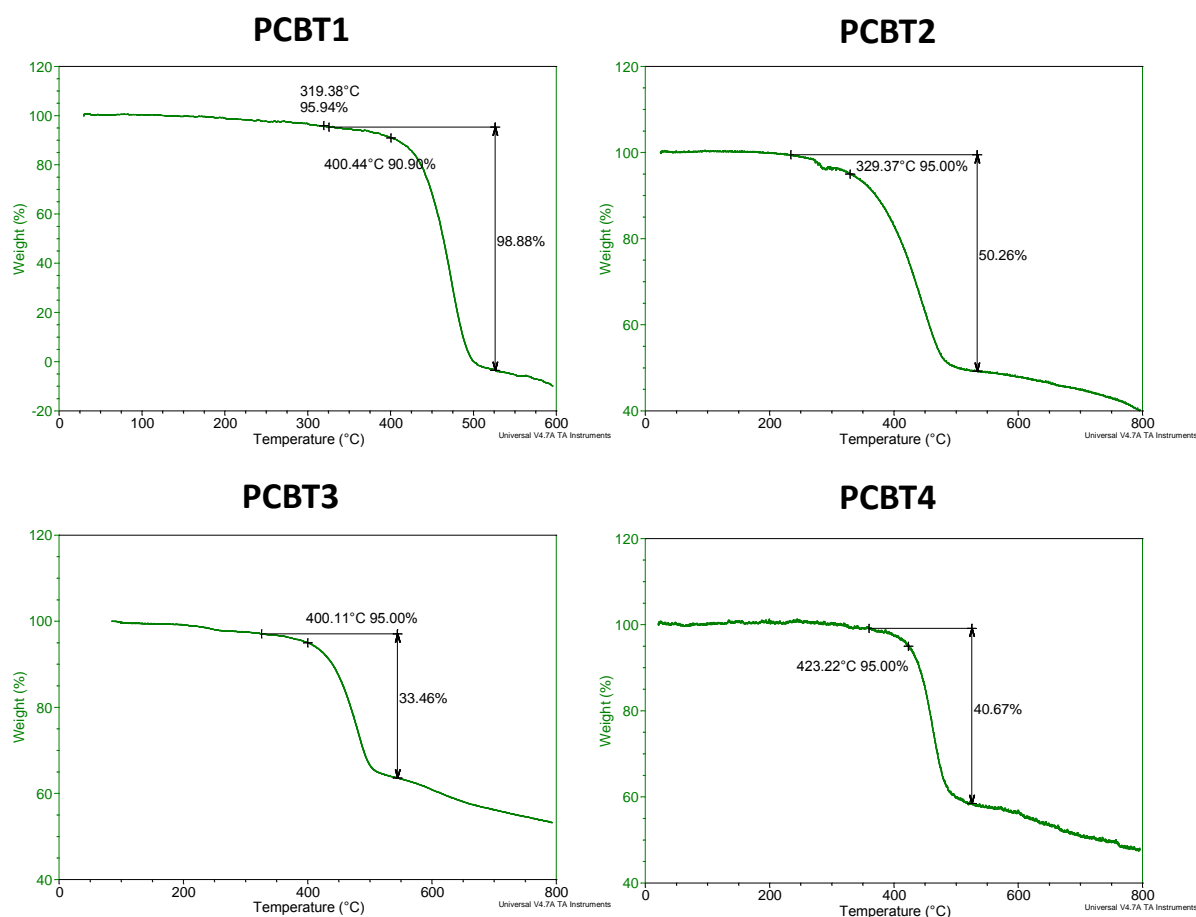


Figure 2 - 35: TGA analyses of PCBTs.

### 2.6.3 DIFFERENTIAL SCANNING CALORIMETRY

DSC data were recorded under helium flow (25 ml/min) at a scan rate of 10°C/min, between 0°C and 250°C.

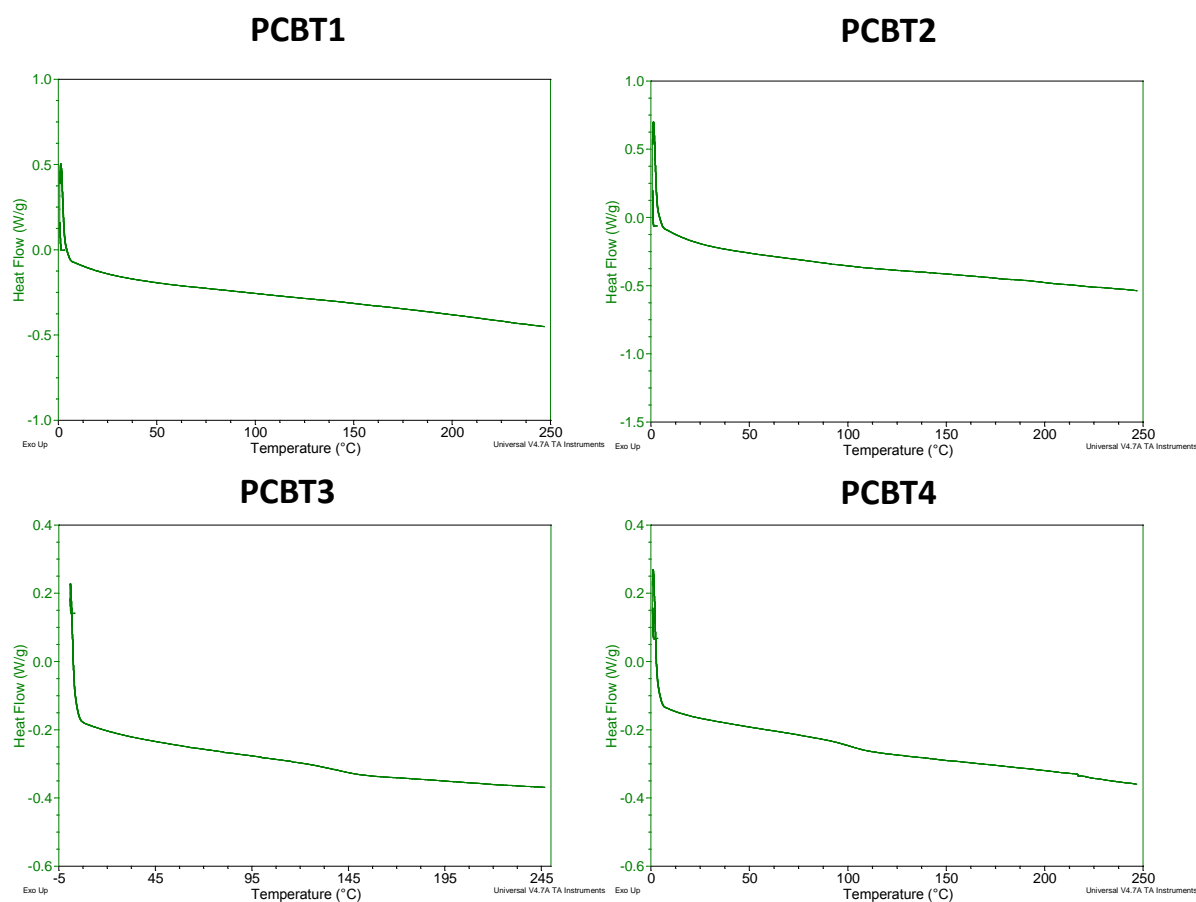


Figure 2 - 36: DSC analyses of PCBTs.

## 2.6.4 ELECTROCHEMISTRY

A solution of  $0.1 \text{ g.l}^{-1}$  of the investigated polymer in  $\text{CH}_2\text{Cl}_2$  with  $0.1 \text{ M}$  tetrabutylammonium hexafluorophosphate ( $\text{TBAPF}_6$ ) as electrolyte was prepared in a glove box under  $\text{N}_2$ . CV measurements were then performed on the solution under  $\text{N}_2$ , using a silver wire as reference electrode and platinum for the working and counter electrodes. A solution of ferrocene ( $1 \text{ mM}$  in  $\text{CHCl}_3$ ) was prepared in the same conditions and the redox potential of  $\text{Fc}/\text{Fc}^+$  vs  $\text{Ag}$  ( $E_{\text{Fc}/\text{Fc}^+ \text{ vs Ag}}$ ) was measured.

### PCBT1

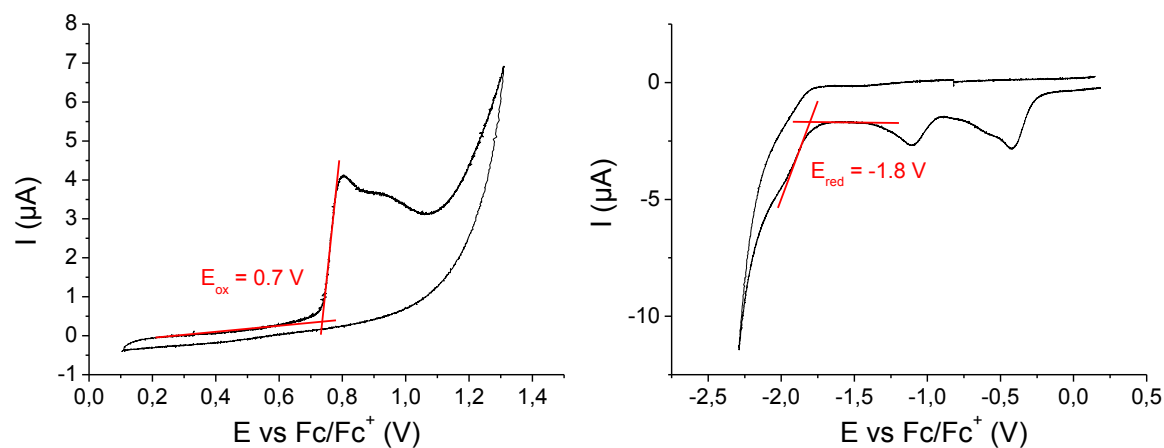


Figure 2 - 37: Cyclic voltammograms of PCBT1 in  $\text{CH}_2\text{Cl}_2$  solution ( $0.1 \text{ g.l}^{-1}$ ). Left-oxidation; right-reduction.

### PCBT2

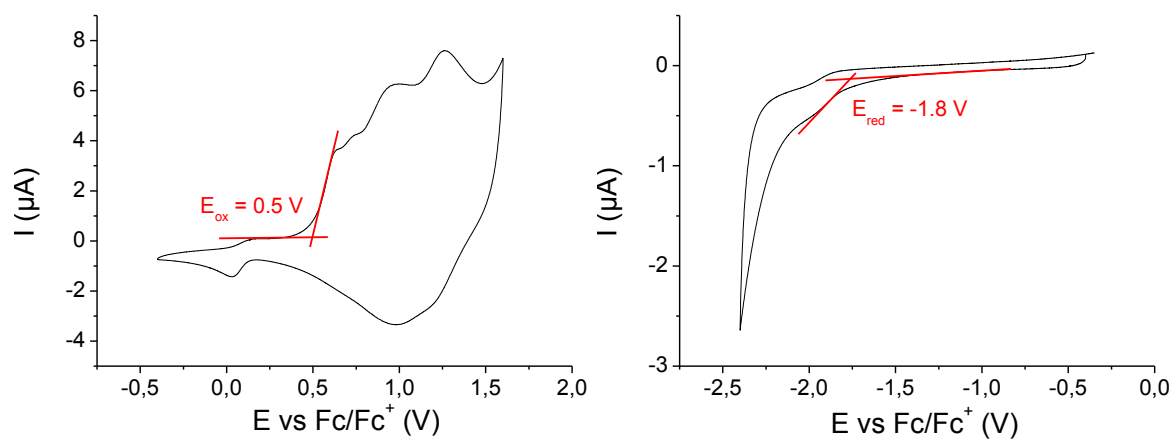


Figure 2 - 38: Cyclic voltammograms of PCBT2 in  $\text{CH}_2\text{Cl}_2$  solution ( $0.1 \text{ g.l}^{-1}$ ). Left-oxidation; right-reduction.

### PCBT3

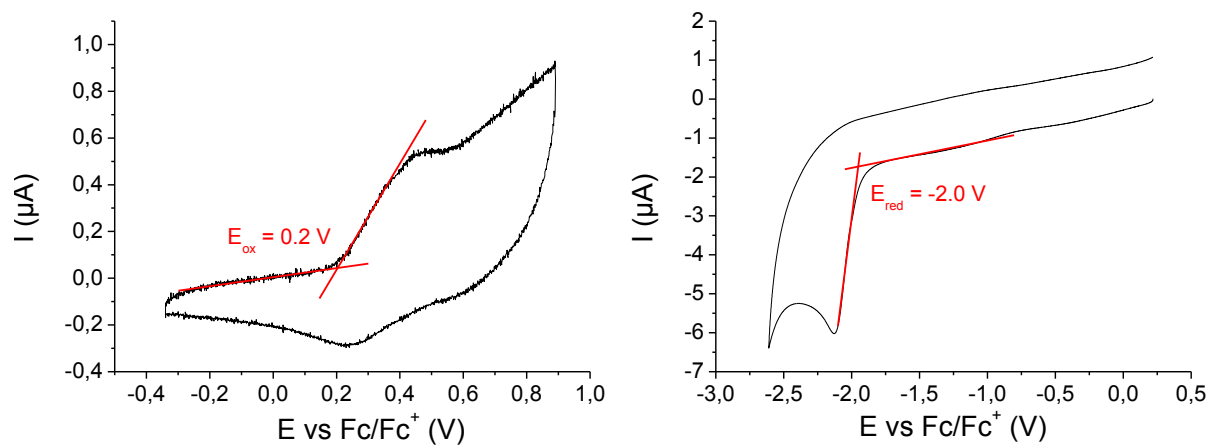


Figure 2 - 39: Cyclic voltammograms of PCBT3 in  $\text{CH}_2\text{Cl}_2$  solution ( $0.1 \text{ g.l}^{-1}$ ). Left-oxidation; right-reduction.

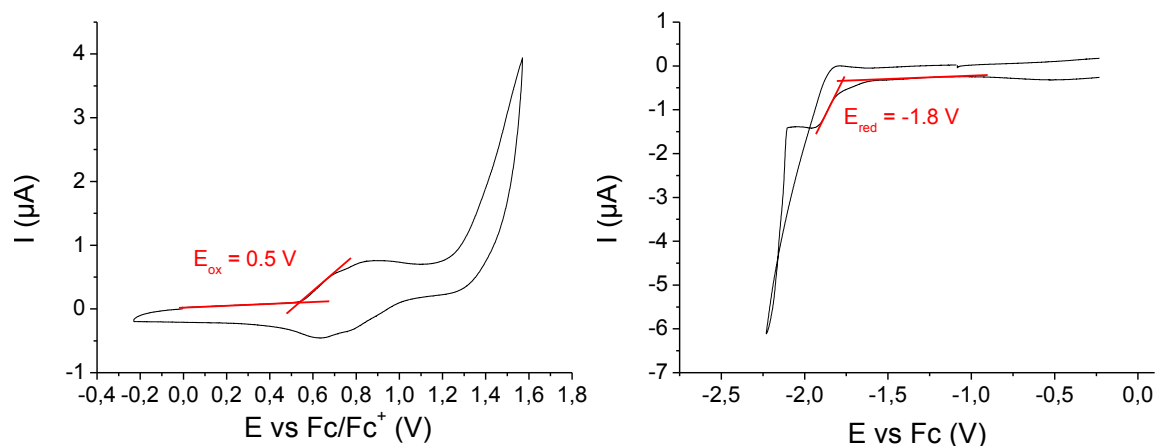
**PCBT4**

Figure 2 - 40: Cyclic voltammograms of PCBT4 in  $CH_2Cl_2$  solution ( $0.1 \text{ g.l}^{-1}$ ). Left-oxidation; right-reduction.

### 2.6.5 OPTICAL CHARACTERIZATIONS OF PCBT-PCBM BLENDS

ODCB solutions of PCBTs mixed with PCBM at different ratios were spin-casted onto glass substrates coated with a PEDOT-PSS layer. The concentration of PCBT was kept constant ( $12 \text{ g.l}^{-1}$ ).

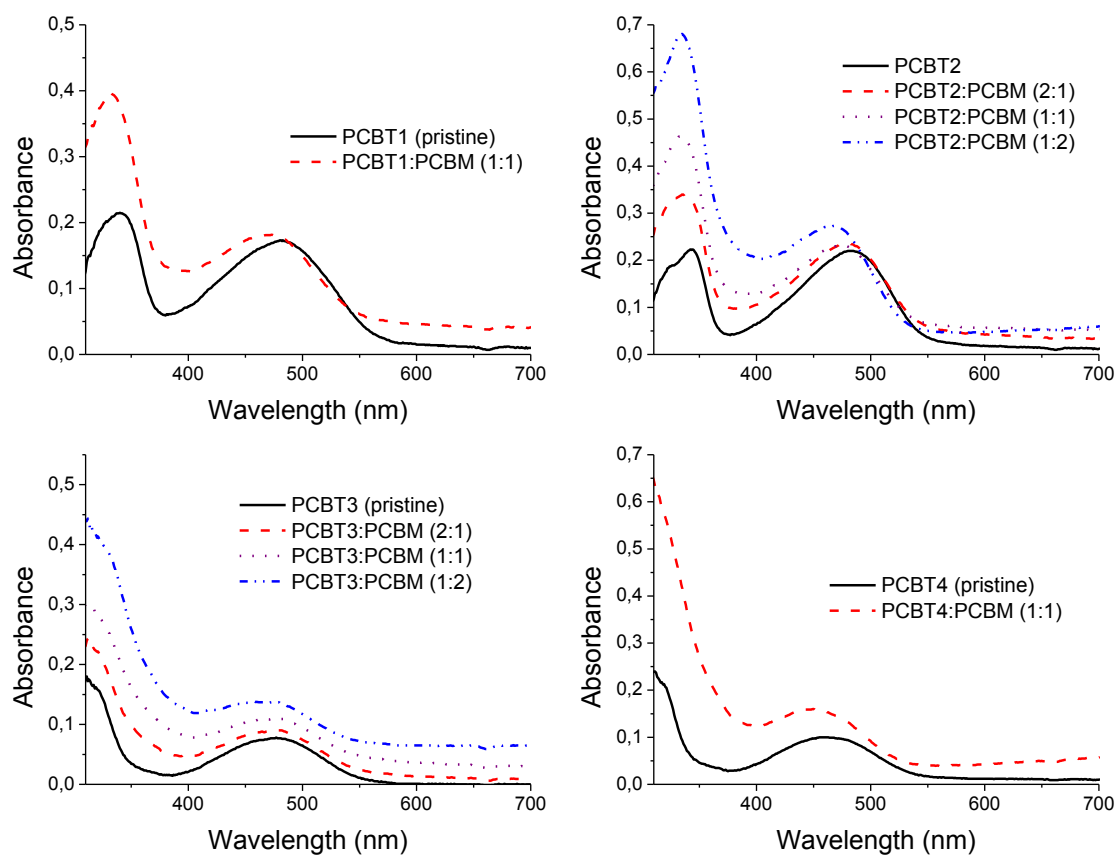


Figure 2 - 41: Absorption spectra of PCBT:PCBM blends in film at different ratios, spin-coated from ODCB solutions onto PEDOT-PSS coated glass substrates.

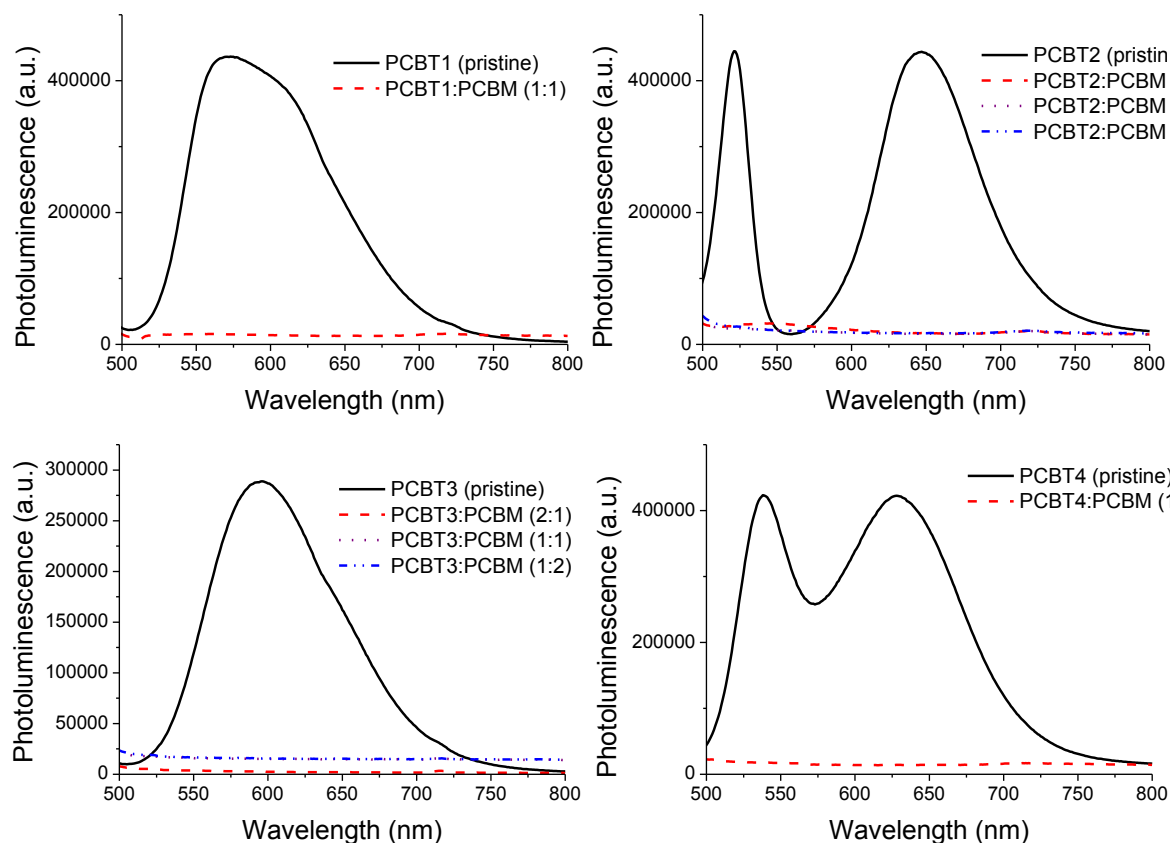


Figure 2 - 42: Photoluminescence spectra of PCBT:PCBM blends in film at different ratios, spin-coated from ODCB solutions onto PEDOT-PSS coated glass substrates. Excitations were according to the absorption maxima of PCBTs in solid-state (see section 2.3.2).

## 2.6.6 PHOTOVOLTAIC CHARACTERIZATION

Photovoltaic devices with a direct architecture were fabricated under inert atmosphere. ITO coated onto a glass substrate bearing an additional PEDOT-PSS layer was used as anode, and aluminium as cathode. The active layer was deposited by spin-coating from an ODCB solution of PCBT and PCBM (overall concentration of  $24 \text{ g.l}^{-1}$ ). Three different ratios of donor and acceptor materials were tested. In Table 2 - 11 are presented the performances of devices made from 1:1 blends, which proved to be the most efficient ratios. Measurements were carried out before and after annealing of the devices at  $150^\circ\text{C}$  for 20 minutes. Values of PCE are not shown because of values below the error bar.

Table 2 - 11: Photovoltaic performances of devices using PCBT:PCBM (1:1) blends as active layer.

Polymer	Annealing	Voc (V)	Jsc ( $\text{mA.cm}^{-2}$ )	FF
PCBT1	None	0,31	0,31	0,38
	$150^\circ\text{C}$ 20min	0,38	0,53	0,38
PCBT3	None	0,42	0,24	0,32
	$150^\circ\text{C}$ 20min	0,39	0,45	0,39





---

## Chapter 3    SYNTHESIS AND CHARACTERIZATION OF BRIDGED POLYSQUARAINES



## Table of contents

<b>3.1</b>	<b>Literature overview .....</b>	<b>107</b>
<b>3.2</b>	<b>Synthesis of bridged polysquaraine .....</b>	<b>110</b>
3.2.1	Squaraine monomer.....	110
3.2.2	Bridged polysquaraines .....	113
<b>3.3</b>	<b>Properties of the bridged polysquaraines .....</b>	<b>117</b>
3.3.1	Thermal properties .....	117
3.3.2	Optical properties .....	118
3.3.3	Electrochemical properties .....	120
3.3.4	Preliminary tests for photovoltaic applications .....	122
<b>3.4</b>	<b>Conclusion.....</b>	<b>125</b>
<b>3.5</b>	<b>Bibliography .....</b>	<b>126</b>
<b>3.6</b>	<b>Experimental .....</b>	<b>127</b>
3.6.1	Syntheses and structural characterizations .....	127
3.6.2	Thermogravimetric analyses (TGA) .....	136
3.6.3	Differential Scanning Calorimetry (DSC).....	136
3.6.4	Electrochemistry .....	137
3.6.5	Optical characterizations .....	139



### 3.1 LITERATURE OVERVIEW

Due to their strong and red-shifted light absorption, organic dyes are attractive building blocks for conjugated polymers employed in light-emission or light-harvesting devices. Additionally, they usually present very planar structures which favor enhanced intermolecular interactions in the solid state.<sup>[1]</sup> Various dyes were used as monomers for synthesis of CPs, such as diketopyrrolopyrrole, isoindigo or BODIPY.<sup>[2-4]</sup> Amongst them, squaraine (SQ) dyes attracted much attention due to their remarkable donor-acceptor-donor structure. The first report of such dyes was published by Triebs and Jacob.<sup>[5]</sup> Different types of electron-rich structures can be condensed with squaric acid to give squaraine derivatives, but a common general feature is the presence of an aromatic moiety bearing an amino group. Aniline, pyrrole and indole are examples of units able to form SQ dyes (see Figure 3 - 1).<sup>[6-8]</sup>

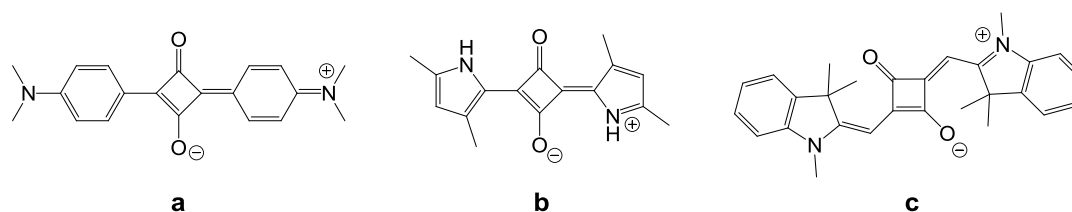


Figure 3 - 1: Examples of squaraine dyes made from (a) aniline, (b) pyrrole, (c) indole derivatives.<sup>[6-8]</sup>

As already mentioned in the first chapter, two different products (1,2- and 1,3-isomers) can be obtained when synthesizing squaraine, and only the 1,3-isomer leads to the zwitterionic structure with strong and red-shifted absorption.<sup>[9]</sup> This isomer can be represented by several canonical structures as depicted in Figure 3 - 2. The central representation is often preferred because its character is in agreement with the absence of carbonyl peak in the IR absorption spectra of such compounds.<sup>[6]</sup> Moreover, this configuration of the cyclobutene core fulfills Hückel's rule and is thus aromatic.

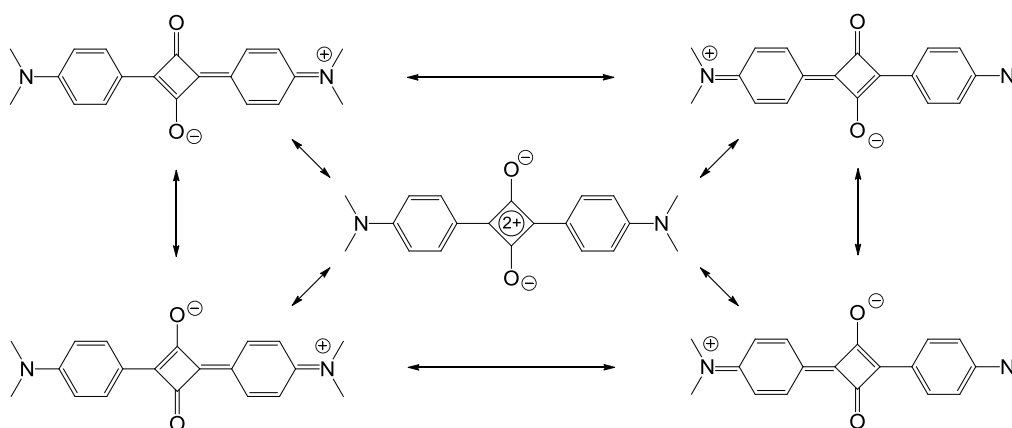
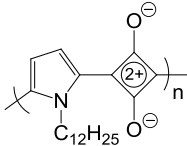
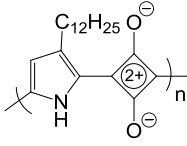
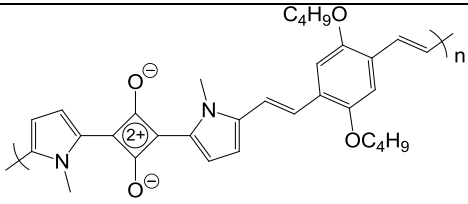
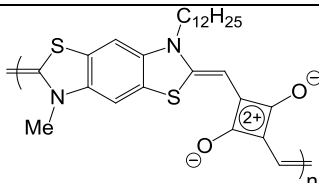


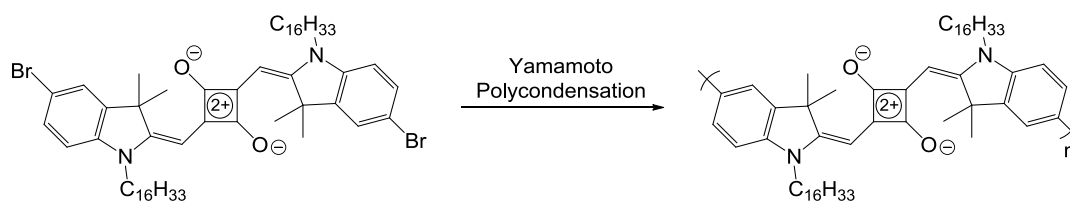
Figure 3 - 2: The different resonant structures for a squaraine dye.<sup>[6]</sup>

Synthesis of conjugated polymers containing SQ units is a promising strategy which was successfully employed to achieve materials with small band-gaps. The first example was reported by Treibs and co-workers, who described the preparation of an insoluble material obtained from pyrrole and squaric acid. However, no further investigation could be performed due to its intractable nature.<sup>[5]</sup> Since then, variety of N-alkyl or 3-alkyl substituted derivatives were developed, showing improved solubilities and optical band-gaps around 1.8 eV (see Table 3 - 1).<sup>[10]</sup> Many research efforts were focused to further decrease the band-gaps and it was found that extension of the conjugation and inclusion of electron-rich units in the backbone accomplished the desired effect.<sup>[11]</sup> By enhancing the planarity and electron-donating character of difunctional monomers, Havinga et al. achieved very small band-gaps polysquaraines.<sup>[12]</sup>

Table 3 - 1: Examples of polysquaraines.

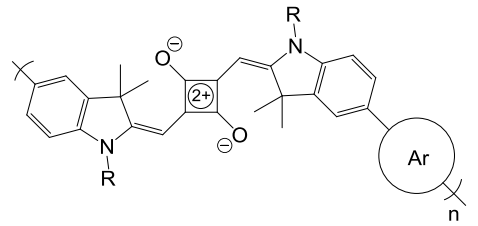
Polymer/dye	$\lambda_{\text{max}}$ (nm)	$E_g^{\text{opt}}$ (eV)	Ref
	581	1.77	[10]
	604	-	
	880	0.79	[13]
	-	0.8	[12]

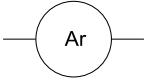
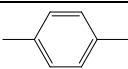
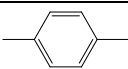
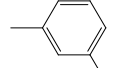
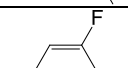
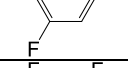
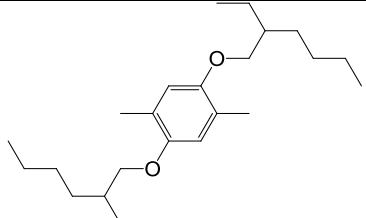
If a SQ-based monomer is appropriately functionalized, polysquaraines can be obtained via classical synthetic routes such as Yamamoto or Suzuki couplings. For instance, Lambert and co-workers developed an indole-based squaraine dye bearing bromide functions that was subsequently polymerized by Yamamoto coupling (see Figure 3 - 3).<sup>[14]</sup> The resulting polymer showed an optical band-gap around 1.6 eV in film. Although, further decrease to 1.5 eV was acquired after thermal annealing causing an intermolecular rearrangement.

Figure 3 - 3: Example of an indole-based polysquaraine.<sup>[14]</sup>

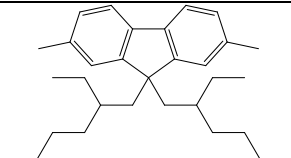
Other research groups studied the influence of bridging similar squaraine units with different aromatic moieties (see Table 3 - 2).<sup>[15-16]</sup> Based on the reported data, it was concluded that increasing the electron-withdrawing strength of the bridge induced an increase of the band-gap, also confirmed by the blue-shift in absorption between the phenylene ( $\lambda_{\max}^{\text{sol}} = 681 \text{ nm}$ ) and tetrafluorophenylene ( $\lambda_{\max}^{\text{sol}} = 614 \text{ nm}$ ) linkers. However this effect could be attributed to a stronger twist angle between units when replacing hydrogen by fluorine atoms, as already mentioned in Chapter 1 (see section 1.2.2). On the contrary, only a slight red-shift could be observed when using electron-donating units. Generally, the light absorptions of these materials were blue-shifted compared with the non-bridged polymer ( $\lambda_{\max}^{\text{sol}} = 738 \text{ nm}$ ). This was attributed to a strong torsion angle induced by the spacing units.

Table 3 - 2: Polysquaraines with different bridging units.



Bridging unit 	Solubilizing group R	$\lambda_{\max}^{\text{solution}}$ (nm)	$E_g^{\text{opt}}$ (eV)	Ref
	dodecyl	681	1.61 <sup>a</sup>	[16]
	octyl	688	1.74 <sup>b</sup>	[15]
	dodecyl	670	1.64 <sup>a</sup>	[16]
	dodecyl	679	1.67 <sup>a</sup>	[16]
	octyl	614	1.78 <sup>b</sup>	[15]
	octyl	685	1.76 <sup>b</sup>	[15]



Bridging unit	Solubilizing group R	$\lambda_{\max}^{\text{solution}}$ (nm)	$E_g^{\text{opt}}$ (eV)	Ref
	octyl	684	1.76 <sup>b</sup>	[15]

<sup>a</sup> Optical band-gap calculated from the onset of absorption in solid state; <sup>b</sup> Optical band-gap calculated from the onset of absorption in CHCl<sub>3</sub> solution.

On the basis of this literature overview, it was decided to develop similar polysquaraines with new linkers. Firstly, thiophene was selected as an electron-donor bridge preventing strong torsion angle. Similar structure was already reported on size-controlled oligomers (up to pentamers) but their optical properties were only studied in order to observe two-photon absorption.<sup>[17]</sup> Secondly, a stronger donor, benzodithiophene (BDT), was used. The two solubilizing groups on this unit should provide an enhancement of the material solubility in organic solvents, since squaraine-based materials commonly show a tendency to aggregate in solution.<sup>[11]</sup> Finally, incorporation of benzothiadiazole (BT) unit should give a clear indication on the influence of electron-withdrawing bridge between SQ moieties.

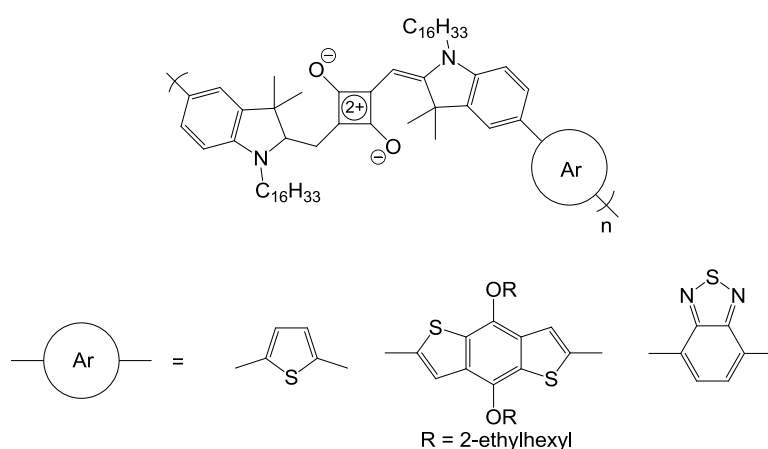


Figure 3 - 4: The investigated bridged polysquaraines.

## 3.2 SYNTHESIS OF BRIDGED POLYSQUARINE

### 3.2.1 SQUARINE MONOMER

In order to obtain a squaraine-based monomer which could be polymerized with various other comonomers, versatile functionalities compatible with Suzuki and Stille conditions were required. Hence, halide and more particularly bromide functions were selected due to their ease of synthesis, low-cost reagents and satisfactory reactivity in the subsequent transformations. Such

difunctionalized squaraine-based monomers bearing various alkyl chains were already reported.<sup>[14, 16]</sup> To achieve a suitable solubility of the resulting polymers, *n*-hexadecyl chains were chosen (see Figure 3 - 5). Despite their length, the linear geometry should allow good intermolecular interactions in the solid-state.

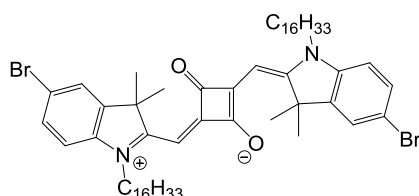


Figure 3 - 5: The selected dibromide squaraine-based monomer.<sup>[14]</sup>

Synthesis of the monomer was performed in four steps. 5-Bromo-1-hexadecyl-2,3,3-trimethyl-3H-indolium iodide **11** was synthesized according to a reported procedure (see Figure 3 - 6).<sup>[18]</sup> Firstly, *p*-bromoaniline was converted into *p*-bromophenylhydrazine hydrochloride **9**. Then, a Fischer indole condensation of **9** with 3-methyl-2-butanone afforded compound **10** in good yield. To attach solubilizing groups on the final monomer, the bromo-indole **10** was refluxed with 1-iodohexadecane in a polar solvent (nitromethane) to obtain the desired 5-bromo-1-hexadecyl-2,3,3-trimethyl-3H-indolium iodide **11** in moderate yield.

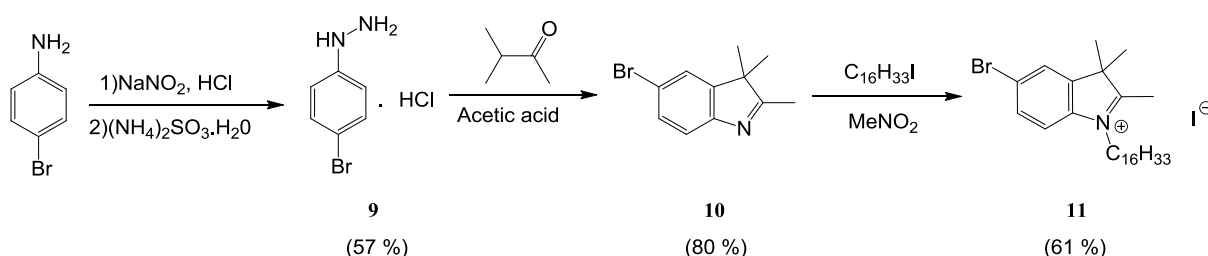
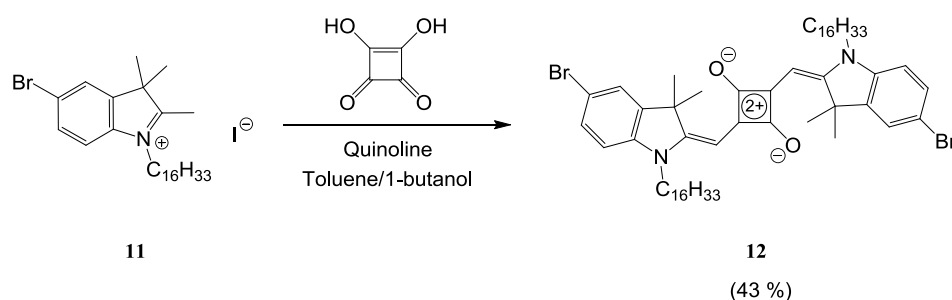


Figure 3 - 6: Synthesis of the indolium precursor **11**.

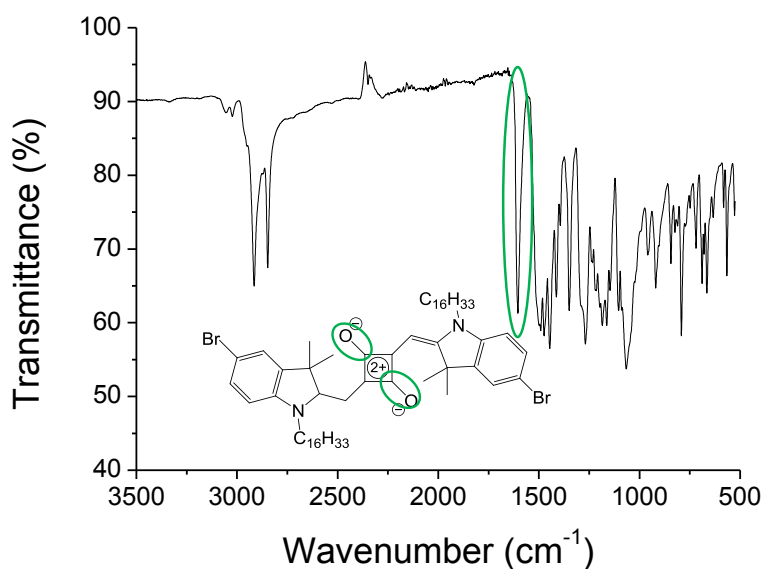
The structures and purities of these intermediates were confirmed by NMR (<sup>1</sup>H, <sup>13</sup>C and <sup>1</sup>H-<sup>13</sup>C HSQC) and IR (see experimental section). Their melting points were relevant with values found in the literature.<sup>[14, 18]</sup>

Subsequent condensation of the indolium salt **11** with squaric acid was carried out following reported procedure (see Figure 3 - 7).<sup>[15]</sup> Additionally to the base catalysis provided by small amounts of quinoline, refluxing the reactants using a Dean-Stark apparatus, which enables azeotropic removal of the formed water, shifted the reaction equilibrium towards product formation. Furthermore, the selective formation of the 1,3-condensation isomer **12** as a major product was ensured by the use of mixture of toluene and 1-butanol, as already reported.<sup>[10]</sup>

Figure 3 - 7: Synthesis of the alkylated dibromosquaraine monomer **12**.

The structure of **12** was confirmed by NMR ( $^1\text{H}$ ,  $^{13}\text{C}$  and  $^1\text{H}$ - $^{13}\text{C}$  HSQC), IR and HRMS (see experimental section). Moreover, its melting point was in good agreement with the literature.<sup>[14]</sup>

In the IR spectrum, the strong absorption band at  $1604\text{ cm}^{-1}$  was associated with the C-O stretching frequency in cyclobutene-diylum-1,3-diolate moiety, and no signal in the  $1700\text{--}1800\text{ cm}^{-1}$  region corresponding to the carbonyl absorption in 1,2 isomer<sup>[10]</sup> could be observed, which was a clear indication that only the 1,3 condensation isomer was produced (see Figure 3 - 8).

Figure 3 - 8: IR spectrum (ATR) of compound **12**.

The  $^1\text{H}$  NMR spectrum of compound **12** in  $\text{CDCl}_3$  is presented in Figure 3 - 9. All the protons of the molecule could be attributed with consistent integration values.

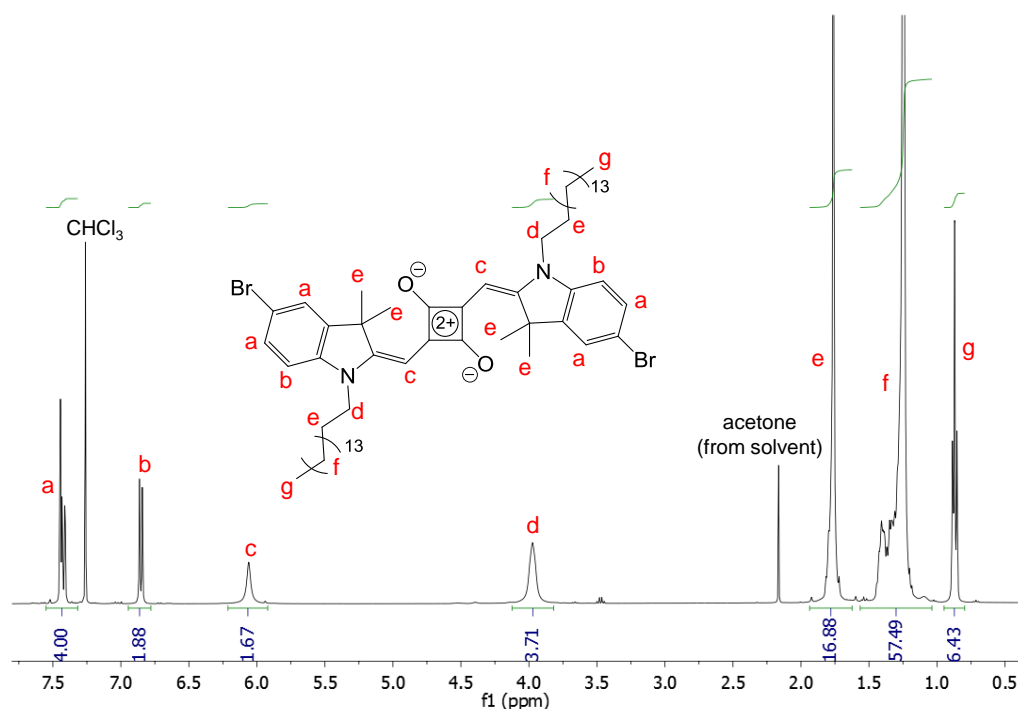


Figure 3 - 9: <sup>1</sup>H NMR spectrum (400 MHz) of compound **12** in CDCl<sub>3</sub>, taking the symmetry into account.

### 3.2.2 BRIDGED POLYSQUARAINES

Three different bridged polysquaraines were synthesized. As illustrated in Figure 3 - 10, poly(squaraine-*alt*-benzothiadiazole) (**PSQBT**) was obtained by a Suzuki polycondensation of the dibromosquaraine **12** with the commercially available 4,7-bis(4,4,5,5-tetramethyl-1,3,2-dioxaborolan-2-yl)benzo[c][1,2,5]thiadiazole. Experimental conditions were similar to the syntheses of poly(carbazole-*alt*-benzothiadiazole) (**PCBTs**) described in the previous chapter. Poly(squaraine-*alt*-thiophene) (**PSQT**) and poly(squaraine-*alt*-benzodithiophene) (**PSQBDT**) were both prepared by a Stille polycondensation of the monomer **12** with commercially available 2,5-bis(tributylstannyl)thiophene and bis(2-ethylhexyloxy)benzo[1,2-b:4,5-b']dithiophene-4,8-bis(trimethylstannane). The Stille polycondensations were carried out in a mixture of 90 % (vol.) of degassed toluene and 10 % (vol.) of degassed dimethylformamide (DMF). It was reported that highly polar solvents such as DMF acted as coordination ligand on the catalytic system, thus improving the reaction yields and molecular weights.<sup>[19]</sup> Its mixing in small proportions with toluene provides a better solubility of the reactants and formed products. As for the Suzuki polycondensations, the ratio of monomers was 1:1 to reach high molecular weights following Carothers equation. A common feature of the three polymerizations is the highly visible color change from deep-blue (due to SQ monomer in solution) to dark green.

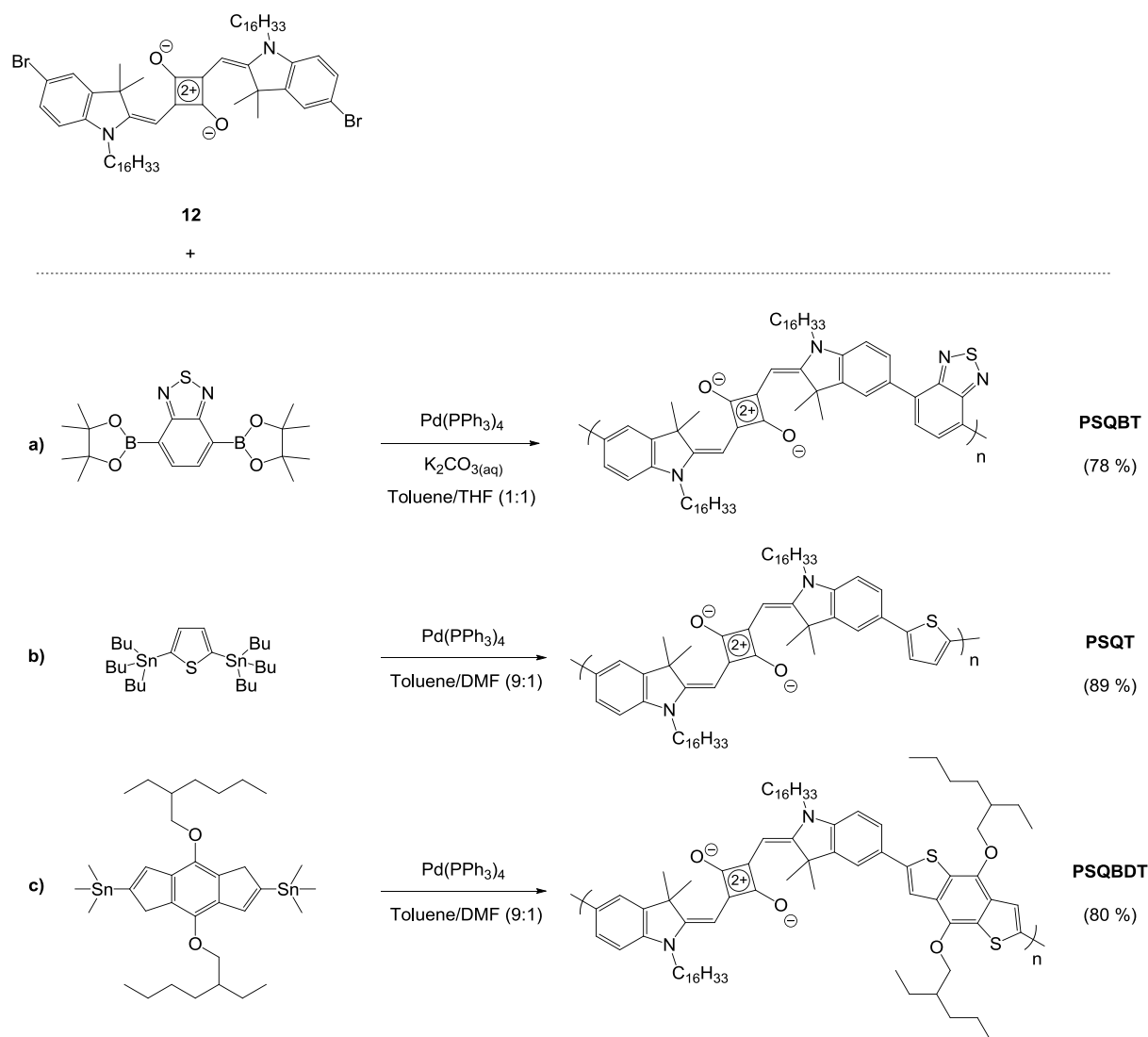


Figure 3 - 10: Syntheses of the bridged polysquaraines via: a) Suzuki coupling; b), c) Stille coupling. Heated at reflux for 48h.

All synthesized materials were subsequently purified by Soxhlet extraction with MeOH, acetone, THF and  $\text{CHCl}_3$ . The THF and  $\text{CHCl}_3$  fractions were recovered separately to afford the resulting materials, and yield of the reactions were calculated from both fractions. The polymers were obtained in good yields as dark purple powders with a strong green color in solution. The THF fractions were soluble in THF,  $\text{CH}_2\text{Cl}_2$ ,  $\text{CHCl}_3$  and ODCB whereas the  $\text{CHCl}_3$  fractions only showed good solubility in  $\text{CHCl}_3$  and ODCB. As can be seen in Table 3 - 3, a higher mass proportion was obtained from  $\text{CHCl}_3$  for **PSQBT** and **PSQT**. On the contrary, most of **PSQBDT** was recovered from the THF fraction, which could be attributed to an enhanced solvation in organic solvents due to the solubilizing groups on the bridging moieties.

Table 3 - 3: Weight proportions of the THF and CHCl<sub>3</sub> fractions recovered from Soxhlet extraction.

Polymer	THF (%w)	CHCl <sub>3</sub> (%w)
PSQBT	30	70
PSQT	29	71
PSQBDT	65	35

The chemical structures of the materials (CHCl<sub>3</sub> fractions) were confirmed by IR and NMR (<sup>1</sup>H, <sup>13</sup>C and <sup>1</sup>H-<sup>13</sup>C HSQC, see experimental section for details). IR spectra of the materials were similar to the squaraine monomer (see Figure 3 - 11). A slightly stronger absorption peak at 2954 cm<sup>-1</sup> was observed for PSQBDT, which is associated with the increased amount of alkyl groups per repeating unit.

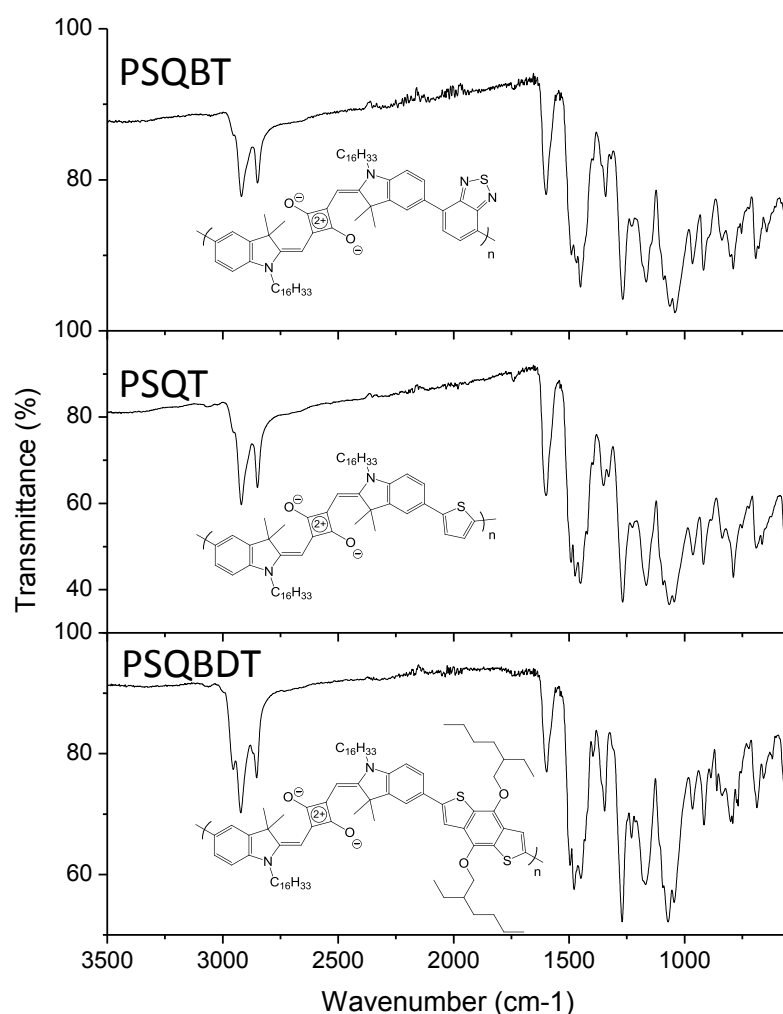


Figure 3 - 11: IR spectra (ATR) of the synthesized polymers.

The <sup>1</sup>H NMR spectra of the PSQs confirmed the expected structures (see Figure 3 - 12). The protons linked to the sp<sup>2</sup> carbons close to the cyclobutene core are well isolated in the 6-6.5 ppm region and were thus used as reference for signals integration.

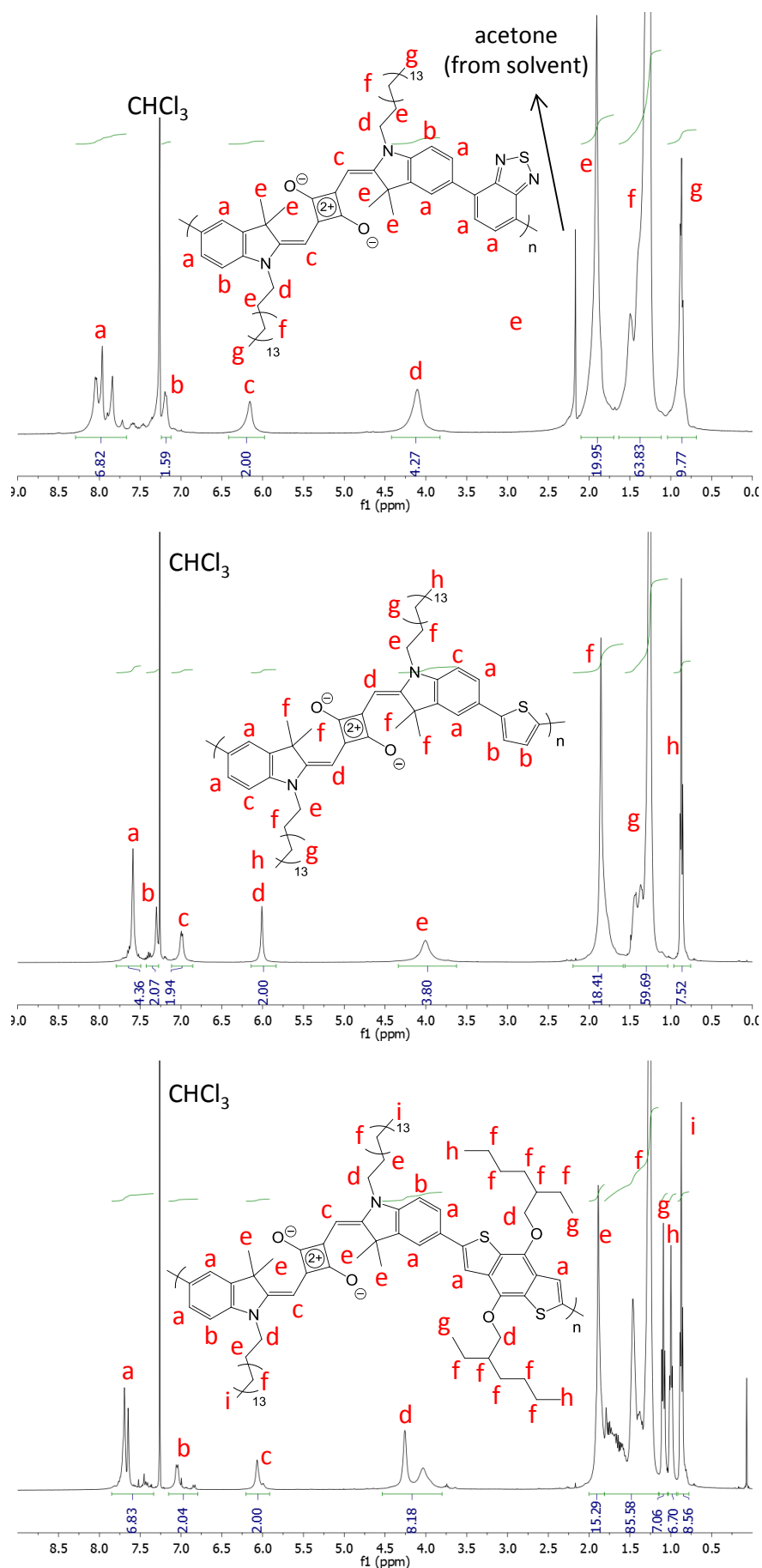


Figure 3 - 12:  $^1\text{H}$  NMR spectra (400 MHz) of the synthesized PSQs in  $\text{CDCl}_3$ .

Molecular weights of the materials were measured by SEC in chloroform with 1 % (vol.) of triethylamine at 30°C (see Table 3 - 4). Previous measurements using CHCl<sub>3</sub> only as eluent led to poorly intense signals with longer elution time, probably due to interactions of the macromolecules in solution with the immobile phase of the columns. Therefore Et<sub>3</sub>N was used as an additive. Values were obtained by conventional calibration on PS standards with a refractive index (RI) detector and also by universal calibration using both RI and viscosimetric detector.

Table 3 - 4: Molecular weights of PSQs determined by SEC in CHCl<sub>3</sub> at 30°C.

Polymer	Fraction	Conventional calibration (PS std)			Universal calibration		
		$\overline{M}_n$ (g/mol)	$\overline{D}^a$	$\overline{DP}_n^b$	$\overline{M}_n$ (g/mol)	$\overline{D}^a$	$\overline{DP}_n^b$
PSQBT	THF	5 800	1.7	5.9	4 300	3.4	4.4
	CHCl <sub>3</sub>	13 500	1.3	13.8	-	-	-
PSQT	THF	9 300	2.5	10.0	5 600	3.4	6.1
	CHCl <sub>3</sub>	19 900	2.7	21.5	11 000	3.9	11.9
PSQBDT	THF	6 100	1.3	4.7	8 400	1.4	6.5
	CHCl <sub>3</sub>	13 500	1.4	10.5	-	-	-

$$^a \text{Dispersity } \overline{D} = \frac{\overline{M}_w}{\overline{M}_n}; ^b \text{Number-average degree of polymerization } \overline{DP}_n = \frac{\overline{M}_n}{M_{rep.unit}}.$$

Given the low  $\overline{DP}_n$  obtained for some of the THF fractions, it was decided to focus the rest of the study on the CHCl<sub>3</sub> fractions only.

## 3.3 PROPERTIES OF THE BRIDGED POLYSQUARAINES

### 3.3.1 THERMAL PROPERTIES

Thermogravimetric analysis (TGA) was performed on the materials, and they all demonstrated good stabilities upon heating with decomposition temperatures above 300°C (see Table 3 - 5). The weight losses of the CHCl<sub>3</sub> fractions were in agreement with a decomposition occurring on the solubilizing groups first (the weight proportion of solubilizing groups compared with the whole repeating unit were 46 %, 49 % and 55 % for **PSQBT**, **PSQT** and **PSQBDT**, respectively). Characterization of the synthesized polymers by differential scanning calorimetry (DSC) gave their glass transition temperatures, but no semi-cristalline features could be observed.



Table 3 - 5: TGA and DSC data of the PSQs.

Polymer	TGA		DSC
	Decomposition temperature (°C) <sup>a</sup>	Weight loss (%)	T <sub>g</sub> (°C) <sup>b</sup>
PSQBT	353	36.2	20
PSQT	353	37.6	26
PSQBDT	314	53.6	27

<sup>a</sup> Evaluated under N<sub>2</sub> at 5% weight loss at a heating rate of 10°C/min; <sup>b</sup> Measured under He flow at 20°C/min on the 2<sup>nd</sup> heating run.

### 3.3.2 OPTICAL PROPERTIES

Figure 3 - 13 shows the UV-visible absorption spectra of the synthesized materials in chloroform solution and as spin-coated films on glass substrate, and the related data are listed in Table 3 - 6. As a comparison, the absorption spectrum of the squaraine monomer **12** in chloroform solution is also presented. Absorption spectra of the THF fractions showed slight hypsochromic shifts between 5 and 10 nm associated to their lower molecular weights (see experimental section).

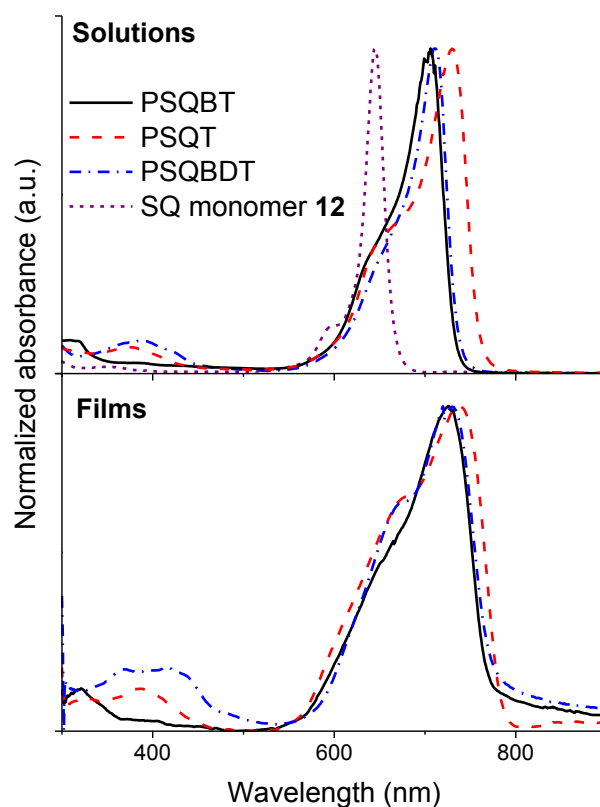


Figure 3 - 13: UV-vis absorption spectra of PSQs in CHCl<sub>3</sub> solutions (0.01 g.l<sup>-1</sup>) and in films spin-coated from CHCl<sub>3</sub> solutions (10 g.l<sup>-1</sup>).

Table 3 - 6: UV-vis absorption data of PSQs in CHCl<sub>3</sub> solutions and in films spin-coated from CHCl<sub>3</sub> solutions.

	Solution (CHCl <sub>3</sub> )		Film		$E_g^{opt}(\text{eV})^c$
	$\lambda_{max}^{sol}(\text{nm})^a$	$\lambda_{onset}^{sol}(\text{nm})^a$	$\lambda_{max}^{film}(\text{nm})^b$	$\lambda_{onset}^{film}(\text{nm})^b$	
<b>SQ mon.</b>	645	670	-	-	-
<b>PSQBT</b>	706	732	726	767	1.6
<b>PSQT</b>	732	756	739	783	1.6
<b>PSQBDT</b>	711	735	730	771	1.6

<sup>a</sup> Determined in CHCl<sub>3</sub> solutions (0.01 g.l<sup>-1</sup>); <sup>b</sup> Determined in film casted on glass from an ODCB solution (10 g.l<sup>-1</sup>);

<sup>c</sup> Estimated from the onset point of the absorption edge in a film with the following formula:  $E_g^{opt} = \frac{1240}{\lambda(nm)}$ .

All three polymers showed a very pronounced red-shift when compared to the single SQ dye **12** ( $\Delta\lambda_{max}^{pol-mon}$  of 61 nm, 87 nm and 66 nm for **PSQBT**, **PSQT** and **PSQBDT**, respectively), confirming the extended conjugation. A similar effect was observed in the non-bridged polysquaraine (PSQ) developed by Lambert and co-workers,<sup>[14]</sup> indicating that the  $\pi$ -electrons delocalization along several squaraine dyes was mainly responsible for this red-shift. When comparing the reported bridged polysquaraines in the literature with the non-bridged PSQ of Lambert et al., a strong blue-shift of the UV-visible absorption was observed (shift of  $\lambda_{max}$  between 50 and 124 nm).<sup>[15-16]</sup> Here the absorptions were only slightly blue-shifted (shift of  $\lambda_{max}$  between 6 and 22 nm). This could be attributed to a decrease in the steric hindrance generated by the bridging units, thus reducing the dihedral angle between repeating units and increasing the planarity of the backbone. The thiophene unit is expected to induce less steric hindrance than the benzodithiophene due to the incorporated alkyl chains. In addition, BDT is less hindered than benzothiadiazole which is linked through a phenyl ring. Hence, the absorption maxima of the corresponding polymers in solution are shifted to longer wavelength when the steric effect is reduced ( $\lambda_{max}^{PSQBT} < \lambda_{max}^{PSQBDT} < \lambda_{max}^{PSQT}$ ).

As expected, films of the materials showed a bathochromic shift of their absorption, in addition to a broadening of the peaks. Surprisingly, the presence of bulky 2-ethylhexyl substituents in PSQBDT did not influence the UV-vis absorption maxima, thus one can presume that intermolecular arrangement in the solid state remains unaffected. Indeed, the red-shift of the absorption peak was similar in PSQBDT and PSQBT ( $\Delta\lambda_{max}$  from solution to film of 19-20 nm), and stronger than PSQT ( $\Delta\lambda_{max}$  from solution to film of 7 nm). The three PSQs were found to have optical band-gaps around 1.6 eV, which is a highly desired feature for active materials in photovoltaic devices. The three absorption spectra were quite similar, therefore, it can be concluded that no (or weak) ICT involving the bridging unit takes place, whether the bridging unit is electron-donating or withdrawing.

The previously prepared solutions and films were also used for photoluminescence (PL) measurements that are depicted in Figure 3 - 14. Excitations performed at different wavelengths

(650 nm to 720 nm) resulted in the same emission, therefore PL was recorded with an excitation at 650 nm in order to record spectra over a wider range of wavelengths. Stokes shift values, which corresponds to the difference between the absorption and emission maxima, were smaller for the PSQs than for the PCBTs. This could be explained by small structural differences between the ground and excited state in polysquaraines. Once again, PSQT presented the most red-shifted spectrum.

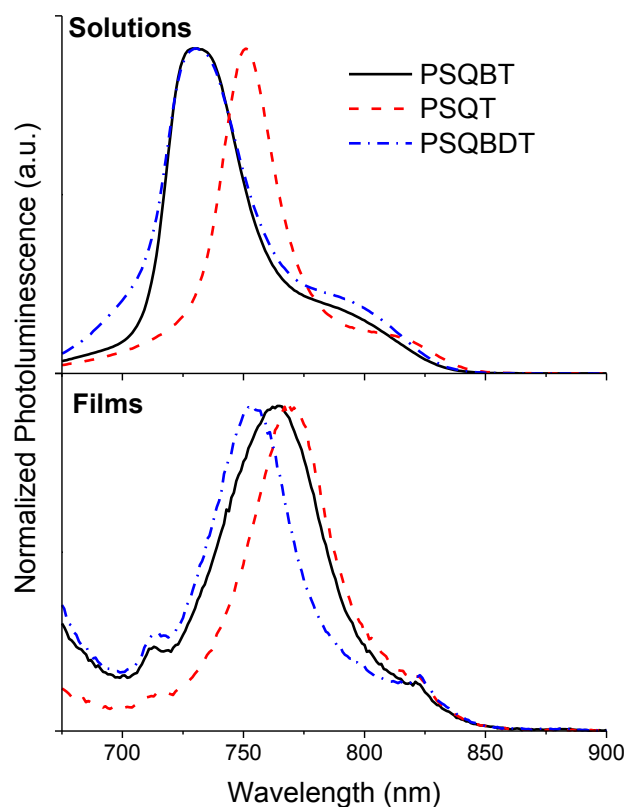


Figure 3 - 14: Photoluminescence spectra of PSQs in  $\text{CHCl}_3$  solutions ( $0.01 \text{ g.l}^{-1}$ ) and in films spin-coated from  $\text{CHCl}_3$  solutions ( $10 \text{ g.l}^{-1}$ ). Excitation at 650 nm.

Table 3 - 7: Photoluminescence data of PSQs in  $\text{CHCl}_3$  solutions and in films spin-coated from  $\text{CHCl}_3$  solutions. Excitation at 650 nm.

Polymer	Solution ( $\text{CHCl}_3$ )	Film
	$\lambda_{\text{max em.}}^{\text{sol}}$ (nm) <sup>a</sup>	$\lambda_{\text{max em.}}^{\text{film}}$ (nm) <sup>b</sup>
PSQBT	729	764
PSQT	751	769
PSQBDT	730	754

<sup>a</sup> Determined in  $\text{CHCl}_3$  solutions ( $0.01 \text{ g.l}^{-1}$ ); <sup>b</sup> Determined in film casted on glass from an ODCB solution ( $10 \text{ g.l}^{-1}$ )

### 3.3.3 ELECTROCHEMICAL PROPERTIES

Electrochemical measurements (CV) were performed in order to determine the HOMO and LUMO levels positions of the three PSQs. CV was carried out on  $0.1 \text{ g.l}^{-1}$  solutions of the materials in  $\text{CHCl}_3$ , using the same conditions as in case of the PCBTs (TBAPF<sub>6</sub> as electrolyte, silver wire as reference

electrode and platinum for the working and counter-electrodes). All the three materials showed similar behavior (see experimental section), and the oxidation and reduction cyclic voltammograms of **PSQT** are shown as an example in Figure 3 - 15. Two reversible oxidation peaks could be identified, as already reported for similar conjugated polymers, corresponding to the formation of dicationic species. The reduction, however, only showed one irreversible peak.

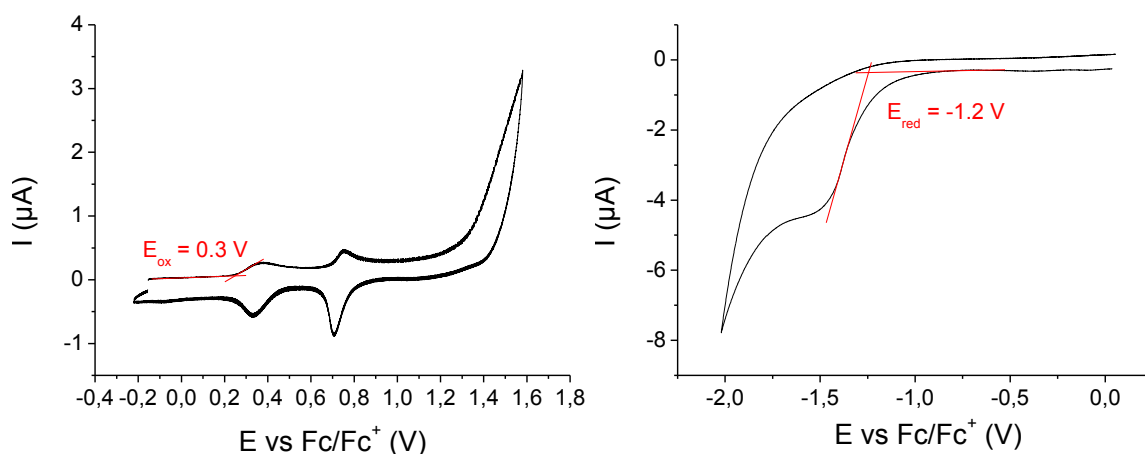


Figure 3 - 15: Cyclic voltammograms (left- oxidation; right- reduction) of PSQT in  $\text{CHCl}_3$  solution ( $0.1 \text{ g.l}^{-1}$ ).

HOMO and LUMO levels were calculated from the obtained data according to previously mentioned equations (see Chapter 2 and experimental section).

Table 3 - 8: CV data of PSQs.

Polymer	$E_{\text{HOMO}}(\text{eV})^a$	$E_{\text{LUMO}}(\text{eV})^b$	$E_g^{\text{CV}}(\text{eV})^c$	$E_g^{\text{opt}}(\text{eV})^d$
PSQBT	-5.1	-3.7	1.4	1.7
PSQT	-5.1	-3.6	1.5	1.6
PSQBDT	-5.0	-3.8	1.2	1.7

<sup>a</sup>Calculated from the onset of the oxidation peak ( $E_{\text{onsetox}}$ ); <sup>b</sup> Calculated from the onset of the reduction peak ( $E_{\text{onsetred}}$ ); <sup>c</sup> Calculated as following:  $E_g = E_{\text{ox}} - E_{\text{red}}$ ; <sup>d</sup> Optical band-gaps in solution calculated from  $\lambda_{\text{onset}}^{\text{sol}}$ .

The electrochemical measurements confirmed the achievement of narrow band-gap materials. The obtained electrochemical band-gap of **PSQT** was smaller than the optical band-gaps in solution, however within the experimental error. In the case of **PSQBT** and **PSQBDT**, the measured electrochemical band-gaps showed a stronger difference with the optical band-gaps, which could be attributed to localized charge states. Moreover, **PSQBDT** showed a hardly detectable reduction signal, therefore its calculated LUMO value should be interpreted carefully. Nevertheless, only slight differences were observed when comparing the HOMO of the three CPs, indicating that the squaraine moiety is mainly responsible for their oxidation behaviour. Interestingly, the polysquaraine

bridged with the BDT unit demonstrated the highest HOMO level, which is consistent with the commonly observed effect of electron-donating groups (see Chapter 1).

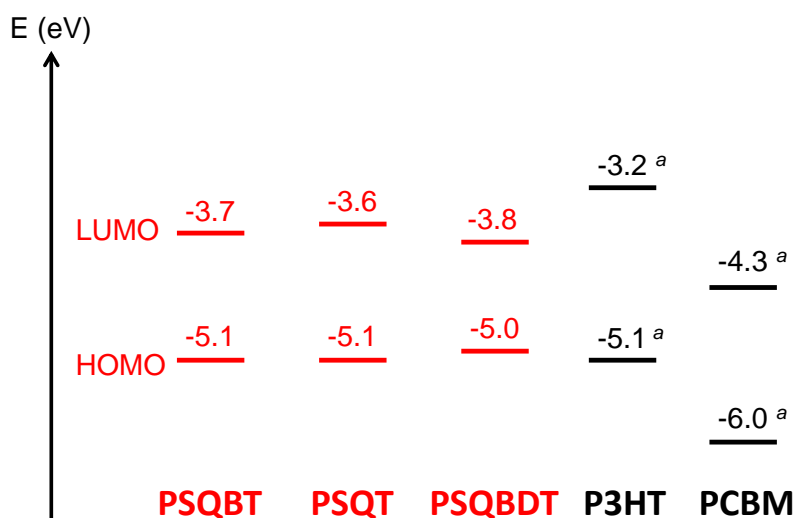


Figure 3 - 16: Energetic representation of the PSQs. <sup>a</sup> Values for P3HT and PCBM are from the literature.<sup>[20]</sup>

The three polymers demonstrated HOMO levels similar to the one of P3HT, with smaller band-gaps, which is a desired property of donor materials in the active layer of BHJ solar cells.

### 3.3.4 PRELIMINARY TESTS FOR PHOTOVOLTAIC APPLICATIONS

Prior to any photovoltaic characterization, films of PSQs and PCBM blends at different ratios were prepared by spin-coating from ODCB solutions on PEDOT-PSS coated glass slides using similar conditions as for the PCBTs (see Chapter 2). Firstly, the UV-visible absorption spectra of the blends were compared to the pristine materials. As anticipated, a peak around 330 nm occurred when increasing the ratio of PCBM, and no significant changes were observed in the polymer absorption in the 600-800 nm region (see experimental section). The absorption spectra of pristine PSQT and PSQT:PCBM blends are shown in Figure 3 - 17 as an example.

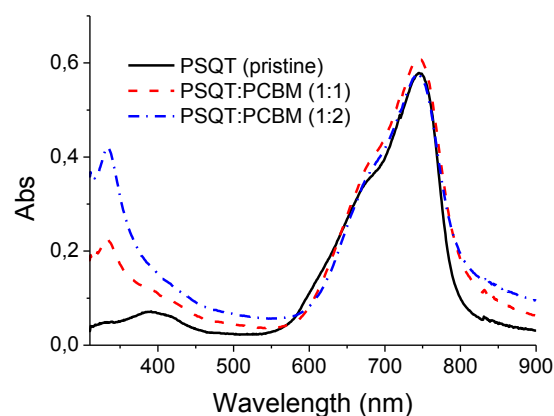


Figure 3 - 17: Solid-state light absorption of PSQT:PCBM blends.

The films were excited at 650 nm to induce the photoluminescence of the PSQs. In all three cases, a strong decrease of fluorescence was observed when increasing the ratio of PCBM, which could indicate an efficient dissociation of the generated excitons in the PSQs (see experimental section). Figure 3 - 18 shows the fluorescence quenching in the PSQT:PCBM blends.

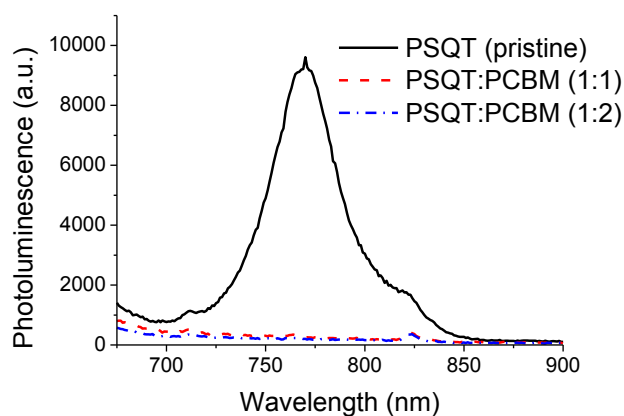


Figure 3 - 18: Solid-state PL of PSQT:PCBM blends excited at 650 nm.

As morphology of the polymer-PCBM blends is an important parameter in BHJ solar cells, images of the prepared films were observed by AFM (see Figure 3 - 19).

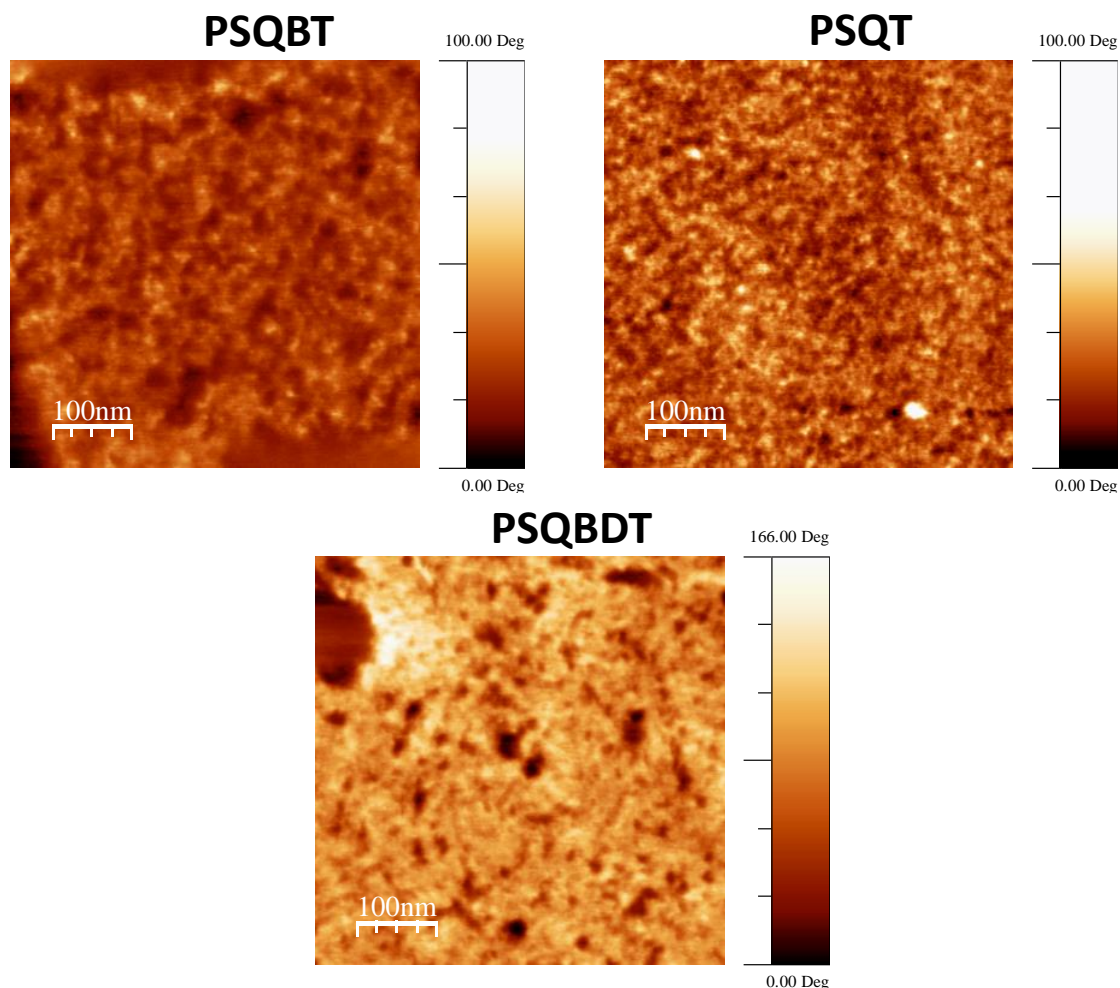


Figure 3 - 19: AFM phase images of PSQ:PCBM (1:1) blends.

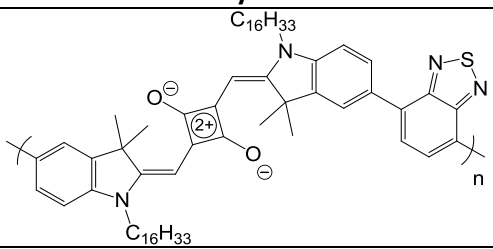
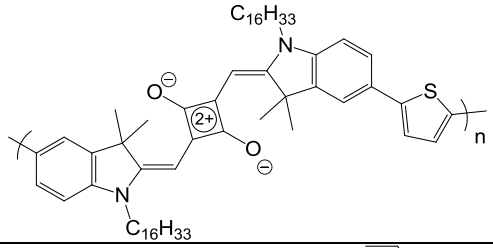
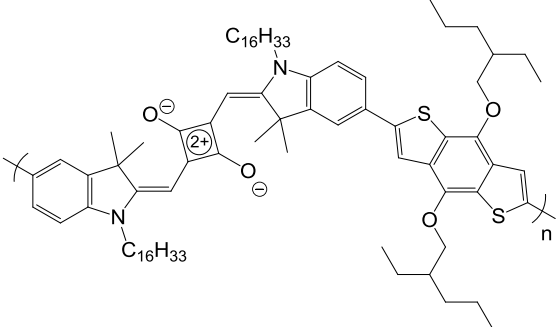
The surface of the films showed phase-separated blends of two materials. In the case of PSQT:PCBM, the blend was finely mixed with domains smaller than 50 nm. PSQBT:PCBM demonstrated bigger domains and less contrast between the two phases, which could indicate a preferential phase-segregation of one material at the surface of the film. Finally, large domains could be observed in the PSQBDT:PCBM blend.

The nanoscale phase separations observed in the AFM were relevant with the measured decrease of PL intensity of the PSQ:PCBM films. The morphology observed for PSQT:PCBM is the most favorable for photovoltaic application, and blends of PSQBT and PSQBDT require an optimization of the films preparation conditions to achieve a more finely mixed structure.

### 3.4 CONCLUSION

Three novel conjugated polymers based on squaraine units alternated with benzothiadiazole, thiophene and benzodithiophene were successfully synthesized via Suzuki and Stille cross-coupling. Their structures were confirmed by NMR, IR and SEC, and their thermal properties by DSC and TGA.

The materials demonstrated strong light absorption and emission in the red-near IR region. The bridging unit (BT, Th or BDT) between squaraine moieties demonstrated a small influence on the optical properties. Electrochemical measurements confirmed narrow band-gaps of the materials.

Polymer	$E_{\text{HOMO}}(\text{eV})^a$	$E_{\text{LUMO}}(\text{eV})^a$	$E_g^{\text{CV}}(\text{eV})^a$	$E_g^{\text{opt film}}(\text{eV})^b$
	-5.1	-3.7	1.4	1.6
	-5.1	-3.6	1.5	1.6
	-5.0	-3.8	1.2	1.6

<sup>a</sup> Determined by cyclic voltammetry in solution; <sup>b</sup> Optical band-gaps in film calculated from  $\lambda_{\text{onset}}^{\text{film}}$ .

Due to their interesting HOMO levels and band-gaps, preliminary studies on blends of polymers with PCBM were carried out and showed encouraging results in terms of exciton dissociation, but the morphology of **PSQBT** and **PSQBDT** blends with PCBM require further optimization.

Finally, it would be interesting to reach lower energetic levels in order to achieve higher  $V_{\text{OC}}$  in BHJ solar cells, but also to obtain n-type semiconducting polymers. This could be realized by using bridging units with a stronger electron-withdrawing feature for instance.



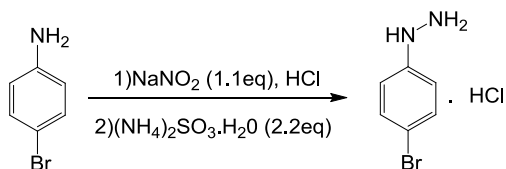
## 3.5 BIBLIOGRAPHY

- [1] A. Mishra, P. Bäuerle, *Angewandte Chemie International Edition* **2012**, *51*, 2020-2067.
- [2] C. B. Nielsen, M. Turbiez, I. McCulloch, *Advanced Materials* **2013**, *25*, 1859-1880.
- [3] G. K. Dutta, A. R. Han, J. Lee, Y. Kim, J. H. Oh, C. Yang, *Advanced Functional Materials* **2013**, n/a-n/a.
- [4] B. C. Popere, A. M. Della Pelle, S. Thayumanavan, *Macromolecules* **2011**, *44*, 4767-4776.
- [5] A. Treibs, K. Jacob, *Angewandte Chemie International Edition in English* **1965**, *4*, 694-694.
- [6] K.-Y. Law, F. C. Bailey, *Canadian Journal of Chemistry* **1986**, *64*, 2267-2273.
- [7] L. Beverina, R. Ruffo, M. M. Salamone, E. Ronchi, M. Binda, D. Natali, M. Sampietro, *Journal of Materials Chemistry* **2012**, *22*, 6704-6710.
- [8] S. H. Kim, S. H. Hwang, *Dyes and Pigments* **1998**, *36*, 139-148.
- [9] L. Beverina, P. Salice, *European Journal of Organic Chemistry* **2010**, *2010*, 1207-1225.
- [10] C. R. Chenthamarakshan, J. Eldo, A. Ajayaghosh, *Macromolecules* **1999**, *32*, 251-257.
- [11] A. Ajayaghosh, *Accounts of Chemical Research* **2005**, *38*, 449-459.
- [12] W. t. H. E. E. Havinga, H. Wynberg, *Polymer Bulletin* **1992**, *29*, 119-126.
- [13] J. Eldo, A. Ajayaghosh, *Chemistry of Materials* **2001**, *14*, 410-418.
- [14] S. F. Völker, S. Uemura, M. Limpinsel, M. Mingebach, C. Deibel, V. Dyakonov, C. Lambert, *Macromolecular Chemistry and Physics* **2010**, *211*, 1098-1108.
- [15] S. Kuster, T. Geiger, *Dyes and Pigments* **2012**, *95*, 657-670.
- [16] T. Maeda, T. Tsukamoto, A. Seto, S. Yagi, H. Nakazumi, *Macromolecular Chemistry and Physics* **2012**, *213*, 2590-2597.
- [17] D. Scherer, R. Dörfler, A. Feldner, T. Vogtmann, M. Schwoerer, U. Lawrentz, W. Grahn, C. Lambert, *Chemical Physics* **2002**, *279*, 179-207.
- [18] M. V. Reddington, *Bioconjugate Chemistry* **2007**, *18*, 2178-2190.
- [19] B. Carsten, F. He, H. J. Son, T. Xu, L. Yu, *Chemical Reviews* **2011**, *111*, 1493-1528.
- [20] M. C. Scharber, D. Mühlbacher, M. Koppe, P. Denk, C. Waldauf, A. J. Heeger, C. J. Brabec, *Advanced Materials* **2006**, *18*, 789-794.

## 3.6 EXPERIMENTAL

### 3.6.1 SYNTHESIS AND STRUCTURAL CHARACTERIZATIONS

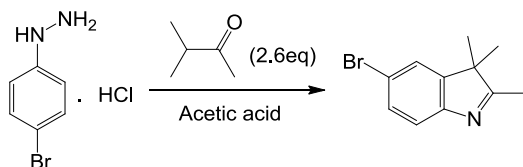
#### *p*-Bromophenylhydrazine hydrochloride (9)



A mixture of *p*-bromoaniline (34.51 g, 0.200 mol), 100 ml of water and 50 ml of hydrochloric acid (36 %w) was stirred and cooled down to 0°C. Then, a solution of sodium nitrite (15.00 g, 0.217 mol) in 45 ml of water was added dropwise. The mixture was stirred for an additional 30 min at 0°C, and the precipitate was filtered off. The resulting filtrate was then added dropwise to a solution of ammonium sulfite (59.02 g, 0.440 mol) in 125 ml of water which was previously cooled down to 0°C, forming a yellow precipitate. The mixture was stirred for 1h at 0°C, and the precipitate was filtered off. The resulting filtrate was added to 60 ml of hydrochloric acid (36 %w) and heated to reflux until a red solid formed and redissolved. The solution was then allowed to cool to room temperature, during which pink crystals formed, and left at 5°C overnight. The crystals were recovered by filtration, washed with a small amount of 1 M hydrochloric acid and dried for 4h at 50°C under vacuum to give the final product (25.66 g, 57 %).

Degradation at 230°C. <sup>1</sup>H NMR (400 MHz, DMSO): δ (ppm) 10.41 (s, 3H), 8.50 (s, 1H), 7.47 – 7.40 (m, 2H), 6.99 – 6.93 (m, 2H). <sup>13</sup>C NMR (101 MHz, DMSO): δ (ppm) 145.04, 131.54, 116.51, 112.70. FT-IR (ATR): ν = 3203, 2937, 2669, 1581, 1487, 1406, 1164, 1078, 1012, 867, 809, 757, 612 cm<sup>-1</sup>.

#### 5-Bromo-2,3,3-trimethyl-3H-indole (10)



*p*-Bromophenylhydrazine hydrochloride **9** (25.55 g, 0.114 mol), 3-methyl-2-butanone (32 ml, 0.300 mol) and 160 ml of acetic acid were heated up to reflux for 3h. The solution was then allowed to cool down to room temperature, during which a red precipitate formed. The volatile components were

removed under vacuum. 50 ml of water was added, and the mixture was extracted 3 times with 40 ml of diethyl ether, followed by 4 washing with 30 ml of water. The combined organic phases were dried ( $\text{MgSO}_4$ ), filtered on celite and the solvent was removed under vacuum. The resulting red oil was purified by distillation under vacuum (b.p.  $140^\circ\text{C}$ ) to give the final product as a pale yellow oil which turned into light pink-orange crystals after few hours (21.78 g, 80%).

m.p.  $< 50^\circ\text{C}$ .  $^1\text{H}$  NMR (400 MHz,  $\text{CDCl}_3$ ):  $\delta$  (ppm) 7.44 (m, 2H), 7.42 – 7.41 (m, 1H), 2.32 (s, 3H), 1.32 (s, 6H).  $^{13}\text{C}$  NMR (101 MHz,  $\text{CDCl}_3$ ):  $\delta$  (ppm) 188.55, 152.75, 147.91, 130.75, 124.95, 121.36, 118.96, 54.23, 23.03, 15.51. FT-IR (ATR):  $\nu = 3050, 2960, 2924, 2867, 1571, 1447, 1246, 1199, 1051, 911, 819, 675, 537\text{ cm}^{-1}$ .

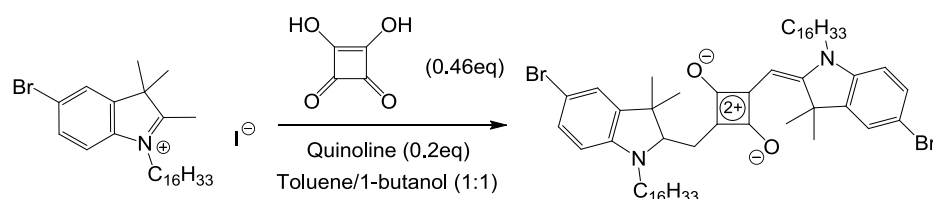
### **5-Bromo-1-hexadecyl-2,3,3-trimethyl-3H-indolium iodide (11)**



**10** (10.00 g, 42.0 mmol), 1-iodohexadecane (19.80 g, 56.2 mmol) and 30 ml of nitromethane were bubbled under argon and then heated to reflux overnight. The solvent was removed under vacuum, and 70 ml of diethyl ether was added. The solution was cooled down at  $5^\circ\text{C}$  for 6h, and a precipitate formed, which was recovered by filtration and rinsed with cold diethyl ether. The resulting solid was dried at  $40^\circ\text{C}$  under vacuum to yield a light brown powder (15.15 g, 61 %).

m.p.  $154^\circ\text{C}$ .  $^1\text{H}$  NMR (400 MHz,  $\text{CDCl}_3$ ):  $\delta$  (ppm) 7.73 – 7.67 (m, 2H), 7.61 (d,  $J = 8.5\text{ Hz}$ , 1H), 4.66 (t,  $J = 7.4\text{ Hz}$ , 2H), 3.09 (s, 3H), 1.95 – 1.85 (m, 2H), 1.67 (s, 6H), 1.48 – 1.17 (m, 26H), 0.87 (t,  $J = 6.9\text{ Hz}$ , 3H).  $^{13}\text{C}$  NMR (101 MHz,  $\text{CDCl}_3$ ):  $\delta$  (ppm) 195.87, 143.65, 140.22, 132.88, 126.93, 124.67, 117.19, 54.91, 50.70, 32.02, 29.79, 29.78, 29.75, 29.72, 29.66, 29.57, 29.45, 29.42, 29.24, 28.00, 26.93, 23.29, 17.37, 14.22. FT-IR (ATR):  $\nu = 2917, 2849, 1583, 1467, 1413, 1254, 1129, 986, 935, 872, 822, 796, 719\text{ cm}^{-1}$ .

### **2,5-Bis[(5-bromo-1-hexadecyl-3,3-dimethyl-2,3-dihydroindole-2-ylidene)methyl]cyclobutendiylum-1,3-diolate (12)**



**11** (11.60 g, 19.6 mmol), 3,4-dihydroxy-3-cyclobutene-1,2-dione (squaric acid, 1.03 g, 9 mmol), quinoline (0.51 g, 4 mmol) and 10 ml of a 1-butanol/toluene mixture (1:1 vol) were bubbled under argon and then heated to reflux overnight with a Dean-Stark trap. The solution turned green in the first minutes of the reaction, and then deep blue. Solvent was removed under vacuum. The raw product was purified by flash chromatography (petroleum ether/ethyl acetate 4:1) to yield a shiny red sticky solid. A subsequent recrystallization in diethyl ether followed by a drying under vacuum at 40°C overnight afforded the final product as shiny green crystals (8.44 g, 43%).

m.p. 82°C.  $^1\text{H}$  NMR (400 MHz,  $\text{CDCl}_3$ ):  $\delta$  (ppm) 7.44 (d,  $J = 1.8$  Hz, 2H), 7.41 (dd,  $J = 8.3, 1.9$  Hz, 2H), 6.84 (d,  $J = 8.4$  Hz, 2H), 5.96 (s, 2H), 3.94 (s, 4H), 1.77 (s, 12H), 1.65 (br, 4H), 1.44 – 1.18 (m, 52H), 0.87 (t,  $J = 6.8$  Hz, 6H).  $^{13}\text{C}$  NMR (101 MHz,  $\text{CDCl}_3$ ):  $\delta$  (ppm) 181.98, 170.10, 144.40, 141.61, 130.91, 125.87, 117.01, 111.02, 87.53, 77.36, 49.55, 44.19, 32.06, 31.06, 29.84, 29.83, 29.81, 29.79, 29.78 (s), 29.73, 29.66, 29.60, 29.49, 27.19, 27.15, 27.09, 22.83, 14.26. FT-IR (ATR):  $\nu = 3054, 3023, 2914, 2847, 1604, 1474, 1446, 1413, 1349, 1269, 1185, 1066, 958, 919, 843, 792, 719, 689, 665, 565\text{ cm}^{-1}$ . HRMS (EI+,  $m/z$ ) [ $M$ ] $^+$  calculated (%) for  $\text{C}_{58}\text{H}_{86}\text{Br}_2\text{N}_2\text{O}_2$ : 1000.5056, found 1000.5031.

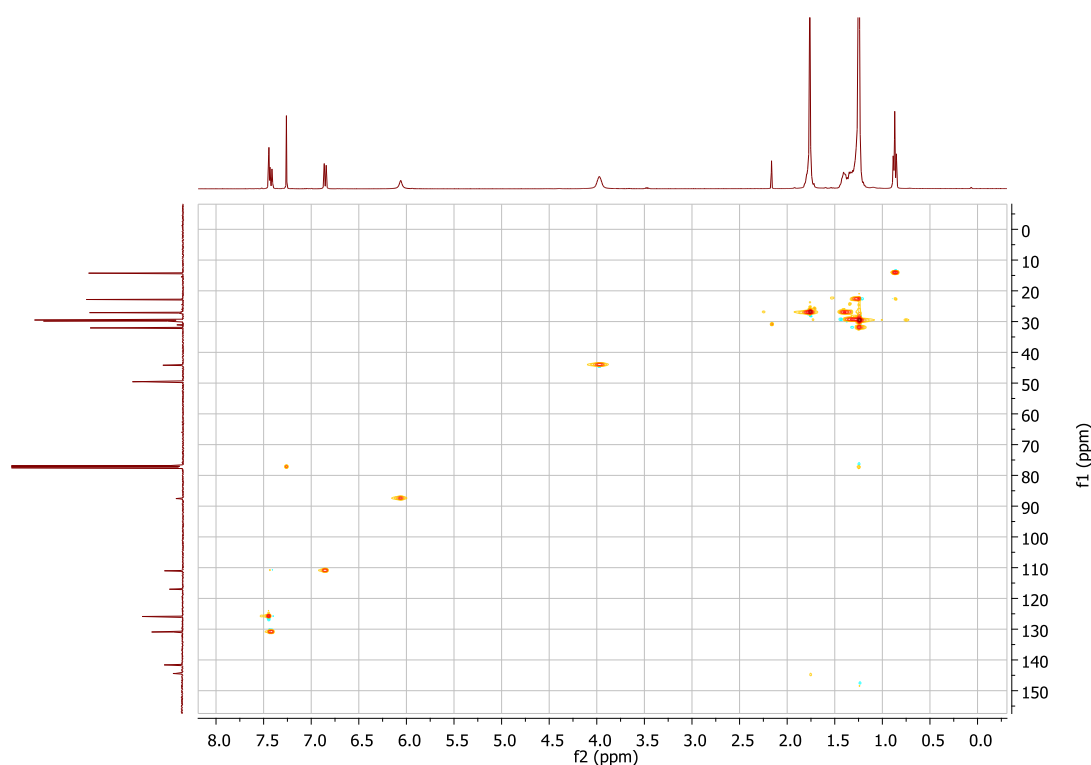
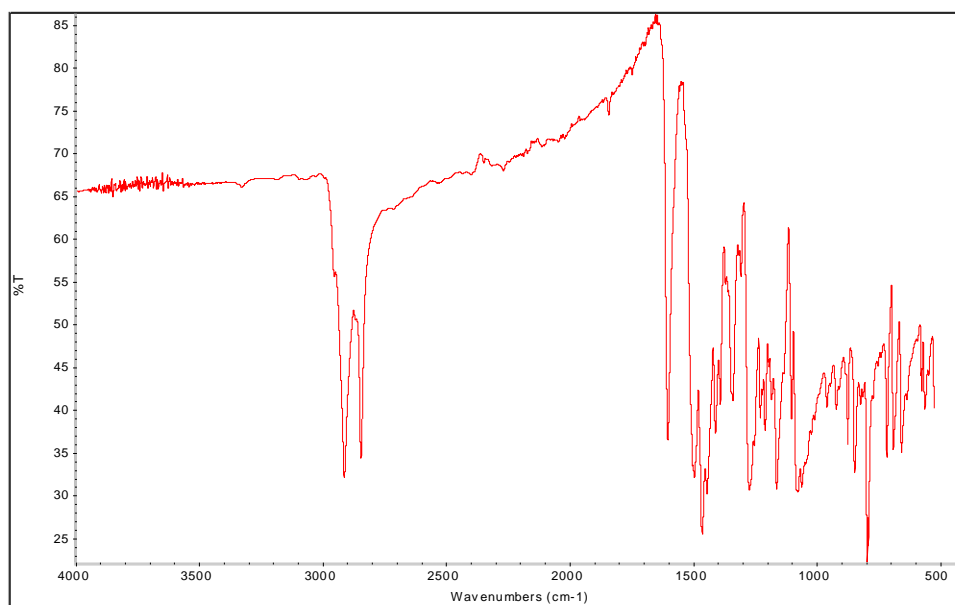
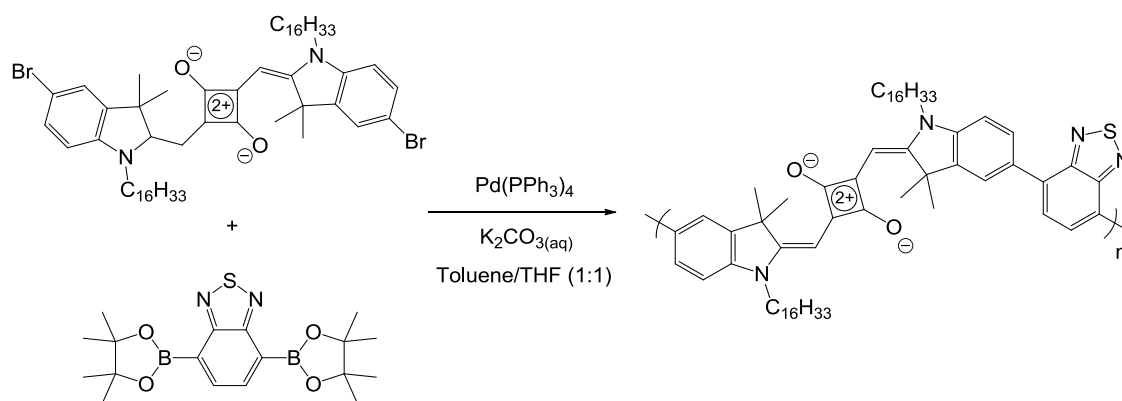


Figure 3 - 20:  $^1\text{H}$ - $^{13}\text{C}$  HSQC NMR spectra (400 MHz) of **12** in  $\text{CDCl}_3$ .

Figure 3 - 21: IR spectrum (ATR) of **12**.

**Poly(bis(hexadecyl)squaraine-*alt*-benzothiadiazole) (PSQBT) via Suzuki polycondensation**



**12** (502 mg, 0.5 mmol), 2,1,3-Benzothiadiazole-4,7-bis(boronic acid pinacol ester) (194 mg, 0.5 mmol) and tetrakis(triphenylphosphine)palladium(0) (15 mg, 0.013 mmol) were dissolved in 10 mL of a degassed THF/toluene mixture (1:1 vol) in a 50 mL round-bottom flask, followed by several cycles vacuum/argon. Then, 10 mL of a degassed 2 M potassium carbonate aqueous solution was added. The reaction was refluxed under argon for 48h. A dark green coloration of the solution could be observed. The reaction mixture was then poured into 200 mL of methanol. The dark purple precipitate was collected by filtration, rinsed with water and methanol, followed by purification on Soxhlet apparatus (methanol, acetone, THF and CHCl<sub>3</sub>). The THF and CHCl<sub>3</sub> fractions were separately precipitated in methanol. The resulting dark purple solids were recovered by filtration and dried under vacuum at 40°C overnight ( $m_{\text{THF}}$ =115 mg,  $m_{\text{CHCl}_3}$ =268 mg, 78 %).

$^1\text{H}$  NMR (400 MHz,  $\text{CDCl}_3$ ):  $\delta$  (ppm) 8.15 – 7.94 (m, 4H), 7.84 (s, 2H), 7.19 (d,  $J = 7.3$  Hz, 2H), 6.16 (s, 2H), 4.10 (s, 4H), 2.09 – 1.79 (m, 16H), 1.64 – 1.16 (m, 52H), 0.87 (t,  $J = 6.6$  Hz, 6H).  $^{13}\text{C}$  NMR (101 MHz,  $\text{CDCl}_3$ ):  $\delta$  (ppm) 154.36, 143.01, 142.85, 133.51, 132.88, 129.62, 127.92, 123.41, 111.88, 109.94, 87.86, 49.61, 32.06, 29.84, 29.80, 29.77, 29.72, 29.66, 29.57, 29.49, 27.44, 27.27, 22.82, 14.26. FT-IR (ATR):  $\nu = 2918, 2849, 1599, 1450, 1341, 1267, 1166, 1041, 965, 917, 789, 691, 565\text{ cm}^{-1}$ .

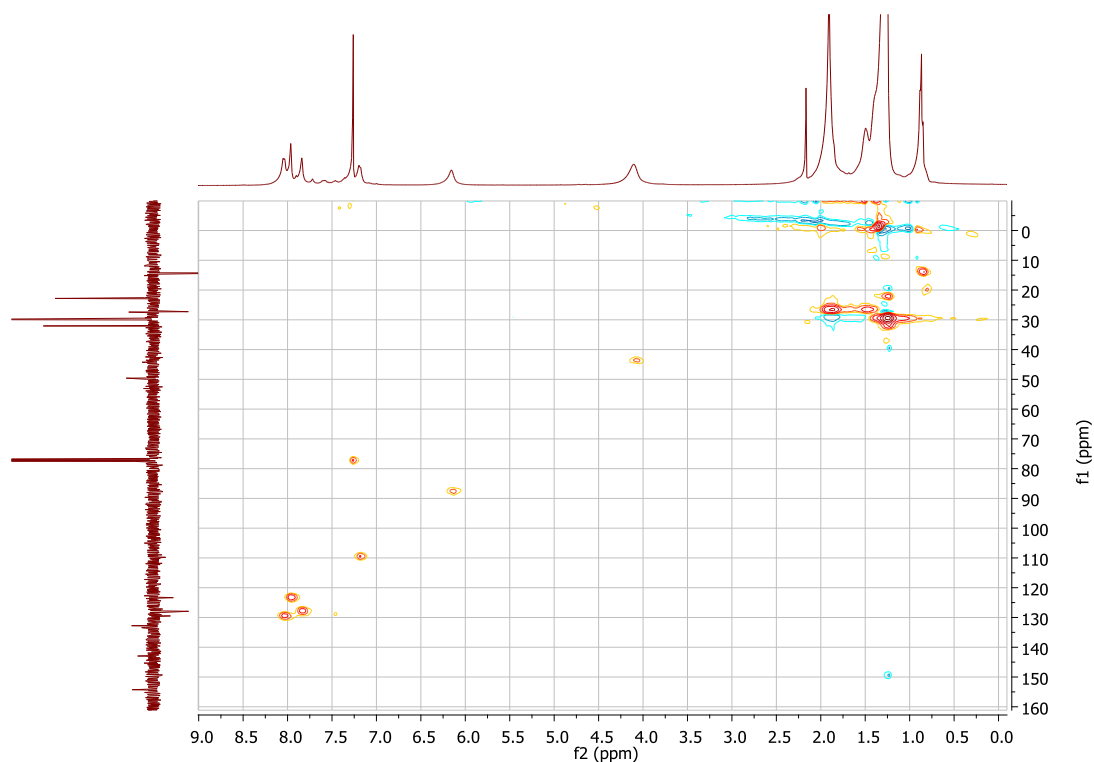


Figure 3 - 22:  $^1\text{H}$ - $^{13}\text{C}$  HSQC NMR spectra (400 MHz) of PSQBT in  $\text{CDCl}_3$ .

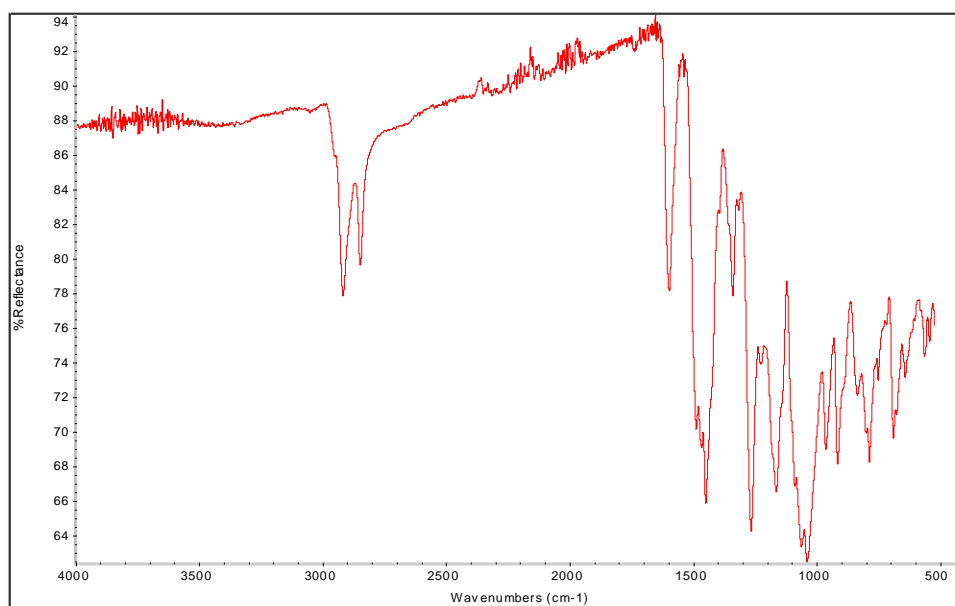
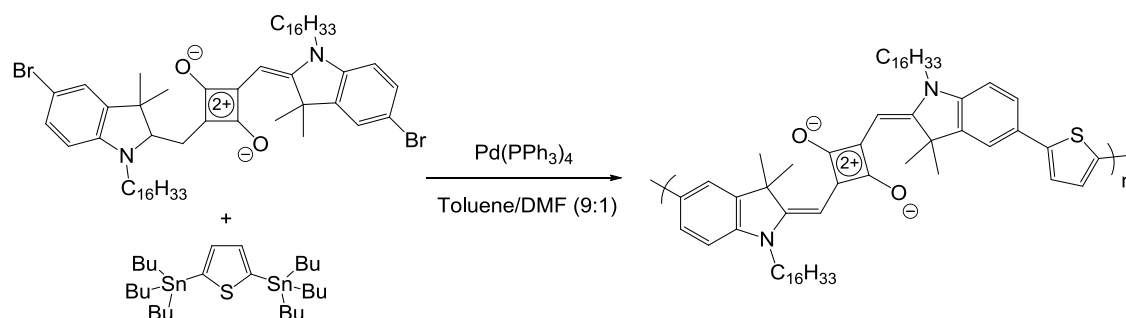


Figure 3 - 23: IR spectrum (ATR) of PSQBT.

**Poly(bis(hexadecyl)squaraine-*alt*-thiophene) (PSQT) via Stille polycondensation**

**12** (502 mg, 0.5 mmol), 2,5-bis(tributylstannyl)thiophene (331 mg, 0.5 mmol) and tetrakis(triphenylphosphine)palladium(0) (15 mg, 0.013 mmol) were dissolved in 10 mL of a degassed toluene/DMF mixture (9:1 vol) in a 50 mL round-bottom flask, followed by several cycles vacuum/argon. The reaction was refluxed under argon for 48h. A dark green coloration of the solution could be observed. The reaction mixture was then poured into 100 mL of methanol. The dark purple precipitate was collected by filtration, rinsed with methanol, followed by purification on Soxhlet apparatus (methanol, acetone, THF and CHCl<sub>3</sub>). The THF and CHCl<sub>3</sub> fractions were separately precipitated in methanol. The resulting dark purple solids were recovered by filtration and dried under vacuum at 40°C overnight ( $m_{\text{THF}}$ =119 mg,  $m_{\text{CHCl}_3}$ =293 mg, 89 %).

<sup>1</sup>H NMR (400 MHz, CDCl<sub>3</sub>):  $\delta$  (ppm) 7.65 – 7.52 (m, 4H), 7.30 (s, 2H), 6.99 (d,  $J$  = 5.5 Hz, 2H), 6.01 (s, 2H), 4.00 (s, 4H), 1.86 (s, 12H), 1.79 – 1.67 (m, 2H), 1.52 – 1.16 (m, 52H), 0.87 (t,  $J$  = 6.7 Hz, 6H). <sup>13</sup>C NMR (101 MHz, CDCl<sub>3</sub>):  $\delta$  (ppm) 169.55, 143.15, 142.14, 130.37, 129.08, 125.70, 125.59, 125.53, 123.98, 119.65, 109.87, 87.37, 49.44, 44.04, 32.06, 29.84, 29.83, 29.80, 29.75, 29.69, 29.64, 29.53, 29.50, 27.33, 27.25, 22.83, 14.26. FT-IR (ATR):  $\nu$  = 2919, 2849, 1599, 1450, 1351, 1267, 1165, 1066, 963, 918, 788, 689, 567 cm<sup>-1</sup>.

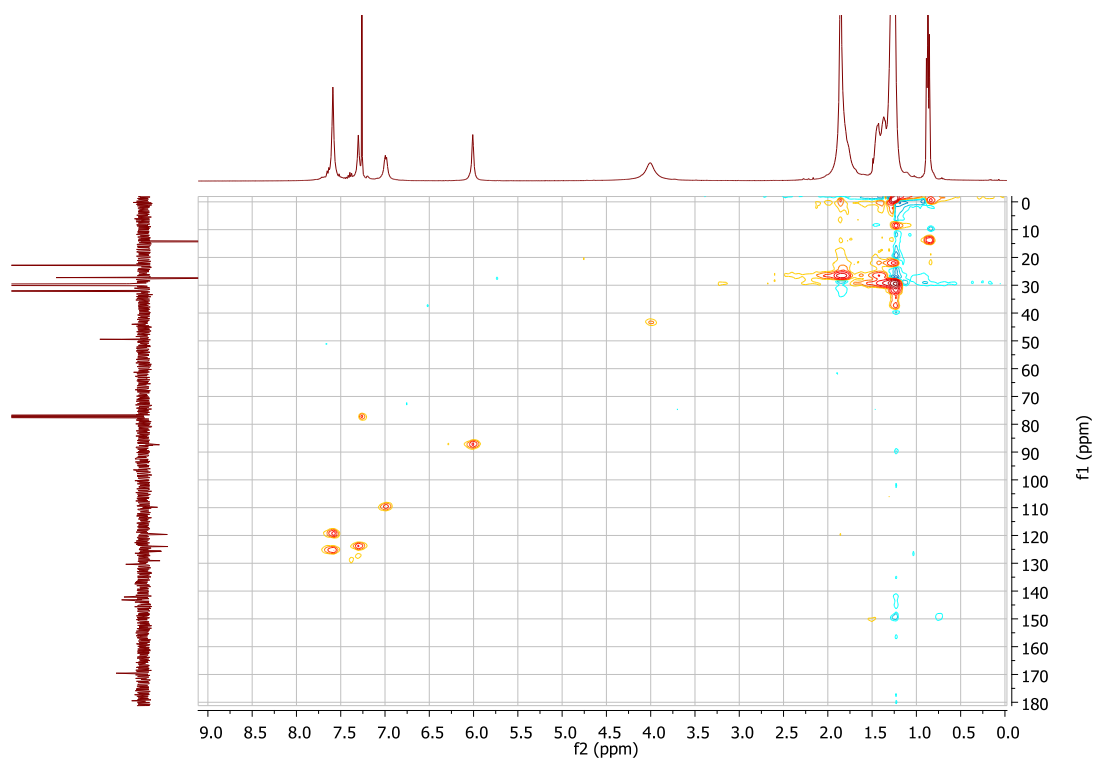


Figure 3 - 24:  $^1\text{H}$ - $^{13}\text{C}$  HSQC NMR spectra (400 MHz) of PSQT in  $\text{CDCl}_3$ .

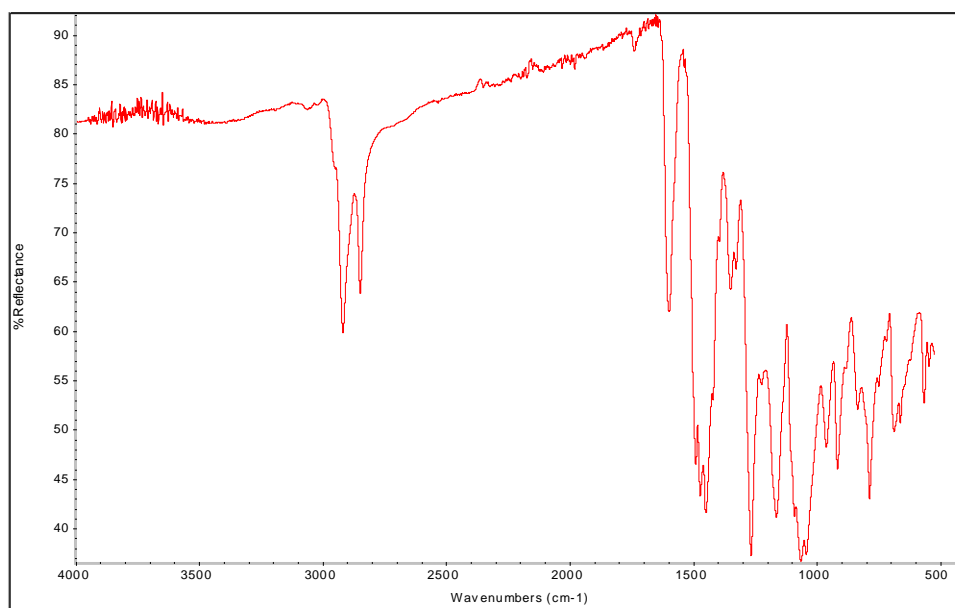
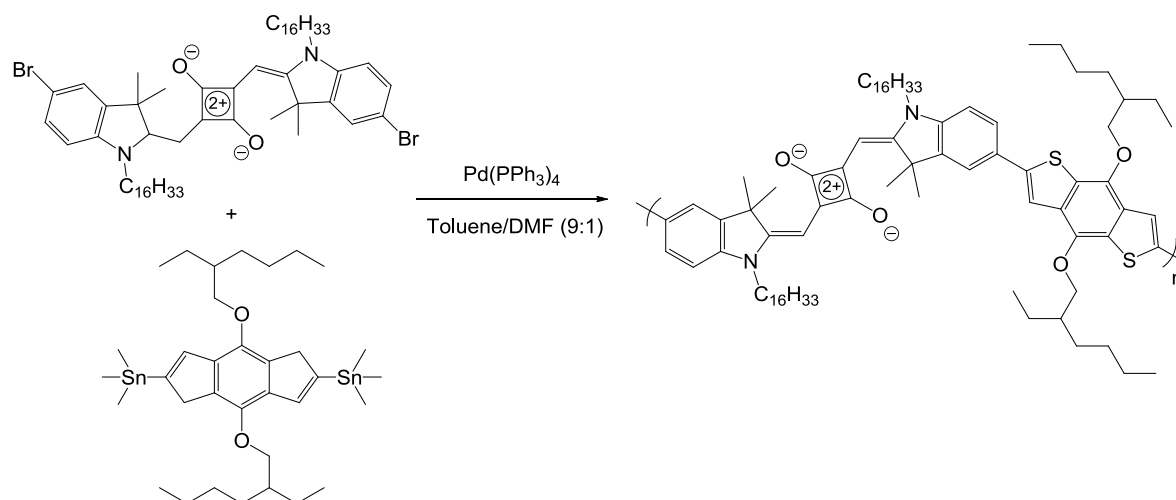


Figure 3 - 25: IR spectrum (ATR) of PSQT.



**Poly(bis(hexadecyl)squaraine-*alt*-bis(2-ethylhexyloxy)benzodithiophene) (PSQBDT)**

**12** (502 mg, 0.5 mmol), bis(2-ethylhexyloxy)benzo[1,2-b:4,5-b']dithiophene -4,8-bis(trimethylstannane) (368 mg, 0.5 mmol) and tetrakis(triphenylphosphine)palladium(0) (15 mg, 0.013 mmol) were dissolved in 10 mL of a degassed toluene/DMF mixture (9:1 vol) in a 50 mL round-bottom flask, followed by several cycles vacuum/argon. The reaction was refluxed under argon for 48h. A dark green coloration of the solution could be observed. The reaction mixture was then poured into 100 mL of methanol. The dark purple precipitate was collected by filtration, rinsed with methanol, followed by purification on Soxhlet apparatus (methanol, acetone, THF and  $\text{CHCl}_3$ ). The THF and  $\text{CHCl}_3$  fractions were separately precipitated in methanol. The resulting dark purple solids were recovered by filtration and dried under vacuum at 40°C overnight ( $m_{\text{THF}}$ =336 mg,  $m_{\text{CHCl}_3}$ =181 mg, 80 %).

$^1\text{H}$  NMR (400 MHz,  $\text{CDCl}_3$ ):  $\delta$  (ppm) 7.77 – 7.67 (m, 4H), 7.65 (s, 2H), 7.05 (d,  $J$  = 7.5 Hz, 2H), 6.07 (s, 2H), 4.26 (s, 4H), 4.03 (s, 4H), 1.89 (s, 12H), 1.81 – 1.16 (m, 74H), 1.09 (t,  $J$  = 7.4 Hz, 6H), 1.00 (t,  $J$  = 7.0 Hz, 6H), 0.87 (t,  $J$  = 6.8 Hz, 6H).  $^{13}\text{C}$  NMR (101 MHz,  $\text{CDCl}_3$ ):  $\delta$  (ppm) 144.42, 143.32, 143., 132.95 (s), 129.52, 126.66, 120.54, 115.61, 109.99, 76.22, 49.48, 43.47, 40.86, 32.07, 30.66, 29.84, 29.81, 29.77, 29.71, 29.66, 29.56, 29.51, 29.38, 27.32, 27.26, 24.07, 23.37, 22.83, 14.42, 14.26, 11.55. FT-IR (ATR):  $\nu$  = 2921, 2852, 1596, 1478, 1346, 1270, 1168, 1071, 965, 915, 791, 686, 568  $\text{cm}^{-1}$ .

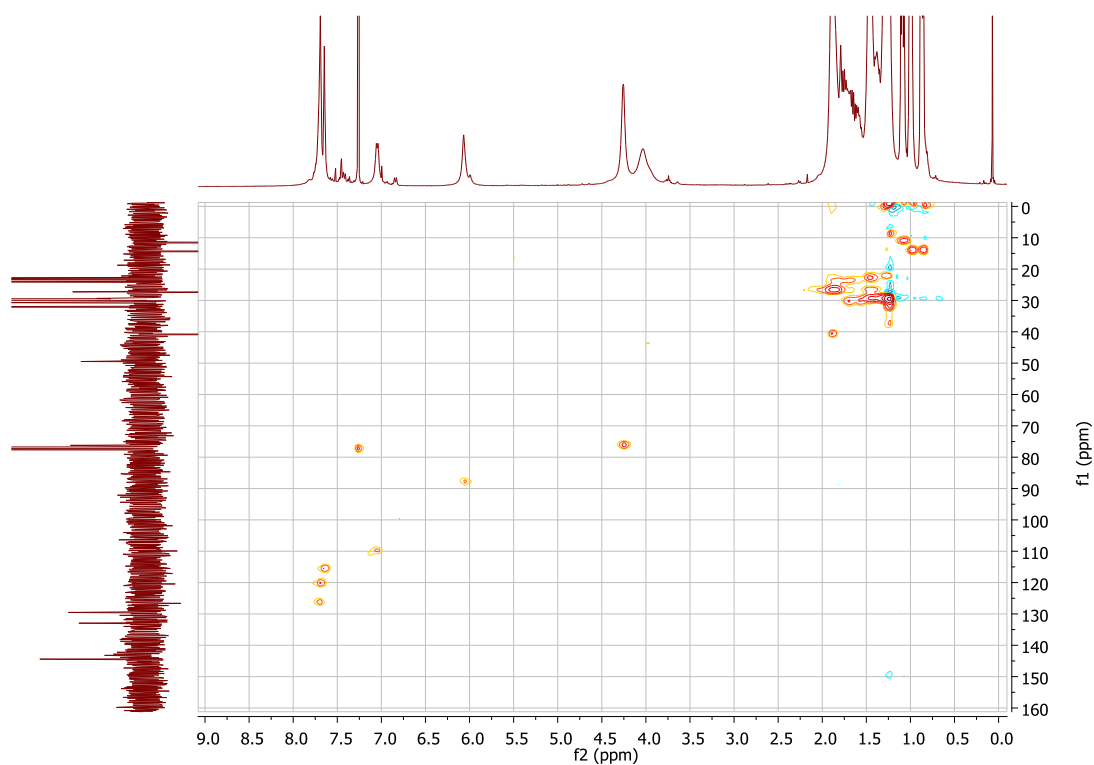


Figure 3 - 26:  $^1\text{H}$ - $^{13}\text{C}$  HSQC NMR spectra (400 MHz) of PSQBDT in  $\text{CDCl}_3$ .

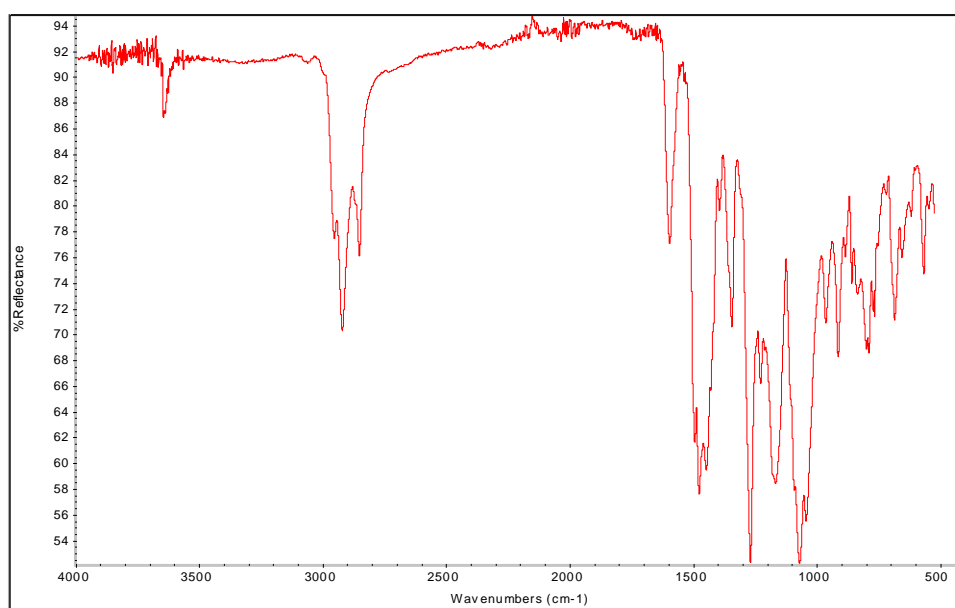


Figure 3 - 27: IR spectrum (ATR) of PSQT.

### 3.6.2 THERMOGRAVIMETRIC ANALYSES (TGA)

TGA data were measured under N<sub>2</sub> atmosphere at 10°C/min.

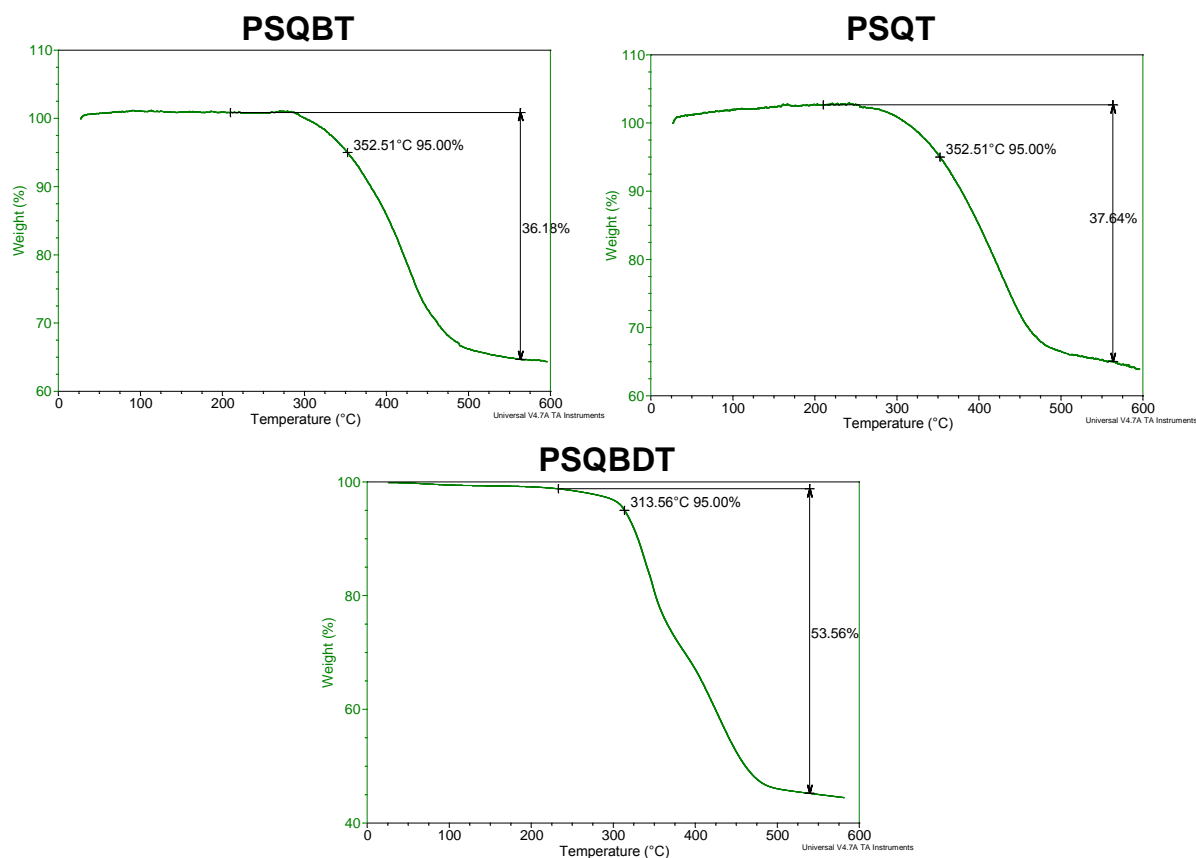


Figure 3 - 28: TGA analyses of PSQs.

### 3.6.3 DIFFERENTIAL SCANNING CALORIMETRY (DSC)

DSC data were measured under helium flow (25 ml/min) at a scan rate of 20°C/min, between -150°C and 250°C.

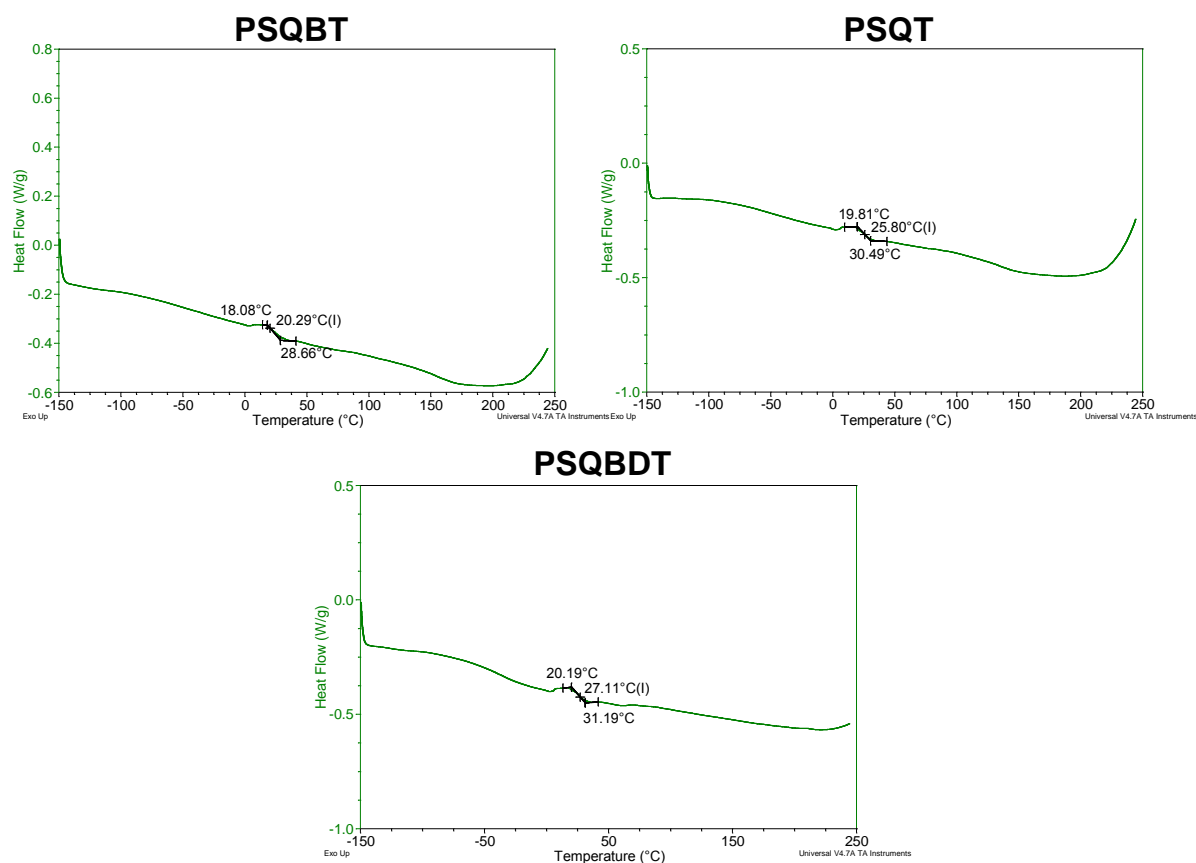


Figure 3 - 29: DSC analyses of PSQs.

### 3.6.4 ELECTROCHEMISTRY

A solution of  $0.1 \text{ g.l}^{-1}$  of the investigated polymer in  $\text{CHCl}_3$  (according to solubility) with  $0.1 \text{ M}$  tetrabutylammonium hexafluorophosphate (TBAPF6) as electrolyte was prepared in a glove box under  $\text{N}_2$ . CV measurements were then performed on the solution under  $\text{N}_2$ , using a silver wire as reference electrode and platinum for the working and counter electrodes. A solution of ferrocene ( $1 \text{ mM}$  in  $\text{CHCl}_3$ ) was prepared in the same conditions and the redox potential of  $\text{Fc}/\text{Fc}^+$  vs  $\text{Ag}$  ( $E_{\text{Fc}/\text{Fc}^+ \text{ Ag}}$ ) was measured.

### PSQBT

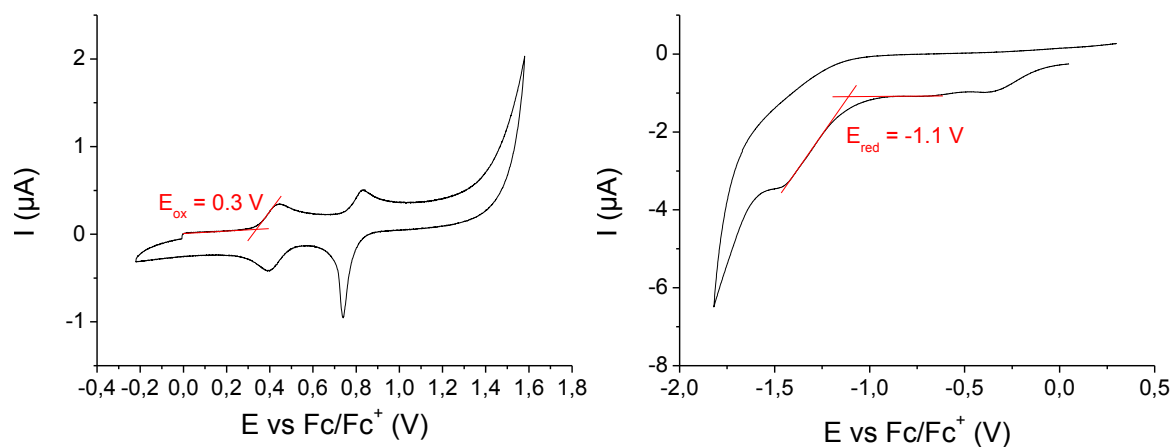


Figure 3 - 30: Cyclic voltammograms of PSQBT in  $\text{CHCl}_3$  solution ( $0.1 \text{ g.l}^{-1}$ ). Left-oxidation; right-reduction.

### PSQT

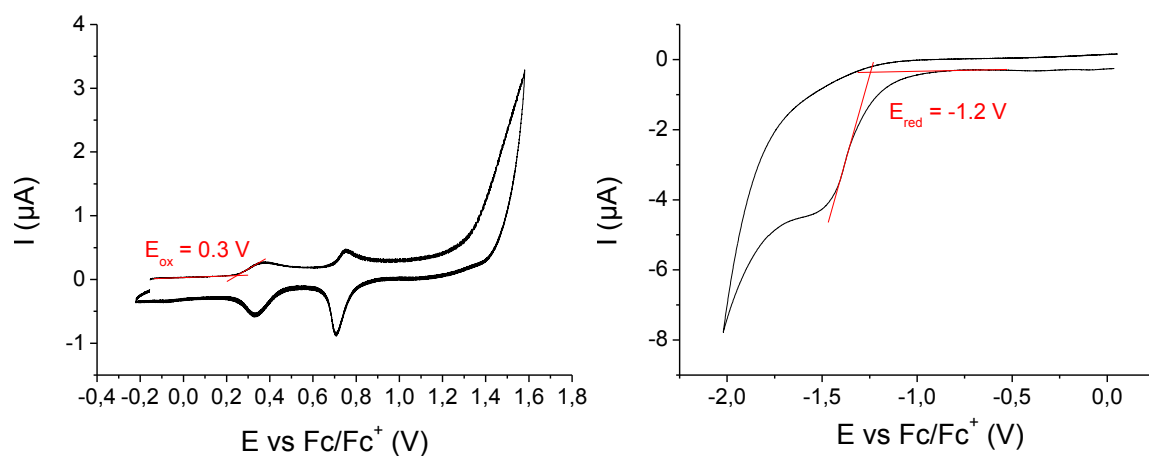


Figure 3 - 31: Cyclic voltammograms of PSQT in  $\text{CHCl}_3$  solution ( $0.1 \text{ g.l}^{-1}$ ). Left-oxidation; right-reduction.

### PSQBDT

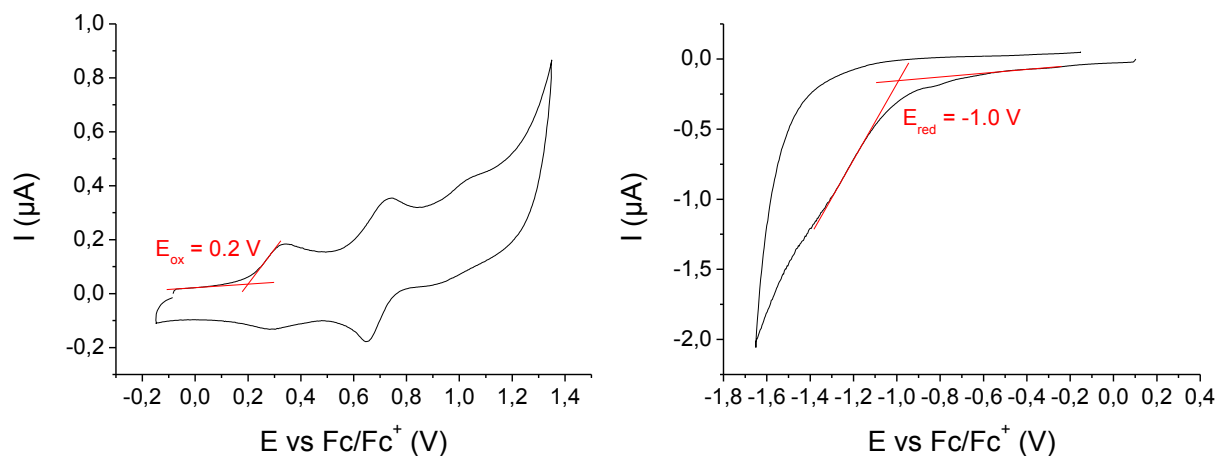


Figure 3 - 32: Cyclic voltammograms of PSQBDT in CHCl<sub>3</sub> solution (0.1 g.l<sup>-1</sup>). Left-oxidation; right-reduction.

## 3.6.5 OPTICAL CHARACTERIZATIONS

### THF fractions

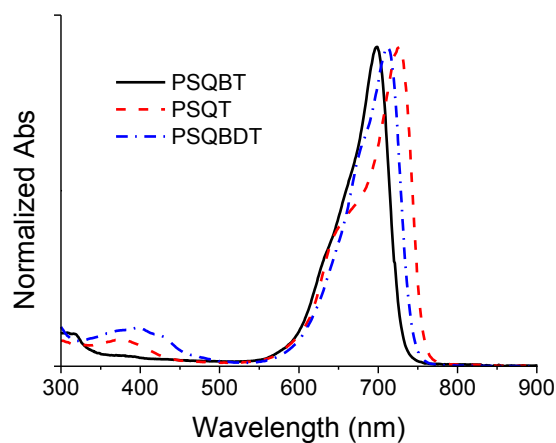


Figure 3 - 33: Normalized UV-visible absorption spectra of the PSQs THF fractions in CHCl<sub>3</sub> solution (0.01 g.l<sup>-1</sup>).

### PSQ:PCBM blends

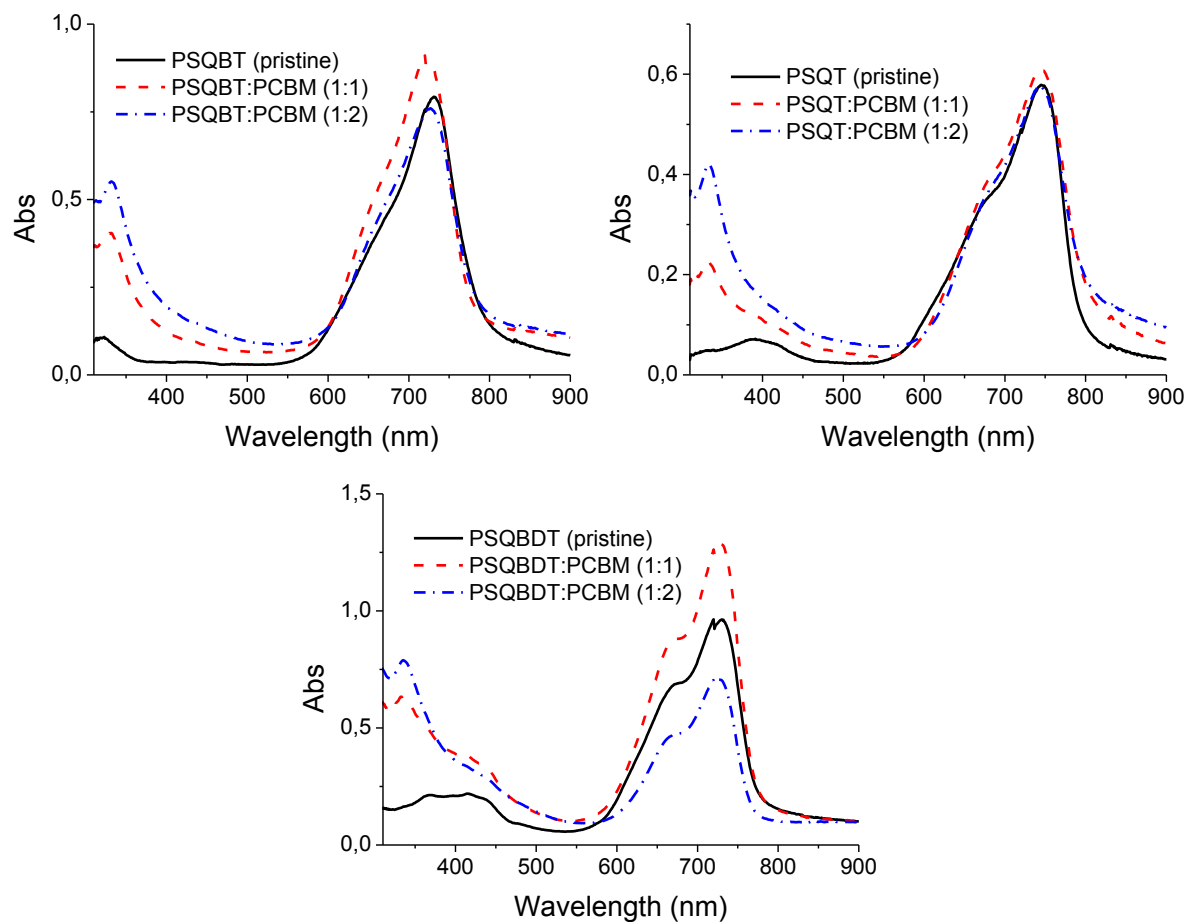


Figure 3 - 34: UV-visible absorption spectra of pristine PSQs in films and PSQ:PCBM blends in films at different ratios, spin-coated from ODCB solutions onto PEDOT-PSS coated glass substrates.

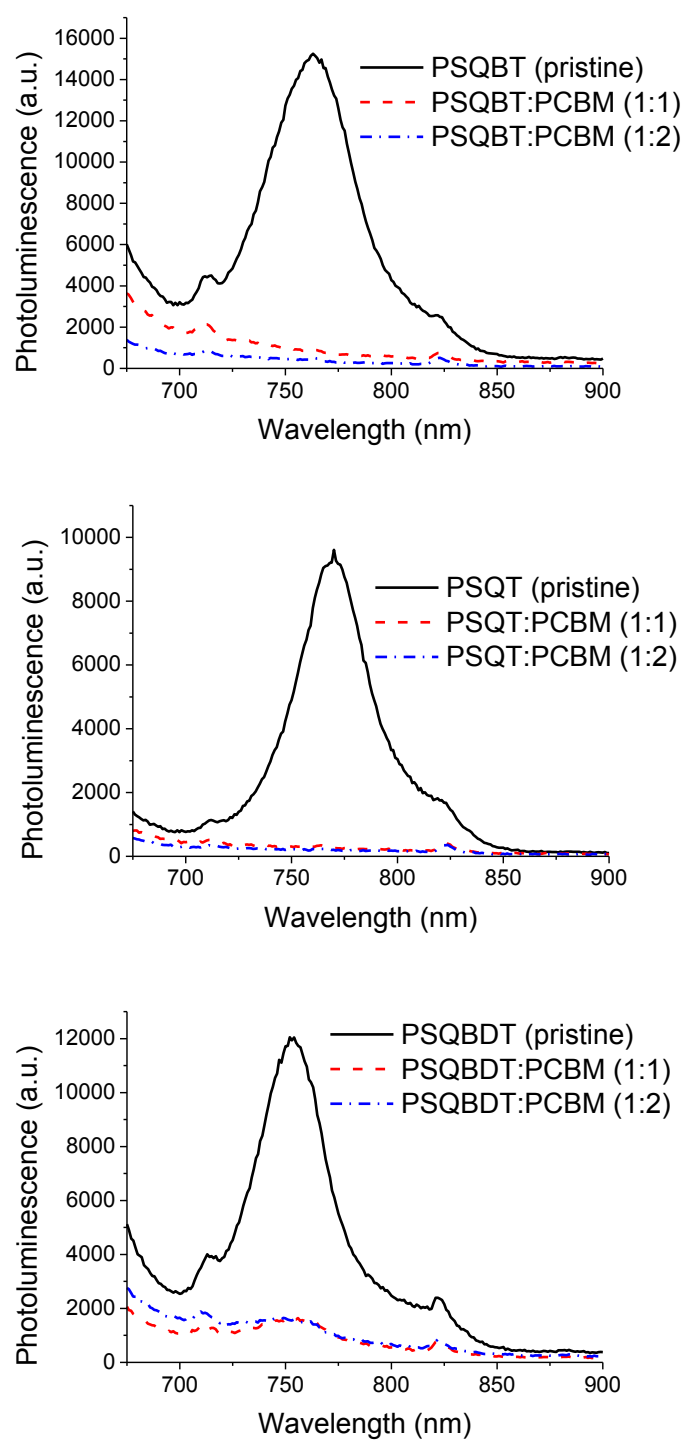


Figure 3 - 35: Photoluminescence spectra of pristine PSQs in films and PSQ:PCBM blends in films at different ratios, excited at 650 nm.





---

Chapter 4      NOVEL CONJUGATED POLYMERS  
PREPARED BY METAL-FREE  
POLYCONDENSATIONS



## Table of contents

<b>4.1</b>	<b>Literature overview .....</b>	<b>147</b>
<b>4.1.1</b>	<b>Polycondensation with squaric acid .....</b>	<b>147</b>
<b>4.1.2</b>	<b>Polymerization by arylimino-de-oxo-bisubstitution .....</b>	<b>151</b>
<b>4.1.3</b>	<b>Strategy .....</b>	<b>153</b>
<b>4.2</b>	<b>Polysquaraines .....</b>	<b>155</b>
<b>4.2.1</b>	<b>Synthesis.....</b>	<b>155</b>
4.2.1.1	Monomers .....	155
4.2.1.2	Polymers.....	161
<b>4.2.2</b>	<b>Characterization.....</b>	<b>165</b>
4.2.2.1	Thermal properties.....	165
4.2.2.2	Optical properties.....	166
4.2.2.3	Electrochemical properties .....	168
<b>4.3</b>	<b>Polyimines.....</b>	<b>169</b>
<b>4.3.1</b>	<b>Synthesis.....</b>	<b>169</b>
4.3.1.1	Monomers .....	169
4.3.1.2	Polymers .....	170
<b>4.3.2</b>	<b>Characterization.....</b>	<b>171</b>
4.3.2.1	Thermal properties.....	171
4.3.2.2	Optical properties.....	172
<b>4.4</b>	<b>Conclusion.....</b>	<b>174</b>
<b>4.5</b>	<b>Experimental .....</b>	<b>177</b>
<b>4.5.1</b>	<b>Syntheses.....</b>	<b>178</b>
<b>4.5.2</b>	<b>Thermogravimetric analyses (TGA) .....</b>	<b>200</b>
<b>4.5.3</b>	<b>Differential Scanning Calorimetry (DSC).....</b>	<b>201</b>
<b>4.5.4</b>	<b>Optical .....</b>	<b>203</b>
<b>4.6</b>	<b>Bibliography .....</b>	<b>177</b>



## 4.1 LITERATURE OVERVIEW

Since the discovery of transition metal-catalyzed reactions, they have been intensively exploited in the synthesis of conjugated polymers (CPs). They provide efficient coupling between  $sp^2$  carbons and can be used in variety of transformations including a wide range of substrates, which makes them a versatile tool in preparation of organic materials.<sup>[1-4]</sup> However, their main drawback is the use of non-environmental friendly solvents and metallic-based catalytic systems. Metals used to catalyze such couplings (e.g. palladium or nickel) are expensive due to their rare abundance and the high cost of their commercial production. Also, traces of remaining metal catalysts in an organic material are a significant issue when considering electronic applications, since it can induce doping or act as charges trap, thus disturbing the semiconductor properties. Therefore, time and solvent-consuming purification techniques must be applied to remove these impurities (e.g. Soxhlet extraction), which has a large impact on the final cost of the produced material. As the potential low-cost production of organic semiconductors is considered as one of the greatest advantages over their inorganic counterparts, new synthetic routes are extensively sought after.

### 4.1.1 POLYCONDENSATION WITH SQUARIC ACID

In this context, different condensation reactions emerge as potential candidates able to fulfill these requirements. For instance, the condensation of 3,4-dihydroxycyclobut-3-ene-1,2-dione, also known as squaric acid (SA), with electron-rich heteroaromatic compounds (usually containing nitrogen) is a promising path towards conjugated macromolecules with small band-gaps. The main advantage lies in the fact that it can be catalyzed with an organic base or even be performed without catalysis, and produces water as the main by-product. This can significantly simplify the purification procedures and lead to synthesis implementing “green chemistry” protocols, which is highly demanded in modern scientific society. The mechanism of formation of a squaraine dye is presented in Figure 4 - 1.

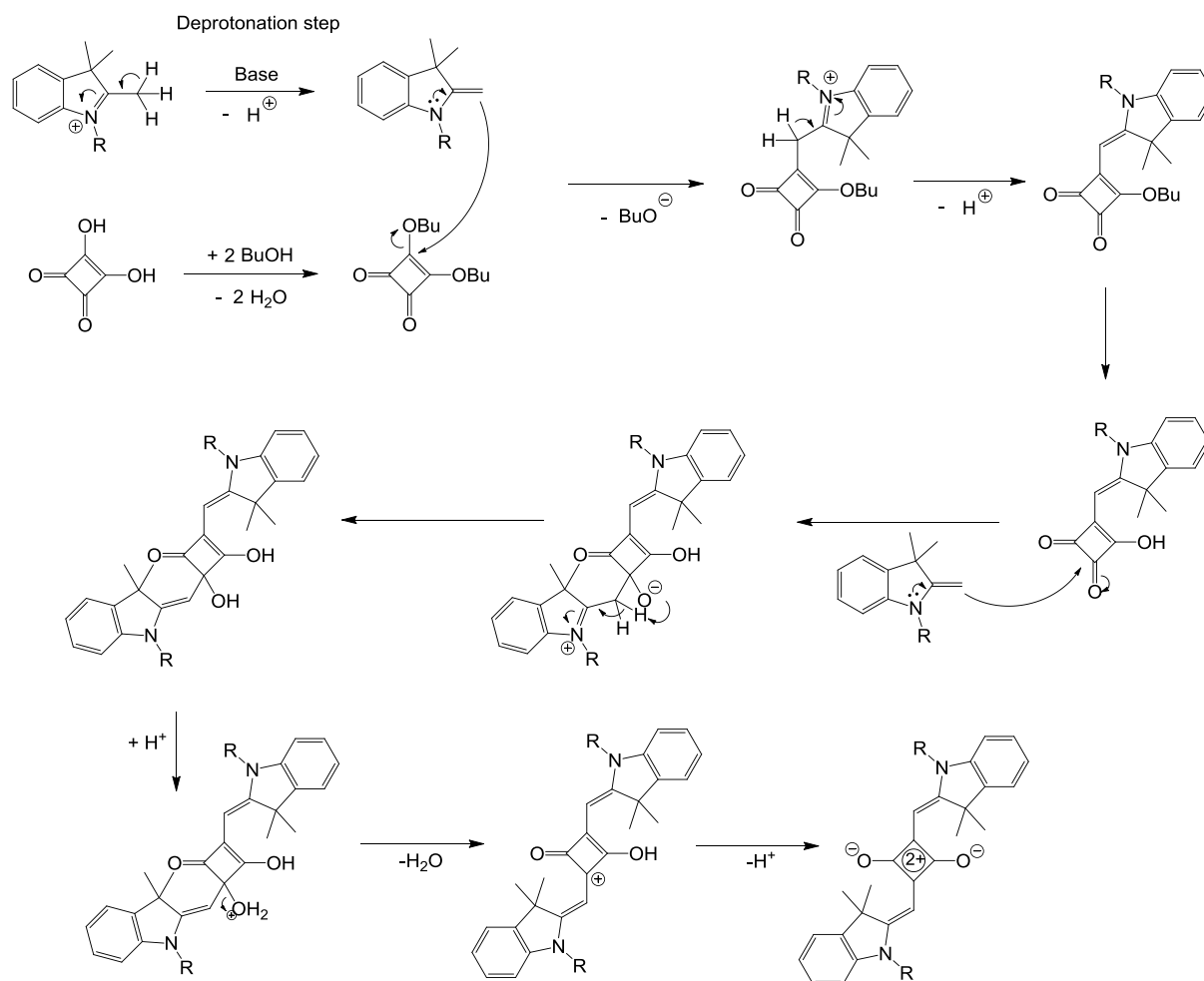


Figure 4 - 1: Mechanism of formation of a squaraine dye.<sup>[5-6]</sup>

The first report on CPs synthesis via such polycondensation dates back to 1965, when Treibs and Jacob prepared an insoluble material from pyrrole and SA (see Figure 4 - 2).<sup>[7]</sup>

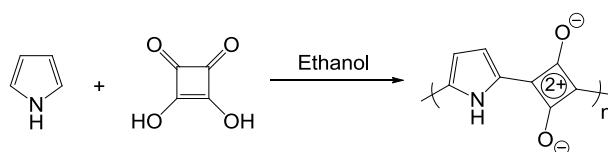
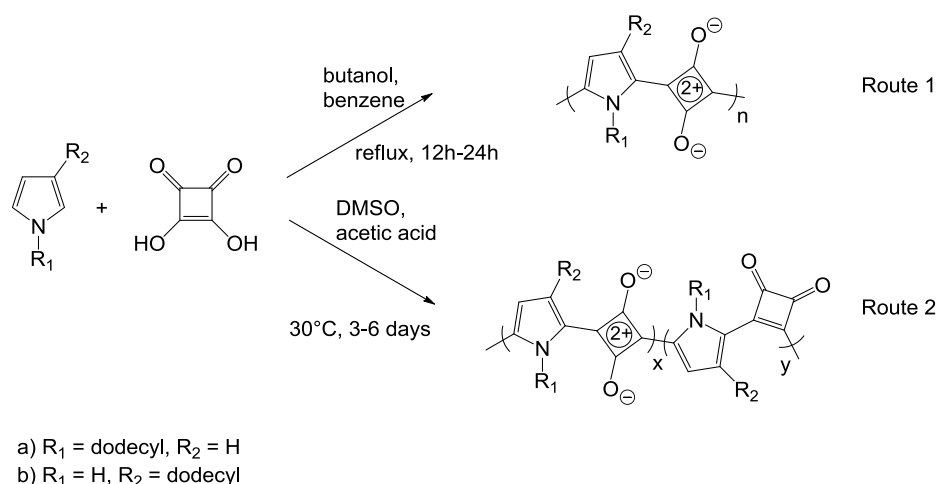


Figure 4 - 2: Synthesis of the insoluble polymer from pyrrole and SA. The structure shown here is hypothetical since it could not be confirmed due to the intractable nature of the material.<sup>[7]</sup>

As already mentioned in the previous chapter, Ajayagosh and co-workers achieved similar soluble CPs by substituting the 1 (nitrogen) or 3 positions in the pyrrole unit with alkyl chains (see Figure 4 - 3).<sup>[8]</sup> They also highlighted the possibility of tuning the composition of the final product depending on the reaction conditions (1,3-isomeric unit or both 1,3- and 1,2-isomeric units along the polymer backbone). Higher molecular weights were obtained when 1,2-isomeric moieties were present in the polymer backbone, as well as enhanced solubility in non-polar solvents. These CPs showed band-gaps down to 1.13 eV.



Synth. route/ solubilizing groups	$M_n$ (g.mol <sup>-1</sup> )	Solubility			
		MeOH	DMF	CHCl <sub>3</sub>	hexane
<b>1/a</b>	6000	±	+	+	--
<b>2/a</b>	14300	--	--	++	++
<b>1/b</b>	4500	±	+	+	--
<b>2/b</b>	10900	--	--	++	++

±: partial; +: good; ++: very good; --: bad.

Figure 4 - 3: Influence of reaction conditions on the structure and solubility of pyrrole-based polysquaraines.<sup>[8]</sup>

Carbazole (Cz) is another electron-rich unit which can be condensed with squaric acid. Chen and Hall developed a series of polymers synthesized from N-alkylated Cz and SA (see Figure 4 - 4).<sup>[9]</sup> However, the employed solubilizing groups (ethyl and butyl) were not sufficient enough to dissolve the obtained materials in common organic solvents, thus limiting their characterization.

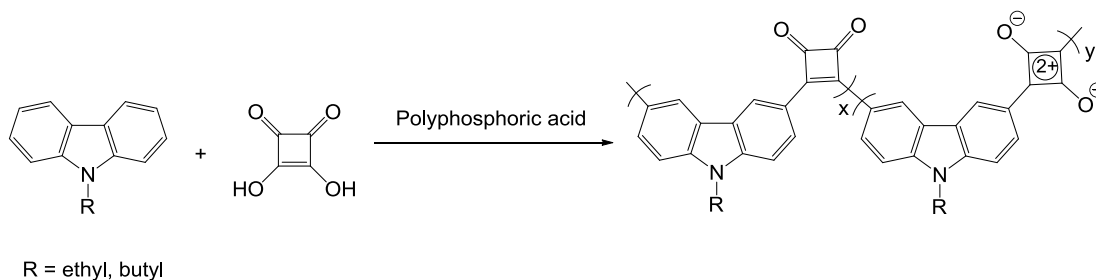
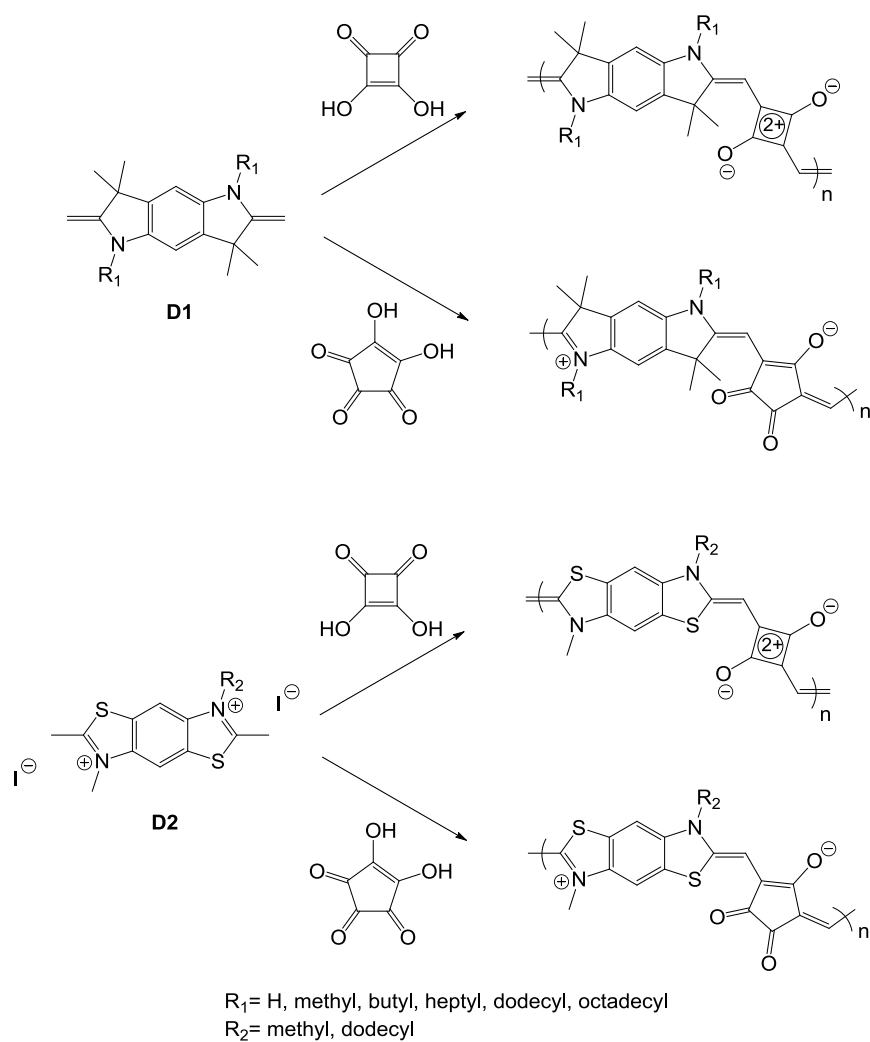


Figure 4 - 4: Carbazole-based polysquaraine.<sup>[9]</sup>

By selecting suitable electron-rich molecule with two reactive sites towards SA and refluxing them in alcohols (butanol, cyclohexanol or propanol), Havinga and co-workers achieved semiconducting polymers showing very small band-gaps (see Figure 4 - 5).<sup>[10-11]</sup> They also demonstrated that a similar reaction could be carried out by replacing SA with croconic acid (CA), leading to even smaller band-gaps. Introducing ionic functional groups on the side chains allowed them to obtain water-soluble polysquaraines.<sup>[12]</sup>



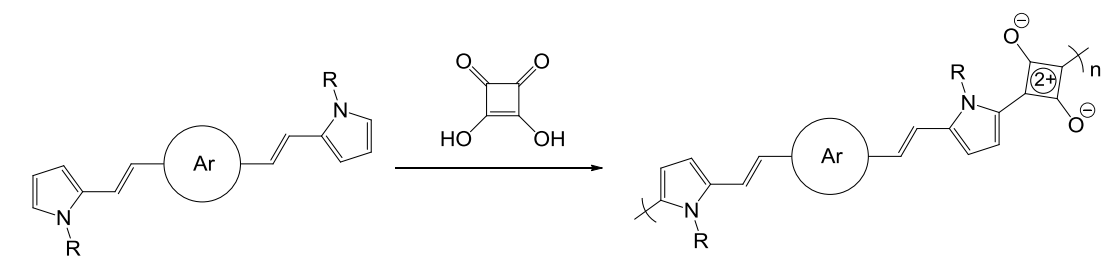


Donor	Acceptor	E <sub>g</sub> <sup>opt</sup> (eV) <sup>a</sup>
<b>D1</b>	SA	1.15
	CA	1.2
<b>D2</b>	SA	0.8
	CA	0.5

<sup>a</sup> Data for R = dodecyl

Figure 4 - 5: Small band-gaps polysquaraines based on SA and CA.<sup>[10-11]</sup>

Other research groups took advantage of the pyrrole reactivity to develop difunctional monomers suitable for condensation with SA. As illustrated in Figure 4 - 6, a wide variety of conjugated polymers was achieved following that strategy.




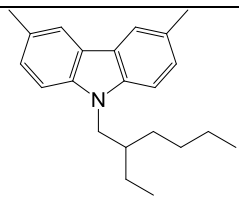
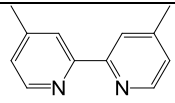
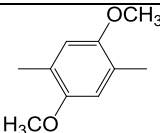
	Solubilizing group R	$M_n / M_w$ (g.mol <sup>-1</sup> )	$\lambda_{\max}^{\text{solution}}$ (nm)	$E_g^{\text{opt}}$ (eV)	Ref
	hexadecyl	8300 / 20900	685 727	1.38	[13]
	2-ethylhexyl	10000 / 20200	636 718	1.38	
	dodecyl	15800 / 124300	870 978	0.89	[14]

Figure 4 - 6: Examples of polysquaraines obtained by condensation of pyrrole-based difunctional monomers with SA.

#### 4.1.2 POLYMERIZATION BY ARYLIMINO-DE-OXO-BISUBSTITUTION

Another example of metal-free synthesis of CPs is the arylimino-de-oxo-bisubstitution, as already mentioned in Chapter 1. In this reaction, imine bonds are formed from aldehyde and primary amine by simple elimination of water. Polymers obtained via this transformation are known as polyimines or polymeric Schiff bases.

One of the first reports of a conjugated polymer obtained via arylimino-de-oxo-bisubstitution dates back to 1923, where dialdehydes and diamines were condensed in bulk, leading to insoluble products.<sup>[15]</sup> Over the years, conjugated polyimines have been extensively studied in order to achieve thermally stable polymers with high mechanical strength for application in aircraft industry.<sup>[16-17]</sup> In the late 1980s - 1990s, several research groups investigated conjugated polyimines as potential candidates for electronic applications. For instance, Jenekhe and co-workers synthesized a series of polymers by condensing aromatic diamines and dialdehydes in solution (see Figure 4 - 7), and characterized their opto-electronic properties.<sup>[18]</sup> The obtained materials with band-gaps ranging from 2.1 to 2.8 eV were poorly soluble in organic solvents. However, better solubility was achieved when complexing them with a Lewis acid such as GaCl<sub>3</sub>, and a decrease of the band-gaps to 1.7 - 2.1

eV was also observed. This effect was explained by an enhanced planarity of the backbone via complexation of the imine's nitrogen atoms.

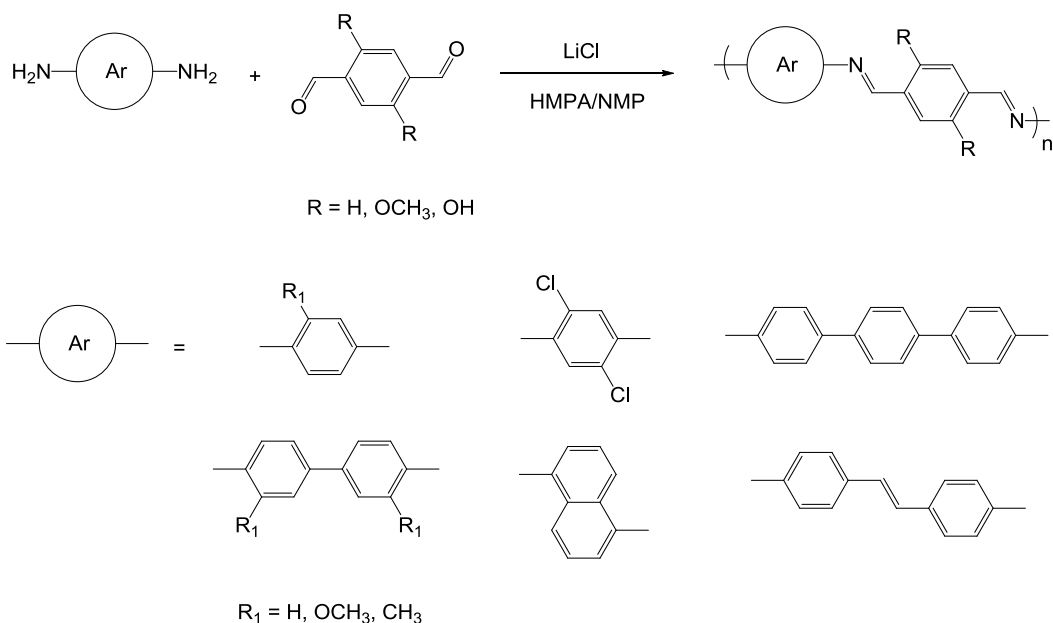


Figure 4 - 7: Examples of conjugated polyimines developed by Jenekhe et al.<sup>[18]</sup>

Electronic properties of polyimines incorporating different heteroaromatic units were also investigated. As an example, a diketonic derivative of selenophene was employed in condensations with different aromatic diamines.<sup>[19]</sup> Investigations on the electrical conductivity of these insoluble CPs revealed a semiconducting behavior upon doping with iodine.

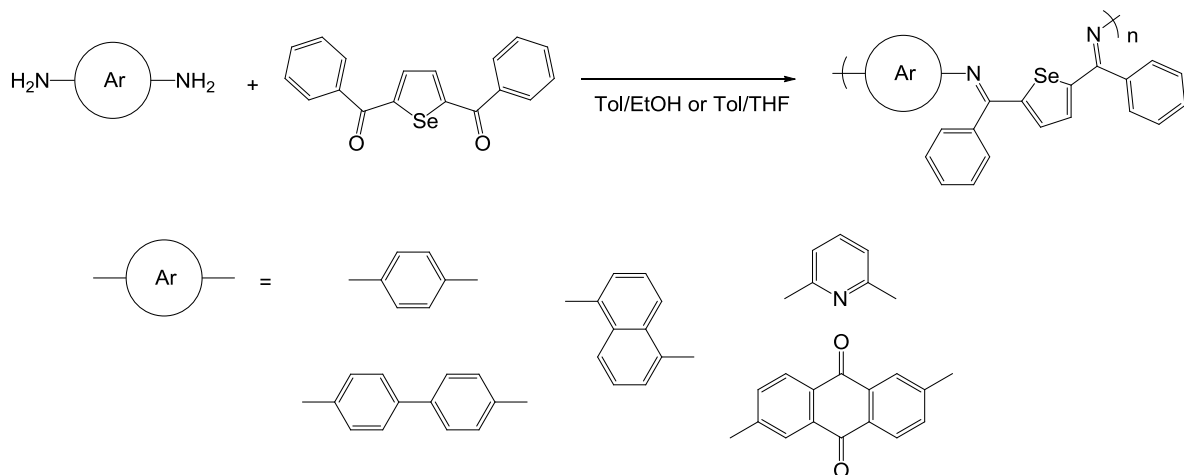


Figure 4 - 8: Examples of selenophene-based conjugated polyimines.<sup>[19]</sup>

More recently, a series of soluble conjugated polyimines were developed by Skene and co-workers.<sup>[20-21]</sup> The materials were synthesized by condensing a diamine derivative of fluorene with various dialdehydes. The resulting CPs showed fluorescence, which is rarely observed for polyimines

presumably due to a quenching from the imine bond.<sup>[22]</sup> It was revealed that the efficient fluorescence was related to the alkyl substitution of the fluorene unit.

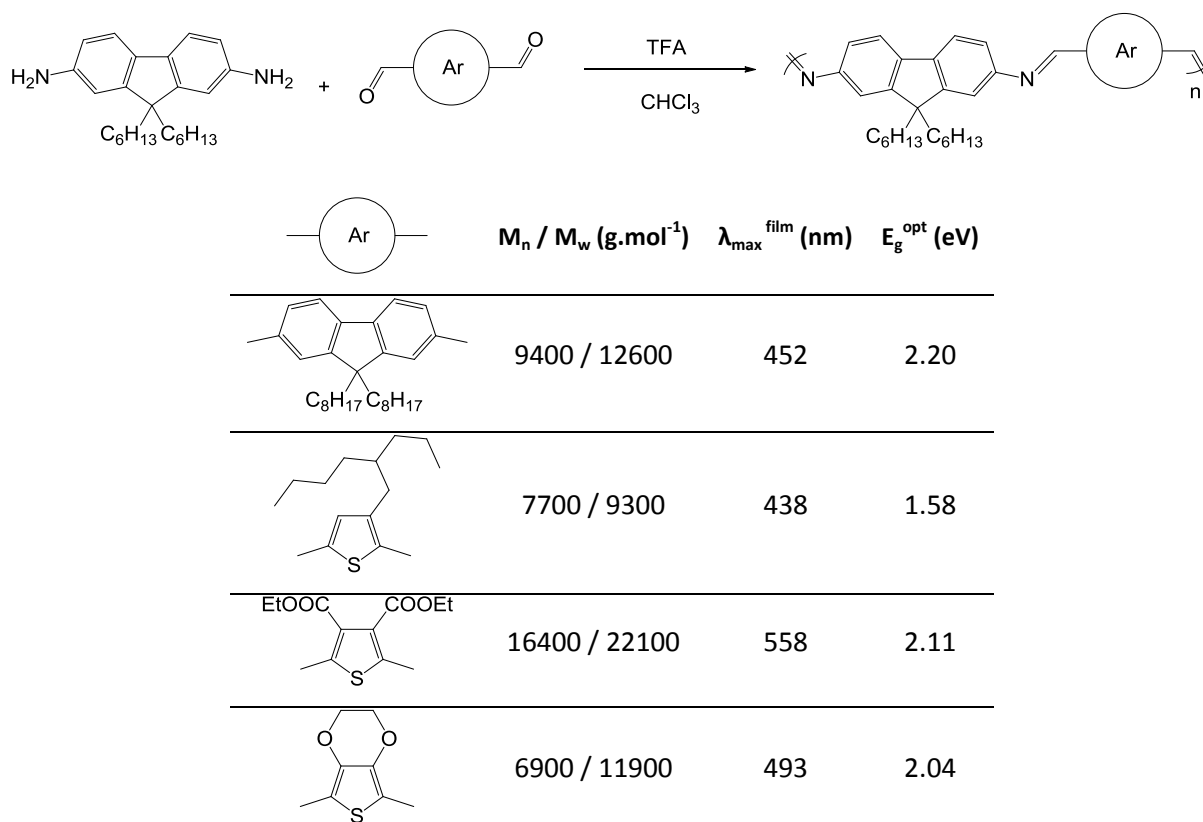


Figure 4 - 9: Conjugated polyimines based on fluorene.<sup>[20-21]</sup>

### 4.1.3 STRATEGY

Due to the numerous advantages offered by the metal-free condensations, it was decided to synthesize novel conjugated material via condensation with squaric acid and arylimino-de-oxo-bisubstitution.

The first objective involved a metal-free synthesis of previously prepared polymers (**PSQT** and **PSQBT**, see Figure 4 - 10).

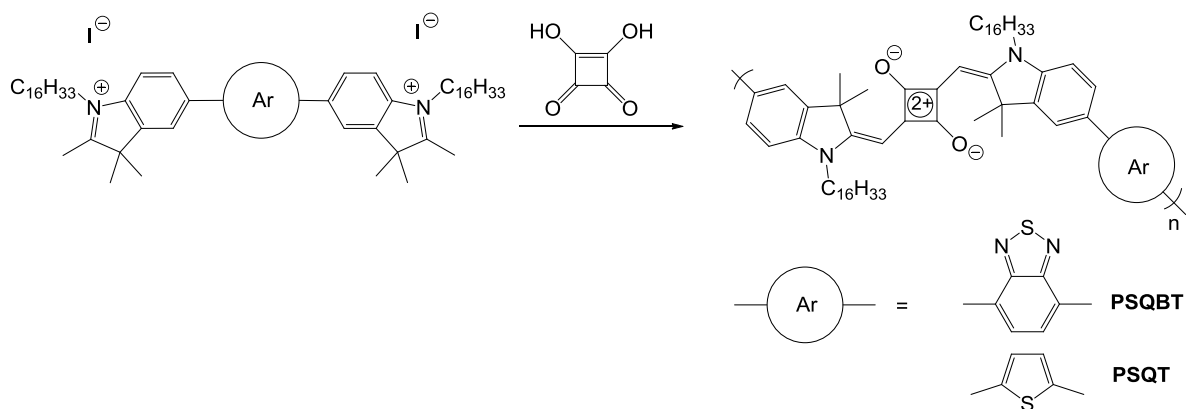


Figure 4 - 10: Metal-free approach to PSQT and PSQBT.

Furthermore, aniline derivative, which is known to condense with SA,<sup>[5]</sup> was exploited to achieve a novel CP (see Figure 4 - 11). Alkyl chains were incorporated to provide solubility of the resulting material.

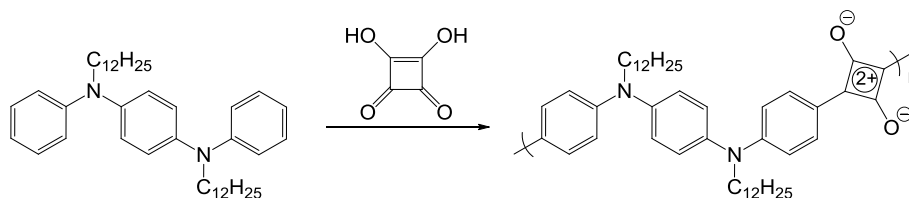


Figure 4 - 11: Polycondensation of aniline derivative with SA.

The second approach included the synthesis of aromatic diamines and dialdehydes based on the well-known carbazole and EDOT moieties, which were subsequently polymerized via the arylimino-de-oxo-bisubstitution reaction.

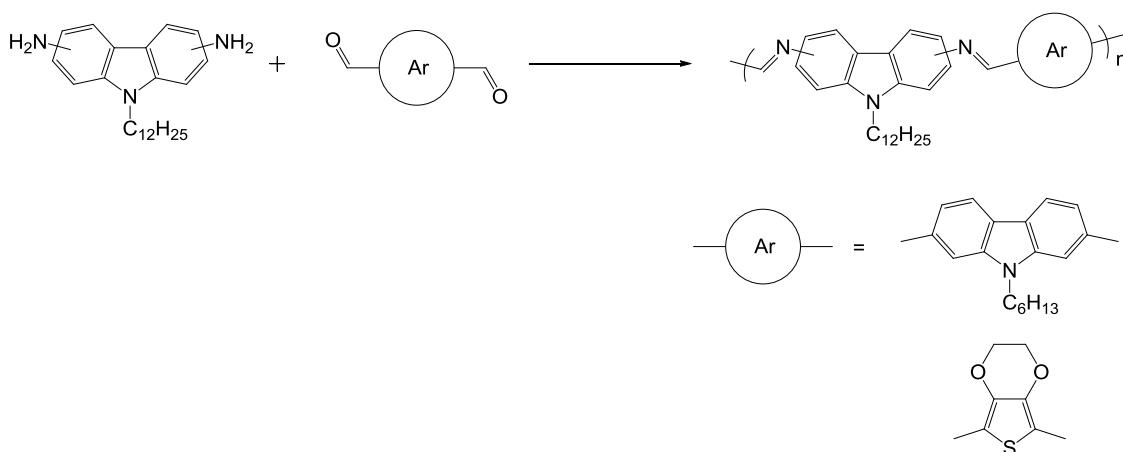


Figure 4 - 12: Polycondensations via arylimino-de-oxo-bisubstitution between 3,6- and 2,7-diaminocarbazole and bisaldehydes derivatives of EDOT and carbazole.

## 4.2 SYNTHESIS AND CHARACTERIZATION OF POLYSQUARAINES

### 4.2.1 SYNTHESIS OF POLYSQUARAINES

#### 4.2.1.1 INDOLE-BASED MONOMERS

Taking inspiration from the condensation of indole derivative with squaric acid, we focused on the synthesis of monomers composed of a central heteroaromatic unit (Th or BT) bonded with two indole moieties (see Figure 4 - 13). Furthermore, hexadecyl chains are attached on the indole units to ensure solubility of the resulting polymers.

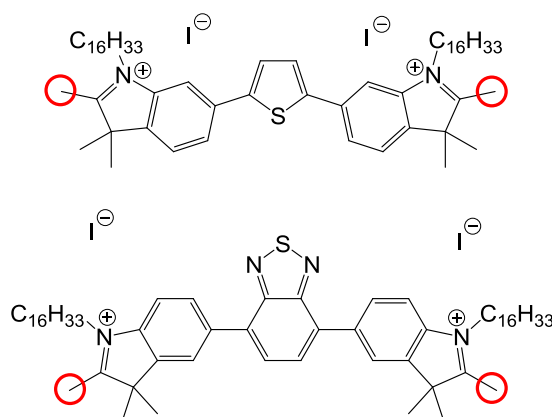


Figure 4 - 13: Bis-indolium iodide monomers. Circled in red: reactive sites towards SA.

The thiophene-based monomer was prepared in two steps (see Figure 4 - 14). Stille coupling of the commercially available bis(tributylstannyl)thiophene with two equivalents of the previously prepared 5-bromoindole **10**, catalyzed by tetrakis(triphenylphosphine)palladium(0) in a toluene/DMF (9:1 vol.) mixture afforded the bis(indolyl)thiophene **13**. Characterization of compound **13** (NMR, IR, HRMS and melting point) was in agreement with the literature (see experimental section).<sup>[23]</sup> The indolium iodide salt **14** was obtained by reaction of compound **13** with an excess of 1-iodohexadecane, using nitromethane as a solvent.

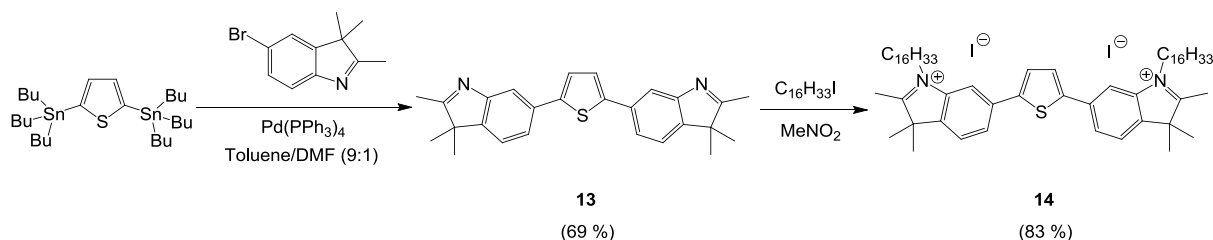
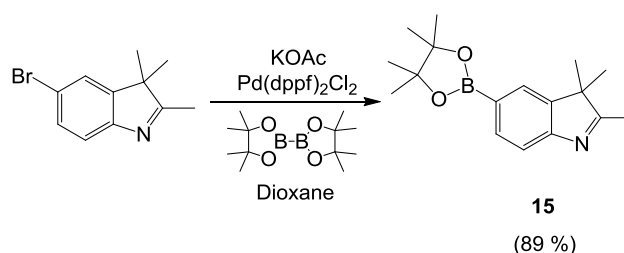
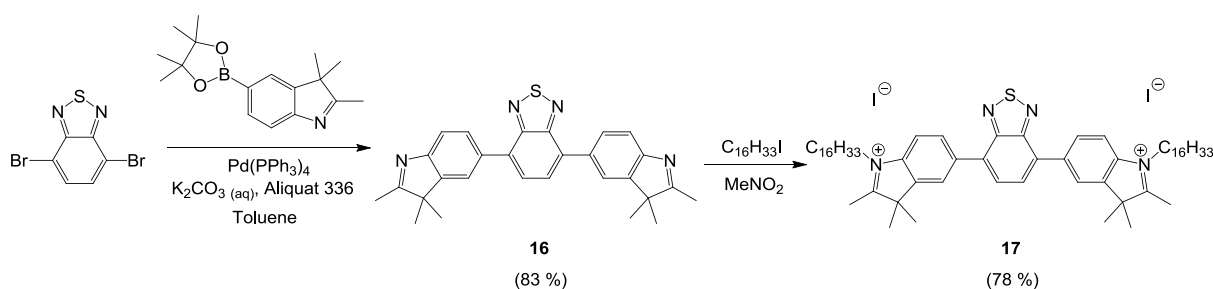


Figure 4 - 14: Synthesis of bis(indolium)thiophene **14**.

The benzothiadiazole-based monomer was synthesized in three steps. Suzuki coupling reaction between the commercially available 4,7-bis(4,4,5,5-tetramethyl-1,3,2-dioxaborolan-2-yl)benzothiadiazole and the bromo-indole **10** did not afford the desired bis(indolyl)benzothiadiazole in sufficient yields. Therefore the bromo-indole **10** was first turned into a boronic ester **15** in order to be subsequently reacted with the commercially available 4,7-dibromobenzothiadiazole (see Figure 4 - 15). Following a reported procedure, **10** was reacted with bis(pinacolato)diboron in dioxane, in the presence of potassium acetate and dichloro[1,1'-bis(diphenylphosphino)-ferrocen]-palladium(II) as catalyst, affording the boronic ester **15** in good yield (see **Error! Reference source not found.**).<sup>[24]</sup> Structure of **15** was confirmed by NMR (<sup>1</sup>H, <sup>13</sup>C and <sup>1</sup>H-<sup>13</sup>C HSQC) and IR, and its melting point was consistent with the literature.

Figure 4 - 15: Synthesis of the boronic ester indole **15**.

Subsequently, the bis(indolyl)benzothiadiazole **16** was synthesized by a Suzuki coupling between 4,7-dibromobenzothiadiazole and two equivalents of **15**, using tetrakis(triphenylphosphine)palladium(0) as catalyst in the presence of potassium carbonate and Aliquat 336, a phase-transfer agent. Finally, synthesis of the indolium derivative **17** was performed in the same conditions as for the thiophene-based monomer **14** (see Figure 4 - 16).

Figure 4 - 16: Synthesis of bis(indolium)BT **17**.

Structures of compounds **14**, **16** and **17** were confirmed by NMR (<sup>1</sup>H, <sup>13</sup>C and <sup>1</sup>H-<sup>13</sup>C HSQC), IR and HRMS (see experimental section). The <sup>1</sup>H NMR spectra are presented in Figure 4 - 17 and Figure 4 - 18. In the case of the thiophene-based compounds **13** and **14**, the signals of b and b' protons in the aromatic region were assigned with help of <sup>1</sup>H-<sup>13</sup>C heteronuclear single quantum correlation NMR (see experimental section).

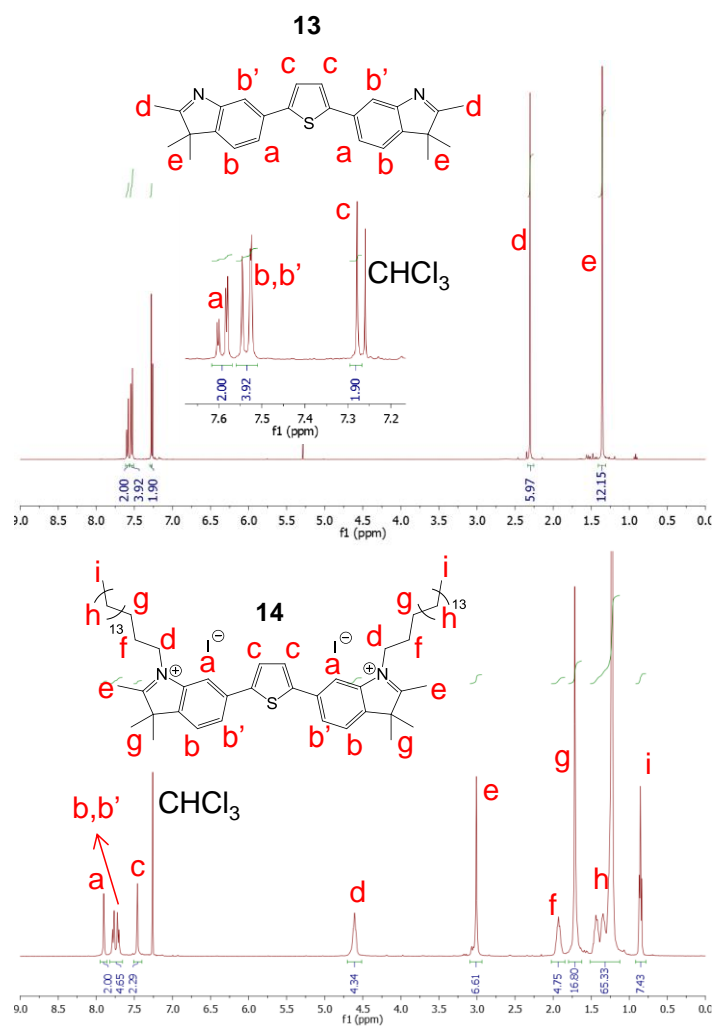


Figure 4 - 17:  $^1\text{H}$  NMR spectra (400 MHz) of the thiophene-based compounds 13 and 14 in  $\text{CDCl}_3$ .



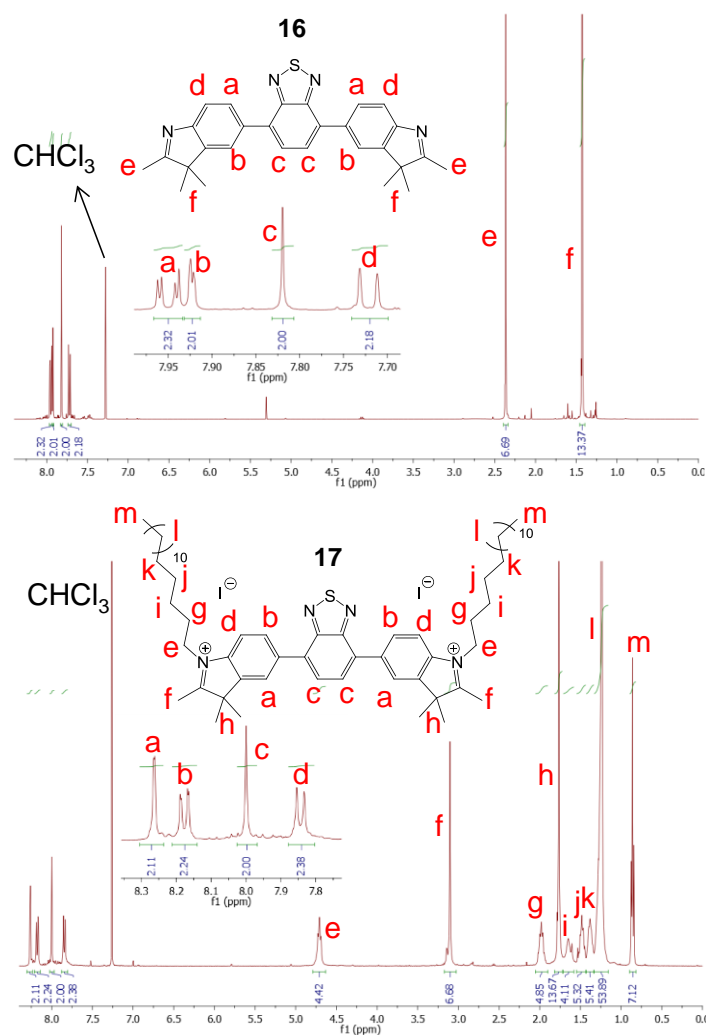


Figure 4 - 18: <sup>1</sup>H NMR spectra (400 MHz) of the BT-based compounds 16 and 17 in CDCl<sub>3</sub>.

The IR spectra provided additional confirmation of the functional groups present in compounds **13-17** (see Figure 4 - 19). At first, the attachment of the hexadecyl chains was supported by a strong increase of the relative intensities of absorption peaks in the 2800-3000 cm<sup>-1</sup> region when comparing the alkylated derivatives **14** and **17** with their precursors **13** and **16**. Additionally, a shift towards higher wavenumbers of the peak corresponding to the C=N stretch was observed, which is consistent with the formation of quaternary ammonium functions.

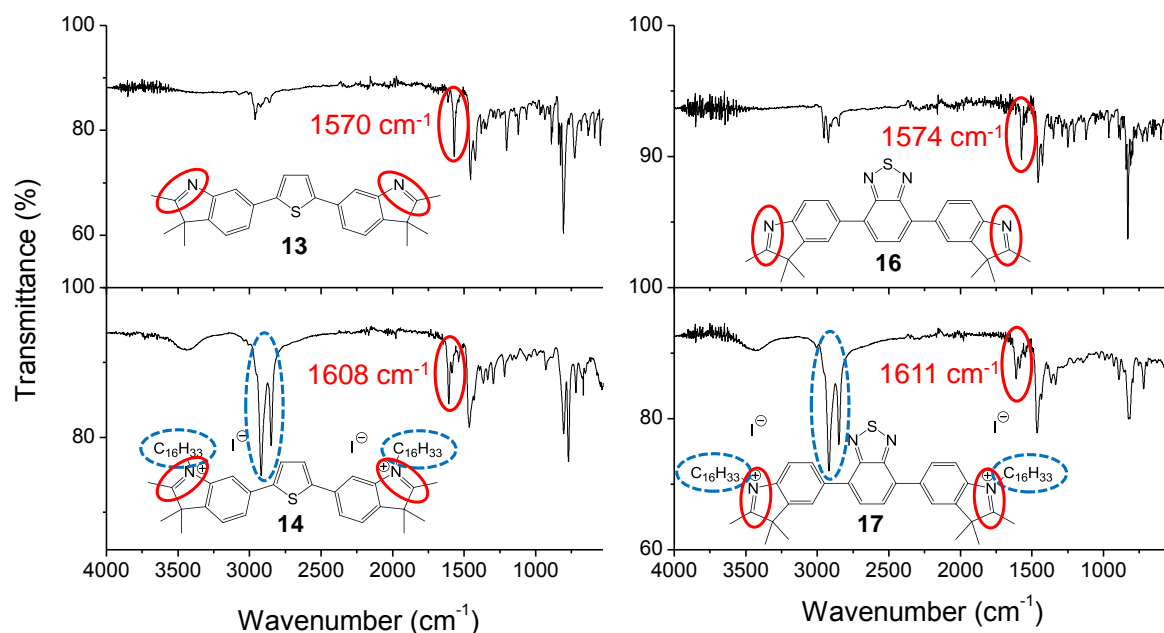


Figure 4 - 19: IR spectra (ATR) of compounds 13-17. Red solid line: C=N stretch. Blue dotted line: alkyl C-H stretch.

The mass measured in high resolution mass spectrometry (HRMS) of **14** and **17** were smaller by 2 Da than the expected values (see experimental section). It is assumed that ionization of the samples could induce a chemical reaction eliminating two protons originating from the indolium moieties.

#### 4.2.1.2 ANILINE-LIKE MONOMER

The reactivity of aniline derivative with SA to form squaraine compounds has been widely reported in the literature (see Figure 4 - 20 a).<sup>[5, 25-26]</sup> Hence, a third monomer derived from aniline was developed, presenting two potential reactive sites and bearing dodecyl side-chains to ensure good solubility of the resulting polymer (see Figure 4 - 20 b).

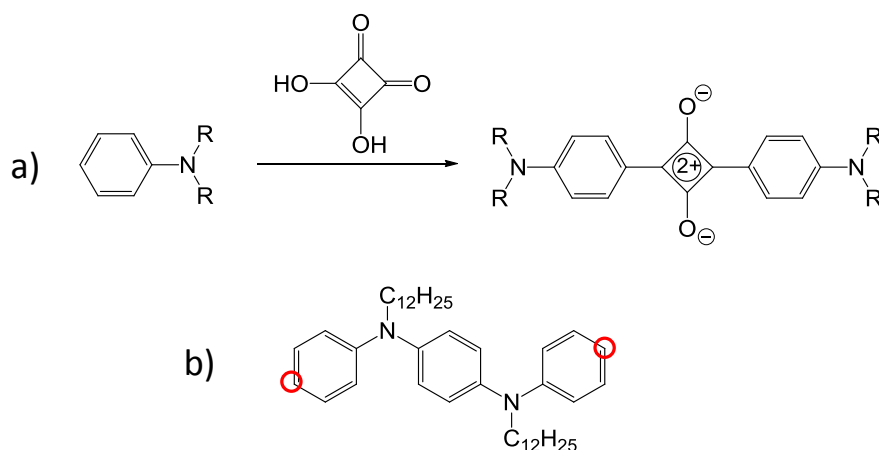


Figure 4 - 20: a) Example of squaraine dye from aniline derivative. b) Developed monomer; circled in red: reactive sites towards SA.

The monomer **18** was synthesized in one step from the commercially available  $N^1,N^4$ -diphenylbenzene-1,4-diamine, which was reacted with 1-bromododecane in the presence of potassium hydroxide (see Figure 4 - 21).

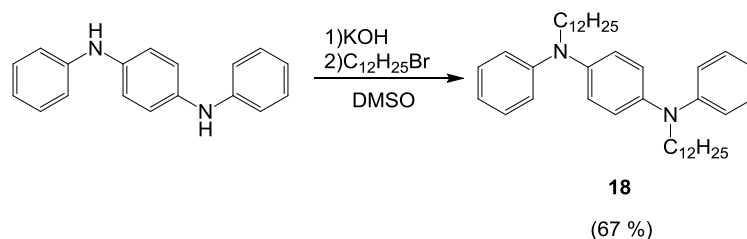


Figure 4 - 21: Synthesis of compound **18**.

IR, NMR ( $^1\text{H}$ ,  $^{13}\text{C}$  and  $^1\text{H}$ - $^{13}\text{C}$  HSQC) and HRMS analyses were performed to confirm the structure of **18** and were in good agreement with previously reported similar structure.<sup>[27]</sup>  $\text{CDCl}_3$  and  $\text{CD}_2\text{Cl}_2$  proved to be unsuitable solvents for NMR analysis, because they caused undesirable change of colour from colorless to blue, which can be attributed to an oxidized state.<sup>[27]</sup> When using deuterated THF (THF- $d_8$ ), compound **18** remained stable and gave clear  $^1\text{H}$  NMR spectrum (see Figure 4 - 22). No peak corresponding to amine protons were observed, confirming the double alkylation of the product. Additionally, integrations values were consistent with the presence of two dodecyl chains in the molecule.

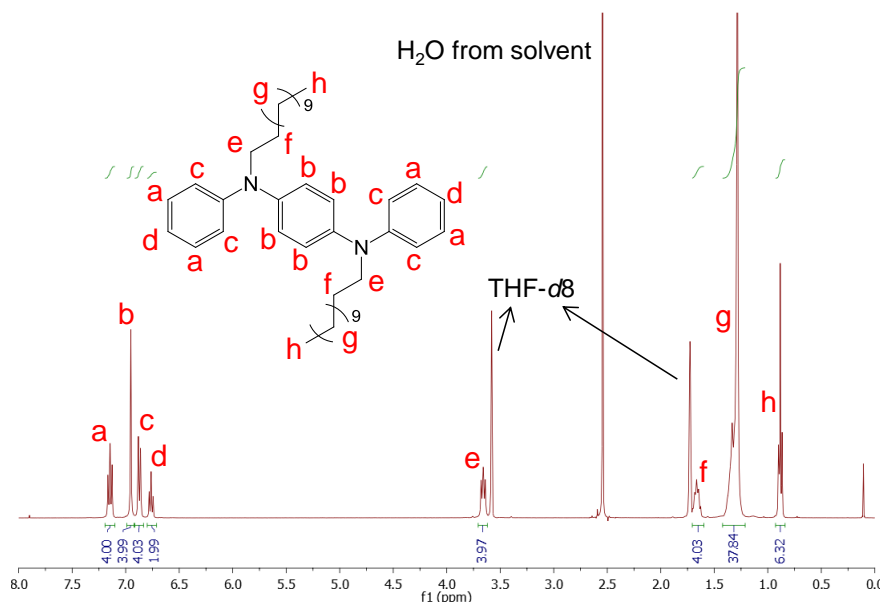


Figure 4 - 22:  $^1\text{H}$  NMR spectrum of **18** in THF- $d_8$ .

The double alkylation of compound **18** was also confirmed from its IR spectrum, where no peaks corresponding to N-H stretch (ca.  $3300\text{--}3400\text{ cm}^{-1}$ ) was observed (see Figure 4 - 23).

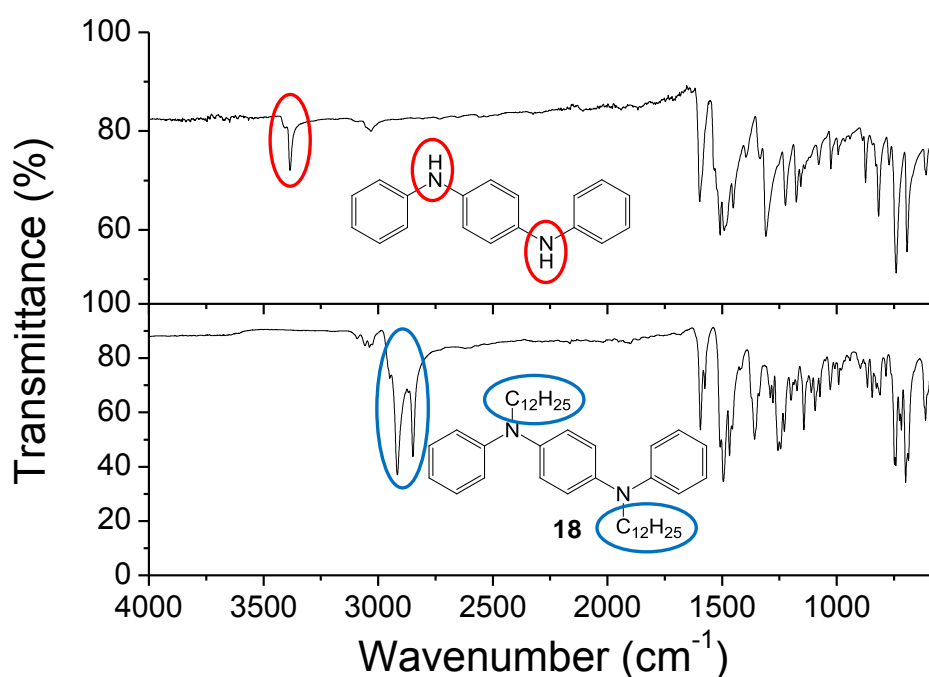


Figure 4 - 23: IR spectrum of **18** and its precursor. Circled in red: peaks corresponding to N-H stretch. Circled in blue: absorption due to alkyl C-H stretch.

#### 4.2.1.3 POLYMERIZATIONS WITH SQUARIC ACID

Firstly, the indole-based monomers **14** and **17** were condensed with SA (in 1:1 molar ratio) in a mixture of toluene and 1-butanol (1:1 vol.), which is known to favor the formation of 1,3-isomeric squaraine moieties (see Figure 4 - 24). Azeotropic removal of water and use of quinoline as base catalyst helped to afford the resulting polysquaraines in good yields. A strong color change of the reaction mixture from yellow-orange to dark green was observed, which was associated with the formation of squaraine units.

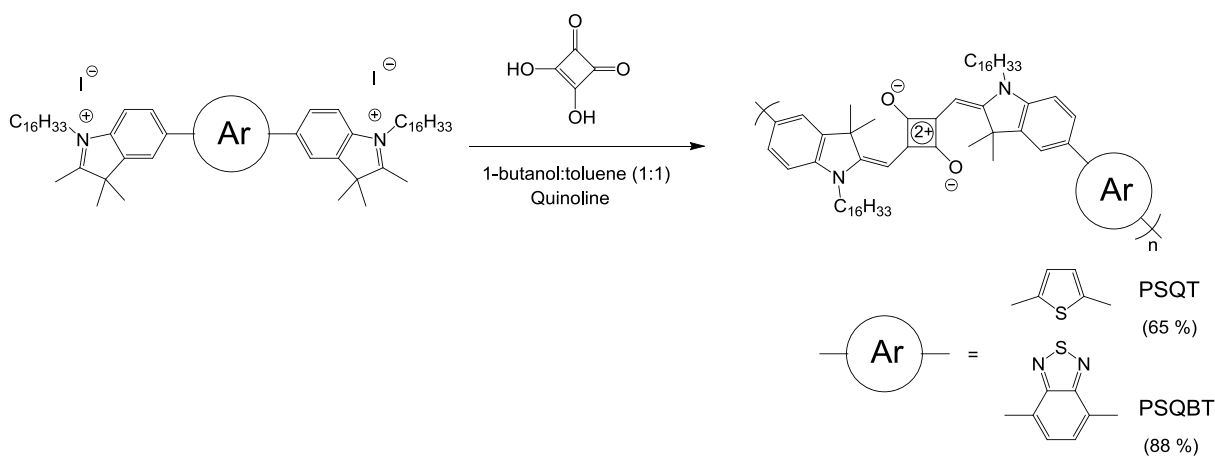


Figure 4 - 24: Synthesis of PSQT and PSQBT from compounds **14** and **17**.

Subsequently, Soxhlet extraction in MeOH, acetone, THF and CHCl<sub>3</sub> of the crude mixture was performed in order to remove the residual quinoline, monomers and small oligomers from the final products, but also to obtain fractions of the polymeric material with narrow dispersity. Recovery of the THF and CHCl<sub>3</sub> fractions separately afforded the resulting materials, and yield of the reactions were calculated by summing the mass of both fractions. A small insoluble fraction remained in the Soxhlet cartridge after CHCl<sub>3</sub> extraction and could not be recovered. The materials presented the same dark purple aspect, and their solubility in organic solvents was similar as for their analogous obtained via Suzuki or Stille coupling (see Chapter 3). However, the biggest difference was the higher yield obtained for the polycondensation of SA with the BT-based monomer, as well as a higher mass ratio of CHCl<sub>3</sub> fraction, when compared with the thiophene-based monomer (84 %w of the final material recovered from the CHCl<sub>3</sub> fraction for **PSQBT**, and only 40 %w in the case of **PSQT**, see Table 4 - 1). In that regards, the polycondensation of indolium derivatives with SA is more activated when an electron-withdrawing unit is present in the monomer.

Table 4 - 1: Weight proportions of the THF and CHCl<sub>3</sub> fractions recovered from Soxhlet extraction.

Polymer	THF (%w)	CHCl <sub>3</sub> (%w)
<b>PSQT</b>	60	40
<b>PSQBT</b>	16	84

As expected, the NMR and IR spectra of **PSQT** and **PSQBT** synthesized from **14** and **17** were similar to their analogous obtained via metal-catalyzed polycondensations (see experimental section). The formation of 1,3-isomeric squaraine units in the polymers backbone was confirmed by the absence of absorption peak corresponding to the C=O stretch in 1,2-isomer in the IR spectra.

SEC in chloroform with 1 % (vol.) of triethylamine at 30°C was performed to measure the molecular weights of the synthesized polymers (see Table 3 - 4). The higher molecular weights achieved for the CHCl<sub>3</sub> fraction of **PSQBT** was consistent with a higher reactivity of monomer **17** compared to **14**. The degrees of polymerization ( $\overline{DP}_n$ ) achieved via these polycondensations were higher than the  $\overline{DP}_n$  obtained via metal-catalyzed couplings (see chapter 3).

Table 4 - 2: Molecular weights of PSQT and PSQBT obtained by polycondensation with squaric acid, measured by SEC in CHCl<sub>3</sub> at 30°C.

Polymer	Fraction	Conventional calibration (PS std)			Universal calibration		
		$\overline{M}_n$ (g/mol)	$\overline{D}^a$	$\overline{DP}_n^b$	$\overline{M}_n$ (g/mol)	$\overline{D}^a$	$\overline{DP}_n^b$
PSQT	THF	12 100	2.2	13.1	11 400	2.7	12.3
	CHCl <sub>3</sub>	23 600	2.0	25.5	34 200	2.3	37.0
PSQBT	THF	8 500	2.3	8.7	5 200	2.8	5.3
	CHCl <sub>3</sub>	36 500	2.2	37.3	33 800	3.0	34.6

<sup>a</sup> Dispersity  $\overline{D} = \frac{\overline{M}_w}{\overline{M}_n}$ ; <sup>b</sup> Number-average degree of polymerization  $\overline{DP}_n = \frac{\overline{M}_n}{M_{rep.unit}}$ .

The aniline-like monomer **18** was polymerized in similar conditions, using toluene/1-butanol (1:1 vol.) as solvent to favor the formation of 1,3-squaraine units and an azeotropic removal of the formed water to shift the reaction equilibrium (see Figure 4 - 25). The resulting poly(squaraine-*alt*-N,N'-didodecyldiphenyl-1,4-benzenediamine) (**PSQDA**) was purified by repeated precipitation in MeOH. It showed good solubility in organic solvents such as THF CH<sub>2</sub>Cl<sub>2</sub> or toluene. Aniline derivatives are known to produce polyaniline under oxidizing conditions, which could be a competitive reaction for the squaraine condensation. In order to exclude this possibility, a blank experiment was carried out, where the aniline derivative **18** was reacted on its own in the same conditions. An equivalent quantity of dichloroacetic acid, which has a similar pKa like SA, was added in the medium to obtain the same pH. No formation of polymer (verified in SEC) was observed after 24 h of heating at reflux, assuring the unability of **18** to form polyaniline.

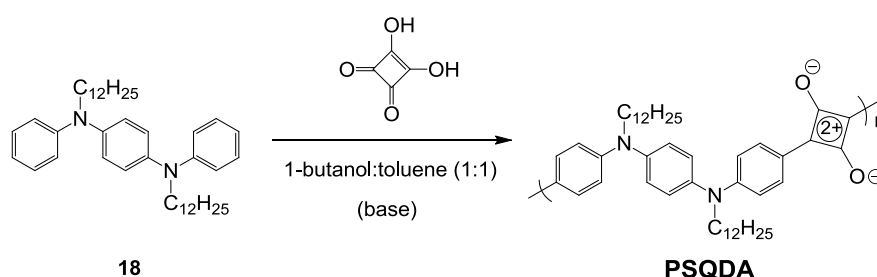


Figure 4 - 25: Synthesis of PSQDA.

The reported procedure for preparation of squaraine dyes from aniline do not mention any use of a base as catalyst.<sup>[5, 25-26]</sup> Indeed, the reactivity of the indolium derivatives is enhanced when a deprotonation of the reactive methyl is assisted by a base. This allows the formation of a sp<sup>2</sup> carbon which can be subsequently subject to an electrophilic attack by squaric acid (see Figure 4 - 1 in section 4.1). In the case of aniline, the reactive carbon is already sp<sup>2</sup> and thus does not require a deprotonation step. However, since a comprehensive study on the influence of base in the squaraine synthetic mechanism is still missing, the polymerization of **18** with SA was performed with and without different bases to determine its effect.

In Table 4 - 3 are presented the achieved molecular weights and yields of polycondensation when changing the reaction conditions (reaction time was kept constant). It was observed that employing a base led to lower molecular weights of the resulting polymers. This could be attributed to an acid-base exchange with squaric acid, which could be responsible for a decrease in reactivity of SA. Furthermore, it was found that increasing the concentration allowed a slight enhancement of the polymer chains length.

Table 4 - 3: Investigations on the polycondensation conditions of PSQDA. Reaction medium heated at reflux for 3 days in a Dean-Stark apparatus.

Base	Normalized concentration of monomers	Yield (%)	$\overline{M}_n$ (g/mol) <sup>a</sup>	$\overline{DP}_n$ <sup>a</sup>	$\overline{DP}_n$
-	1	70	4 100	1.5	6.1
Quinoline (0.2 eq)	1	51	3 200	1.2	4.7
Quinoline (1 eq)	1	68	3 200	1.3	4.7
K <sub>3</sub> PO <sub>4</sub> (0.2 eq)	1	79	2 600	1.1	3.8
-	2.5	42	5 100	1.8	7.5

<sup>a</sup> Measured by SEC in THF at 40°C with RI detector and PS standards; <sup>b</sup> Number-average degree of polymerization  $\overline{DP}_n = \frac{\overline{M}_n}{M_{rep.unit}}$ .

The chemical structure of **PSQDA** was investigated by NMR and IR spectroscopy. The <sup>1</sup>H NMR spectrum of **PSQDA** was in good agreement with the expected structure, although the aromatic region did not allow a good assignment of the different protons in the repeating unit (see Figure 4 - 26).

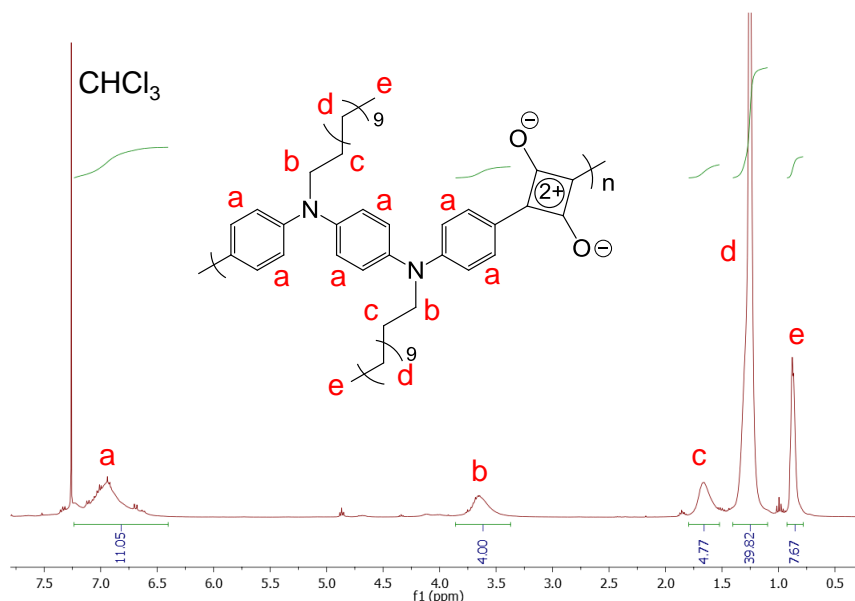


Figure 4 - 26: <sup>1</sup>H NMR spectrum (400 MHz) of PSQDA in CDCl<sub>3</sub>.

When comparing the IR spectra of the monomer **18** and **PSQDA**, appearance of a new peak at  $1733\text{ cm}^{-1}$  was observed which was assigned to the insertion of the SA moiety. The wavenumber value of this peak corresponds to carbonyl stretching, indicating that the squaraine moieties in the polymer backbone were mainly 1,2-isomers, as depicted in Figure 4 - 27. This was unexpected since the polymerization conditions were set up in order to favor the formation of 1,3-isomers.

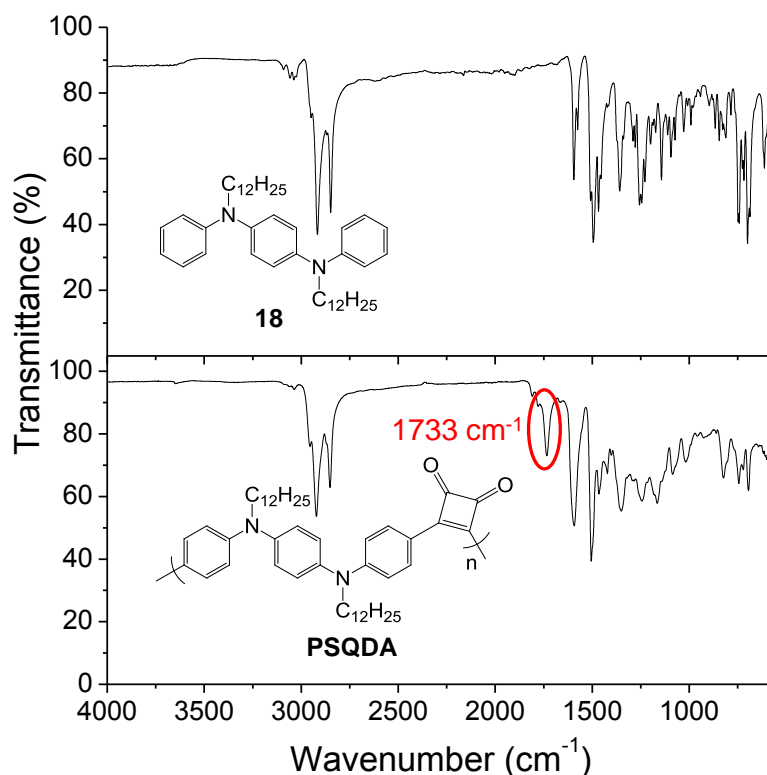


Figure 4 - 27: IR spectra of **18** (top) and **PSQDA** bottom. Circled in red: the peak corresponding to C=O stretching.

## 4.2.2 CHARACTERIZATION OF POLYSQUARAINES

### 4.2.2.1 THERMAL PROPERTIES

Thermal stability of the synthesized materials was studied by TGA (see Table 4 - 4). Their decomposition temperature and weight loss are shown in Table 4 - 4. The measured degradation temperatures of **PSQT** and **PSQBT** were in agreement with what was already observed. Nevertheless, the weight losses were more important. This could be related to a possible reactivity of the chain-ends at high temperatures, since they are the main difference (as well as the molecular weights) with the polysquaraines described in chapter 3. **PSQDA** also showed a good thermal stability, in addition to a weight loss inconsistent with the degradation of the side-chains only (theoretically 50 %). Additionally, DSC measurements provided the glass transition temperatures, which were in close range of  $19 - 20^{\circ}\text{C}$  (see Table 4 - 4). They did not demonstrate any semi-crystalline behavior (see experimental section).



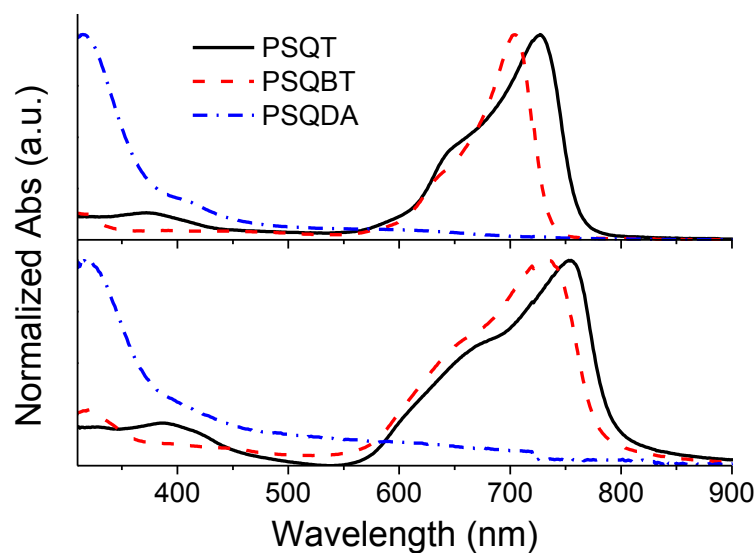
Table 4 - 4: TGA and DSC data of the polysquaraines.

Polymer	TGA		DSC
	Decomposition temperature (°C) <sup>a</sup>	Weight loss (%) <sup>a</sup>	T <sub>g</sub> (°C) <sup>b</sup>
PSQT	352	84	20
PSQBT	346	56	20
PSQDA	322	88	19

<sup>a</sup> Evaluated under N<sub>2</sub> at 5% weight loss, at a heating rate of 10°C/min; <sup>b</sup> Measured under He flow at 20°C/min.

#### 4.2.2.2 OPTICAL PROPERTIES

Optical properties of the materials were recorded and their absorption spectra in CHCl<sub>3</sub> solutions and films on glass substrates are presented in Figure 4 - 28.



	Solution (CHCl <sub>3</sub> )		Film		E <sub>g</sub> <sup>opt</sup> (eV) <sup>c</sup>
	λ <sub>max</sub> <sup>sol</sup> (nm) <sup>a</sup>	λ <sub>onset</sub> <sup>sol</sup> (nm) <sup>a</sup>	λ <sub>max</sub> <sup>film</sup> (nm) <sup>b</sup>	λ <sub>onset</sub> <sup>film</sup> (nm) <sup>b</sup>	
PSQT	727	762	753	790	1.6
PSQBT	704	735	735	776	1.6
PSQDA	315	446	318	460	2.7

<sup>a</sup> Determined in CHCl<sub>3</sub> solutions (0.01 g.l<sup>-1</sup>); <sup>b</sup> Determined in film casted on glass substrate from an CHCl<sub>3</sub> solution (10 g.l<sup>-1</sup>); <sup>c</sup> Estimated from the onset point of the absorption edge in a film with the following formula:

$$E_g^{opt} = \frac{1240}{\lambda(nm)}.$$

Figure 4 - 28: Normalized absorption spectra and data of the polysquaraines in CHCl<sub>3</sub> solution (top) and spin-coated films on glass substrate (bottom).

The UV-visible absorption spectra of **PSQT** and **PSQBT** were comparable to their analogous prepared by Stille and Suzuki coupling. This confirms that the maximum extent of conjugation (in relation with

optical absorption) was already achieved in materials with lower molecular weights. As expected, the optical band-gaps of **PSQT** and **PSQBT** were estimated around 1.6 eV.

On the contrary, the absorption spectrum of **PSQDA** shows a strong blue-shift, with an absorption maximum in the UV region (318 nm) and an optical band-gap of 2.7 eV. These results are in agreement with the formation of 1,2-isomeric squaraine units, as observed in the IR spectrum. Since no typical absorption of zwitterionic 1,3-units in the red or near-IR part of the spectrum was detected, it was concluded that the backbone was composed with a great majority of 1,2-squaraine moieties. Furthermore, no strong red-shift was observed in the film absorption of **PSQDA**, probably due to limited intermolecular interactions in the solid-state.

The photoluminescence of **PSQT** and **PSQBT** in  $\text{CHCl}_3$  solutions is presented in Figure 4 - 29. As anticipated, both polymers showed the same PL in solution like their previously synthesized analogous (see chapter 3). However, no fluorescence was observed in solid state. It is assumed that the spin-coating conditions in this case did not produce films with a sufficient thickness, thus leading to an unmeasurable photoluminescence.

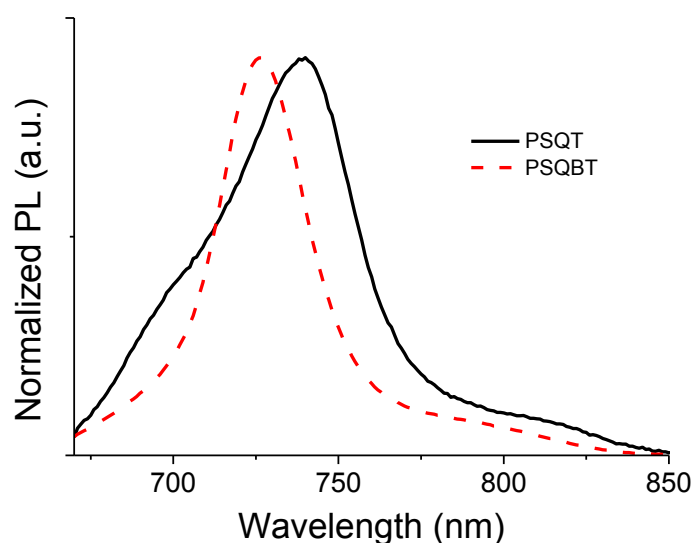


Figure 4 - 29: Normalized photoluminescence spectra of **PSQT** and **PSQBT** in  $\text{CHCl}_3$  solutions ( $0.01 \text{ g.l}^{-1}$ ). Excitation at 650 nm.

**PSQDA** photoluminescence is shown in Figure 4 - 30. The material demonstrated broad emission in both solution and film. Additionally, the observed Stokes shift was significant (202 nm in solution), indicating a strong difference between the ground and excited states.

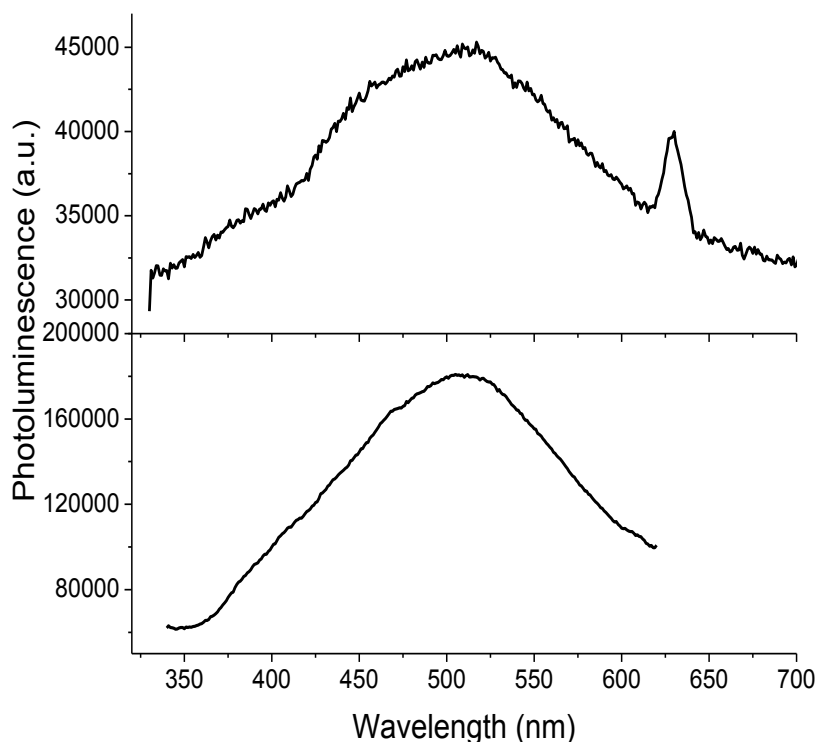


Figure 4 - 30: Photoluminescence spectra of PSQDA in  $\text{CHCl}_3$  solution (top) and in film (bottom) spin-coated onto glass substrate from  $\text{CHCl}_3$  solution ( $10 \text{ g.l}^{-1}$ ). Excitation at 315 nm.

Table 4 - 5: Photoluminescence data of PSQs in  $\text{CHCl}_3$  solutions and as spin-coated films.

Polymer	Solution ( $\text{CHCl}_3$ )	Film
	$\lambda_{\text{max em.}}^{\text{sol}} (\text{nm})^a$	$\lambda_{\text{max em.}}^{\text{film}} (\text{nm})^b$
PSQT	740	-
PSQBT	726	-
PSQDA	517	505

<sup>a</sup> Determined in  $\text{CHCl}_3$  solutions ( $0.01 \text{ g.l}^{-1}$ ); <sup>b</sup> Determined in film casted on glass from a  $\text{CHCl}_3$  solution ( $10 \text{ g.l}^{-1}$ )

#### 4.2.2.3 ELECTROCHEMICAL PROPERTIES

Energetic levels and band-gaps of the materials were measured by cyclic voltammetry in solution, using the same conditions as previously (see experimental section).

Table 4 - 6: CV data of PSQs.

Polymer	$E_{\text{HOMO}}(\text{eV})^a$	$E_{\text{LUMO}}(\text{eV})^b$	$E_{\text{g}}^{\text{CV}}(\text{eV})^c$	$E_{\text{g}}^{\text{opt}}(\text{eV})^d$
PSQT	-5.0	-3.9	1.1	1.6
PSQBT	-5.1	-3.7	1.4	1.6
PSQDA	-4.7	-	-	2.78

<sup>a</sup> Calculated from the onset of the oxidation peak ( $E_{\text{onset ox}}$ ); <sup>b</sup> Calculated from the onset of the reduction peak ( $E_{\text{onset red}}$ ); <sup>c</sup> Calculated as following:  $E_{\text{g}} = E_{\text{onset ox}} - E_{\text{onset red}}$ ; <sup>d</sup> Optical band-gaps in solution calculated from

$$\lambda_{\text{onset}}^{\text{sol}}$$

Surprisingly, the HOMO and LUMO levels of **PSQT** differed from the polymer prepared via metal-catalyzed cross-coupling (see Chapter 3). It exhibited a much smaller band-gap than its analogous synthesized by Stille which was less consistent with the optical band-gap. This could be the result of localized reduction and oxidation sites in the conjugated backbone. Unfortunately the LUMO level of **PSQDA** could not be measured since the reduction of the solvent occurred first.

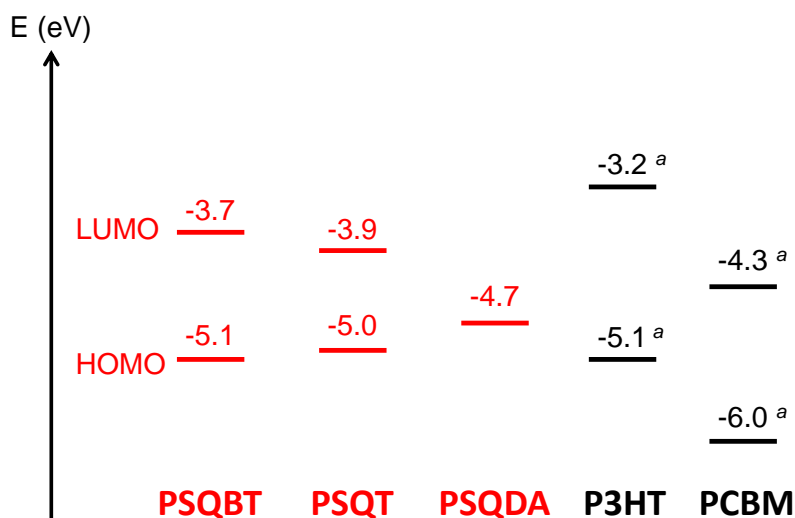


Figure 4 - 31: Energetic representation of the PSQs. <sup>a</sup> Values for P3HT and PCBM are from the literature.<sup>[28]</sup>

## 4.3 SYNTHESIS AND CHARACTERIZATION OF POLYIMINES

### 4.3.1 SYNTHESIS OF POLYIMINES

#### 4.3.1.1 CARBAZOLE AND EDOT-BASED MONOMERS

Difunctionalized heteroaromatic monomers bearing aldehyde or amino groups were synthesized in order to be used in polycondensation to form polyimines. Firstly, a dialdehyde derivative of 3,4-ethylenedioxythiophene (EDOT) was prepared in one step following a reported procedure (see Figure 4 - 32).<sup>[29]</sup> Commercially available EDOT was treated with n-butyllithium to form a dilithium intermediate, which was then reacted with DMF to afford compound **19**.

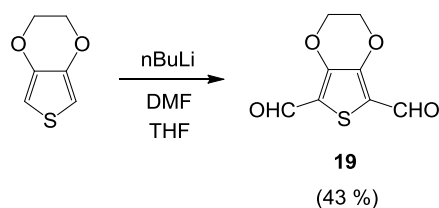
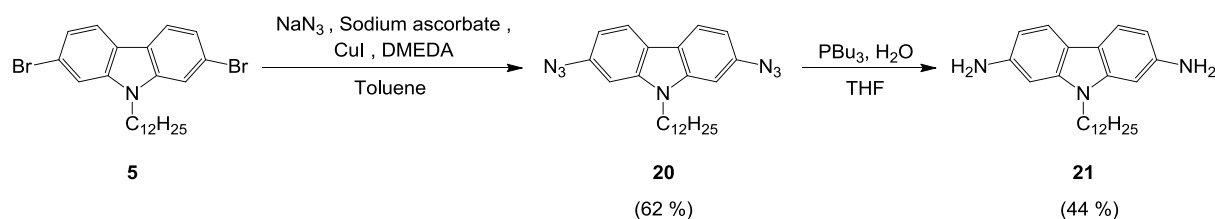
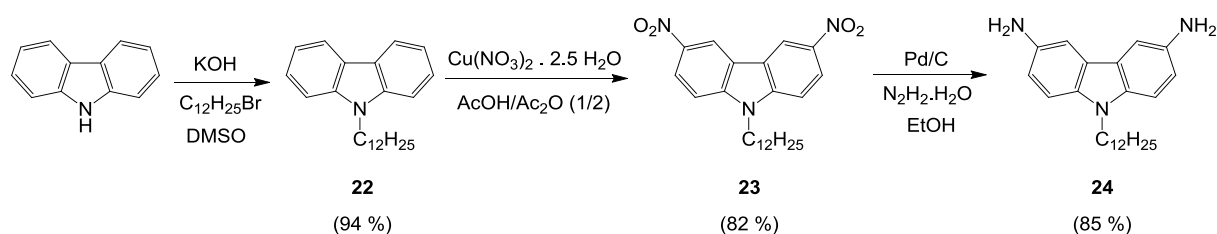


Figure 4 - 32: Synthesis of the EDOT-dialdehyde **19**.

Secondly, two carbazole-based derivatives bearing amino groups in 2,7 and 3,6 positions were synthesized. Similarly to the investigation presented in chapter 2, this would allow a further understanding of the dependence of carbazole linkage positions on the properties of the resulting polyimines. The 2,7-diaminocarbazole **21** was obtained in 2 steps from the previously prepared 2,7-dibromo-N-dodecylcarbazole **5**, following already reported procedures (see Figure 4 - 33).<sup>[30-31]</sup> The diazido compound **20** was achieved via an Ullmann-type reaction catalyzed by CuI, followed by a Staudinger reduction in the presence of tributylphosphine to produce **21** in moderate yields.

Figure 4 - 33: Synthesis of the 2,7-diaminocarbazole **21**.

The 3,6-diaminocarbazole **24** was achieved in three steps (see Figure 4 - 34). The commercially available carbazole was first alkylated with bromododecane in basic conditions, and subsequently nitrated under Menke conditions to afford the 3,6-dinitrocarbazole **23**. The resulting dinitrocarbazole **23** was then reduced by hydrazine, which was catalyzed by palladium supported on carbon, and the 3,6-diaminocarbazole **24** was obtained in good yields.<sup>[32]</sup>

Figure 4 - 34: Synthesis of the 3,6-diaminocarbazole **24**.

Structures of the monomer **19**, **21** and **24** were confirmed by  $^1\text{H}$  and  $^{13}\text{C}$  NMR. The obtained spectra were in good agreement with similar compounds already reported in the literature (see experimental section).<sup>[29, 32-33]</sup>

#### 4.3.1.2 POLYMERIZATIONS BY ARYLIMINO-DE-OXO-BISUBSTITUTION

Novel conjugated polyimines were synthesized from the above described diamines **21** and **24** and dialdehyde **19** (see Figure 4 - 35). Additionally, a dialdehyde derivative of carbazole (2,7-dicarbaldehyde-N-hexyl-carbazole) which was already prepared in the laboratory, was used. Even if this compound bears a shorter hexyl side-chain, it was assumed that its polycondensation with the diamino derivatives bearing dodecyl side-chains (**21** and **24**) should provide polymers with adequate solubility in organic solvents. The polycondensations were carried out in toluene using 1:1 molar

ratio of monomers and azeotropic removal of water maintained by using a Dean-Stark apparatus. Moreover, catalytic amount of *p*-toluenesulfonic acid was added to enhance the product formation. The polymeric products precipitated during the reaction, and the resulting solids were dried under vacuum. Their colorless solutions in deuterated chloroform ( $\text{CDCl}_3$ ) were analyzed by  $^1\text{H}$  NMR. No signal was attributed to residual monomers, hence it was concluded that all starting materials were consumed in the reaction.

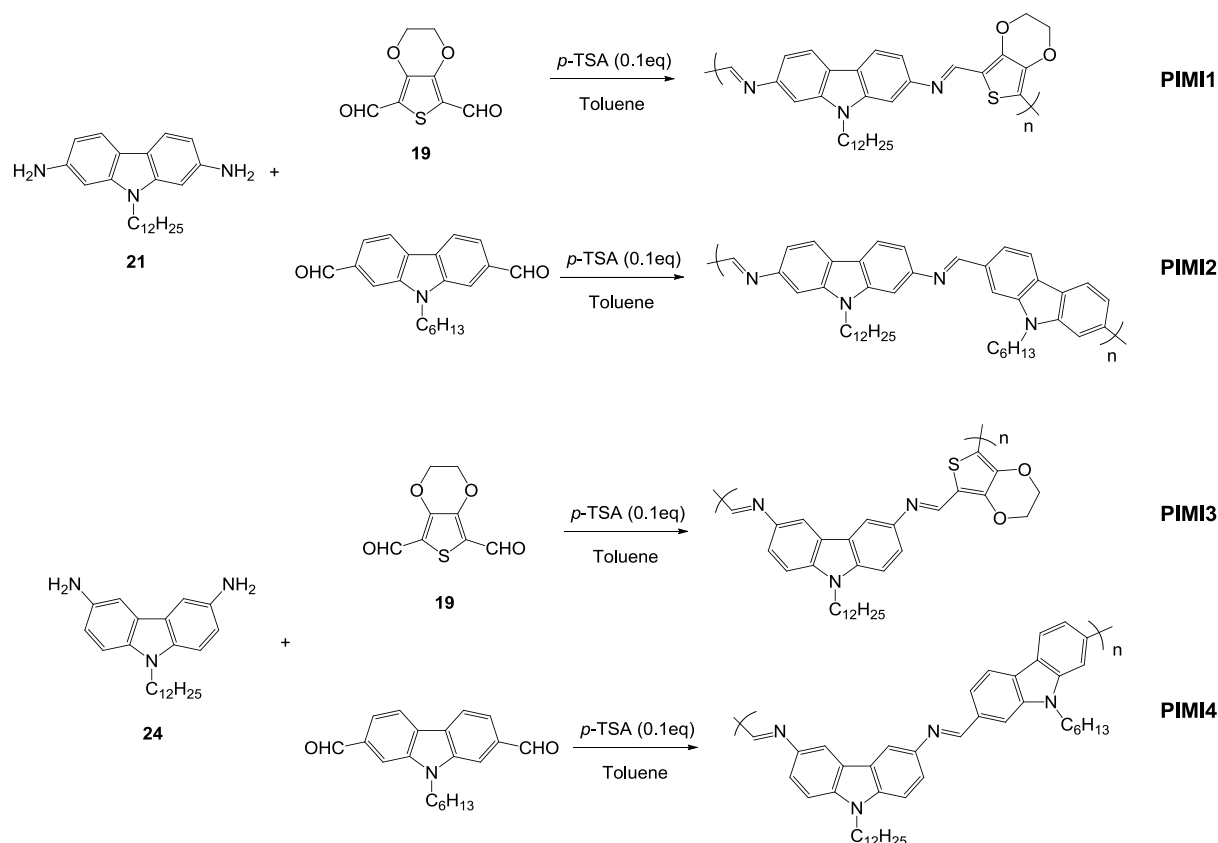


Figure 4 - 35: Synthesis of polyimines PIMI1-4.

Despite the presence of solubilizing side-chains, all the four polyimines were poorly soluble in common organic solvents. A limited solubility was observed in DMF, however the concentrations were not sufficient to obtain NMR spectra. Only IR spectroscopy could be used as a structural indication of the materials, and it proved to be consistent with the expected structures (see experimental section).

## 4.3.2 CHARACTERIZATION OF POLYIMINES

### 4.3.2.1 THERMAL PROPERTIES

The thermal behavior of **PIMI1-4** was investigated by TGA and DSC (see Table 4 - 7). The materials containing only carbazole units in the backbone (**PIMI2** and **4**) showed high decomposition temperatures, whereas the presence of EDOT moieties reduced the thermal stability (**PIMI1** and **3**).

Additionally, the observed weight loss of **PIMI2** and **4** were consistent with a degradation occurring on the alkyl side-chains (theoretically 40 %). This was not the case for **PIMI1** and **3** (theoretically 32 %), supporting the assumption of an instability brought by the EDOT units. Finally, DSC measurements showed no sign of crystallinity, and the measured glass transition temperatures ( $T_g$ ) were similar when the repeating unit of the polyimines were similar, independently from the position linkage on the carbazole moieties.

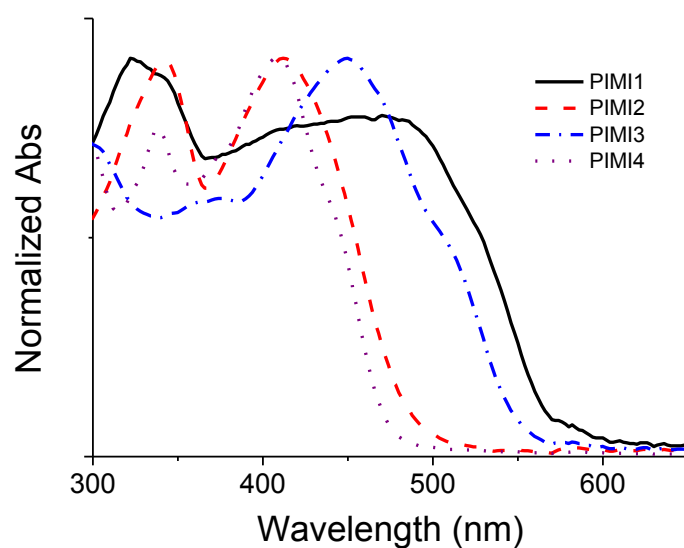
Table 4 - 7: TGA and DSC data of the polyimines.

Polymer	TGA		DSC
	Decomposition temperature (°C) <sup>a</sup>	Weight loss (%) <sup>a</sup>	$T_g$ (°C) <sup>b</sup>
<b>PIMI1</b>	179	53	25
<b>PIMI2</b>	397	39	18
<b>PIMI3</b>	281	48	25
<b>PIMI4</b>	374	42	18

<sup>a</sup> Evaluated under N<sub>2</sub> at 5% weight loss, at a heating rate of 10°C/min; <sup>b</sup> Measured under He flow at 20°C/min.

#### 4.3.2.2 OPTICAL PROPERTIES

The slight solubility of the polyimines **PIMI1-4** in DMF allowed the characterization of their optical properties, and their UV-visible spectra are shown in Figure 4 - 36. The materials demonstrated two or more absorption peaks, and the absorption maxima at the two highest wavelengths are referenced in Figure 4 - 36. The formation of conjugated polymers or oligomers was supported by a bathochromic shift compared to the corresponding monomers (see experimental section). A remarkable observation is the red-shift in absorption of the two polyimines containing EDOT moieties, which could be attributed to an intramolecular charge transfer between the carbazole and EDOT units. The optical band-gaps were also dependent on the position of the imine nitrogen in the carbazole unit. The optical band-gaps were higher in case of 3,6-positions in the carbazole unit ( $E_g^{\text{opt}} \text{PIMI1} < E_g^{\text{opt}} \text{PIMI3}$ , and  $E_g^{\text{opt}} \text{PIMI2} < E_g^{\text{opt}} \text{PIMI4}$ ). This could be explained by a better conjugation extent in the case of 2,7-linkage, thus reducing the band-gap.



	$\lambda_{\max 1}^{\text{sol}}(\text{nm})^a$	$\lambda_{\max 2}^{\text{sol}}(\text{nm})^a$	$\lambda_{\text{onset}}^{\text{sol}}(\text{nm})^a$	$E_g^{\text{opt}}(\text{eV})^b$
<b>PIMI1</b>	322	470	569	2.2
<b>PIMI2</b>	342	412	486	2.6
<b>PIMI3</b>	286	450	549	2.3
<b>PIMI4</b>	338	410	474	2.6

<sup>a</sup> Determined in DMF solutions; <sup>b</sup> Estimated from the onset point of the absorption edge in solution with the following formula:  $E_g^{\text{opt}} = \frac{1240}{\lambda(\text{nm})}$ .

Figure 4 - 36: Normalized absorption spectra and data of PIMI1-4 in DMF solutions.

Photoluminescence was also studied, and their PL spectra are presented in Figure 4 - 37. **PIMI3** showed an emission in longer wavelengths compared to the three other materials. Large Stokes shifts ranging from 66 to 133 nm were measured, indicating strong structural differences between the ground and excited states of these materials.



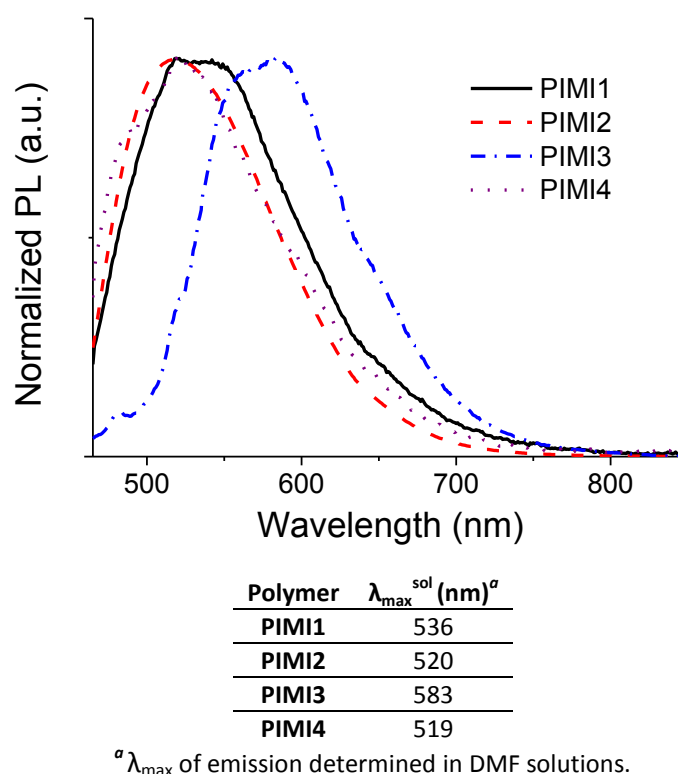


Figure 4 - 37: PL spectra and data of PIMI1-4 in DMF (excitation at 450 nm).

## 4.4 CONCLUSION

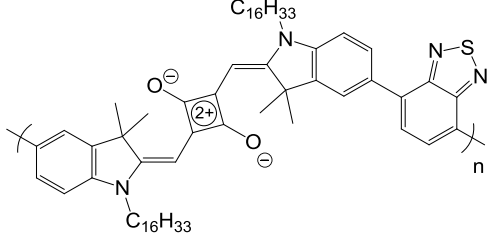
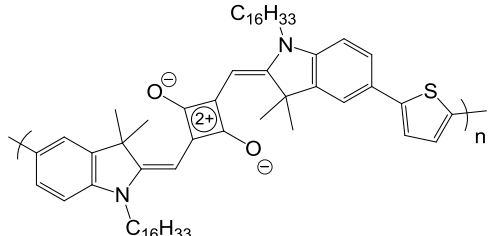
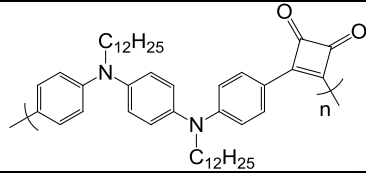
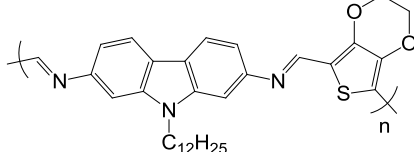
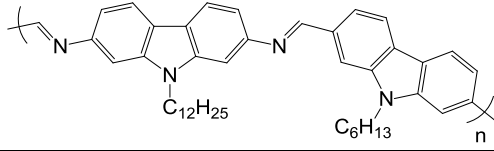
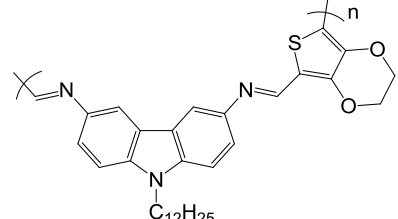
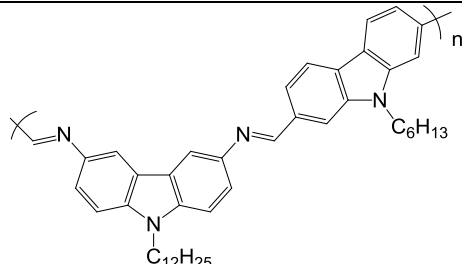
Seven novel conjugated materials were successfully synthesized via polycondensations which did not require the use of metal-based catalyst.

The condensation of indolenium derivatives with squaric acid proved to be a more efficient way towards polysquaraines in comparison to the Stille and Suzuki couplings as it resulted in higher molecular weights.

A new conjugated polymer prepared by condensation of an aniline derivative with SA was developed. This material occurred to bear only 1,2-isomers of squaraine units in the main chain, and further investigations are required in order to fully understand the mechanism of this reaction. Optimization of the reaction conditions leading to the formation of 1,3-isomers are highly desirable in order to obtain materials with more red-shifted absorption.

The arylimino-de-oxo-bisubstitution reaction was successfully employed to obtain conjugated materials from diamino and dialdehydes compounds. Despite the presence of alkyl side-chains, the solubility of the resulting polyimines in common organic solvents was limited. However, their slight solubility in DMF allowed their optical characterization, which suggests the achievement of

conjugated materials bearing imine bonds in the main chain, as well as the existence of an ICT between the carbazole and EDOT moieties. In a future work, the use of longer and/or bulkier alkyl side-chains should allow a better solubility of such materials, allowing further characterization.

Polymer	$E_{\text{HOMO}}(\text{eV})^a$	$E_{\text{LUMO}}(\text{eV})^a$	$E_{\text{g}}^{\text{CV}}(\text{eV})^a$	$E_{\text{g}}^{\text{opt film}}(\text{eV})^b$
	-5.1	-3.7	1.4	1.6
	-5.0	-3.9	1.1	1.6
	-5.0	-	-	2.7
	-	-	-	2.2
	-	-	-	2.6
	-	-	-	2.3
	-	-	-	2.6

<sup>a</sup> Determined by cyclic voltammetry in solution; <sup>b</sup> Optical band-gaps in film calculated from  $\lambda_{\text{onset}}^{\text{film}}$ .

- [1] J. Sakamoto, M. Rehahn, G. Wegner, A. D. Schlüter, *Macromolecular Rapid Communications* **2009**, *30*, 653-687.
- [2] B. Carsten, F. He, H. J. Son, T. Xu, L. Yu, *Chemical Reviews* **2011**, *111*, 1493-1528.
- [3] M. C. Iovu, E. E. Sheina, R. R. Gil, R. D. McCullough, *Macromolecules* **2005**, *38*, 8649-8656.
- [4] T. Yamamoto, A. Yamamoto, *Chemistry Letters* **1977**, *6*, 353-356.
- [5] P. Marks, M. Levine, *Journal of Chemical Education* **2012**, *89*, 1186-1189.
- [6] K.-Y. Law, F. C. Bailey, *Canadian Journal of Chemistry* **1986**, *64*, 2267-2273.
- [7] A. Treibs, K. Jacob, *Angewandte Chemie International Edition in English* **1965**, *4*, 694-694.
- [8] C. R. Chenthamarakshan, J. Eldo, A. Ajayaghosh, *Macromolecules* **1999**, *32*, 251-257.
- [9] Y.-Y. Chen, H. K. Hall, Jr., *Polymer Bulletin* **1986**, *16*, 419-425.
- [10] W. t. H. E. E. Havinga, H. Wynberg, *Polymer Bulletin* **1992**, *29*, 119-126.
- [11] E. E. Havinga, W. ten Hoeve, H. Wynberg, *Synthetic Metals* **1993**, *55*, 299-306.
- [12] E. E. Havinga, A. Pomp, W. ten Hoeve, H. Wynberg, *Synthetic Metals* **1995**, *69*, 581-582.
- [13] W. Zhang, Z. Wang, Y. S. Tang, Z. G. Xu, Y. Li, Q. Jiang, *Chinese Chemical Letters* **2010**, *21*, 245-248.
- [14] J. Eldo, A. Ajayaghosh, *Chemistry of Materials* **2001**, *14*, 410-418.
- [15] R. Adams, J. E. Bullock, W. C. Wilson, *Journal of the American Chemical Society* **1923**, *45*, 521-527.
- [16] G. F. D'Alelio, J. V. Crivello, R. K. Schoenig, T. F. Huemmer, *Journal of Macromolecular Science: Part A - Chemistry* **1967**, *1*, 1321-1330.
- [17] P. W. Morgan, S. L. Kwolek, T. C. Pletcher, *Macromolecules* **1987**, *20*, 729-739.
- [18] C.-J. Yang, S. A. Jenekhe, *Macromolecules* **1995**, *28*, 1180-1196.
- [19] F. R. Diaz, J. Moreno, L. H. Tagle, G. A. East, D. Radic, *Synthetic Metals* **1999**, *100*, 187-193.
- [20] S. Barik, T. Bletzacker, W. G. Skene, *Macromolecules* **2012**, *45*, 1165-1173.
- [21] S. Barik, W. G. Skene, *Polymer Chemistry* **2011**, *2*, 1091-1097.
- [22] S. Dufresne, W. G. Skene, *Journal of Physical Organic Chemistry* **2012**, *25*, 211-221.
- [23] D. Scherer, R. Dörfler, A. Feldner, T. Vogtmann, M. Schwoerer, U. Lawrentz, W. Grahn, C. Lambert, *Chemical Physics* **2002**, *279*, 179-207.
- [24] S. Kuster, T. Geiger, *Dyes and Pigments* **2012**, *95*, 657-670.
- [25] M. Tian, M. Furuki, I. Iwasa, Y. Sato, L. S. Pu, S. Tatsuura, *The Journal of Physical Chemistry B* **2002**, *106*, 4370-4376.
- [26] L. Beverina, P. Salice, *European Journal of Organic Chemistry* **2010**, *2010*, 1207-1225.
- [27] W.-Y. Zheng, K. Levon, J. Laakso, J.-E. Oesterholm, *Macromolecules* **1994**, *27*, 7754-7768.
- [28] M. C. Scharber, D. Mühlbacher, M. Koppe, P. Denk, C. Waldauf, A. J. Heeger, C. J. Brabec, *Advanced Materials* **2006**, *18*, 789-794.
- [29] A. K. Mohanakrishnan, A. Hucke, M. A. Lyon, M. V. Lakshmikantham, M. P. Cava, *Tetrahedron* **1999**, *55*, 11745-11754.
- [30] J. Andersen, U. Madsen, F. Björkling, X. Liang, *Synlett* **2005**, *2005*, 2209-2213.
- [31] K. Hemming, M. N. Khan, P. A. O'Gorman, A. Pitard, *Tetrahedron* **2013**, *69*, 1279-1284.
- [32] S. Koyuncu, İ. Kaya, F. B. Koyuncu, E. Ozdemir, *Synthetic Metals* **2009**, *159*, 1034-1042.
- [33] J. F. Morin, M. Leclerc, *Macromolecules* **2001**, *34*, 4680-4682.

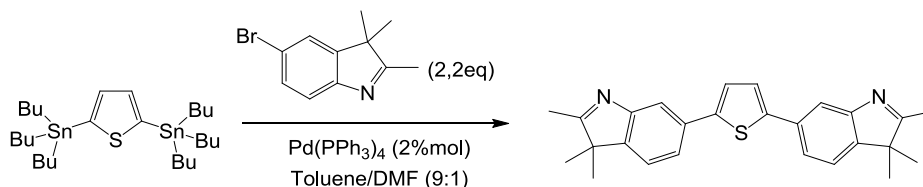
## 4.5 BIBLIOGRAPHY

- [1] J. Sakamoto, M. Rehahn, G. Wegner, A. D. Schlüter, *Macromolecular Rapid Communications* **2009**, *30*, 653-687.
- [2] B. Carsten, F. He, H. J. Son, T. Xu, L. Yu, *Chemical Reviews* **2011**, *111*, 1493-1528.
- [3] M. C. Iovu, E. E. Sheina, R. R. Gil, R. D. McCullough, *Macromolecules* **2005**, *38*, 8649-8656.
- [4] T. Yamamoto, A. Yamamoto, *Chemistry Letters* **1977**, *6*, 353-356.
- [5] P. Marks, M. Levine, *Journal of Chemical Education* **2012**, *89*, 1186-1189.
- [6] K.-Y. Law, F. C. Bailey, *Canadian Journal of Chemistry* **1986**, *64*, 2267-2273.
- [7] A. Treibs, K. Jacob, *Angewandte Chemie International Edition in English* **1965**, *4*, 694-694.
- [8] C. R. Chenthamarakshan, J. Eldo, A. Ajayaghosh, *Macromolecules* **1999**, *32*, 251-257.
- [9] Y.-Y. Chen, H. K. Hall, Jr., *Polymer Bulletin* **1986**, *16*, 419-425.
- [10] W. t. H. E. E. Havinga, H. Wynberg, *Polymer Bulletin* **1992**, *29*, 119-126.
- [11] E. E. Havinga, W. ten Hoeve, H. Wynberg, *Synthetic Metals* **1993**, *55*, 299-306.
- [12] E. E. Havinga, A. Pomp, W. ten Hoeve, H. Wynberg, *Synthetic Metals* **1995**, *69*, 581-582.
- [13] W. Zhang, Z. Wang, Y. S. Tang, Z. G. Xu, Y. Li, Q. Jiang, *Chinese Chemical Letters* **2010**, *21*, 245-248.
- [14] J. Eldo, A. Ajayaghosh, *Chemistry of Materials* **2001**, *14*, 410-418.
- [15] R. Adams, J. E. Bullock, W. C. Wilson, *Journal of the American Chemical Society* **1923**, *45*, 521-527.
- [16] G. F. D'Alelio, J. V. Crivello, R. K. Schoenig, T. F. Huemmer, *Journal of Macromolecular Science: Part A - Chemistry* **1967**, *1*, 1321-1330.
- [17] P. W. Morgan, S. L. Kwolek, T. C. Pletcher, *Macromolecules* **1987**, *20*, 729-739.
- [18] C.-J. Yang, S. A. Jenekhe, *Macromolecules* **1995**, *28*, 1180-1196.
- [19] F. R. Diaz, J. Moreno, L. H. Tagle, G. A. East, D. Radic, *Synthetic Metals* **1999**, *100*, 187-193.
- [20] S. Barik, T. Bletzacker, W. G. Skene, *Macromolecules* **2012**, *45*, 1165-1173.
- [21] S. Barik, W. G. Skene, *Polymer Chemistry* **2011**, *2*, 1091-1097.
- [22] S. Dufresne, W. G. Skene, *Journal of Physical Organic Chemistry* **2012**, *25*, 211-221.
- [23] D. Scherer, R. Dörfler, A. Feldner, T. Vogtmann, M. Schwoerer, U. Lawrentz, W. Grah, C. Lambert, *Chemical Physics* **2002**, *279*, 179-207.
- [24] S. Kuster, T. Geiger, *Dyes and Pigments* **2012**, *95*, 657-670.
- [25] M. Tian, M. Furuki, I. Iwasa, Y. Sato, L. S. Pu, S. Tatsuura, *The Journal of Physical Chemistry B* **2002**, *106*, 4370-4376.
- [26] L. Beverina, P. Salice, *European Journal of Organic Chemistry* **2010**, *2010*, 1207-1225.
- [27] W.-Y. Zheng, K. Levon, J. Laakso, J.-E. Oesterholm, *Macromolecules* **1994**, *27*, 7754-7768.
- [28] M. C. Scharber, D. Mühlbacher, M. Koppe, P. Denk, C. Waldauf, A. J. Heeger, C. J. Brabec, *Advanced Materials* **2006**, *18*, 789-794.
- [29] A. K. Mohanakrishnan, A. Hucke, M. A. Lyon, M. V. Lakshmikantham, M. P. Cava, *Tetrahedron* **1999**, *55*, 11745-11754.
- [30] J. Andersen, U. Madsen, F. Björkling, X. Liang, *Synlett* **2005**, *2005*, 2209-2213.
- [31] K. Hemming, M. N. Khan, P. A. O'Gorman, A. Pitard, *Tetrahedron* **2013**, *69*, 1279-1284.
- [32] S. Koyuncu, İ. Kaya, F. B. Koyuncu, E. Ozdemir, *Synthetic Metals* **2009**, *159*, 1034-1042.
- [33] J. F. Morin, M. Leclerc, *Macromolecules* **2001**, *34*, 4680-4682.

## 4.6 EXPERIMENTAL

### 4.6.1 SYNTHESSES

#### 2,5-bis(2,3,3-trimethyl-3H-indol-6-yl)thiophene (13)



The previously prepared 5-bromo-2,3,3-trimethyl-3H-indole **10** (1.61 g, 3.1 mmol), 2,5-bis(tributylstannyl)thiophene (2.02 g, 6.8 mmol) and tetrakis(triphenylphosphine)palladium(0) (67 mg, 0.06 mmol) were degassed via three vacuum/argon cycles, and 5 mL of a degassed toluene/DMF mixture (9:1 vol) was added under argon. The reaction mixture was refluxed under argon overnight. 10 ml of a 10%w KF aqueous solution was added, and the mixture was stirred for 1h at room temperature. The resulting white precipitate was filtered off, rinsed with toluene and the filtrate was washed three times with 20 ml of water. The organic phase was dried with  $\text{MgSO}_4$  and the solvent was removed under vacuum to give the crude product as an orange solid. A subsequent purification by flash chromatography (toluene:EtOH 96:4) followed by drying at 40°C under vacuum overnight afforded the pure compound as orange crystals (0.84 g, 69 %).

m.p. 173°C.  $^1\text{H}$  NMR (400 MHz,  $\text{CDCl}_3$ ):  $\delta$  (ppm) 7.59 (dd,  $J = 8.0, 1.8$  Hz, 2H), 7.55 – 7.51 (m, 4H), 7.28 (s,  $J = 3.7$  Hz, 2H), 2.30 (s, 6H), 1.35 (s, 12H).  $^{13}\text{C}$  NMR (101 MHz,  $\text{CDCl}_3$ )  $\delta$  188.56, 153.38, 146.62, 143.75, 131.69, 125.42, 123.97, 120.30, 118.88, 53.91, 23.28, 15.63. FT-IR (ATR):  $\nu = 2962, 1570, 1456, 1423, 1381, 1204, 1123, 891, 841, 828, 807, 728, 635, 589, 549$ . HRMS (EI+,  $m/z$ )  $[\text{M}]^+$  calculated (%) for  $\text{C}_{26}\text{H}_{26}\text{N}_2\text{S}$ : 398.1817, found 398.1799.

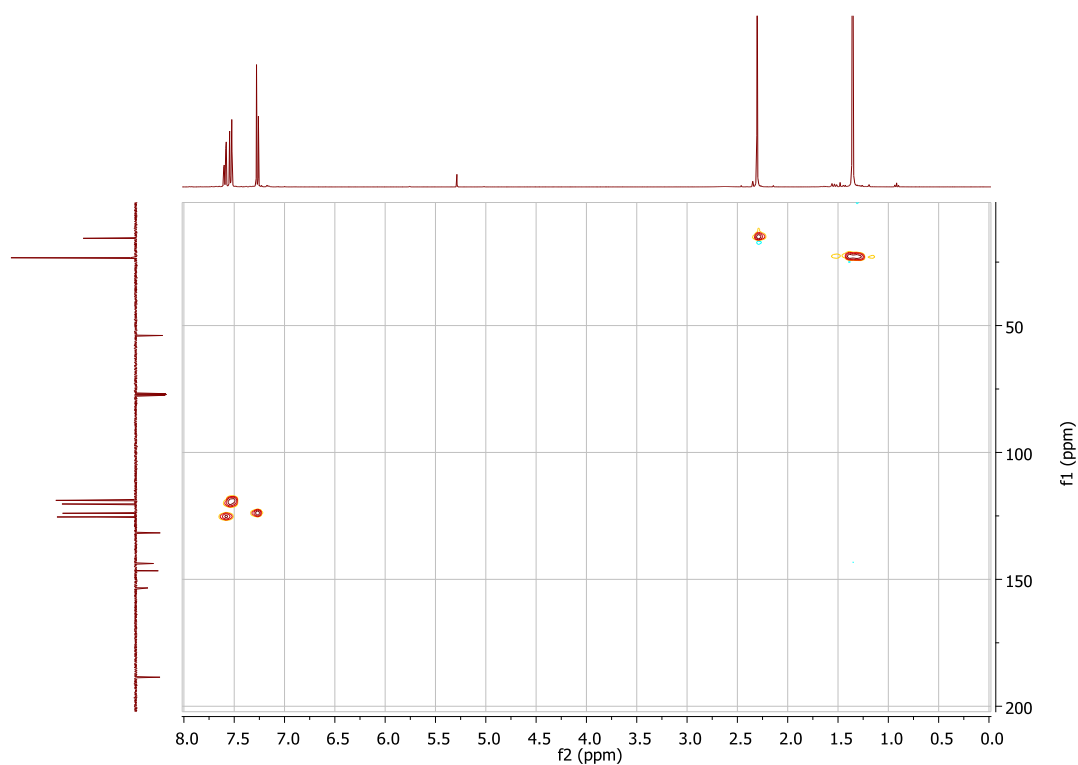


Figure 4 - 38:  $^1\text{H}$ - $^{13}\text{C}$  HSQC NMR (400 MHz) spectra of 13 in  $\text{CDCl}_3$ .

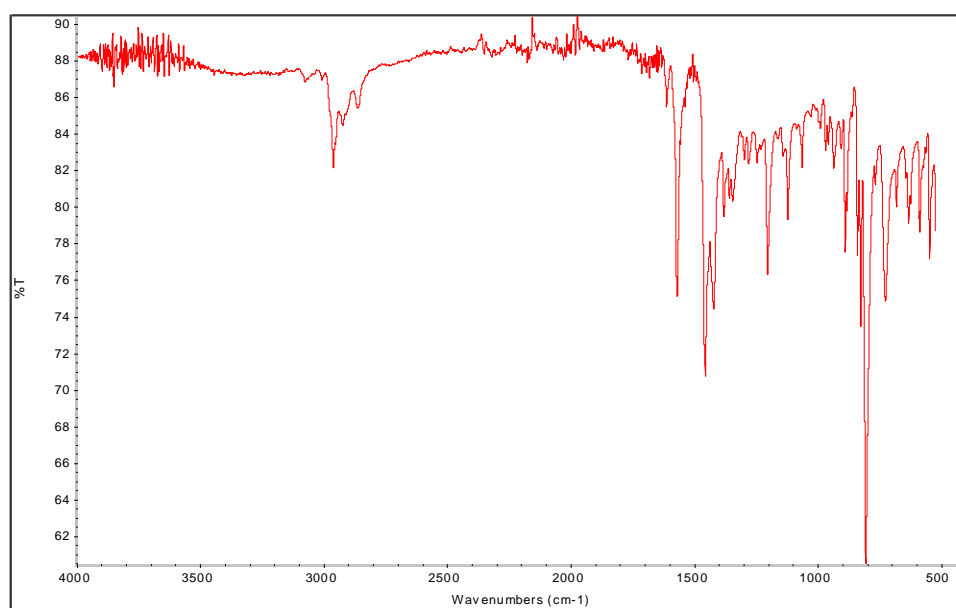
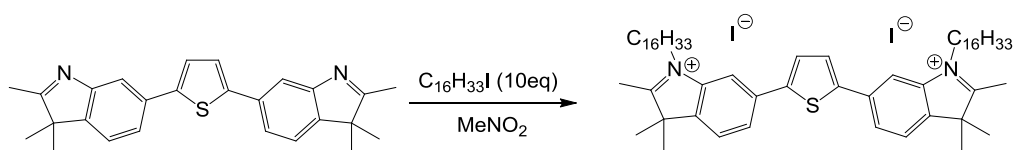


Figure 4 - 39: IR spectrum (ATR) of 13.

**2,5-bis(1-hexadecyl-2,3,3-trimethyl-3H-indol-6-ium)thiophene diiodide (14)**



**13** (0.80 g, 2.0 mmol), 1-iodohexadecane (7.03 g, 20.0 mmol) and 20 ml of nitromethane were bubbled under argon and then heated to reflux overnight. The solvent was removed under vacuum, and 50 ml of diethyl ether was added. The solution was cooled down at 5°C overnight, and a dark brown precipitate formed, which was recovered by filtration and rinsed with cold diethyl ether. The resulting solid was dried at 40°C under vacuum overnight to yield a brown powder (1.83 g, 83 %).

Degradation at 125°C.  $^1\text{H}$  NMR (400 MHz,  $\text{CDCl}_3$ ):  $\delta$  (ppm) 7.90 (s, 2H), 7.74 (dd,  $J = 26.0, 8.4$  Hz, 4H), 7.46 (s, 2H), 4.61 (t,  $J = 6.7$  Hz, 4H), 3.01 (s, 6H), 1.92 (d,  $J = 6.8$  Hz, 4H), 1.73 - 1.67 (m, 16H), 1.50 - 1.13 (m, 52H), 0.85 (t,  $J = 6.7$  Hz, 6H).  $^{13}\text{C}$  NMR (101 MHz,  $\text{CDCl}_3$ ):  $\delta$  (ppm) 194.80, 142.81, 142.70, 140.25, 135.99, 127.05, 126.80, 120.57, 116.51, 55.02, 50.42, 32.01, 29.79, 29.78, 29.75, 29.70, 29.62, 29.49, 29.45, 29.30, 28.19, 27.01, 23.50, 22.78, 16.77, 14.22. FT-IR (ATR):  $\nu=3443, 2920, 2850, 1608, 1586, 1539, 1465, 1367, 1337, 1297, 1219, 1164, 1065, 930, 805, 772, 720, 668, 538\text{ cm}^{-1}$ . HRMS (EI+,  $m/z$ )  $[\text{M}-2\text{H}]^+$  calculated (%) for  $\text{C}_{58}\text{H}_{90}\text{N}_2\text{S}$ : 848.6981, found 846.7.

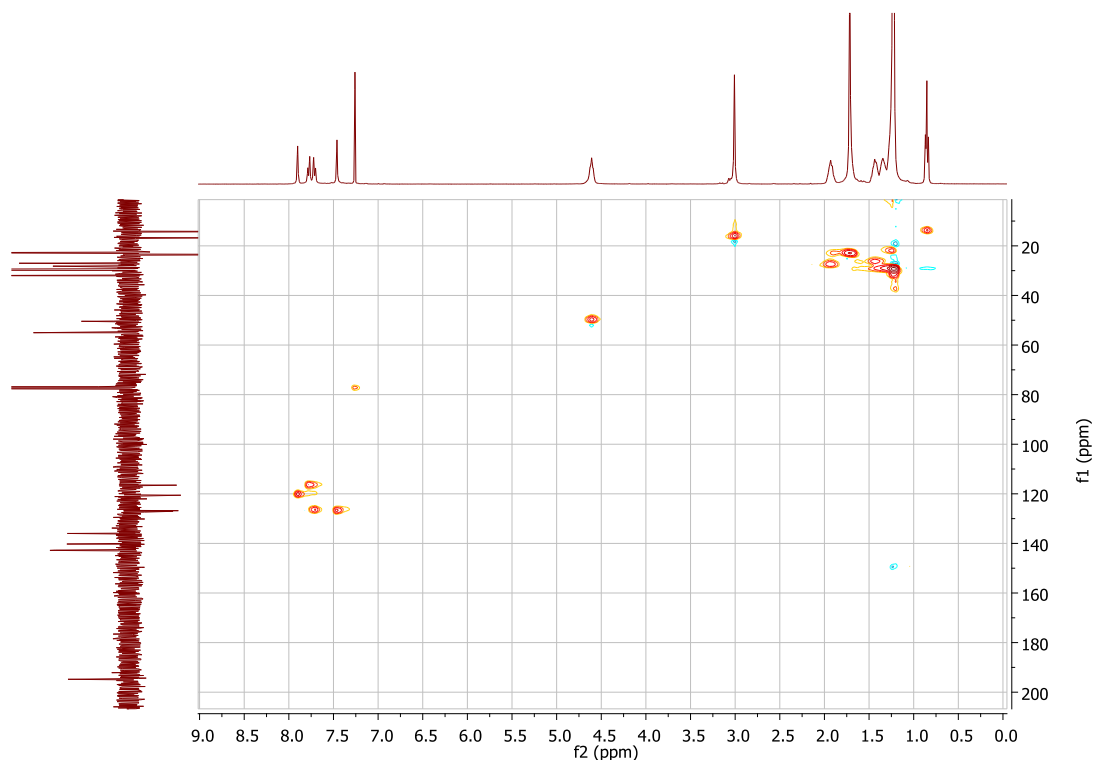


Figure 4 - 40:  $^1\text{H}$ - $^{13}\text{C}$  HSQC NMR spectra (400 MHz) of **14** in  $\text{CDCl}_3$ .

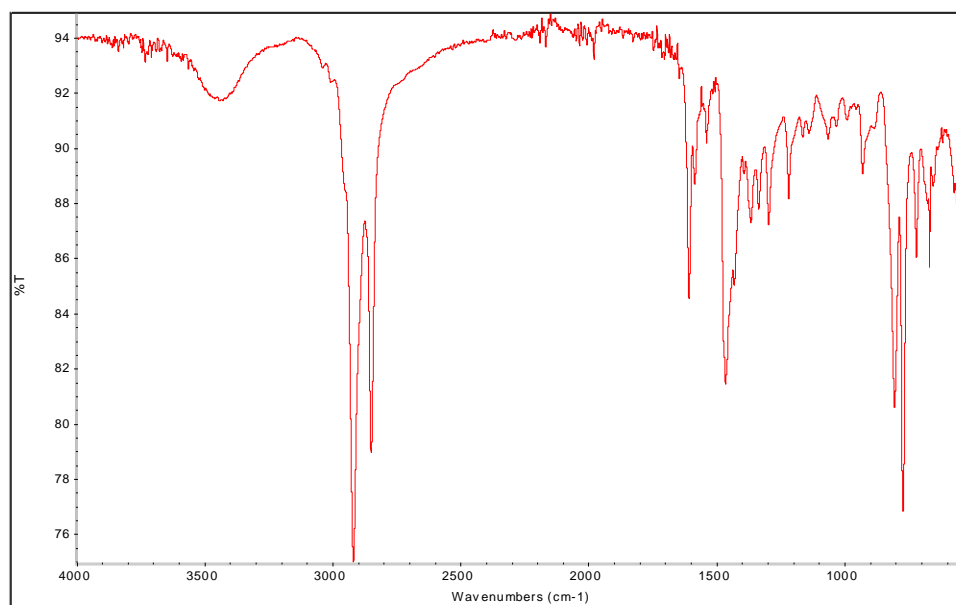
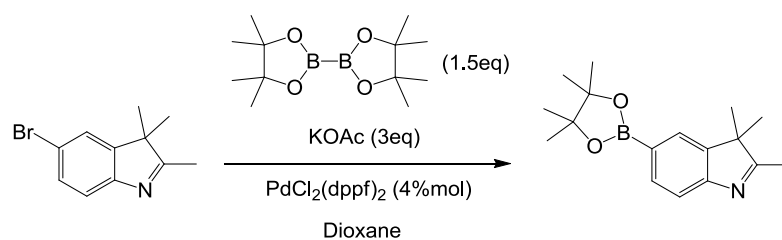


Figure 4 - 41: IR spectrum (ATR) of 14.

### **2,3,3-trimethyl-5-(4,4,5,5-tetramethyl-1,3,2-dioxaborolan-2-yl)-3H-indole (15)**



**10** (3.01 g, 12.6 mmol), bis(pinacolato)diboron (4.80 g, 18.9 mmol), anhydrous potassium acetate (3.72 g, 37.9 mmol) and dichloro[1,1'-bis(diphenylphosphino)-ferrocen]-palladium(II) (0.37 g, 0.5 mmol) were introduced in a 500 ml, and degassed three times with vacuum/argon cycles. Dry dioxane (200 ml) was then added via an addition funnel under argon, and the mixture was stirred and heated up to 90°C for 5h, during which a dark brown coloration in solution appeared. The solid residues in the reaction mixture were filtered off over a thin silica layer and the solvent was removed under vacuum. Flash chromatography with CH<sub>2</sub>Cl<sub>2</sub>:Et<sub>3</sub>N as eluent (99:1) yielded the pure product as a pink powder (3.21 g, 89 %).

m.p. 121 °C. <sup>1</sup>H NMR (400 MHz, CDCl<sub>3</sub>): δ (ppm) 7.79 (dd, *J* = 7.7, 1.1 Hz, 1H), 7.72 (s, 1H), 7.52 (d, *J* = 7.7 Hz, 1H), 2.29 (s, 3H), 1.35 (s, 12H), 1.30 (s, 6H). <sup>13</sup>C NMR (101 MHz, CDCl<sub>3</sub>): δ (ppm) 189.83, 156.46, 145.01, 135.01, 127.51, 119.46, 83.85, 24.98, 23.13, 15.63. FT-IR (ATR): ν = 2955, 1615, 1575, 1479, 1425, 1371, 1351, 1329, 1300, 1252, 1208, 1148, 1093, 1061, 961, 911, 854, 833, 776, 706, 685, 582 cm<sup>-1</sup>.



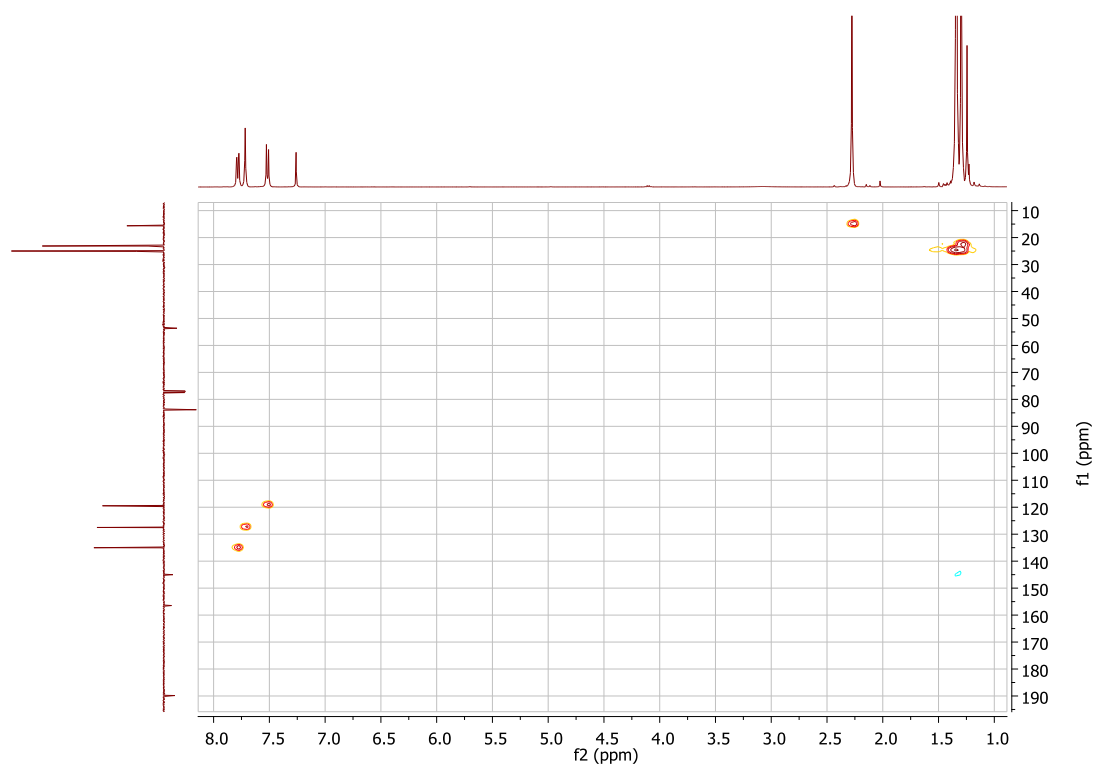


Figure 4 - 42:  $^1\text{H}$ - $^{13}\text{C}$  HSQC NMR (400 MHz) spectra of 15 in  $\text{CDCl}_3$ .

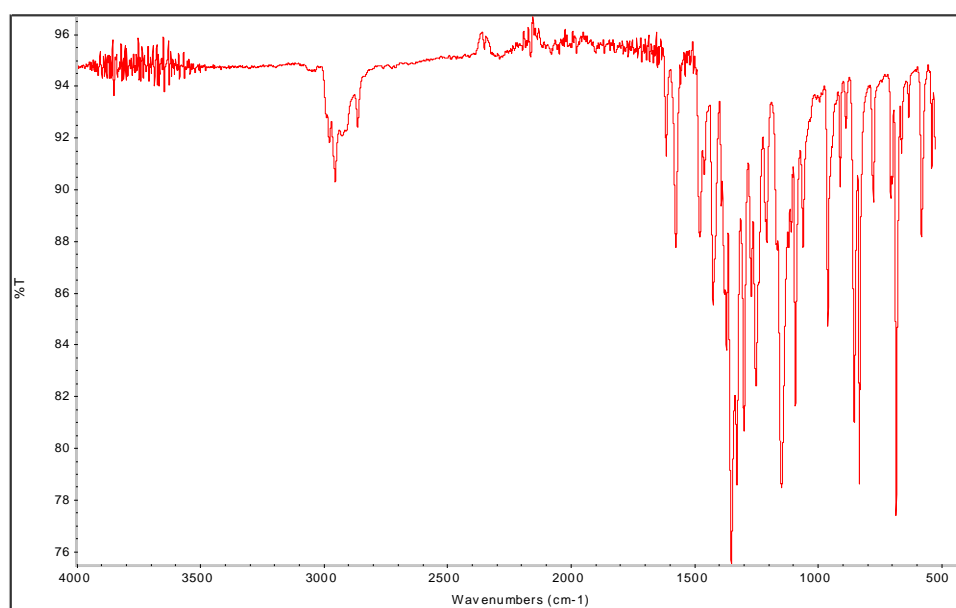
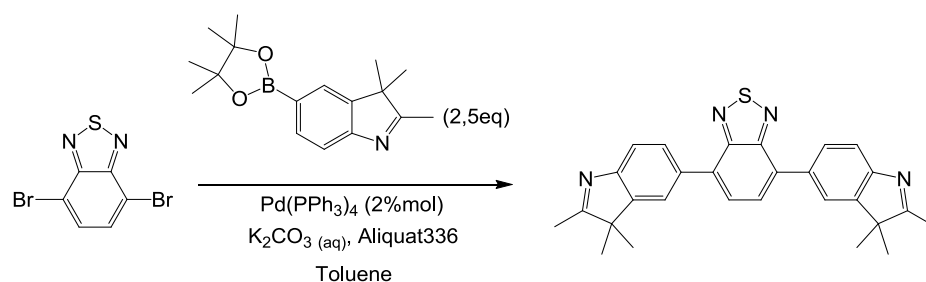


Figure 4 - 43: IR spectrum (ATR) of 15.

**4,7-bis(2,3,3-trimethyl-3H-indol-5-yl)benzothiadiazole (16)**

4,7-dibromobenzothiadiazole (301 mg, 1 mmol), **15** (729 mg, 2.6 mmol), tetrakis(triphenylphosphine)palladium(0) (25 mg, 0.02 mmol) and one drop of Aliquat 336 were degassed via three vacuum/argon cycles, and 10 mL of degassed toluene was added under argon. Then, 10 mL of a degassed 2 M potassium carbonate aqueous solution was added. The reaction mixture was refluxed under argon overnight. The reaction was stopped by pouring it in 100 ml of water, and the mixture was extracted three times with toluene. The combined organic phases were washed two times with 50 ml of water. The organic phase was dried with  $\text{MgSO}_4$  and the solvent was removed under vacuum. A subsequent purification by flash chromatography ( $\text{CH}_2\text{Cl}_2$ :ethyl acetate 85:15) followed by drying at 40°C under vacuum overnight afforded the pure compound as a yellow-orange powder (384 mg, 83 %).

m.p. 218°C.  $^1\text{H}$  NMR (400 MHz,  $\text{CDCl}_3$ ):  $\delta$  (ppm) 7.93 (dd,  $J = 8.0, 1.8$  Hz, 2H), 7.91 (d,  $J = 1.2$  Hz, 2H), 7.80 (s, 2H), 7.70 (d,  $J = 8.0$  Hz, 2H), 2.35 (s, 3H), 1.41 (s, 7H).  $^{13}\text{C}$  NMR (101 MHz,  $\text{CDCl}_3$ ):  $\delta$  (ppm) 189.24, 154.34, 153.93, 146.13, 134.64, 133.41, 129.14, 128.17, 122.59, 120.03, 54.03, 23.33, 15.71. FT-IR (ATR):  $\nu = 2954, 2924, 1574, 1458, 1428, 1350, 1250, 1207, 1123, 964, 883, 843, 831, 811, 600, 543\text{ cm}^{-1}$ . HRMS (EI+,  $m/z$ )  $[\text{M}]^+$  calculated for  $\text{C}_{28}\text{H}_{26}\text{N}_4\text{S}$ : 450.1878, found 450.1882.

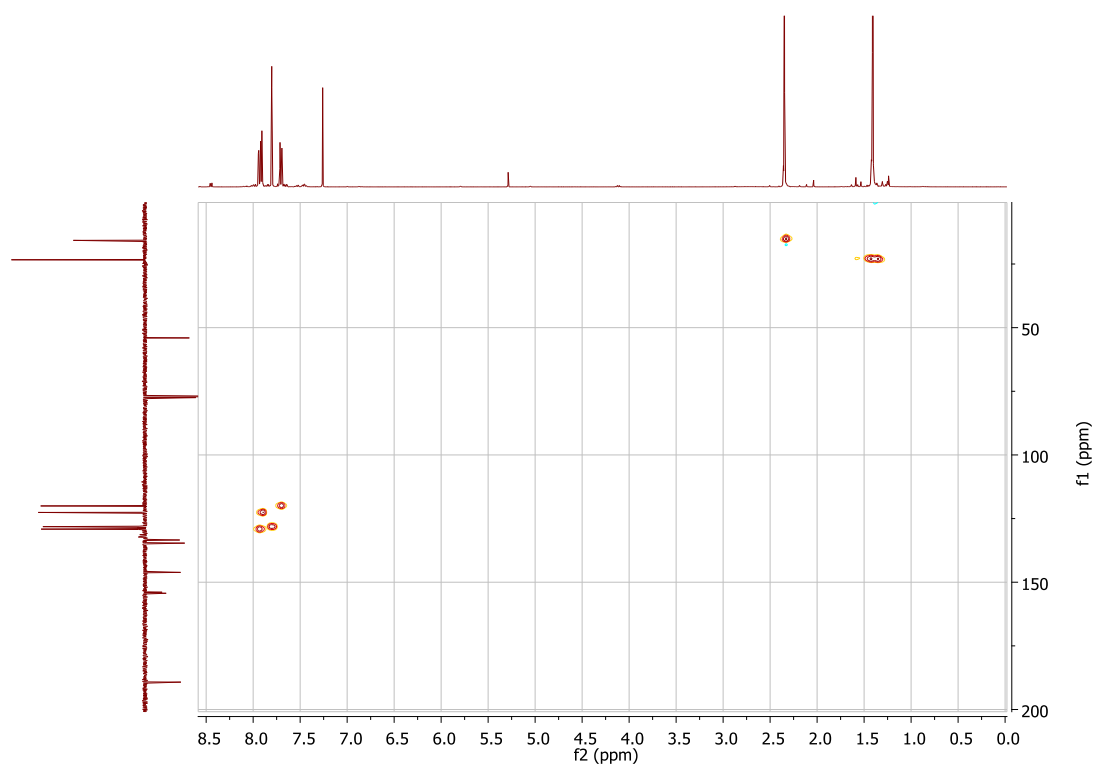


Figure 4 - 44:  $^1\text{H}$ - $^{13}\text{C}$  HSQC NMR spectra (400 MHz) of 16 in  $\text{CDCl}_3$ .

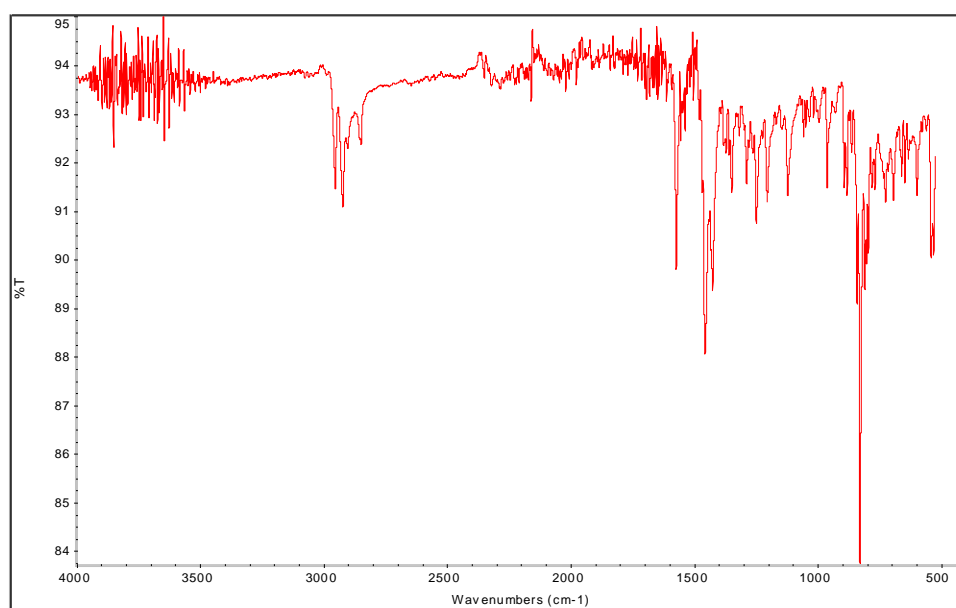
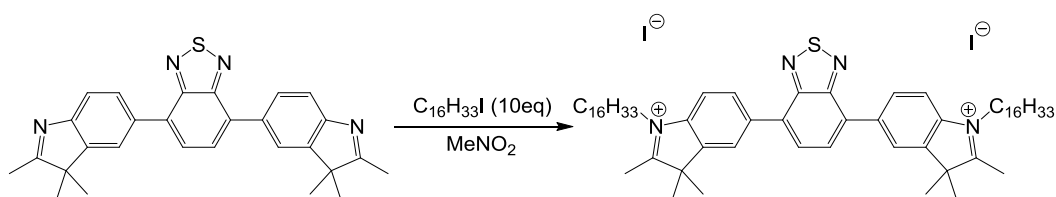


Figure 4 - 45: IR spectrum (ATR) of 16.

**4,7-bis(1-hexadecyl-2,3,3-trimethyl-3H-indol-5-ium)benzothiadiazole diiodide (17)**



**16** (296 mg, 0.7 mmol), 1-iodohexadecane (2.45 g, 7.0 mmol) and 8 ml of nitromethane were bubbled under argon and then heated to reflux overnight. The solvent was removed under vacuum, and 30 ml of diethyl ether was added. The solution was cooled down at 5°C overnight, and a dark brown precipitate formed, which was recovered by filtration and rinsed with cold diethyl ether. The resulting solid was dried at 40°C under vacuum overnight to yield a dark brown powder (592 mg, 78 %).

Degradation at 156°C.  $^1\text{H}$  NMR (400 MHz,  $\text{CDCl}_3$ ):  $\delta$  (ppm) 8.26 (d,  $J = 1.1$  Hz, 2H), 8.18 (dd,  $J = 8.5, 1.4$  Hz, 2H), 8.00 (s, 2H), 7.84 (d,  $J = 8.5$  Hz, 2H), 4.71 (t,  $J = 7.2$  Hz, 4H), 3.10 (s, 6H), 2.03 – 1.91 (m, 4H), 1.76 (s, 12H), 1.70 – 1.59 (m, 4H), 1.54 – 1.43 (m, 4H), 1.38 (s, 4H), 1.26 (d,  $J = 16.8$  Hz, 40H), 0.86 (t,  $J = 6.9$  Hz, 6H).  $^{13}\text{C}$  NMR (101 MHz,  $\text{CDCl}_3$ ):  $\delta$  (ppm) 195.95, 153.55, 142.23, 140.92, 139.13, 131.80, 130.68, 129.65, 124.56, 115.64, 55.11, 50.54, 31.98, 29.75, 29.74, 29.71, 29.66, 29.58, 29.45, 29.41, 29.27, 28.15, 26.99, 23.46, 22.74, 17.15, 14.19. FT-IR (ATR):  $\nu = 3430, 2919, 2850, 1611, 1464, 1335, 893, 826, 720\text{ cm}^{-1}$ . HRMS (EI+,  $m/z$ )  $[\text{M}-2\text{H}]^+$  calculated for  $\text{C}_{60}\text{H}_{90}\text{N}_4\text{S}$ : 898.6886, found 898.6900.

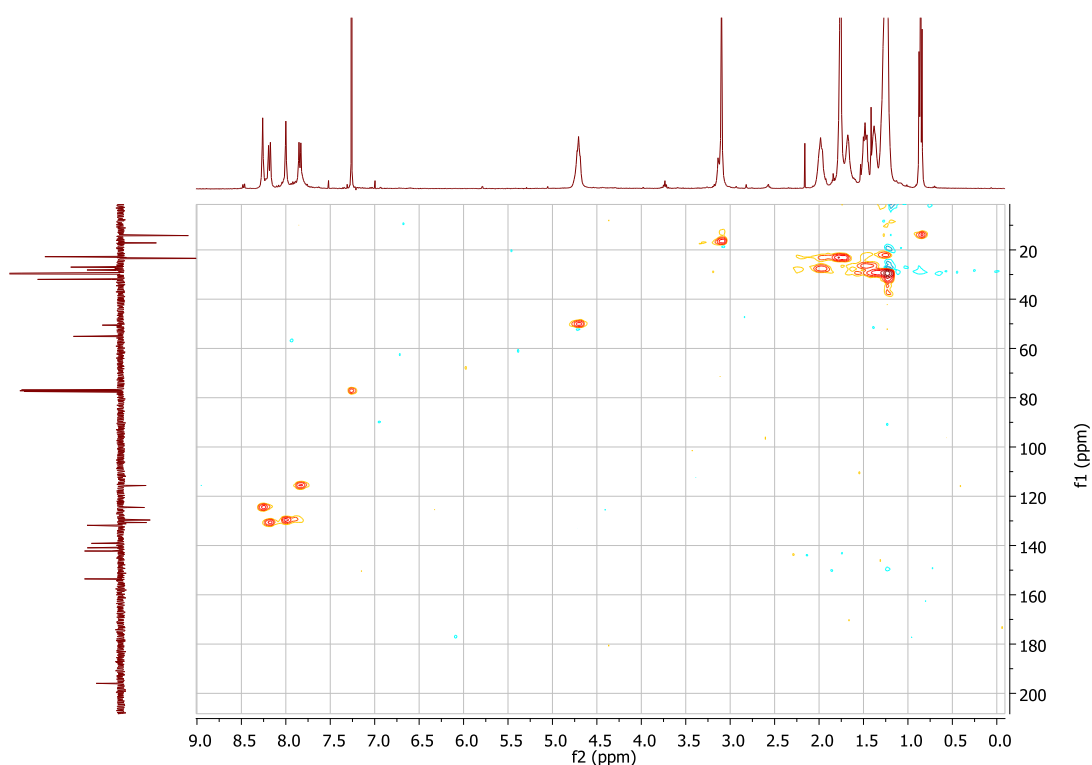


Figure 4 - 46:  $^1\text{H}$ - $^{13}\text{C}$  HSQC NMR spectra (400 MHz) of **17** in  $\text{CDCl}_3$ .

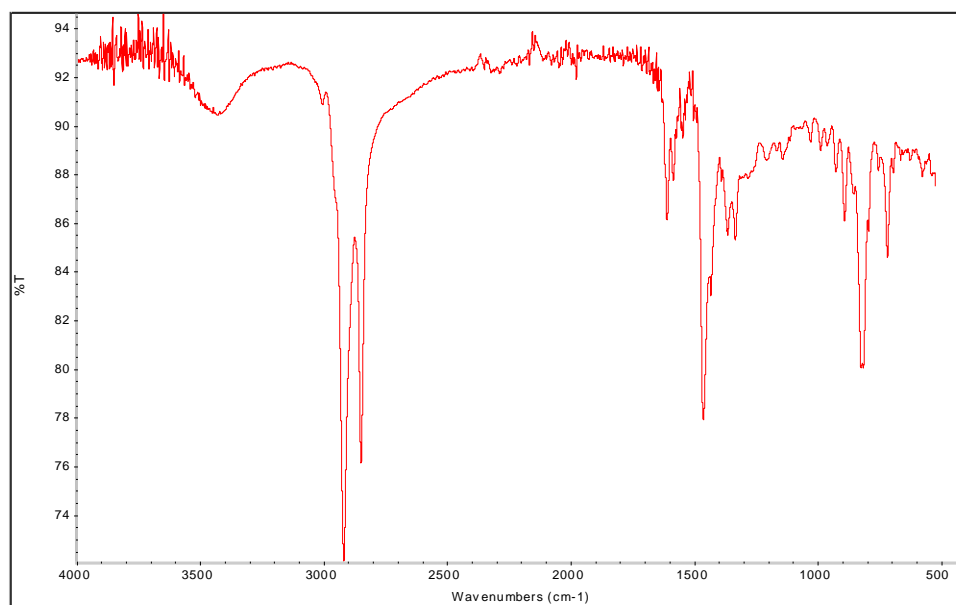
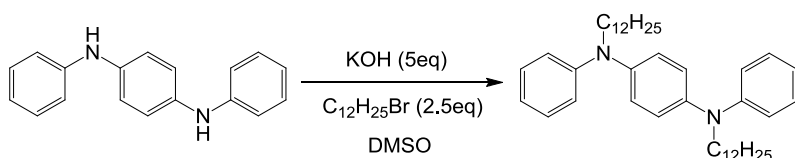


Figure 4 - 47: IR spectrum (ATR) of 17.

**N<sup>1</sup>,N<sup>4</sup>-didodecyl-N<sup>1</sup>,N<sup>4</sup>-diphenylbenzene-1,4-diamine (18)**

N<sup>1</sup>,N<sup>4</sup>-diphenylbenzene-1,4-diamine (10.00 g, 38.4 mmol) and freshly powdered potassium hydroxide (10.78 g, 192.1 mmol) were introduced in a 500 ml round-bottom flask, and subsequently degassed via three vacuum/argon cycles. 200 ml of dry DMSO was then added under argon, and the mixture was stirred at 90°C for 2 h. 1-bromododecane (23.93 g, 23 ml, 96.0 mmol) was then added dropwise and the reaction was allowed to stir for 4 h. The mixture was poured in 2 l of water, and extracted four times with 100 ml of diethyl ether. The combined organic phases were concentrated under vacuum, washed three times with 50 ml of water and dried over MgSO<sub>4</sub>. The solvent was removed under vacuum. Flash chromatography (heptane:ethyl acetate 95:5) followed by a recrystallization in pentane afforded the pure product as a white powder (15.34 g, 67 %).

m.p. 64°C. <sup>1</sup>H NMR (400 MHz, THF): δ (ppm) 7.15 (t, *J* = 7.9 Hz, 4H), 6.95 (s, 4H), 6.87 (d, *J* = 7.9 Hz, 4H), 6.76 (t, *J* = 7.3 Hz, 4H), 3.70 – 3.62 (m, 4H), 1.71 – 1.61 (m, 4H), 1.31 (d, *J* = 19.3 Hz, 36H), 0.88 (t, *J* = 6.8 Hz, 6H). <sup>13</sup>C NMR (101 MHz, THF): δ (ppm) 149.69, 143.83, 129.89, 124.80, 120.48, 119.65, 53.28, 33.03, 30.80, 30.77, 30.74, 30.73, 30.62, 30.46, 28.62, 28.13, 23.72, 14.59. FT-IR (ATR): ν = 3038, 2916, 2848, 1594, 1494, 1467, 1358, 1256, 1143, 1094, 845, 742, 699, 612 cm<sup>-1</sup>. HRMS (EI+, *m/z*) [M]<sup>+</sup> calculated for C<sub>42</sub>H<sub>64</sub>N<sub>2</sub>: 596.5070, found 596.5080.

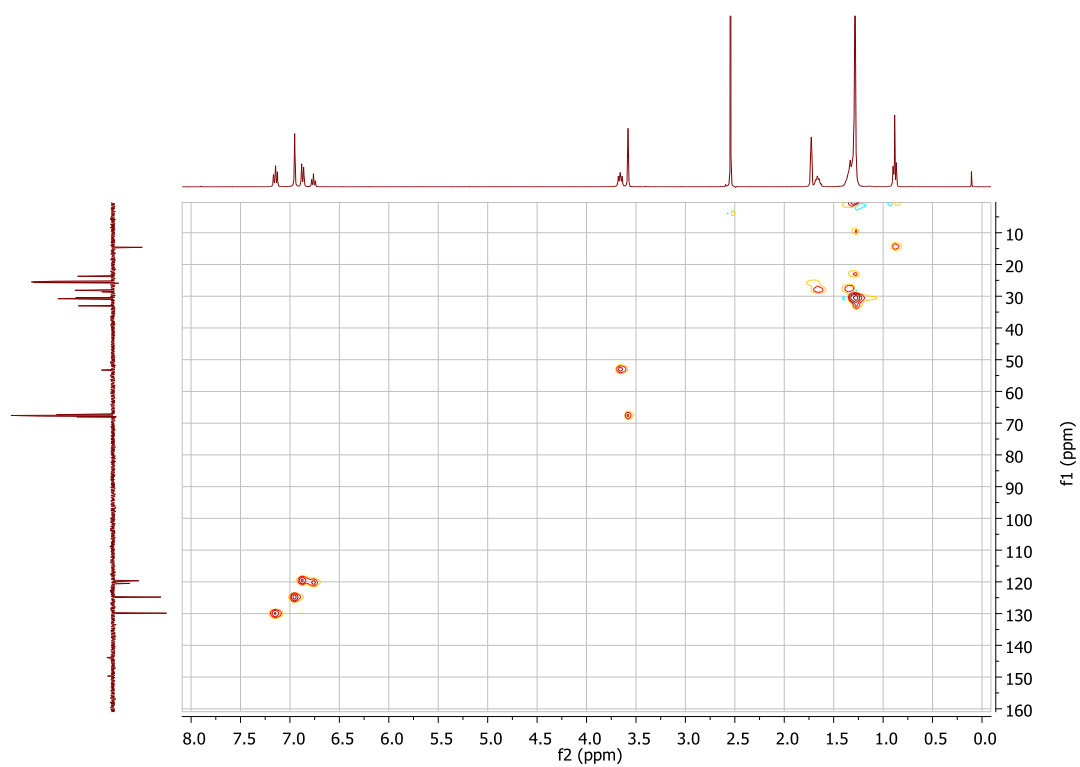


Figure 4 - 48:  $^1\text{H}$ - $^{13}\text{C}$  HSQC NMR spectra (400 MHz) of **17** in  $\text{THF-d}_8$ .

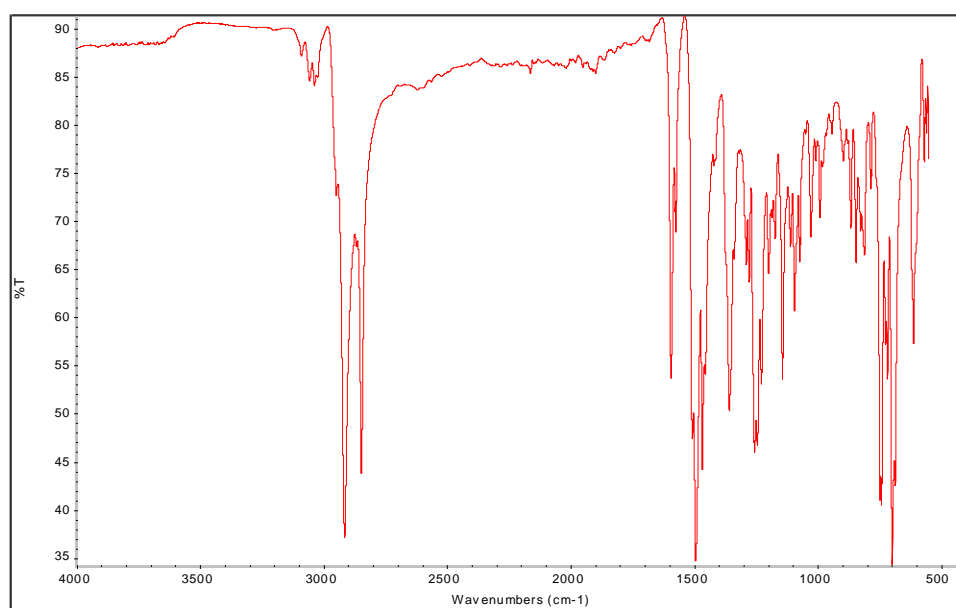
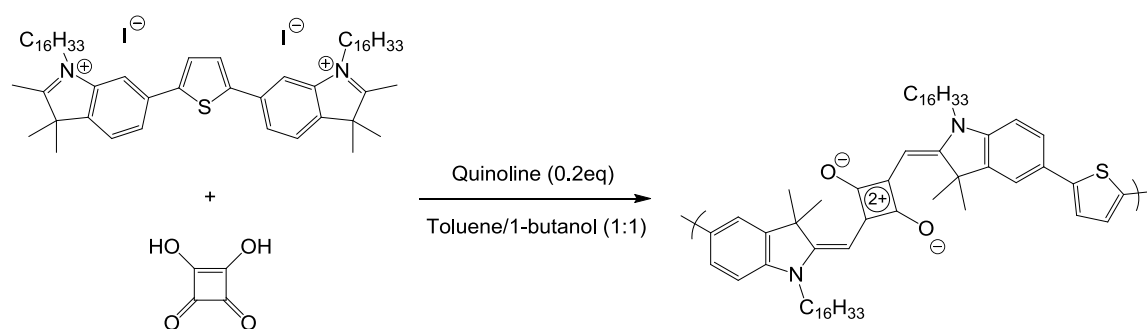


Figure 4 - 49: IR spectrum (ATR) of **18**.

**Poly(bis(hexadecyl)squaraine-*alt*-thiophene) (PSQT) via SA polycondensation**

**14** (776 mg, 0.7 mmol), squaric acid (80 mg, 0.7 mmol) and quinoline (18 mg, 0.014 mmol) were added in a 25 ml round-bottom flask which was then connected to a Dean-Stark apparatus. The reaction media was degassed three times with vacuum/argon cycles, and 10 ml of a toluene/1-butanol mixture (1:1 vol, bubbled under argon) was added. The mixture was then stirred and heated up to reflux for 3 days. Solubilization of the monomers was achieved only after stirring at reflux. A dark green color of the solution could be observed after few hours of reaction. The reaction mixture was then poured into cold MeOH/H<sub>2</sub>O (9:1 vol) and the resulting precipitate was filtered and purified on Soxhlet apparatus with MeOH (12h), acetone (24h), THF (72h) and CHCl<sub>3</sub> (24h). A small insoluble fraction remained in the cartridge and could not be recovered. The THF and CHCl<sub>3</sub> fractions were separately concentrated under vacuum, solubilized in a minimum amount of CHCl<sub>3</sub> and finally precipitated in MeOH/H<sub>2</sub>O (9:1 vol). The resulting dark purple solid was dried at 40°C under vacuum overnight ( $m_{\text{THF}}$ =254 mg,  $m_{\text{CHCl}_3}$ =167 mg, 65 %).

<sup>1</sup>H NMR (400 MHz, CDCl<sub>3</sub>):  $\delta$  (ppm) 7.59 (s,  $J$  = 28.1 Hz, 4H), 7.30 (s, 2H), 7.00 (s, 2H), 6.02 (s, 2H), 4.23 – 3.66 (m,  $J$  = 116.5 Hz, 4H), 2.01 – 1.63 (m, 16H), 1.55 – 1.05 (m, 52H), 0.87 (t,  $J$  = 5.9 Hz, 6H). <sup>13</sup>C NMR (101 MHz, CDCl<sub>3</sub>):  $\delta$  (ppm) 169.66, 143.26, 142.13, 130.43, 125.57, 124.02, 119.66, 109.90, 87.38, 49.45, 44.08, 32.06, 29.84, 29.80, 29.75, 29.69, 29.64, 29.53, 29.50, 27.30, 27.23, 22.82, 14.26. FT-IR (ATR):  $\nu$  = 2919, 2849, 1599, 1450, 1351, 1267, 1165, 1066, 963, 918, 788, 689, 567 cm<sup>-1</sup>.

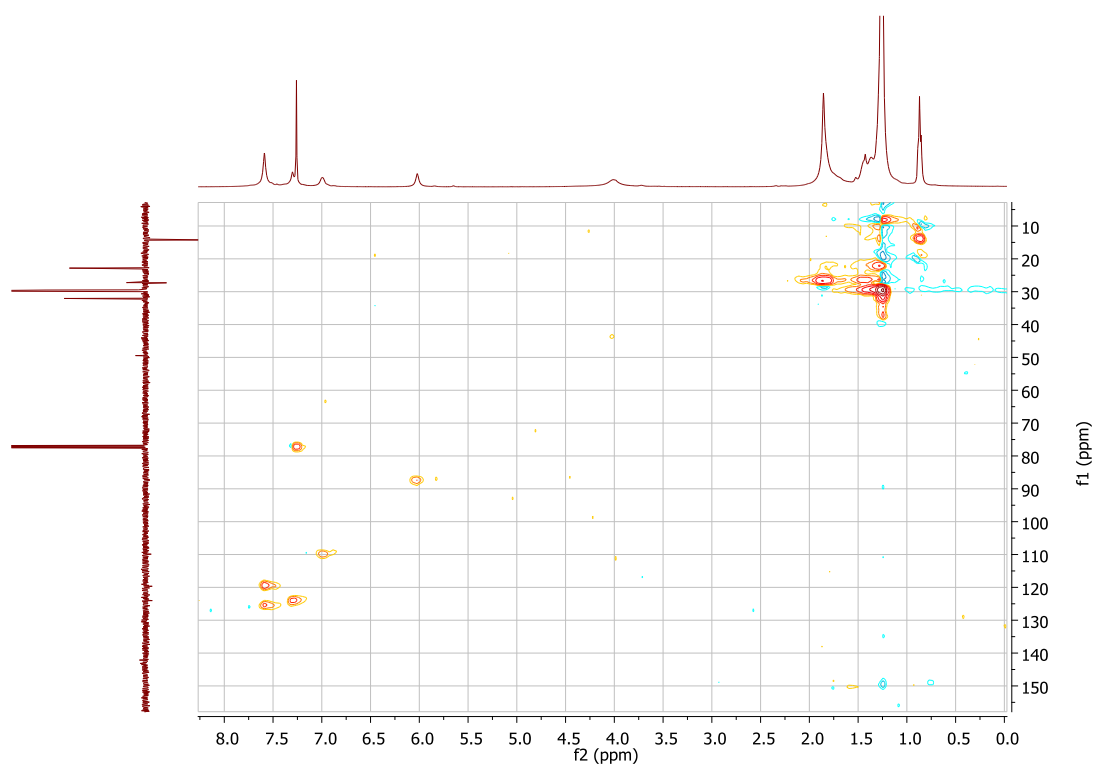


Figure 4 - 50:  $^1\text{H}$ - $^{13}\text{C}$  HSQC NMR spectra (400 MHz) of PSQT synthesized from 14 in  $\text{CDCl}_3$ .

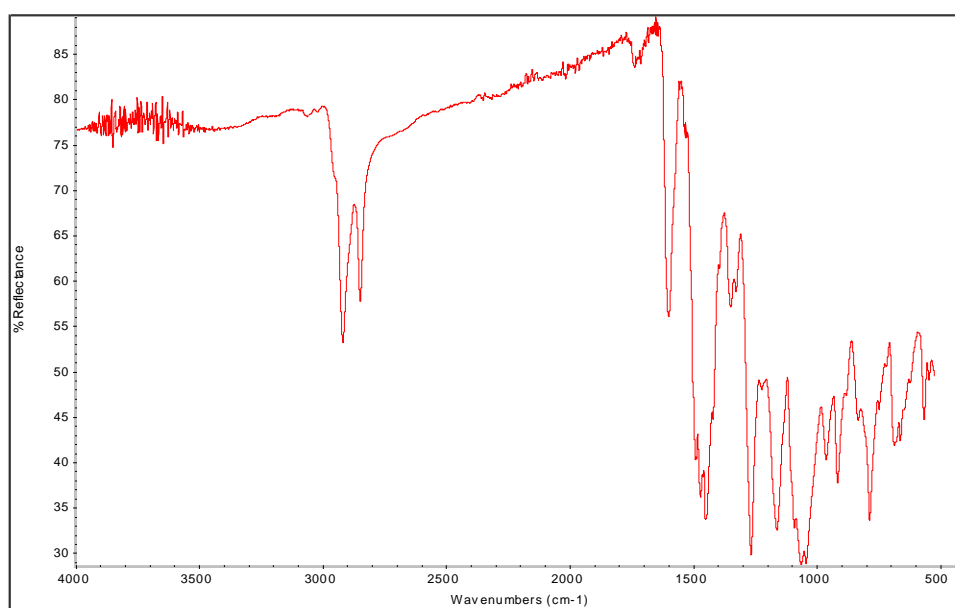
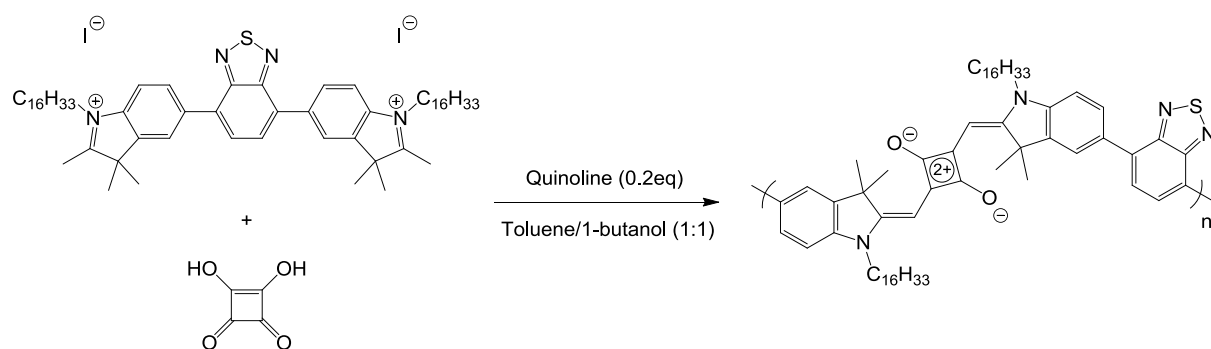


Figure 4 - 51: IR spectrum (ATR) of PSQT synthesized from 14.



**Poly(bis(hexadecyl)squaraine-*alt*-benzothiadiazole) (PSQBT) via SA polycondensation**

**17** (461 mg, 0.4 mmol), squaric acid (46 mg, 0.4 mmol) and quinoline (10 mg, 0.08 mmol) were added in a 25 ml round-bottom flask which was then connected to a Dean-Stark apparatus. The reaction media was degassed three times with vacuum/argon cycles, and 10 ml of a toluene/1-butanol mixture (1:1 vol, bubbled under argon) was added. The mixture was then stirred and heated up to reflux for 3 days. Solubilization of the monomers was achieved only after stirring at reflux. A dark green color of the solution could be observed after few hours of reaction. The reaction mixture was then poured into cold MeOH/H<sub>2</sub>O (9:1 vol) and the resulting precipitate was filtered and purified on Soxhlet apparatus with MeOH (12h), acetone (12h), THF (48h) and CHCl<sub>3</sub> (24h). A small insoluble fraction remained in the cartridge and could not be recovered. The THF and CHCl<sub>3</sub> fractions were separately concentrated under vacuum, solubilized in a minimum amount of CHCl<sub>3</sub> and finally precipitated in MeOH/H<sub>2</sub>O (9:1 vol). The resulting dark purple solid was dried at 40°C under vacuum overnight ( $m_{\text{THF}}$ =53 mg,  $m_{\text{CHCl}_3}$ =273 mg, 88 %).

<sup>1</sup>H NMR (400 MHz, CDCl<sub>3</sub>):  $\delta$  (ppm) 8.15 – 7.67 (m, 6H), 7.18 (s, 2H), 6.09 (s, 2H), 4.07 (s, 4H), 2.23 – 1.70 (m, 16H), 1.60 – 1.03 (m, 52H), 0.87 (t,  $J$  = 6.8 Hz, 6H). <sup>13</sup>C NMR (101 MHz, CDCl<sub>3</sub>):  $\delta$  (ppm) 170.16, 154.27, 142.56, 132.75, 129.43, 127.89, 123.32, 110.26, 109.64, 49.57, 32.05, 29.83, 29.79, 29.76, 29.71, 29.66, 29.56, 29.49, 27.33, 27.26, 22.81, 14.25. FT-IR (ATR):  $\nu$ = 2918, 2849, 1599, 1450, 1341, 1267, 1166, 1041, 965, 917, 789, 691, 565 cm<sup>-1</sup>.

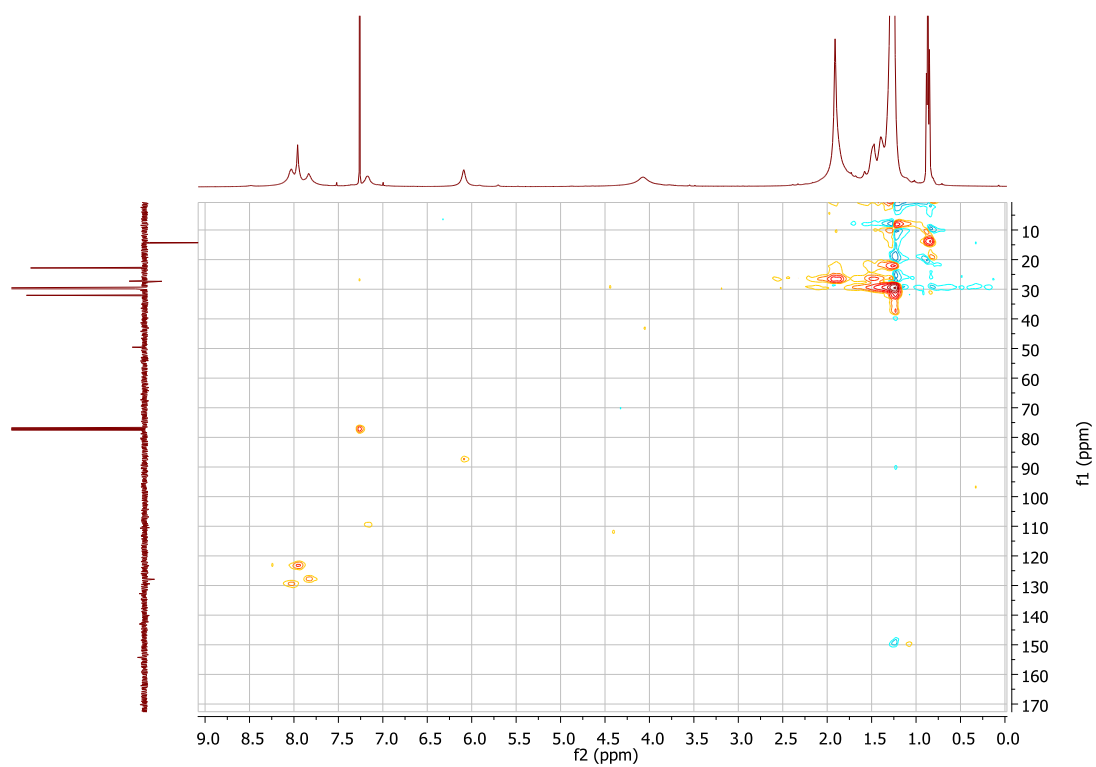


Figure 4 - 52:  $^1\text{H}$ - $^{13}\text{C}$  HSQC NMR spectra (400 MHz) of PSQBT synthesized from 17 in  $\text{CDCl}_3$ .

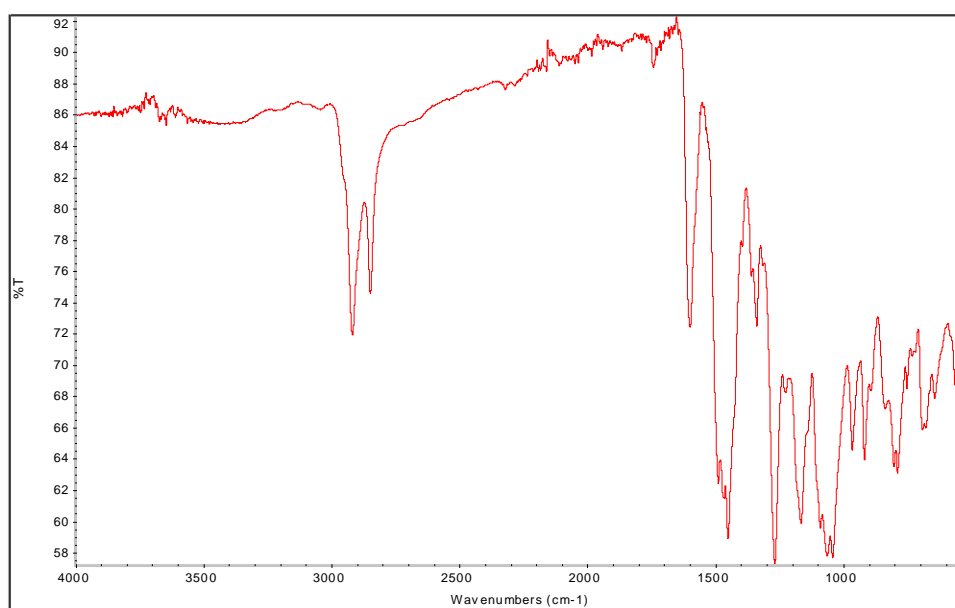
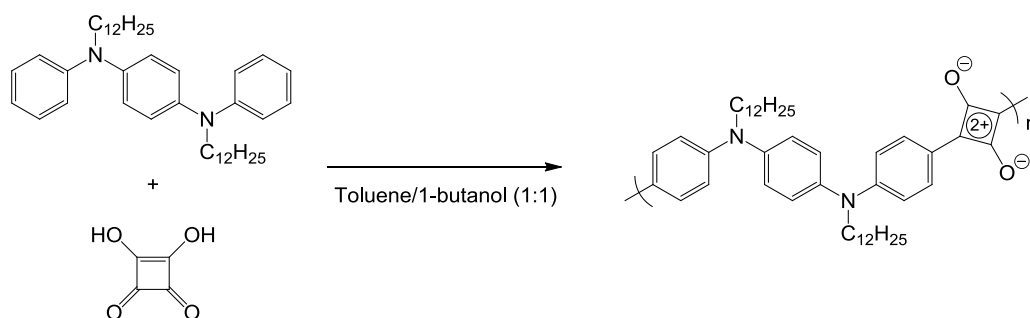


Figure 4 - 53: IR spectrum (ATR) of PSQBT synthesized from 17.

**Poly(squaraine -*alt*-N,N'-didodecyldiphenyl-1,4-benzenediamine) (PSQDA)**

**18** (202 mg, 0.34 mmol) and squaric acid (39 mg, 0.34 mmol) were introduced in a 25 ml round-bottom flask which was then connected to a Dean-Stark apparatus. The reaction media was degassed three times with vacuum/argon cycles, and 5 ml of a toluene/1-butanol mixture (1:1 vol, bubbled under argon) was added. The mixture was then stirred and heated up to reflux for 3 days. Solvent was subsequently removed under reduced pressure. The crude compound was dissolved in 3 ml of  $\text{CHCl}_3$ , and precipitated into 30 ml of cold MeOH. The resulting viscous product was recovered from centrifugation, and the same operation was repeated once. Drying at 50°C under vacuum overnight yielded a dark brown solid (64 mg, 28 %).

$^1\text{H}$  NMR (400 MHz,  $\text{CDCl}_3$ ):  $\delta$  (ppm) 7.20 – 6.47 (m, 12H), 3.83 – 3.40 (m, 4H), 1.78 – 1.50 (m, 4H), 1.44 – 1.08 (m, 36H), 0.92 – 0.77 (m, 6H).  $^{13}\text{C}$  NMR (101 MHz,  $\text{CDCl}_3$ ):  $\delta$  (ppm) 129.96, 129.64, 129.28, 128.59, 123.29, 119.82, 113.31, 74.45, 52.67, 32.06, 29.77, 29.61, 29.48, 27.60, 27.24, 22.83, 14.26.  $^{13}\text{C}$  NMR (101 MHz,  $\text{CDCl}_3$ ):  $\delta$  (ppm) 129.96, 129.64, 129.28, 128.59, 123.29, 119.82, 113.31, 74.45, 52.67, 32.06, 29.77, 29.61, 29.48, 27.60, 27.24, 22.83, 14.26. FT-IR (ATR):  $\nu$ = 2921, 2851, 1733, 1592, 1505, 1465, 1350, 1244, 1165, 1085, 1017, 823, 744, 694  $\text{cm}^{-1}$ .

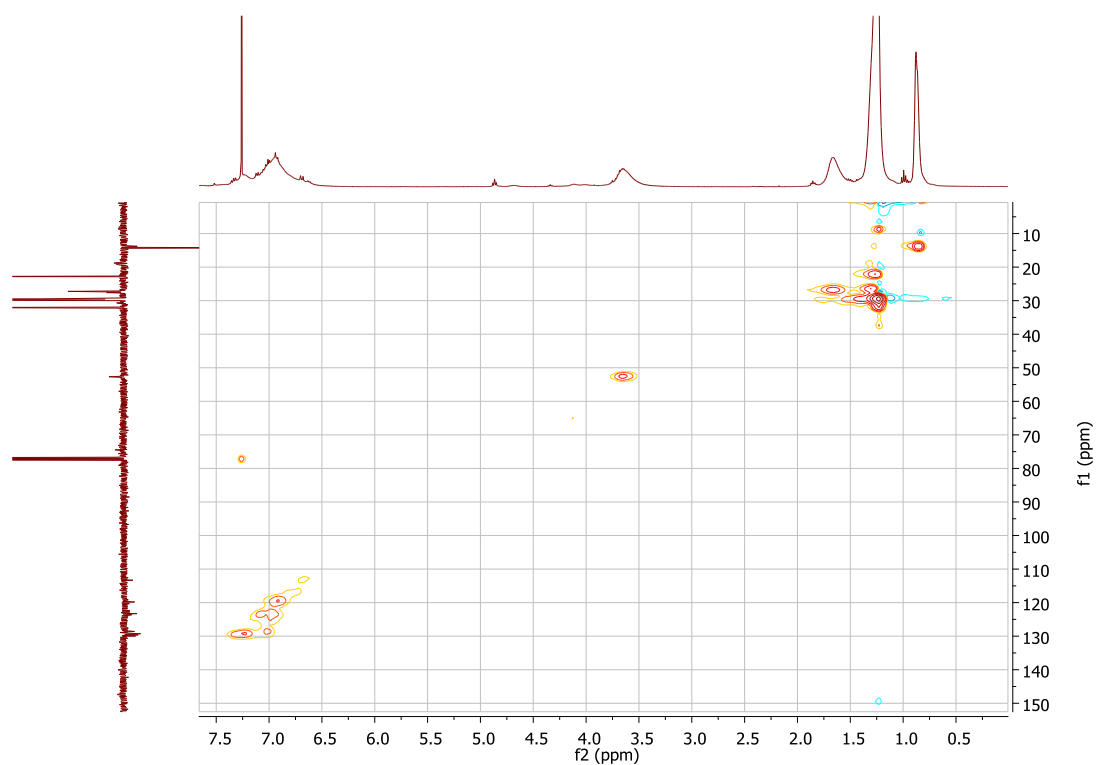


Figure 4 - 54:  $^1\text{H}$ - $^{13}\text{C}$  HSQC NMR spectra (400 MHz) of PSQDA in  $\text{CDCl}_3$ .

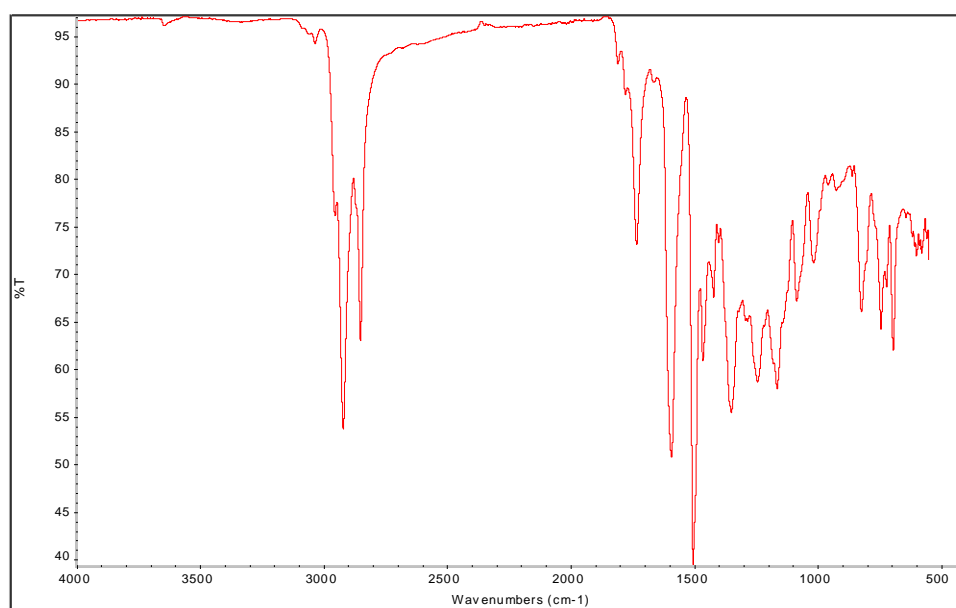
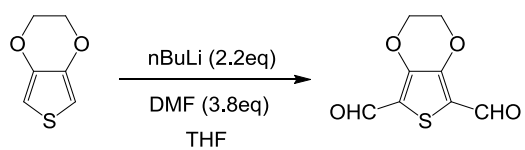


Figure 4 - 55: IR spectrum (ATR) of PSQDA.

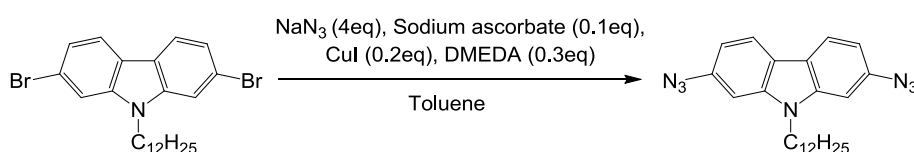
### 3,4-Ethylenedioxythiophene-2,5-dicarbaldehyde (19)



A solution of 3,4-ethylenedioxythiophene (1.00 g, 6.9 mmol) in dry THF (30 ml) was cooled down to -78°C under argon. Then, 9.5 ml of a 1.6 M solution of *n*-BuLi in hexane (15.2 mmol) was added dropwise. The temperature was slowly raised to 0 °C and the mixture was stirred for 20 min. The reaction mixture was cooled down again to -78°C and treated with dry DMF (2 ml, 26.0 mmol). The resulting mixture was then stirred at room temperature for 2 h, and poured into crushed ice containing HCl. The precipitate was recovered by filtration, washed with water and dried at 30°C under vacuum overnight to give light brown crystals (1.40 g, 43 %).

<sup>1</sup>H NMR (400 MHz, CD<sub>2</sub>Cl<sub>2</sub>): δ (ppm) 10.04 (s, 2H), 4.44 (s, 4H). <sup>13</sup>C NMR (101 MHz, CDCl<sub>3</sub>): δ (ppm) 181.08, 147.31, 124.25, 65.27.

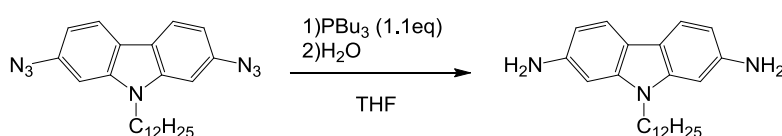
### **2,7-diazido-N-dodecyl-carbazole (20)**



N-dodecyl-2,7-dibromocarbazole **5** (1.00 g, 2.0 mmol), NaN<sub>3</sub> (0.53 g, 8.1 mmol), sodium ascorbate (40 mg, 0.2 mmol), CuI (77 mg, 0.4 mmol) and DMEDA (66 µL, 0.6 mmol) were introduced in a round-bottom flask and subsequently flushed with argon. Toluene (10 mL) was added and the solution was stirred at reflux for 16 h. The reaction mixture was then poured in water and the product was extracted 2 times with ethyl acetate (20 ml). The crude product was purified by flash chromatography in toluene to yield a dark brown solid (518 mg, 62 %).

<sup>1</sup>H NMR (400 MHz, CD<sub>2</sub>Cl<sub>2</sub>): δ (ppm) 7.98 (d, *J* = 8.3 Hz, 2H), 7.01 (d, *J* = 1.9 Hz, 2H), 6.93 (dd, *J* = 8.3, 1.9 Hz, 2H), 4.20 (t, *J* = 7.3 Hz, 2H), 1.87 – 1.77 (m, 2H), 1.40 – 1.19 (m, 18H), 0.88 (t, *J* = 6.8 Hz, 3H). <sup>13</sup>C NMR (101 MHz, CDCl<sub>3</sub>): δ (ppm) 141.93, 137.88, 121.26, 120.26, 110.92, 99.39, 68.12, 43.42, 32.05, 29.74, 29.70, 29.62, 29.50, 29.46, 28.84, 27.33, 25.76, 22.83, 14.26.

### **2,7-diamino-N-dodecyl-carbazole (21)**

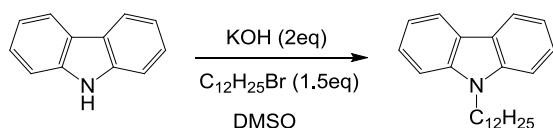


Compound **20** (300 mg, 0.7 mmol) was solubilized in 10 ml of THF under argon and tributylphosphine (195 µl, 0.8 mmol) was added. The reaction medium was stirred at room temperature during 3 h, then water (3 mL) was added and the mixture was stirred for an additional 20 h. The crude product

was purified by flash chromatography (EtOH:Toluene 1:9) to afford **21** as light grey solid (113 mg, 44 %).

$^1\text{H}$  NMR (400 MHz,  $\text{CD}_2\text{Cl}_2$ ):  $\delta$  (ppm) 7.66 (d,  $J$  = 8.2 Hz, 2H), 6.62 (d,  $J$  = 1.8 Hz, 2H), 6.55 (dd,  $J$  = 8.1, 2.0 Hz, 2H), 4.08 (t,  $J$  = 7.3 Hz, 2H), 3.83 (s, 4H), 1.87 – 1.76 (m, 2H), 1.45 – 1.22 (m, 18H), 0.91 (t,  $J$  = 6.9 Hz, 3H).  $^{13}\text{C}$  NMR (101 MHz,  $\text{CDCl}_3$ ):  $\delta$  (ppm) 138.29, 135.88, 123.09, 115.74, 109.27, 106.41, 68.12, 43.32, 32.05, 29.75, 29.74, 29.67, 29.57, 29.47, 29.22, 27.47, 25.75, 22.83, 14.26.

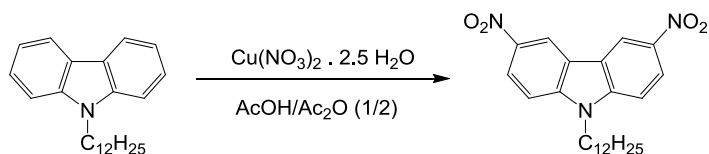
### N-dodecylcarbazole (22)



Carbazole (1.00 g, 6.0 mmol), powdered potassium hydroxide (0.67 g, 12.0 mmol) and 20 ml of DMSO were added in a round-bottom flask. The mixture was stirred at 80°C under argon for 30 min, and 1-bromododecane (2.2 ml, 9 mmol) was added dropwise. The mixture was stirred for 16h at 80°C, and then poured into 100 ml of water. The crude product was extracted 2 times with 40 ml of diethyl ether. The combined organic phases were washed with water and dried over  $\text{MgSO}_4$ . The solvent was removed under vacuum. Flash chromatography (cyclohexane first, then cyclohexane/ethyl acetate 90/10) gave the final product as white crystals (1.88 g, 94 %).

$^1\text{H}$  NMR (400 MHz,  $\text{CD}_2\text{Cl}_2$ ):  $\delta$  (ppm) 8.09 (d,  $J$  = 7.8 Hz, 2H), 7.50 – 7.41 (m, 4H), 7.21 (ddd,  $J$  = 8.0, 6.2, 1.9 Hz, 2H), 4.31 (t,  $J$  = 7.3 Hz, 2H), 1.86 (qt,  $J$  = 7.4 Hz, 2H), 1.43 – 1.20 (m, 18H), 0.88 (t,  $J$  = 6.9 Hz, 3H).

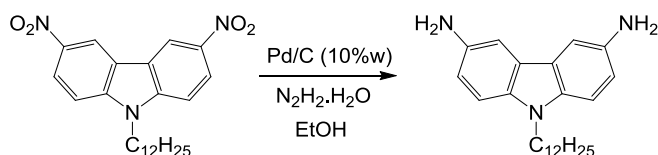
### 3,6-dinitro-N-dodecylcarbazole (23)



A solution of copper nitrate (0.86 g, 3.7 mmol) in acetic anhydride (8 mL) and acetic acid (4 mL) was vigorously stirred at room temperature for 1 h. Compound **22** (1.50 g, 4.5 mmol) was subsequently added and stirring was kept for an additional 3 h. The reaction mixture was then poured into cold water, and the precipitate was recovered by filtration and rinsed with water. The crude product was purified by flash chromatography (toluene) to afford the final product as yellow crystals (1.29 g, 82 %).

$^1\text{H}$  NMR (400 MHz,  $\text{CD}_2\text{Cl}_2$ ):  $\delta$  (ppm) 9.10 (d,  $J = 2.2$  Hz, 2H), 8.47 (dd,  $J = 9.1, 2.2$  Hz, 2H), 7.57 (d,  $J = 9.1$  Hz, 2H), 4.42 (t,  $J = 7.3$  Hz, 2H), 1.92 (qt,  $J = 7.2$  Hz, 2H), 1.44 – 1.17 (m, 18H), 0.87 (t,  $J = 6.9$  Hz, 3H).  $^{13}\text{C}$  NMR (101 MHz,  $\text{CDCl}_3$ ):  $\delta$  (ppm) 144.82, 142.05, 123.14, 122.67, 117.90, 109.70, 68.10, 44.36, 32.01, 31.04, 29.68, 29.60, 29.53, 29.42, 29.38, 29.03, 27.30, 25.74, 22.79, 14.22.

### **3,6-diamino-N-dodecylcarbazole (24)**

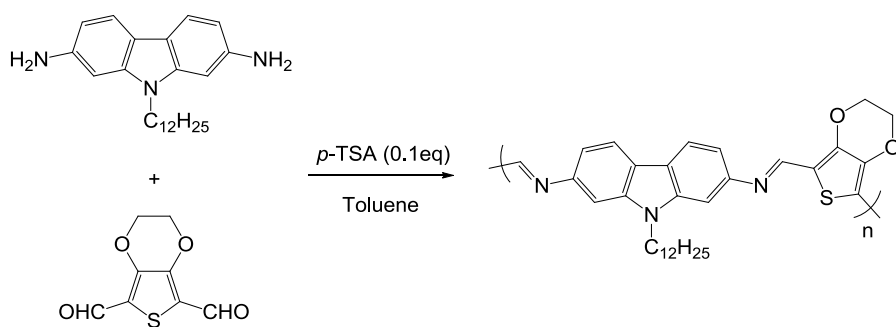


Compound **23** (0.50 g, 1.2 mmol) and Pd/C (0.05 g) was solubilized in dry EtOH (10mL) and heated at reflux under argon for 10 minutes. A solution of hydrazine monohydrate (1.5 mL) in EtOH (3.5 mL) was then added dropwise into the hot solution. The reaction mixture was stirred at 55°C for 36 h. Pd/C was filtered off, and solvent was removed under vacuum. The crude product was purified by recrystallization in methanol and dried at 40°C under vacuum to afford a grey solid (0.37 g, 85 %).

$^1\text{H}$  NMR (400 MHz,  $\text{CD}_2\text{Cl}_2$ ):  $\delta$  (ppm) 7.63 (d,  $J = 8.2$  Hz, 2H), 6.59 (d,  $J = 1.8$  Hz, 2H), 6.51 (dd,  $J = 8.1, 2.0$  Hz, 2H), 4.05 (t,  $J = 7.4$  Hz, 2H), 3.80 (s, 4H), 1.79 (qt,  $J = 7.6$  Hz, 2H), 1.44 – 1.19 (m, 18H), 0.88 (t,  $J = 6.9$  Hz, 3H).  $^{13}\text{C}$  NMR (101 MHz,  $\text{CDCl}_3$ ):  $\delta$  (ppm) 138.29, 135.88, 123.09, 115.74, 109.27, 106.41, 68.12, 43.32, 32.05, 29.75, 29.74, 29.67, 29.57, 29.47, 29.22, 27.47, 25.75, 22.83, 14.26.

### **General procedure for polymerization of diamino and dialdehyde monomers**

Di-amino and di-aldehyde compounds were added in stoichiometric proportion in a 25 ml round bottom-flask equipped with a Dean-Stark trap, and subsequently degassed. Toluene (5 ml) and *p*-toluenesulfonic acid (0.1 eq) were added and the reaction mixture was stirred at reflux for 7 days, during which a dark precipitate formed. The reaction mixture was then allowed to cool down to room temperature and the solvent was removed under vacuum. The resulting solid was dried at 40°C under vacuum overnight.

**Poly(2,7-diimino-N-dodecylcarbazole-*alt*-EDOT) (PIMI1)**

Starting from 2,7-diamino-N-dodecyl-carbazole **21** (50 mg, 0.14 mmol) and 3,4-ethylenedioxythiophene-2,5-dicarbaldehyde **19** (27 mg, 0.14 mmol). The final product was obtained as a dark red solid.

FT-IR (ATR):  $\nu = 2920, 1580, 1442, 1360, 1322, 1266, 1234, 1119, 1080, 856, 834, 802, 641 \text{ cm}^{-1}$ .

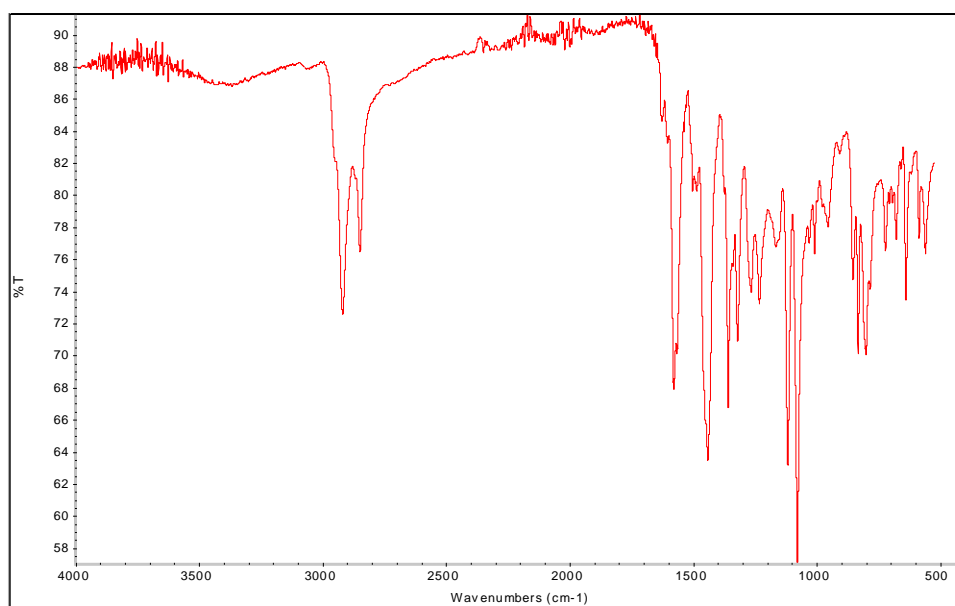
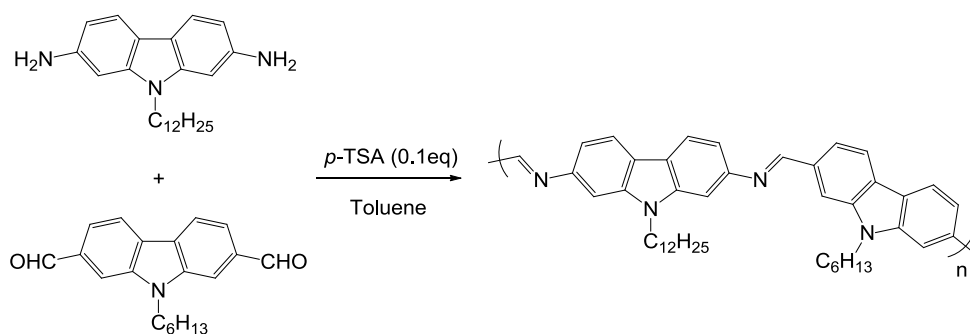


Figure 4 - 56: IR spectrum (ATR) of PIMI1.

**Poly(2,7-diimino-N-dodecylcarbazole-*alt*-2,7-N-hexylcarbazole) (PIMI2)**



Starting from 2,7-diamino-N-dodecyl-carbazole **21** (50 mg, 0.14 mmol) and 2,7-dicarbaldehyde-N-hexylcarbazole (42 mg, 0.14 mmol). The final product was obtained as a dark red solid.

FT-IR (ATR):  $\nu = 3055, 2920, 2850, 1587, 1454, 1323, 1234, 1117, 998, 802, 727, 652 \text{ cm}^{-1}$ .

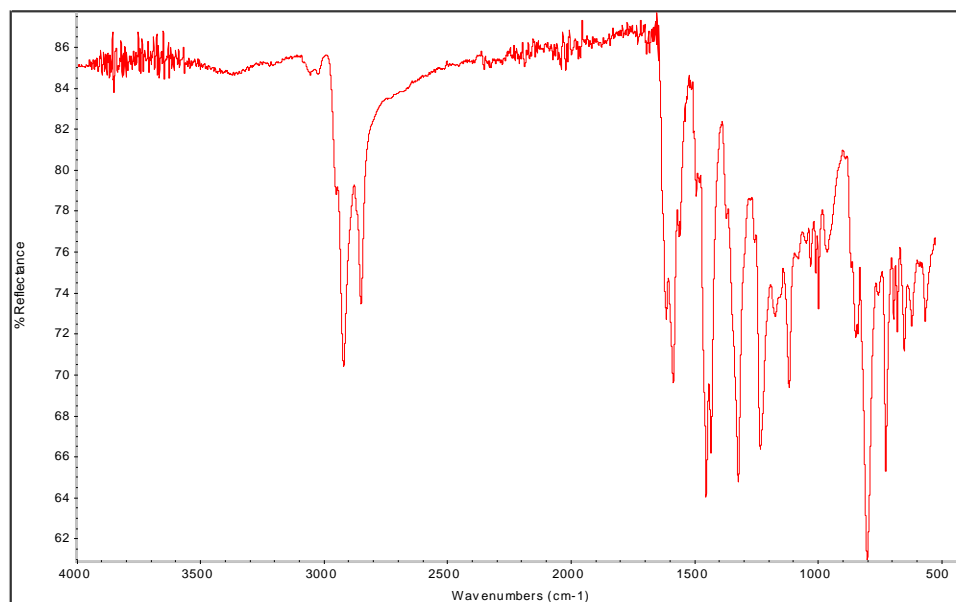
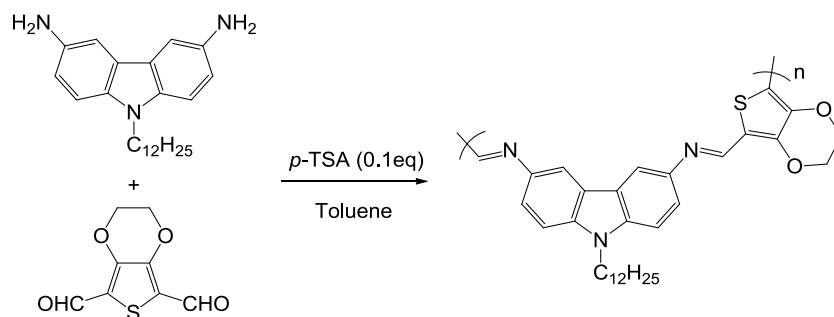


Figure 4 - 57: IR spectrum (ATR) of PIMI2.

### Poly(3,6-diimino-N-dodecylcarbazole-*alt*-EDOT) (PIMI3)



Starting from 3,6-diamino-N-dodecyl-carbazole **24** (50 mg, 0.14 mmol) and 3,4-ethylenedioxythiophene-2,5-dicarbaldehyde **19** (27 mg, 0.14 mmol). The final product was obtained as a black solid.

FT-IR (ATR):  $\nu = 2921, 2850, 1604, 1441, 1361, 1265, 1120, 1081, 1010, 863, 795, 729, 680, 562 \text{ cm}^{-1}$ .

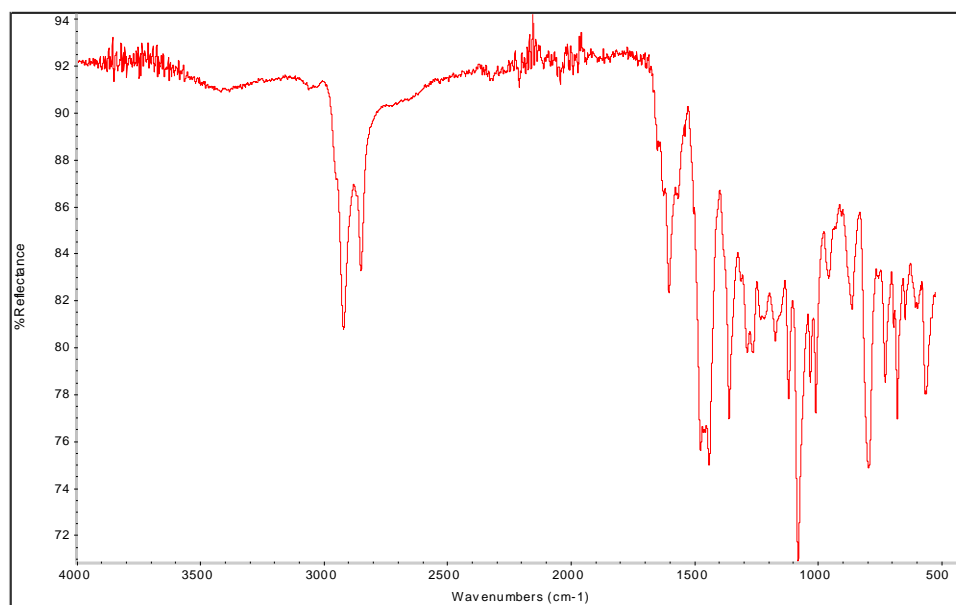
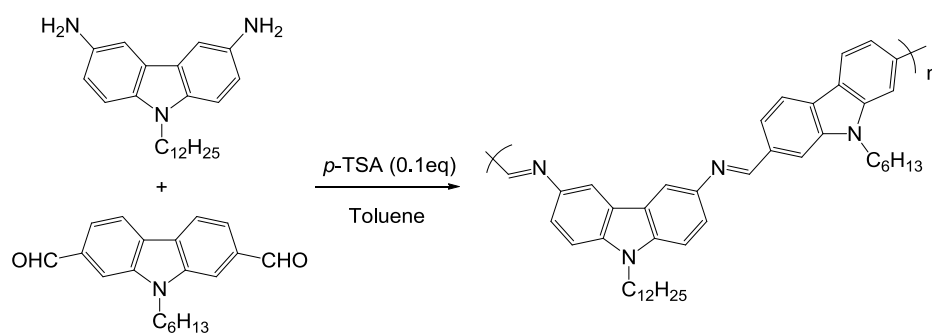


Figure 4 - 58: IR spectrum (ATR) of PIMI3.

**Poly(3,6-diimino-N-dodecylcarbazole-*alt*-2,7-N-hexylcarbazole) (PIMI4)**



Starting from 3,6-diamino-N-dodecyl-carbazole **24** (50 mg, 0.14 mmol) and 2,7-dicarbaldehyde-N-hexylcarbazole (42 mg, 0.14 mmol). The final product was obtained as a black solid.

FT-IR (ATR):  $\nu = 3060, 2921, 2850, 1689, 1615, 1463, 1325, 1236, 1162, 999, 867, 801, 727, 679, 632, 567 \text{ cm}^{-1}$ .

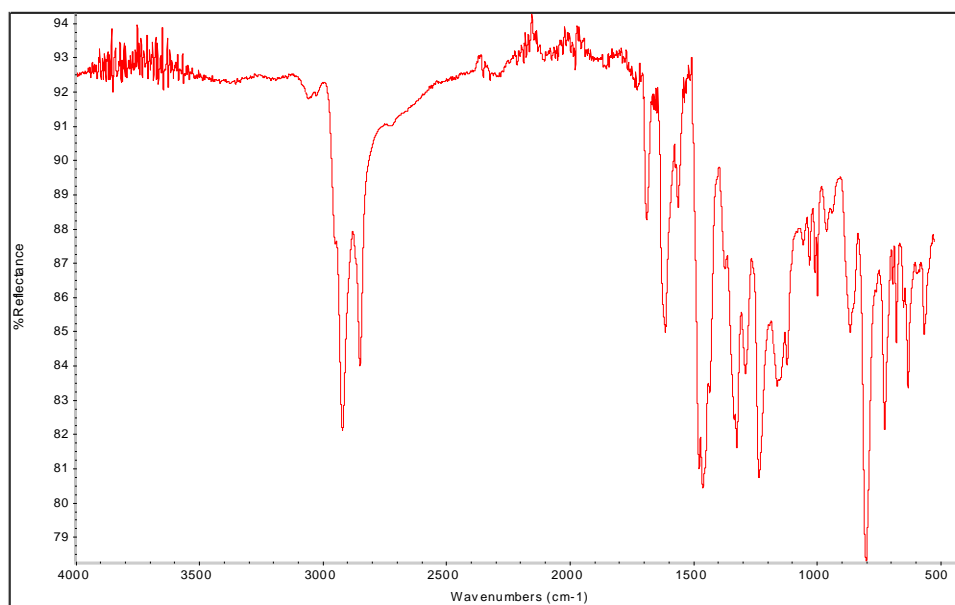


Figure 4 - 59: IR spectrum (ATR) of PIMI4.

## 4.6.2 THERMOGRAVIMETRIC ANALYSES (TGA)

TGA data were measured under N<sub>2</sub> atmosphere at 10°C/min.

### Polysquaraines

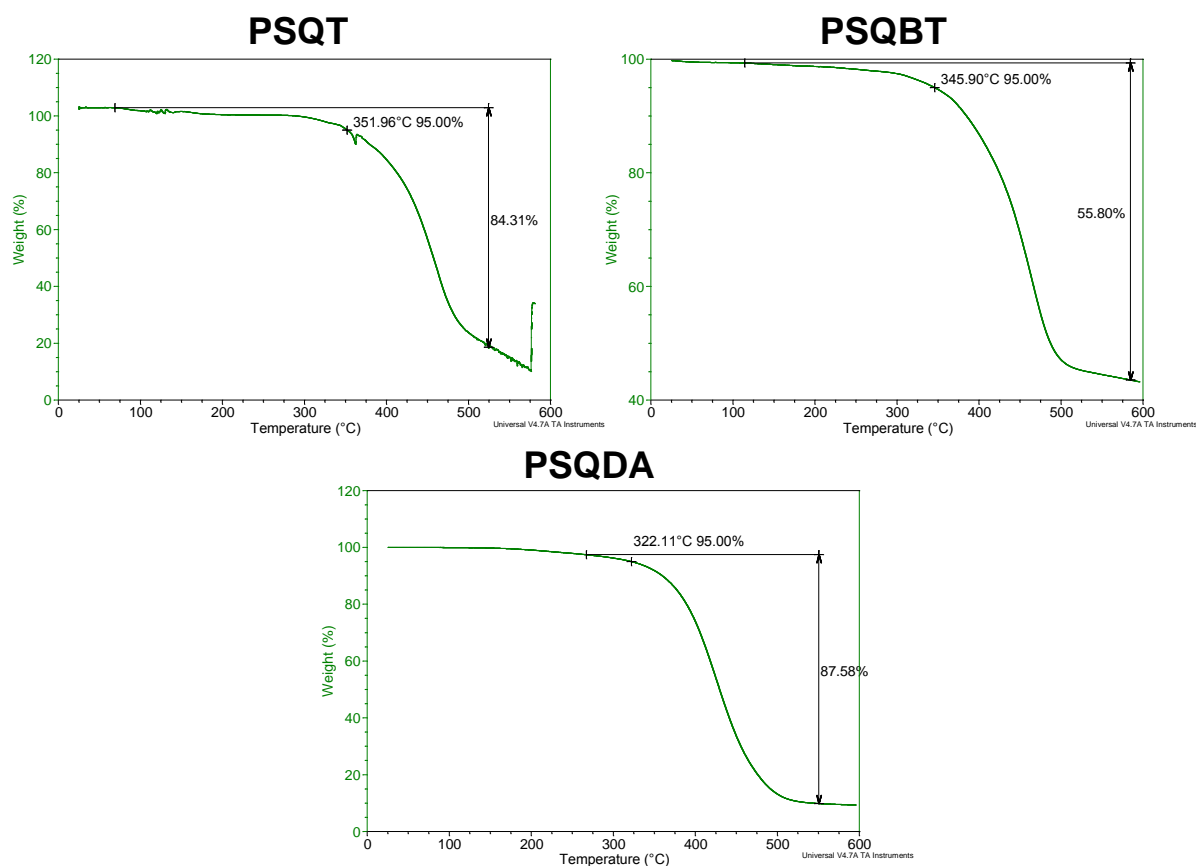


Figure 4 - 60: TGA analyses of PSQs obtained by polycondensation with squaric acid.

## Polyimines

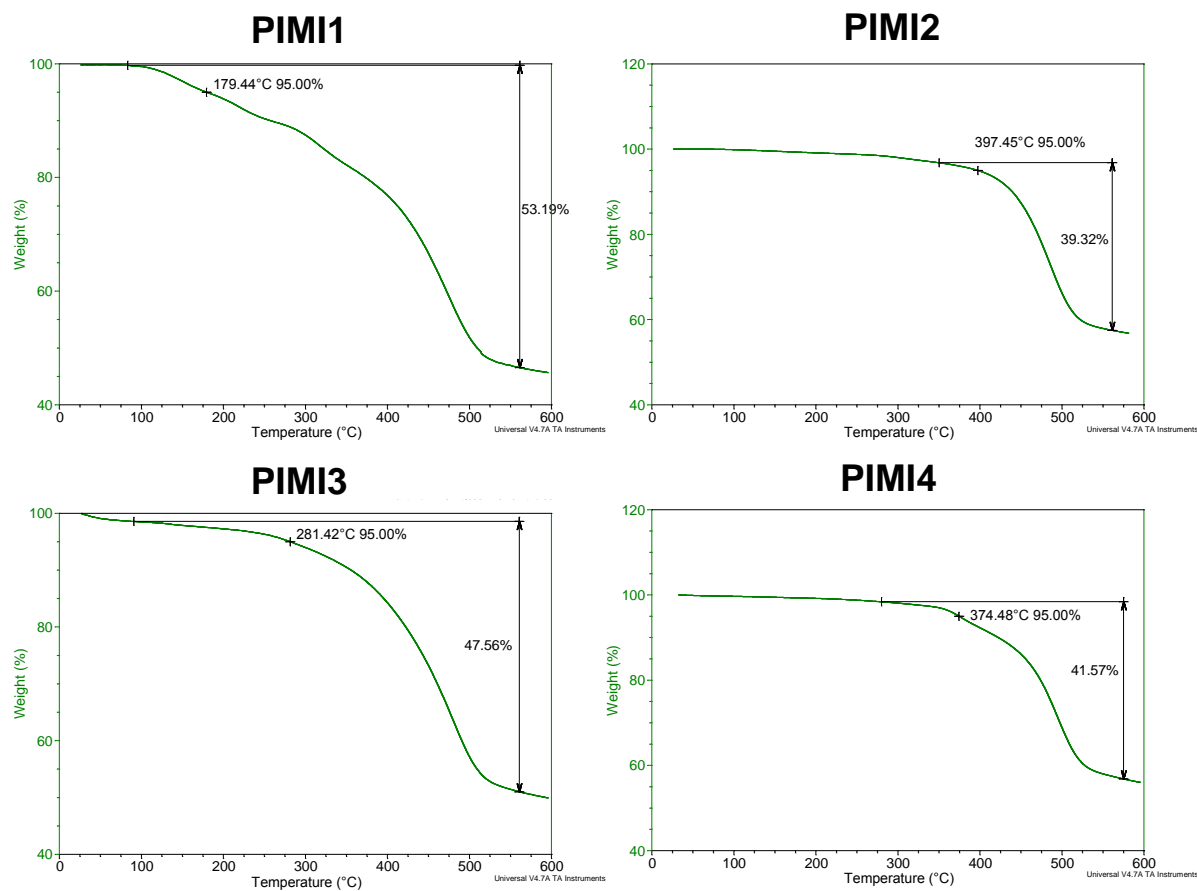


Figure 4 - 61: TGA analyses of polyimines.

### 4.6.3 DIFFERENTIAL SCANNING CALORIMETRY (DSC)

DSC data were measured under helium flow (25 ml/min) at a scan rate of 20°C/min.

## Polysquaraines

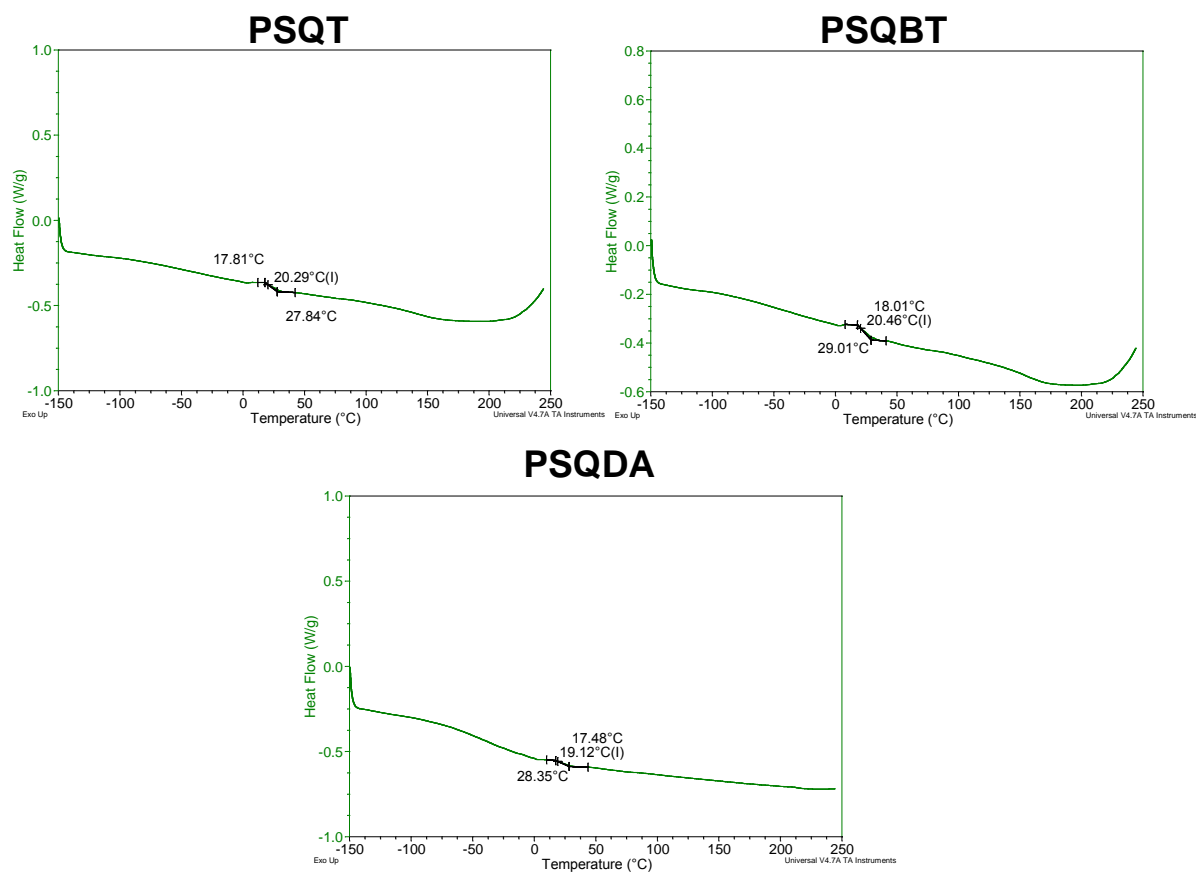


Figure 4 - 62: DSC analyses of PSQs obtained by polycondensation with squaric acid.

## Polyimines

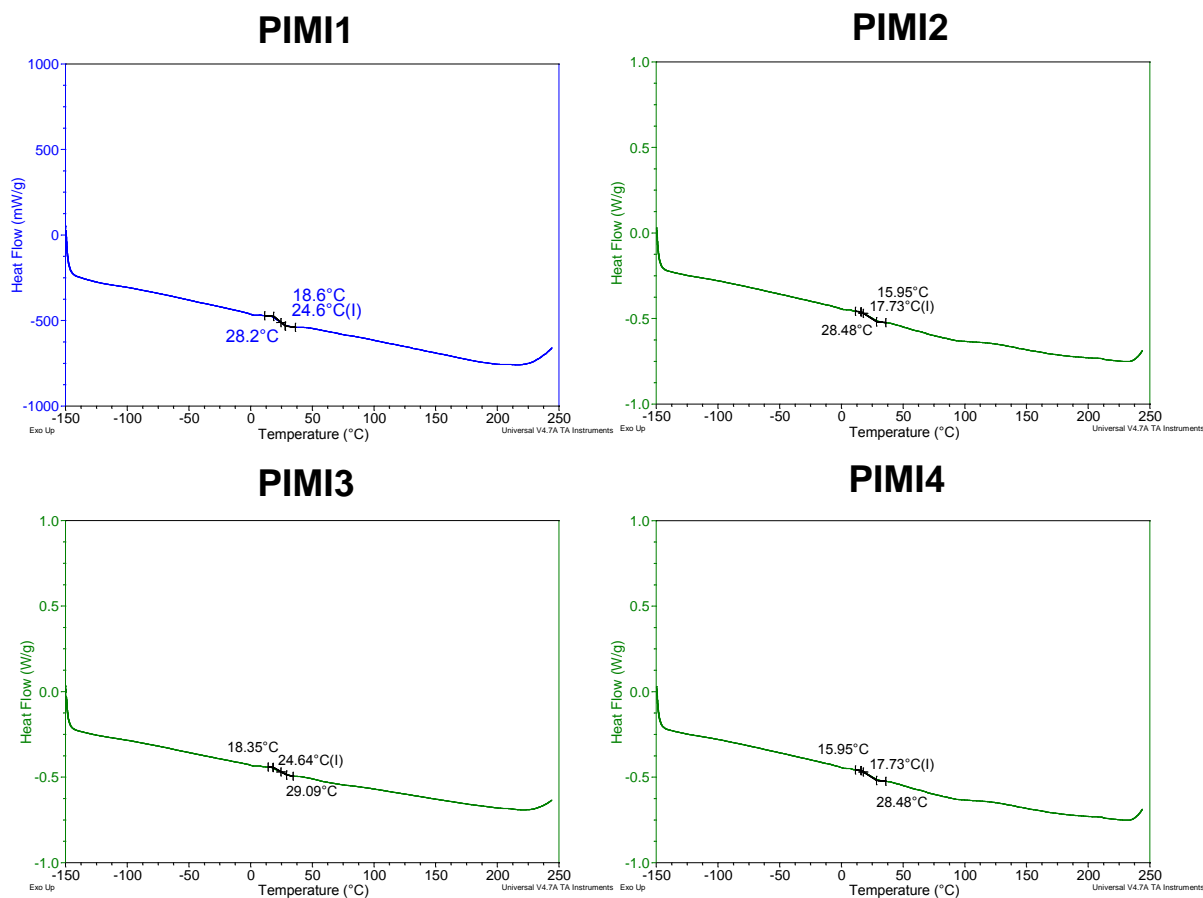


Figure 4 - 63: DSC analyses of polyimines.

## 4.6.4 OPTICAL

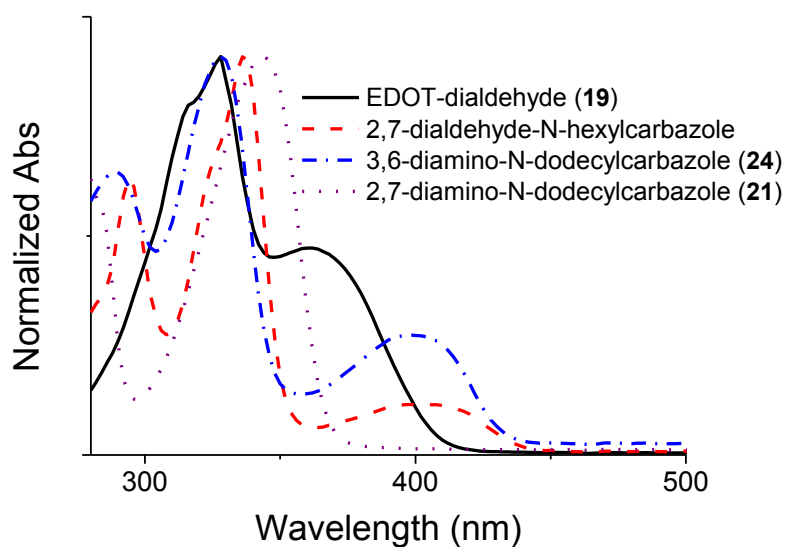


Figure 4 - 64: Normalized UV-visible absorption spectra of the monomers employed in the polyimines syntheses.

### 4.6.5 ELECTROCHEMISTRY

A solution of  $0.1 \text{ g.l}^{-1}$  of the investigated polymer in  $\text{CHCl}_3$  (according to solubility) with  $0.1 \text{ M}$  tetrabutylammonium hexafluorophosphate (TBAPF6) as electrolyte was prepared in a glove box under  $\text{N}_2$ . CV measurements were then performed on the solution under  $\text{N}_2$ , using a silver wire as reference electrode and platinum for the working and counter electrodes. A solution of ferrocene ( $1 \text{ mM}$  in  $\text{CHCl}_3$ ) was prepared in the same conditions and the redox potential of  $\text{Fc}/\text{Fc}^+$  vs Ag ( $E_{\text{Fc}/\text{Fc}^+ \text{ Ag}}$ ) was measured.

#### PSQT

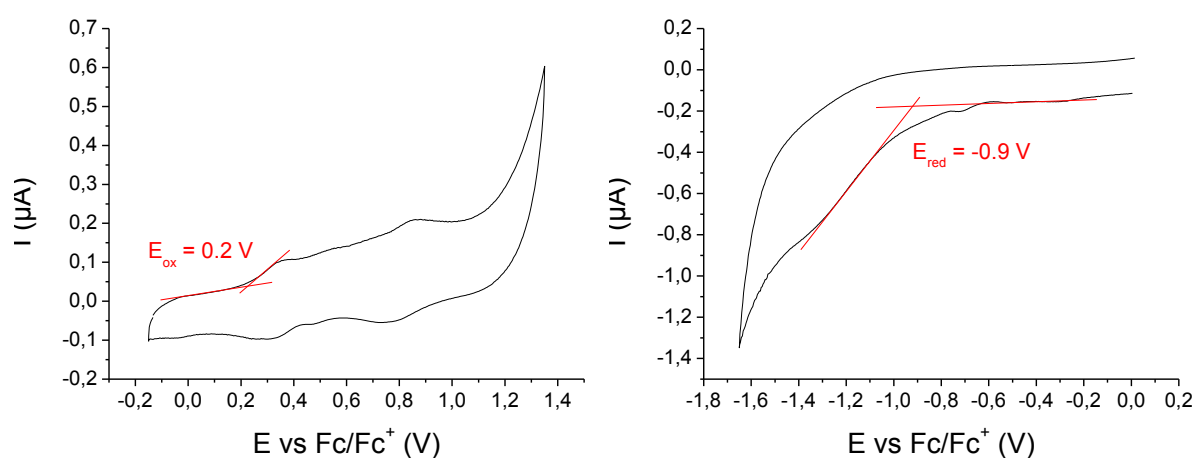


Figure 4 - 65: Cyclic voltammograms of PSQT in  $\text{CHCl}_3$  solution ( $0.1 \text{ g.l}^{-1}$ ). Left-oxidation; right-reduction.

#### PSQBT

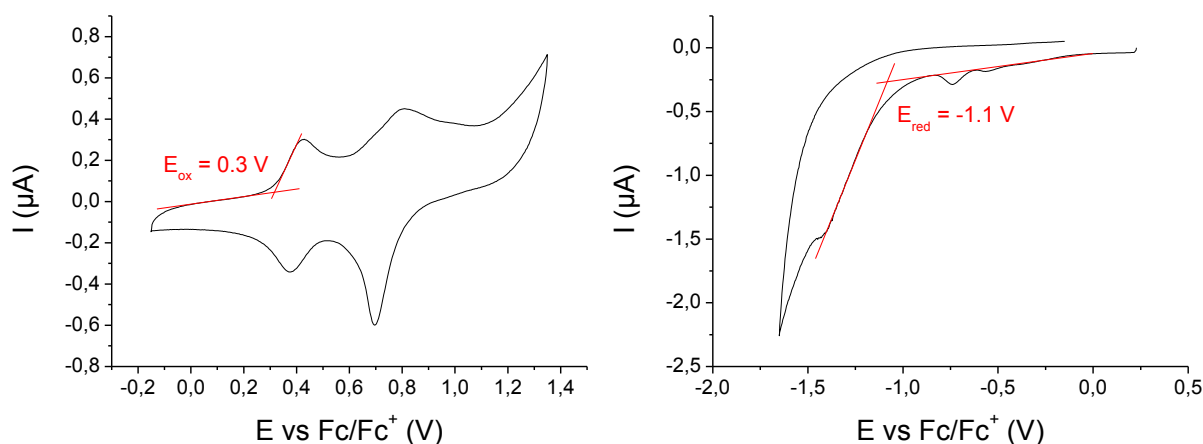


Figure 4 - 66: Cyclic voltammograms of PSQBT in  $\text{CHCl}_3$  solution ( $0.1 \text{ g.l}^{-1}$ ). Left-oxidation; right-reduction.

#### PSQDA

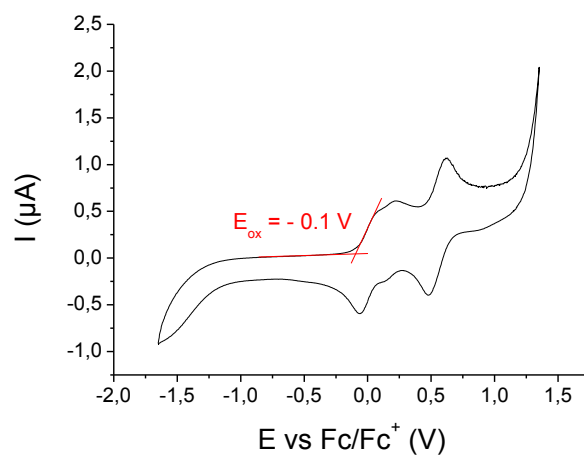


Figure 4 - 67: Cyclic voltammograms of PSQDA in  $CHCl_3$  solution ( $0.1 \text{ g.l}^{-1}$ ). No reduction signal was observed.





## Conclusion and future work

---

Since their discovery, semiconducting polymers have become an exciting research field due to the advantages and novel properties they can bring to electronic applications. However, such technologies require a great variety of materials with different properties. Additionally, the development of environmental-friendly procedures is highly desired.

In that regard, this work was focused on the development of new CPs in order to provide novel organic semiconductors, but also to better understand how the chemical structure affects the final properties in alternated  $\pi$ -conjugated polymers. It was shown that the linkage position on carbazole units had a poor influence on the spectroscopic properties compared to the intramolecular charge transfer between electron-donating and withdrawing moieties. As a future work, a study could be conducted on the effect of substituents inserted on the donor and/or acceptor unit to tune the energetic levels. The alternation of squaraine units with other heteroaromatic moieties proved to be an efficient way to obtain small band-gap materials and the spectroscopic properties seemed to be mainly affected by the squaraine part. Nevertheless, alternating other heteroaromatic units with enhanced electron-withdrawing or donating properties would provide new elements for the understanding of the structure-properties relationship in squaraine-based polymers.

Properties of the developed polymers showed encouraging features to be applied as easily processable materials for organic electronics. Nevertheless, further studies such as measurement of the charge carriers mobility are required to complete the materials characterization. Although photovoltaic cells were initially considered as the target application, the synthesized materials could be of interest for other type of devices. For instance, the strong fluorescences observed in different part of the visible and near-IR spectrum render these materials attractive for light-emitting devices.

The last chapter described the synthesis of conjugated polymers by means of metal catalyst-free reactions. The great advantage is the absence of transition metal in the polycondensation step and production of water as by-product, which can be easily removed from the reaction medium. However, transition metals are still present in some of the monomers syntheses (indole-based, see chapter 4). In a future work, the development of a completely metal-free synthetic route would be a tremendous asset for the production of such polymers. Finally, the solubility issues encountered in the synthesis of polyimines could be addressed by two different approaches. Firstly, the solubilizing groups could be replaced by bulkier and longer side-chains. Secondly, additional alkyl chains could be introduced by the quaternization of nitrogen atoms in the imine bonds. Coupled with suitable side-

chains (bearing ionic groups for example), this could even lead to water and alcohols soluble materials, which is another step towards more environmental-friendly organic electronics.

One of the great challenges in semiconducting polymers is the realization of small band-gaps. The polysquaraines developed in this work showed smaller band-gaps than numerous CPs employed in current organic electronics (e.g. P3HT) and are therefore of great interest. An attractive way to achieve materials with even narrower band-gaps would be the replacement of squaric acid by croconic acid. It was previously demonstrated that polycroconaines have more red-shifted absorption than polysquaraines and the metal-free polycondensations presented in this work could be also applied.

Easily processable, metal-free and more environmental-friendly conjugated polymers remain the issues and challenges in the coming years in order to enter the emerging market of flexible electronic devices.

## Experimental (general)

---

### Materials

Tetrahydrofuran (THF), methylene chloride ( $\text{CH}_2\text{Cl}_2$ ), toluene and dimethylsulfoxide (DMSO) were purified from a solvent purification system (MBraun MB-SPS-800) prior to use. Dioxane was dried over calcium hydride ( $\text{CaH}_2$ ) and distilled prior to use. 2,1,3-Benzothiadiazole-4,7-bis(boronic acid pinacol ester) was purified by sublimation at  $160^\circ\text{C}$  under vacuum prior to use. Squaric acid was recrystallized in boiling water and then rinsed with cold water and acetone, followed by drying under vacuum at  $40^\circ\text{C}$  overnight prior to use. Unless otherwise specified, all other solvents and chemicals were purchased from commercial suppliers (Alfa Aesar, Sigma-Aldrich, TCI, Acros Organics, Scharlau, Orgalight or Strem Chemicals) and used as received. Poly(3,4-ethylenedioxy-thiophene):poly(styrene sulfonate) (PEDOT:PSS) was purchased from Baytron P and passed successively through a  $0.8\ \mu\text{m}$  and a  $0.45\ \mu\text{m}$  PVDF syringe filter before spin-coating. [6,6]-Phenyl- $\text{C}_{61}$ -butyric acid methyl ester (PCBM) was obtained from Solaris.

### Procedure for electrochemical measurements and HOMO-LUMO calculation

A solution of  $0.1\ \text{g.l}^{-1}$  of the investigated polymer in  $\text{CH}_2\text{Cl}_2$  or  $\text{CHCl}_3$  (according to solubility) with  $0.1\ \text{M}$  tetrabutylammonium hexafluorophosphate (TBAPF6) as electrolyte was prepared in a glove box under  $\text{N}_2$ . CV measurements were then performed on the solution under  $\text{N}_2$ , using a silver wire as reference electrode and platinum for the working and counter electrodes. A solution of ferrocene ( $1\ \text{mM}$  in the same solvent) was prepared in the same conditions and the redox potential of  $\text{Fc}/\text{Fc}^+$  vs Ag ( $E_{\text{Fc}/\text{Fc}^+ \text{ Ag}}$ ) was measured. Additionally, the ferrocene solution was brought outside of the glove box and a new CV was performed using saturated calomel electrode (SCE) as reference to obtain  $E_{\text{Fc}/\text{Fc}^+ \text{ SCE}}$ .

### Characterization apparatus

$^1\text{H}$ ,  $^{13}\text{C}$  and  $^1\text{H}$ - $^{13}\text{C}$  HSQC NMR measurements were performed with a Bruker AC-400 NMR spectrometer at room temperature. IR spectra were recorded with Bruker Tensor 27 spectrometer using a  $0.6\ \text{mm}$ -diameter beam and a  $4\ \text{cm}^{-1}$  resolution. Samples were analyzed with the attenuated total reflexion (ATR) method. A Kofler bench (Wagner&Munz Heizbank system Kofler type wme) was used to obtain melting points with a  $\pm 2^\circ\text{C}$  precision. High resolution mass spectroscopy analyses were performed on a AutoSpec-Waters spectrometer (EI). Optical absorption spectra were obtained with a UV-visible spectrophotometer (UV-3600, Shimadzu). Photoluminescence spectra were obtained from a spectrofluorometer (Fluoromax-4, Horiba Scientific). Molecular weights of the polymers were measured by SEC at  $40^\circ\text{C}$  with THF as eluent, using a PL-GPC 50 plus Integrated GPC system from

Polymer laboratories-Varian (one guard column and three columns based on cross-linked polystyrene, pore size = 200 Å, 75 Å and 20 Å), and PS standards were used for calibration.

### **Photovoltaic devices preparation**

The devices were fabricated by using the previously prepared polymers blended with [6,6]-phenyl-C61 butyric acid methyl ester (PCBT:PCBM).

Substrates (glass coated with ITO) were cleaned in an ultrasonic bath in methanol and isopropanol. After drying the substrate a thin layer ( 50 nm) of PEDOT-PSS was spin-coated at 4000 rpm and dried at 110 °C under rotary pump vacuum for 1 h. All procedures after PEDOT:PSS deposition were performed in an inert-atmosphere glovebox of nitrogen ( $O_2$  and  $H_2O < 0.1$  ppm). Different blend ratio of PCBT and PCBM were prepared by making 24 mg/mL solutions in o-dichlorobenzene (o-DCB). As an example, to prepare a blend of 50w% PCBT and 50w% PCBM, 12 mg of PCBT and 12 mg of PCBM were dissolved in 1 mL of o-DCB. The photoactive layer (PCBT:PCBM 1:1 wt%) was spin-coated on the top of the PEDOT-PSS layer from o-dichlorobenzene (o-DCB) solutions at 50 °C. The thickness of the photoactive layer was typically in the range of 80 nm. The aluminium cathode was thermally deposited (100 nm) through a shadow mask with a base pressure of  $10^{-7}$  mbar. The active areas of the devices were ca. 8.4 mm<sup>2</sup>. An annealing treatment was performed at 150°C after the cathode deposition during 20 minutes. The current density-voltage (J-V) characteristics were measured with a Keithley 4200 SCS under an illumination of 100 mW/cm<sup>2</sup> from a K.H.S. Solar Celltest 575 solar simulator with AM1.5 filters and in the dark.

# List of figures

Figure 1: Chemical structure of polyacetylene. ....	1
Figure 2: Examples of organic electronics applications taking advantage of flexibility. solar cells (top left), transistors (top right), displays (bottom left) and electronic contact lens (bottom right). ....	2

## Chapter 1

Figure 1 - 1: Representation of the energetic band structure in metals, semiconductors and insulators. ....	10
Figure 1 - 2: Resonant forms of the butadiene molecule. ....	10
Figure 1 - 3: Representation of molecular orbitals evolution in energy when extending the $\pi$ -system. ....	11
Figure 1 - 4: Sketch of the potential energy curve for a degenerate system (polyacetylene). ....	11
Figure 1 - 5: Sketch of the potential energy curve for a non-degenerate system (polyparaphenylene). ....	12
Figure 1 - 6: Representation of radical cation and radical anion in an organic semiconductor. ....	13
Figure 1 - 7: Creation of a radical cation in degenerated (a) and non-degenerated (b) CP. ....	14
Figure 1 - 8: Charge delocalization in a polyacetylene chain. ....	14
Figure 1 - 9: Hopping transport – a)intramolecular; b)intermolecular. ....	15
Figure 1 - 10: Evolution of the UV-visible absorption with the number of repeating units in oligothiophenes. <sup>[13]</sup> .....	16
Figure 1 - 11: Structural factors determining the band gap of materials derived from linear <i>p</i> -conjugated systems. Reproduced from Roncali. <sup>[16]</sup> .....	16
Figure 1 - 12: Effect of double bonds insertion on phenyl and thiophene-based CPs. <sup>[26-27]</sup> .....	18
Figure 1 - 13: Examples of poly(arylenevinylene)s and poly(aryleneethynylene)s. <sup>[29-31]</sup> .....	19
Figure 1 - 14: Effect of reduced steric hindrance on the optical gap. <sup>[11, 33]</sup> .....	20
Figure 1 - 15: Effect of backbone rigidification via methine-bridging. <sup>[35-38]</sup> .....	21
Figure 1 - 16: LPPP with ethane (LPPP1) and ethene (LPPP2) bridges. <sup>[39-40]</sup> .....	21
Figure 1 - 17: Examples of imine-bridged LPPPs. <sup>[41-43]</sup> .....	22
Figure 1 - 18: PBDCPDTPD, a semiconducting polymer with enhanced planarity obtained by bridging and reduced steric hindrance. <sup>[45]</sup> .....	22
Figure 1 - 19: Examples of soluble CPs. 1: MEH-PPV; 2: poly(3-hexylthiophene) (P3HT); 3: poly(N-octylpyrrole). <sup>[47-49]</sup> .....	23
Figure 1 - 20: Examples of CPs soluble in water and alcoholic solvents. <sup>[50-52]</sup> .....	23
Figure 1 - 21: Effect of steric hindrance generated by alkyl substituents on the optical band-gap. <sup>[54]</sup> .....	24
Figure 1 - 22: Influence of conjugated substituents. <sup>[58]</sup> .....	24
Figure 1 - 23: Ethylenedioxy group insertion on thiophene units and its effect on the polymer band-gap. Red arrow: electron donating effect of the oxygens. Blue dotted lines: sulfur-oxygen interactions. <sup>[60-61]</sup> .....	25
Figure 1 - 24: Examples of electron-donating substituted polythiophenes. <sup>[12, 62-63]</sup> .....	25
Figure 1 - 25: Comparison of thioalkyl and alkoxy substitution on CPs. <sup>[64]</sup> .....	26

Figure 1 - 26: Effect of cyano groups on PTV derivatives. <sup>[65]</sup>	26
Figure 1 - 27: Effect of cyano groups on the band-gap of PPV derivatives. <sup>[66]</sup>	27
Figure 1 - 28: Effect of fluorine insertion. <sup>[67-68]</sup>	27
Figure 1 - 29: Effect of sulfone-based substitution. <sup>[69]</sup>	28
Figure 1 - 30: Influence of nitro group. <sup>[70]</sup>	28
Figure 1 - 31: Aromatic (left) and quinoid (right) forms of poly(isothianaphtene).	29
Figure 1 - 32: Poly(thieno[3,4-b]pyrazine) and poly(thieno[3,4-b]thiophene). <sup>[72-73]</sup>	29
Figure 1 - 33: Isothianaphtene-based CPs obtained by polymeric precursors. <sup>[74-75]</sup>	30
Figure 1 - 34: TPD (1) and TID (2)-based CPs. <sup>[76]</sup>	30
Figure 1 - 35: Quinoid conformation of CPs obtained by elimination reaction. <sup>[77-79]</sup>	31
Figure 1 - 36: Orbital interactions in the case of two identical coupled units (left) and two different units (right).	32
Figure 1 - 37: Geometric influence of the ICT between electron-donating (e-D) and withdrawing (e-W) units....	32
Figure 1 - 38: Small band-gap donor-acceptor polymers based on squaric (left) and croconic (right) acid. <sup>[80]</sup>	32
Figure 1 - 39: Alternated copolymers using benzothiadiazole as electron-withdrawing unit. <sup>[81-83]</sup>	33
Figure 1 - 40: Effect of the D-A ratio on the band-gap. <sup>[24, 84]</sup>	33
Figure 1 - 41: Effect of acceptor strength on the band-gap. <sup>[85]</sup>	34
Figure 1 - 42: Generation of hydrogen-bonding in a donor-acceptor CP. <sup>[86]</sup>	34
Figure 1 - 43: Commonly used electron-donating units in alternated CPs. <sup>[11-12, 57, 89]</sup>	35
Figure 1 - 44: PCDTBT. <sup>[90]</sup>	35
Figure 1 - 45: PBDPP-3, a DPP-based polymer showing high PCE in BHJ solar cells. <sup>[93]</sup>	36
Figure 1 - 46: PBDTPD. <sup>[95-96]</sup>	36
Figure 1 - 47: PTI-3, an isoindigo-based polymer used in BHJ solar cells with PCE of 6.3%. <sup>[100]</sup>	36
Figure 1 - 48: PTB7. <sup>[102]</sup>	37
Figure 1 - 49: Ziegler-Natta (top) and Durham (bottom) routes to polyacetylene. <sup>[103-104]</sup>	37
Figure 1 - 50: PPP obtained by oxidative polymerization of benzene. <sup>[25]</sup>	38
Figure 1 - 51: Gilch (top) and Wessling-Zimmermann (bottom) routes to PPV. <sup>[107-108]</sup>	38
Figure 1 - 52: Examples of metal-catalyzed couplings used in CPs synthesis.	39
Figure 1 - 53: General mechanism of Stille coupling. <sup>[123]</sup>	40
Figure 1 - 54: Synthesis of PBDPP-3 by Stille polycondensation. <sup>[93]</sup>	41
Figure 1 - 55: General mechanisms of Suzuki coupling. <sup>[136]</sup>	42
Figure 1 - 56: Synthesis of PCDTBT by Suzuki polycondensation. <sup>[90]</sup>	43
Figure 1 - 57: Examples of CPs synthesized via Knoevenagel condensation. <sup>[138]</sup>	44
Figure 1 - 58: PPV synthesis by Siegrist polycondensation. <sup>[141]</sup>	44
Figure 1 - 59: Examples of Wittig (top) and aza-Wittig (bottom) polycondensations. <sup>[142-145]</sup>	45
Figure 1 - 60: Examples of semiconducting polymers obtained by arylimino-de-oxo-bisubstitution. <sup>[147-148]</sup>	45
Figure 1 - 61: Synthesis of a well-known squaraine dye (top) and polysquaraine (bottom). <sup>[150]</sup>	46
Figure 1 - 62: Synthesis of the poly(carbazole-alt-benzothiadiazole)s.	47

Figure 1 - 63: Synthesis of the different poly(squaraine)s. ....	48
Figure 1 - 64: Metal-free syntheses of the developed CPs.....	49

## **Chapter 2**

Figure 2 - 1: Representation of the carbazole molecule (left) and oxidation of the fluorene molecule (right). ....	57
Figure 2 - 2: Structures of the developed polymers. ....	62
Figure 2 - 3: Structures of the four Cz monomers developed. ....	63
Figure 2 - 4: Synthesis of 2,7-dibromo-9H-carbazole 2. ....	64
Figure 2 - 5: Synthesis of the 9-heptadecanoyl tosylate 4.....	64
Figure 2 - 6: Synthesis of the alkylated dibromocarbazoles 5-8.....	65
Figure 2 - 7: IR spectra (ATR) of the carbazole derivatives 2 and 5. ....	66
Figure 2 - 8: $^1\text{H}$ NMR spectra (400 MHz) of compounds 2 and 5 in $\text{CD}_2\text{Cl}_2$ . ....	66
Figure 2 - 9: Reaction carried out to optimize the polymerization conditions of PCBTs. ....	67
Figure 2 - 10: Synthesis of PCBTs by Suzuki cross-coupling, using $\text{Pd}(\text{PPh}_3)_4$ as catalyst, $\text{K}_2\text{CO}_3$ as base and toluene/THF mixture (1:1 vol.) as solvent. Reaction medium stirred and heated to reflux.....	68
Figure 2 - 11: $^1\text{H}$ NMR spectra (400 MHz) of PCBT1 in $\text{CDCl}_3$ . ....	69
Figure 2 - 12: Absorption spectra of PCBTs in ODCB solutions (top) and as spin-coated films (bottom). ....	71
Figure 2 - 13: Representation of conjugation extent in 3,6- (left) and 2,7-linked (right) polymers.....	72
Figure 2 - 14: Photoluminescence (PL) spectra of PCBTs in ODCB solutions (top) and spin-coated films (bottom). Each PCBT was excited at $\lambda_{\text{max}}$ determined in absorption spectra. ....	74
Figure 2 - 15: Cyclic voltammograms (left-oxidation, right-reduction) of PCBT3 in $\text{CH}_2\text{Cl}_2$ solution ( $0.1 \text{ g.l}^{-1}$ ). ....	75
Figure 2 - 16: Energetic representation of the four PCBTs. <sup>a</sup> Values for P3HT and PCBM are from the literature. <sup>[34]</sup> .....	76
Figure 2 - 17: Solid-state light absorption of PCBT2:PCBM blends at different ratios, spin-coated from ODCB solutions onto PEDOT-PSS coated glass substrates.....	77
Figure 2 - 18: Solid-state PL of PCBT2:PCBM blends at different ratios, spin-coated from ODCB solutions onto PEDOT-PSS coated glass substrates. Excited at 481 nm.....	77
Figure 2 - 19: AFM phase images of the PCBT:PCBM blends with a 1:1 ratio. ....	78
Figure 2 - 20: $^1\text{H}$ - $^{13}\text{C}$ HSQC NMR spectra (400 MHz) of 5 in $\text{CDCl}_3$ . ....	85
Figure 2 - 21: IR spectrum (ATR) of 5.....	86
Figure 2 - 22: $^1\text{H}$ - $^{13}\text{C}$ HSQC NMR spectra (400 MHz) of 6 in $\text{CDCl}_3$ . ....	87
Figure 2 - 23: IR spectrum (ATR) of 6.....	87
Figure 2 - 24: $^1\text{H}$ - $^{13}\text{C}$ HSQC NMR spectra (400 MHz) of 7 in $\text{CDCl}_3$ . ....	88
Figure 2 - 25: IR spectrum (ATR) of 7.....	89
Figure 2 - 26: $^1\text{H}$ - $^{13}\text{C}$ HSQC NMR spectra (400 MHz) of 8 in $\text{CDCl}_3$ . ....	90
Figure 2 - 27: IR spectrum (ATR) of 8.....	90
Figure 2 - 28: IR spectrum (ATR) of PCBT1. ....	92



Figure 2 - 29: $^1\text{H}$ - $^{13}\text{C}$ HSQC NMR spectra (400 MHz) of PCBT2 in $\text{CDCl}_3$ .....	93
Figure 2 - 30: IR spectrum (ATR) of PCBT2. ....	93
Figure 2 - 31: $^1\text{H}$ - $^{13}\text{C}$ HSQC NMR spectra (400 MHz) of PCBT3 in $\text{CDCl}_3$ .....	94
Figure 2 - 32: IR spectrum (ATR) of PCBT3. ....	95
Figure 2 - 33: $^1\text{H}$ - $^{13}\text{C}$ HSQC NMR spectra (400 MHz) of PCBT4 in $\text{CDCl}_3$ .....	96
Figure 2 - 34: IR spectrum (ATR) of PCBT4. ....	96
Figure 2 - 35: TGA analyses of PCBTs. ....	97
Figure 2 - 36: DSC analyses of PCBTs.....	98
Figure 2 - 37: Cyclic voltammograms of PCBT1 in $\text{CH}_2\text{Cl}_2$ solution ( $0.1 \text{ g.l}^{-1}$ ). Left-oxidation; right-reduction. ....	99
Figure 2 - 38: Cyclic voltammograms of PCBT2 in $\text{CH}_2\text{Cl}_2$ solution ( $0.1 \text{ g.l}^{-1}$ ). Left-oxidation; right-reduction. ....	99
Figure 2 - 39: Cyclic voltammograms of PCBT3 in $\text{CH}_2\text{Cl}_2$ solution ( $0.1 \text{ g.l}^{-1}$ ). Left-oxidation; right-reduction. ....	99
Figure 2 - 40: Cyclic voltammograms of PCBT4 in $\text{CH}_2\text{Cl}_2$ solution ( $0.1 \text{ g.l}^{-1}$ ). Left-oxidation; right-reduction. ....	100
Figure 2 - 41: Absorption spectra of PCBT:PCBM blends in film at different ratios, spin-coated from ODCB solutions onto PEDOT-PSS coated glass substrates.....	100
Figure 2 - 42: Photoluminescence spectra of PCBT:PCBM blends in film at different ratios, spin-coated from ODCB solutions onto PEDOT-PSS coated glass substrates. Excitations were according to the absorption maxima of PCBTs in solid-state (see section 2.3.2). ....	101

### **Chapter 3**

Figure 3 - 1: Examples of squaraine dyes made from (a) aniline, (b) pyrrole, (c) indole derivatives. <sup>[6-8]</sup> .....	107
Figure 3 - 2: The different resonant structures for a squaraine dye. <sup>[6]</sup> .....	107
Figure 3 - 3: Example of an indole-based polysquaraine. <sup>[14]</sup> .....	109
Figure 3 - 4: The investigated bridged polysquaraines.....	110
Figure 3 - 5: The selected dibromide squaraine-based monomer. <sup>[14]</sup> .....	111
Figure 3 - 6: Synthesis of the indolium precursor 11. ....	111
Figure 3 - 7: Synthesis of the alkylated dibromosquaraine monomer 12. ....	112
Figure 3 - 8: IR spectrum (ATR) of compound 12.....	112
Figure 3 - 9: $^1\text{H}$ NMR spectrum (400 MHz) of compound 12 in $\text{CDCl}_3$ , taking the symmetry into account.....	113
Figure 3 - 10: Syntheses of the bridged polysquaraines via: a) Suzuki coupling; b), c) Stille coupling. Heated at reflux for 48h.....	114
Figure 3 - 11: IR spectra (ATR) of the synthesized polymers. ....	115
Figure 3 - 12: $^1\text{H}$ NMR spectra (400 MHz) of the synthesized PSQs in $\text{CDCl}_3$ .....	116
Figure 3 - 13: UV-vis absorption spectra of PSQs in $\text{CHCl}_3$ solutions ( $0.01 \text{ g.l}^{-1}$ ) and in films spin-coated from $\text{CHCl}_3$ solutions ( $10 \text{ g.l}^{-1}$ ).....	118
Figure 3 - 14: Photoluminescence spectra of PSQs in $\text{CHCl}_3$ solutions ( $0.01 \text{ g.l}^{-1}$ ) and in films spin-coated from $\text{CHCl}_3$ solutions ( $10 \text{ g.l}^{-1}$ ). Excitation at 650 nm. ....	120
Figure 3 - 15: Cyclic voltammograms (left- oxidation; right- reduction) of PSQT in $\text{CHCl}_3$ solution ( $0.1 \text{ g.l}^{-1}$ ). ....	121

Figure 3 - 16: Energetic representation of the PSQs. <sup>a</sup> Values for P3HT and PCBM are from the literature. <sup>[20]</sup> ..	122
Figure 3 - 17: Solid-state light absorption of PSQT:PCBM blends. ....	123
Figure 3 - 18: Solid-state PL of PSQT:PCBM blends excited at 650 nm. ....	123
Figure 3 - 19: AFM phase images of PSQ:PCBM (1:1) blends. ....	124
Figure 3 - 20: <sup>1</sup> H- <sup>13</sup> C HSQC NMR spectra (400 MHz) of 12 in CDCl <sub>3</sub> . ....	129
Figure 3 - 21: IR spectrum (ATR) of 12. ....	130
Figure 3 - 22: <sup>1</sup> H- <sup>13</sup> C HSQC NMR spectra (400 MHz) of PSQBT in CDCl <sub>3</sub> . ....	131
Figure 3 - 23: IR spectrum (ATR) of PSQBT. ....	131
Figure 3 - 24: <sup>1</sup> H- <sup>13</sup> C HSQC NMR spectra (400 MHz) of PSQT in CDCl <sub>3</sub> . ....	133
Figure 3 - 25: IR spectrum (ATR) of PSQT. ....	133
Figure 3 - 26: <sup>1</sup> H- <sup>13</sup> C HSQC NMR spectra (400 MHz) of PSQBDT in CDCl <sub>3</sub> . ....	135
Figure 3 - 27: IR spectrum (ATR) of PSQT. ....	135
Figure 3 - 28: TGA analyses of PSQs. ....	136
Figure 3 - 29: DSC analyses of PSQs. ....	137
Figure 3 - 30: Cyclic voltammograms of PSQBT in CHCl <sub>3</sub> solution (0.1 g.Γ <sup>-1</sup> ). Left-oxidation; right-reduction. ....	138
Figure 3 - 31: Cyclic voltammograms of PSQT in CHCl <sub>3</sub> solution (0.1 g.Γ <sup>-1</sup> ). Left-oxidation; right-reduction. ....	138
Figure 3 - 32: Cyclic voltammograms of PSQBDT in CHCl <sub>3</sub> solution (0.1 g.Γ <sup>-1</sup> ). Left-oxidation; right-reduction. ....	139
Figure 3 - 33: Normalized UV-visible absorption spectra of the PSQs THF fractions in CHCl <sub>3</sub> solution (0.01 g.Γ <sup>-1</sup> ). ....	139
Figure 3 - 34: UV-visible absorption spectra of pristine PSQs in films and PSQ:PCBM blends in films at different ratios, spin-coated from ODCB solutions onto PEDOT-PSS coated glass substrates. ....	140
Figure 3 - 35: Photoluminescence spectra of pristine PSQs in films and PSQ:PCBM blends in films at different ratios, excited at 650 nm. ....	141

## Chapter 4

Figure 4 - 1: Mechanism of formation of a squaraine dye. <sup>[5-6]</sup> ..	148
Figure 4 - 2: Synthesis of the insoluble polymer from pyrrole and SA. The structure shown here is hypothetical since it could not be confirmed due to the intractable nature of the material. <sup>[7]</sup> ..	148
Figure 4 - 3: Influence of reaction conditions on the structure and solubility of pyrrole-based polysquaraines. <sup>[8]</sup> ..	149
Figure 4 - 4: Carbazole-based polysquaraine. <sup>[9]</sup> ..	149
Figure 4 - 5: Small band-gaps polysquaraines based on SA and CA. <sup>[10-11]</sup> ..	150
Figure 4 - 6: Examples of polysquaraines obtained by condensation of pyrrole-based difunctional monomers with SA. ....	151
Figure 4 - 7: Examples of conjugated polyimines developed by Jenekhe et al. <sup>[18]</sup> ..	152
Figure 4 - 8: Examples of selenophene-based conjugated polyimines. <sup>[19]</sup> ..	152
Figure 4 - 9: Conjugated polyimines based on fluorene. <sup>[20-21]</sup> ..	153

Figure 4 - 10: Metal-free approach to PSQT and PSQBT. ....	154
Figure 4 - 11: Polycondensation of aniline derivative with SA. ....	154
Figure 4 - 12: Polycondensations via arylimino-de-oxo-bisubstitution between 3,6- and 2,7-diaminocarbazole and bisaldehydes derivatives of EDOT and carbazole. ....	154
Figure 4 - 13: Bis-indolium iodide monomers. Circled in red: reactive sites towards SA. ....	155
Figure 4 - 14: Synthesis of bis(indolium)thiophene 14. ....	155
Figure 4 - 15: Synthesis of the boronic ester indole 15. ....	156
Figure 4 - 16: Synthesis of bis(indolium)BT 17. ....	156
Figure 4 - 17: $^1\text{H}$ NMR spectra (400 MHz) of the thiophene-based compounds 13 and 14 in $\text{CDCl}_3$ . ....	157
Figure 4 - 18: $^1\text{H}$ NMR spectra (400 MHz) of the BT-based compounds 16 and 17 in $\text{CDCl}_3$ . ....	158
Figure 4 - 19: IR spectra (ATR) of compounds 13-17. Red solid line: C=N stretch. Blue dotted line: alkyl C-H stretch. ....	159
Figure 4 - 20: a) Example of squaraine dye from aniline derivative. b) Developed monomer; circled in red: reactive sites towards SA. ....	159
Figure 4 - 21: Synthesis of compound 18. ....	160
Figure 4 - 22: $^1\text{H}$ NMR spectrum of 18 in THF-d8. ....	160
Figure 4 - 23: IR spectrum of 18 and its precursor. Circled in red: peaks corresponding to N-H stretch. Circled in blue: absorption due to alkyl C-H stretch. ....	161
Figure 4 - 24: Synthesis of PSQT and PSQBT from compounds 14 and 17. ....	161
Figure 4 - 25: Synthesis of PSQDA. ....	163
Figure 4 - 26: $^1\text{H}$ NMR spectrum (400 MHz) of PSQDA in $\text{CDCl}_3$ . ....	164
Figure 4 - 27: IR spectra of 18 (top) and PSQDA bottom. Circled in red: the peak corresponding to C=O stretching. ....	165
Figure 4 - 28: Normalized absorption spectra and data of the polysquaraines in $\text{CHCl}_3$ solution (top) and spin-coated films on glass substrate (bottom). ....	166
Figure 4 - 29: Normalized photoluminescence spectra of PSQT and PSQBT in $\text{CHCl}_3$ solutions ( $0.01 \text{ g.l}^{-1}$ ). Excitation at 650 nm. ....	167
Figure 4 - 30: Photoluminescence spectra of PSQDA in $\text{CHCl}_3$ solution (top) and in film (bottom) spin-coated onto glass substrate from $\text{CHCl}_3$ solution ( $10 \text{ g.l}^{-1}$ ). Excitation at 315 nm. ....	168
Figure 4 - 31: Energetic representation of the PSQs. <sup>a</sup> Values for P3HT and PCBM are from the literature. <sup>[28]</sup> ..	169
Figure 4 - 32: Synthesis of the EDOT-dialdehyde 19. ....	169
Figure 4 - 33: Synthesis of the 2,7-diaminocarbazole 21. ....	170
Figure 4 - 34: Synthesis of the 3,6-diaminocarbazole 24. ....	170
Figure 4 - 35: Synthesis of polyimines PIMI1-4. ....	171
Figure 4 - 36: Normalized absorption spectra and data of PIMI1-4 in DMF solutions. ....	173
Figure 4 - 37: PL spectra and data of PIMI1-4 in DMF (excitation at 450 nm). ....	174
Figure 4 - 38: $^1\text{H}$ - $^{13}\text{C}$ HSQC NMR (400 MHz) spectra of 13 in $\text{CDCl}_3$ . ....	179
Figure 4 - 39: IR spectrum (ATR) of 13. ....	179

## List of figures

Figure 4 - 40: $^1\text{H}$ - $^{13}\text{C}$ HSQC NMR spectra (400 MHz) of 14 in $\text{CDCl}_3$ .	180
Figure 4 - 41: IR spectrum (ATR) of 14.	181
Figure 4 - 42: $^1\text{H}$ - $^{13}\text{C}$ HSQC NMR (400 MHz) spectra of 15 in $\text{CDCl}_3$ .	182
Figure 4 - 43: IR spectrum (ATR) of 15.	182
Figure 4 - 44: $^1\text{H}$ - $^{13}\text{C}$ HSQC NMR spectra (400 MHz) of 16 in $\text{CDCl}_3$ .	184
Figure 4 - 45: IR spectrum (ATR) of 16.	184
Figure 4 - 46: $^1\text{H}$ - $^{13}\text{C}$ HSQC NMR spectra (400 MHz) of 17 in $\text{CDCl}_3$ .	185
Figure 4 - 47: IR spectrum (ATR) of 17.	186
Figure 4 - 48: $^1\text{H}$ - $^{13}\text{C}$ HSQC NMR spectra (400 MHz) of 17 in $\text{THF-d}_8$ .	187
Figure 4 - 49: IR spectrum (ATR) of 18.	187
Figure 4 - 50: $^1\text{H}$ - $^{13}\text{C}$ HSQC NMR spectra (400 MHz) of PSQT synthesized from 14 in $\text{CDCl}_3$ .	189
Figure 4 - 51: IR spectrum (ATR) of PSQT synthesized from 14.	189
Figure 4 - 52: $^1\text{H}$ - $^{13}\text{C}$ HSQC NMR spectra (400 MHz) of PSQBT synthesized from 17 in $\text{CDCl}_3$ .	191
Figure 4 - 53: IR spectrum (ATR) of PSQBT synthesized from 17.	191
Figure 4 - 54: $^1\text{H}$ - $^{13}\text{C}$ HSQC NMR spectra (400 MHz) of PSQDA in $\text{CDCl}_3$ .	193
Figure 4 - 55: IR spectrum (ATR) of PSQDA.	193
Figure 4 - 56: IR spectrum (ATR) of PIMI1.	197
Figure 4 - 57: IR spectrum (ATR) of PIMI2.	198
Figure 4 - 58: IR spectrum (ATR) of PIMI3.	199
Figure 4 - 59: IR spectrum (ATR) of PIMI4.	200
Figure 4 - 60: TGA analyses of PSQs obtained by polycondensation with squaric acid.	200
Figure 4 - 61: TGA analyses of polyimines.	201
Figure 4 - 62: DSC analyses of PSQs obtained by polycondensation with squaric acid.	202
Figure 4 - 63: DSC analyses of polyimines.	203
Figure 4 - 64: Normalized UV-visible absorption spectra of the monomers employed in the polyimines syntheses.	203
Figure 4 - 65: Cyclic voltammograms of PSQT in $\text{CHCl}_3$ solution ( $0.1 \text{ g.l}^{-1}$ ). Left-oxidation; right-reduction.	204
Figure 4 - 66: Cyclic voltammograms of PSQBT in $\text{CHCl}_3$ solution ( $0.1 \text{ g.l}^{-1}$ ). Left-oxidation; right-reduction.	204
Figure 4 - 67: Cyclic voltammograms of PSQDA in $\text{CHCl}_3$ solution ( $0.1 \text{ g.l}^{-1}$ ). No reduction signal was observed.	205



# **Introduction, résumé et conclusion de la thèse (french version)**

## **Synthèse et relation structure-propriétés de copolymères alternés $\pi$ -conjugués**

J. Oriou

### **Introduction**

L'émergence de l'électronique représente une avancée technologique majeure au cours du siècle dernier, à tel point qu'elle a envahi notre vie de tous les jours : ordinateurs, appareils domestiques, transport, communication, etc... Ces avancées ont été rendues possibles grâce au développement de composants capables de contrôler des flux d'électrons. Ces composants sont généralement fabriqués à partir de métaux ou de semi-conducteurs inorganiques (par exemple le silicium).<sup>[1]</sup> L'inconvénient principal de tels matériaux réside dans la quantité importante d'énergie nécessaire lors des procédés de purification, ainsi que lors de la fabrication de dispositifs électroniques. La production et la mise en œuvre de composants à base de silicium, par exemple, requiert un très haut degré de pureté et de cristallinité, qui est communément obtenu par fusion du matériau à 1414°C<sup>[2]</sup> (procédé de Czochralski). De par leurs propriétés bien spécifiques, les semi-conducteurs organiques représentent une remarquable alternative aux matériaux inorganiques utilisés actuellement.

Bien que la conductivité électrique dans des matériaux organiques ait été déjà démontrée par le passé, une des plus grandes avancées dans le domaine est celle réalisée par Hideki Shirakawa, Alan G. MacDiarmid et Alan J. Heeger en 1977 avec la découverte des propriétés de conductivité électrique du polyacétylène (voir Figure 1),<sup>[3]</sup> ce qui leur valut le prix Nobel de chimie pour « la découverte et le développement des polymères conducteurs » en 2000.

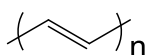
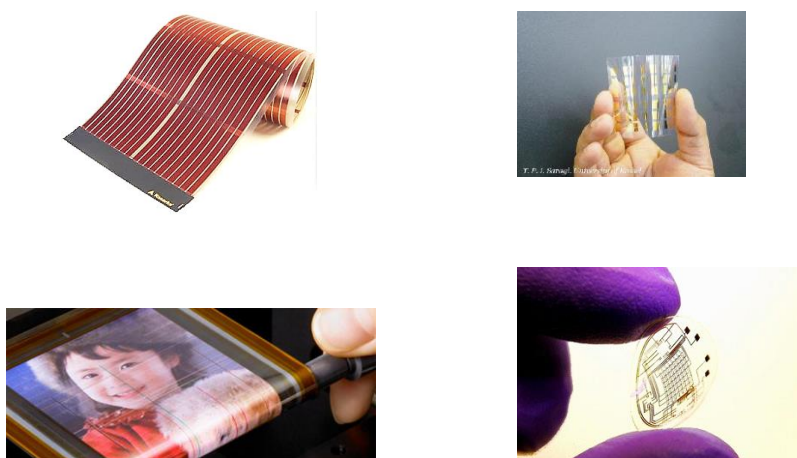


Figure 1 : structure chimique du polyacétylène.

Les semi-conducteurs organiques sont en général basés sur des molécules ou macromolécules  $\pi$ -conjuguées composées de carbone et d'hydrogène, mais peuvent aussi contenir d'autres éléments tels que l'azote, le soufre ou l'oxygène par exemple. Les matériaux organiques sont communément connus comme isolants électriques, mais il est possible d'obtenir une certaine conductivité en

choisissant une structure chimique appropriée.<sup>[4]</sup> Le principal avantage de ces matériaux réside dans les nouvelles propriétés qu'ils apportent. Par exemple, leur solubilité dans des solvants organiques permet de les manipuler sous forme d'encres,<sup>[5]</sup> ou encore de les purifier grâce à des techniques moins coûteuses en énergie telles que la recristallisation, la précipitation ou l'extraction de Soxhlet. De plus, les semi-conducteurs organiques sont généralement légers, et dans le cas de polymères il est possible de créer des dispositifs électroniques flexibles. Toutes ces propriétés offrent un vaste panel d'applications difficiles à réaliser avec des matériaux inorganiques : écrans flexibles, dispositifs photovoltaïques intégrés dans des textiles et dispositifs électroniques biocompatibles en sont quelques exemples (voir Figure 2).



**Figure 2 : Exemples d'applications électroniques organiques tirant parti du caractère flexible des matériaux : panneaux solaires (en haut à gauche), transistors (en haut à droite), écrans souples (en bas à gauche) et lentilles de contact électroniques (en bas à droite).**

Cependant, les propriétés électriques des semi-conducteurs organiques peuvent être limitées, et les rendements des dispositifs électroniques organiques ne sont pas suffisamment élevés pour pouvoir remplacer ceux basés sur des matériaux inorganiques. Même si la relation entre structure chimique et propriétés dans les semi-conducteurs organiques a déjà été intensivement étudiée, il est encore nécessaire de compléter les connaissances acquises par la communauté scientifique dans ce domaine. Dans ce contexte, ce travail de thèse a pour but de synthétiser de nouveaux polymères  $\pi$ -conjugués et d'étudier leur propriétés afin d'ajouter de nouveaux matériaux à la liste de polymères semi-conducteurs existants, ainsi que de permettre une meilleure compréhension de la relation structure-propriétés dans ces matériaux. Enfin, des voies de synthèse originales et plus respectueuses de l'environnement ont été développées pour obtenir de tels matériaux.

## **Chapitre 1 - Relation structure-propriétés des polymères semi-conducteurs : état de l'art**

Le premier chapitre de cette thèse a pour but d'établir un bref état de l'art des connaissances acquises par la communauté scientifique sur la relation entre la structure chimique et les propriétés opto-électroniques des polymères semi-conducteurs. De plus, il fournit un aperçu des différentes méthodes de synthèse permettant l'obtention de polymères  $\pi$ -conjugués.

La première partie se concentre sur la définition de matériau polymère semi-conducteur, en l'illustrant notamment par des diagrammes de bandes énergétiques. L'origine des propriétés semi-conductrices dans les matériaux organiques y est expliquée. La présence d'électrons  $\pi$  ainsi que leur délocalisation via l'alternance de liaisons multiples permet la création d'un système conjugué ayant un profil énergétique de type semi-conducteur, tel qu'illustré en Figure 1-1.<sup>[6]</sup>

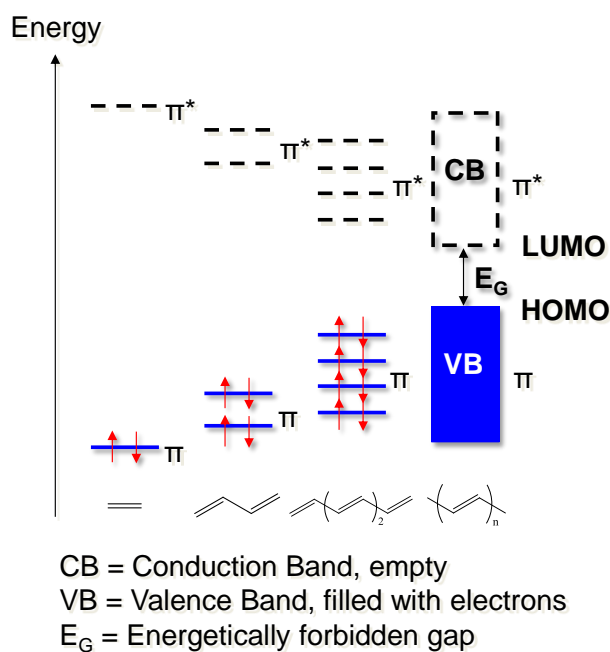


Figure 1-1 : Représentation de l'évolution énergétique des orbitales moléculaires lors de l'extension d'un système  $\pi$ -conjugués.

De plus, la génération et le comportement de charges, nécessaires à l'obtention de propriétés électriques, y est également décrite. Ces charges peuvent être générées via différents stimuli : lumière, température, ou dopage électrochimique par exemple. Elles peuvent se déplacer au sein du matériau le long du système conjugué d'une chaîne polymère, mais aussi par « saut » entre deux fragments de chaîne.<sup>[5]</sup>

En s'appuyant sur les nombreuses publications dans le domaine, la seconde partie décrit comment certaines modifications de la structure chimique d'un polymère  $\pi$ -conjugué peuvent avoir un impact



sur ses propriétés opto-électroniques, en se concentrant principalement sur la position des niveaux énergétiques (orbitale moléculaire la plus haute occupée = HOMO ; orbitale moléculaire la plus basse inoccupée = LUMO) et l'absorption optique du matériau.

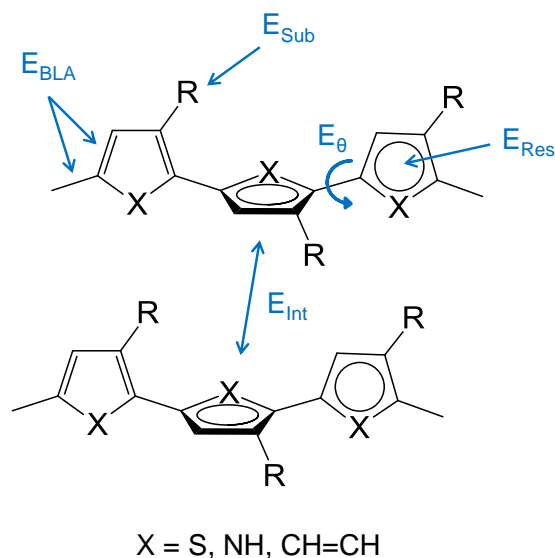


Figure 1-2 : Paramètres structuraux influençant le gap énergétique de matériaux  $\pi$ -conjugués. Reproduction d'une illustration de J. Roncali.<sup>[7]</sup>

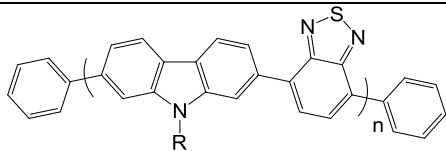
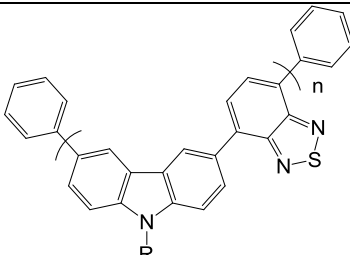
La dernière section se concentre sur les différentes voies de synthèse permettant l'obtention de polymères  $\pi$ -conjugués. Les premières synthèses de polymères semi-conducteurs y sont présentées (obtention de polyacétylène par polymérisation de Ziegler-Natta par exemple),<sup>[8]</sup> ainsi que des méthodes plus récentes et plus communément employées de nos jours (couplages de Stille et Suzuki).<sup>[9-10]</sup> Un aperçu des réactions permettant l'obtention de polymères conjugués sans catalyseurs métallique est aussi fourni, puisque la présence de ces derniers peut impacter grandement les propriétés électriques du matériau final.

## **Chapitre 2 - Synthèse et caractérisation de poly(carbazole-*alt*-benzothiadiazole) (PCBT)**

Ce chapitre décrit la synthèse par polycondensation de type Suzuki de quatre macromolécules  $\pi$ -conjuguées alternant des motifs carbazole et benzothiadiazole. Les motifs carbazole sont liés en position 2,7- ou 3,6-, et deux différents groupes alkyles solubilisant ont été utilisés (n-dodecyle et 9-heptadecanyle). Les structures chimiques des matériaux ont été confirmées par spectroscopie à résonance magnétique nucléaire (RMN), spectroscopie infra-rouge (IR) et par chromatographie d'exclusion stérique (CES), et leur propriétés thermiques ont été étudiées par calorimétrie différentielle à balayage (DSC) et analyse thermo-gravimétrique (ATG).

L'absorption UV-visible et la photoluminescence des polymères ont été mesurées, ainsi que la position de leurs niveaux HOMO et LUMO par voltampérométrie cyclique en solution. Les études spectroscopiques réalisées ont mis en avant la présence d'un transfert de charge intra-moléculaire (ICT) entre motif donneur (carbazole) et motif accepteur (benzothiadiazole) réduisant la bande d'énergie interdite des matériaux, comparés à des homopolymères à base de carbazole ou benzothiadiazole seulement.<sup>[11-13]</sup> Bien que de légères différences soient observées sur les propriétés optiques et électrochimiques, les absorptions optiques des quatre polymères synthétisés sont très similaires, ce qui semble indiquer que l'ICT a un rôle prédominant par rapport à la délocalisation des électrons le long de la chaîne.

Tableau 2-1 : Résumé de quelques propriétés des PCBTs synthétisés.

Polymère	$E_{\text{HOMO}}$ (eV) <sup>a</sup>	$E_{\text{LUMO}}$ (eV) <sup>a</sup>	$E_g^{\text{CV}}$ (eV) <sup>a</sup>	$E_g^{\text{opt film}}$ (eV) <sup>b</sup>	
	R = n-dodecyle (PCBT1)	-5.5	-3.0	2.5	2.2
	R = 9-heptadecanyle (PCBT2)	-5.3	-3.0	2.3	2.3
	R = n-dodecyle (PCBT3)	-5.0	-2.8	2.2	2.2
	R = 9-heptadecanyle (PCBT4)	-5.3	-3.0	2.3	2.3

<sup>a</sup> Mesuré par voltampérométrie cyclique en solution; <sup>b</sup> Bande interdite optique obtenue à partir de  $\lambda_{\text{onset}}^{\text{film}}$ .

Des mélange de ces polymères avec du [6,6]-phényl-C<sub>61</sub>-butanoate de méthyle (PCBM) ont été mis en oeuvre puis étudiés par microscopie à force atomique (AFM) et par photoluminescence afin de démontrer le potentiel de ces matériaux en tant que donneurs dans des cellules solaire à hétérojonction en volume. Des résultats encourageant en sont ressortis, mais malheureusement les cellules solaires fabriquées par la suite ont besoin d'être optimisées pour pouvoir fournir des rendements de conversion en puissance corrects.

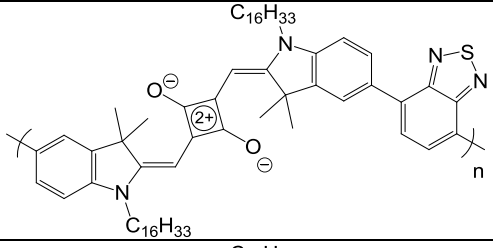
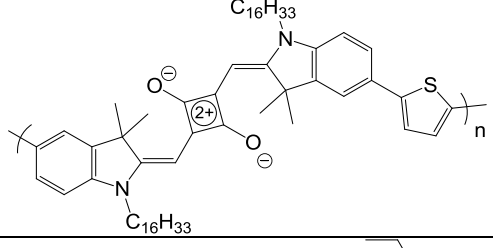
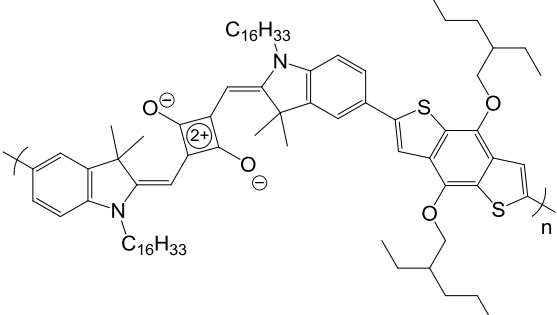
Malgré l'ICT, les bandes interdites de ces matériaux ne sont pas suffisamment réduites lorsqu'on les compare à d'autres polymères  $\pi$ -conjugués plus connus tels que le poly(3-hexylthiophene) (P3HT). Un travail plus approfondi sur le choix des motifs employés permettrait sans doute d'y remédier. De plus, il est possible qu'un important angle dièdre existe entre les motifs carbazole et benzothiadiazole. L'insertion de motifs permettant une meilleure planéité de la chaîne conjuguée devrait donc être envisagée. Enfin, l'utilisation de substituants donneurs ou accepteurs pourrait être une voie intéressante pour changer la position des niveaux HOMO et LUMO.

## Chapitre 3 - Synthèse et caractérisation de polysquaraines alternés

Ce chapitre présente la synthèse par polycondensation de type Suzuki ou Stille de trois différents polymères  $\pi$ -conjugués alternant un motif squaraine avec un motif benzothiadiazole, thiophène ou benzodithiophène. Leurs structures chimiques ont été confirmées par RMN, IR et CES, et leur propriétés thermiques caractérisées par DSC et ATG.

Les trois matériaux présentent une absorption optique et une photoluminescence intenses dans la partie rouge-proche IR du spectre lumineux. Il semble que le type d'unité alternée avec le motif squaraine n'ait qu'une faible influence sur les propriétés optiques. Des mesures électrochimiques ont confirmés les faibles valeurs de bandes interdites observées par absorption optique.

Tableau 3-1 : Résumé de quelques propriétés des polysquaraines synthétisés.

Polymère	$E_{\text{HOMO}}(\text{eV})^a$	$E_{\text{LUMO}}(\text{eV})^a$	$E_g^{\text{CV}}(\text{eV})^a$	$E_g^{\text{opt film}}(\text{eV})^b$
	-5.1	-3.7	1.4	1.6
	-5.1	-3.6	1.5	1.6
	-5.0	-3.8	1.2	1.6

<sup>a</sup> Mesuré par voltampérométrie cyclique en solution; <sup>b</sup> Bande interdite optique obtenue à partir de  $\lambda_{\text{onset}}^{\text{film}}$ .

Les propriétés optiques ainsi que la position des niveaux énergétiques de ces matériaux en font de potentiels donneurs pour la couche active de cellule solaire à hétérojonction en volume. Par conséquent, des mélanges de ces polymères avec du PCBM en film ont été fabriqués puis caractérisés par AFM et photoluminescence. L'extinction de fluorescence des mélanges semble indiquer une bonne dissociation des excitons, mais les morphologies de surface observées en AFM

montrent que des optimisations plus approfondies sont nécessaires au niveau de la fabrication des films.

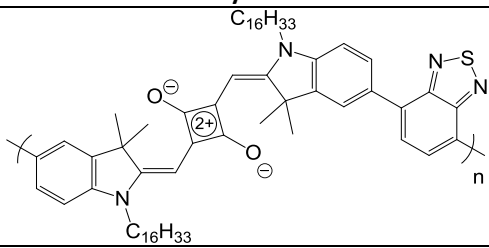
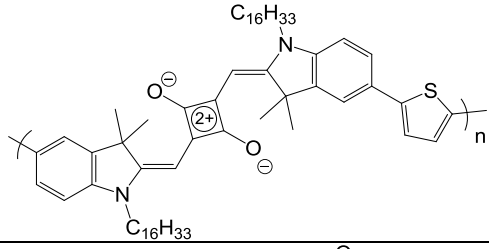
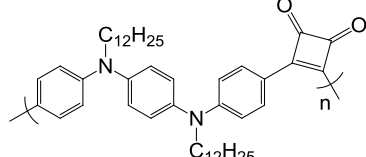
Finalement, il est désirable de baisser les niveaux énergétiques de ces matériaux afin d'atteindre de plus hauts rendements en cellule solaire, mais aussi pour obtenir des polymères semi-conducteurs de type n. Ceci pourrait être réalisé en alternant les unités squaraines avec des motifs encore plus électro-accepteurs.

## **Chapitre 4 - Nouveaux polymères conjugués synthétisés par polycondensation sans catalyseur métallique**

Ce dernier chapitre décrit la synthèse de sept nouveaux matériaux  $\pi$ -conjugués par des polycondensations ne nécessitant pas de catalyseurs métalliques.

Dans un premier temps la condensation de dérivés indoleniums avec de l'acide squarique fut réalisée. Les polysquaraines obtenus par cette méthode présentent des structures et des propriétés similaires à ceux obtenus par condensation de type Suzuki ou Stille, avec des masses molaires encore plus élevées. Puis, un nouveau polymère conjugué fut préparé par condensation d'un dérivé de l'aniline avec de l'acide squarique. Il s'avère que le matériau ne semble contenir que des isomères 1,2- d'unités squaraines (observé en IR), ne produisant ainsi pas les faibles valeurs de bande interdite attendues pour un polysquaraine. De plus amples études sont nécessaires afin de pleinement comprendre le mécanisme de cette réaction.

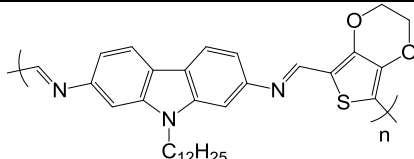
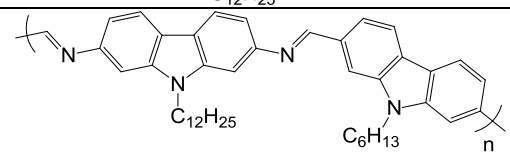
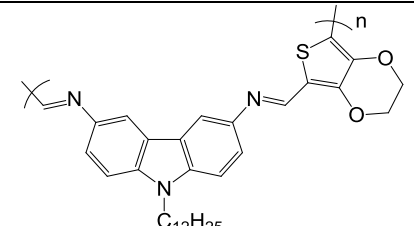
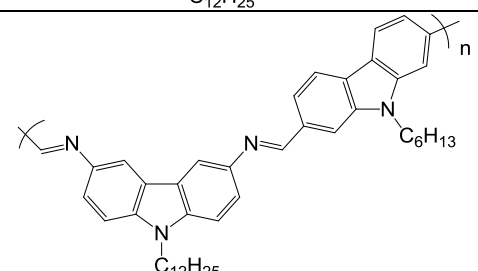
Tableau 3-1 : Résumé de quelques propriétés des polymères synthétisés par condensation avec de l'acide squarique.

Polymère	$E_{\text{HOMO}}(\text{eV})^a$	$E_{\text{LUMO}}(\text{eV})^a$	$E_{\text{g}}^{\text{CV}}(\text{eV})^a$	$E_{\text{g}}^{\text{opt film}}(\text{eV})^b$
	-5.1	-3.7	1.4	1.6
	-5.0	-3.9	1.1	1.6
	-5.0	-	-	2.7

<sup>a</sup> Mesuré par voltampérométrie cyclique en solution; <sup>b</sup> Bande interdite optique obtenue à partir de  $\lambda_{\text{onset}}^{\text{film}}$ .

Dans un second temps, des polycondensations de type aryl-imino-de-oxo-bisubstitution ont été réalisées à partir de motifs conjugués fonctionnalisés par des groupements amine et aldéhydes. Malgré la présence de substituants alkyles, les polyimines obtenues montrent une solubilité limitée dans de nombreux solvants organiques. Une légère solubilité dans le DMF a cependant permis leur caractérisation optique, qui suggère l'obtention de matériaux conjugués, ainsi que la présence d'un transfert de charge intra-moléculaire entre les unités carbazole et EDOT. En perspective, le greffage de chaînes alkyles plus longues ou plus encombrées devrait entraîner une meilleure solubilité des matériaux, permettant ainsi des études plus approfondies.

Tableau 3-2 : Résumé de quelques propriétés des polymères synthétisés par aryl-imino-de-oxo-bisubstitution.

Polymère	$E_{\text{HOMO}}(\text{eV})^a$	$E_{\text{LUMO}}(\text{eV})^a$	$E_g^{\text{CV}}(\text{eV})^a$	$E_g^{\text{opt film}}(\text{eV})^b$
	-	-	-	2.2
	-	-	-	2.6
	-	-	-	2.3
	-	-	-	2.6

<sup>a</sup> Mesuré par voltampérométrie cyclique en solution; <sup>b</sup> Bande interdite optique obtenue à partir de  $\lambda_{\text{onset}}^{\text{film}}$ .

## **Conclusion et perspectives**

Les polymères semi-conducteurs apportent de nouvelles propriétés ainsi que de nombreux avantages au domaine de l'électronique. Cependant cette technologie requiert un vaste panel de matériaux avec des propriétés différentes. De plus, on trouve de nos jours une demande croissante pour des synthèses plus respectueuses de l'environnement.

Dans ce contexte, ce travail de thèse s'est concentré sur le développement de nouveaux polymères  $\pi$ -conjugués dans le but d'obtenir de nouveaux semi-conducteurs organiques, mais aussi afin de mieux comprendre comment la structure chimique influence les propriétés des copolymères alternés  $\pi$ -conjugués. Dans le cas des matériaux à base de carbazole et benzothiadiazole, il semble que la façon de lier le motif carbazole (2,7 ou 3,6) n'ait qu'une faible influence sur les propriétés spectroscopiques par rapport au transfert de charge intra-moléculaire entre unités électro-donneuses et électro-acceptrices. En complément de cette partie, l'utilisation de substituants donneurs ou accepteurs afin de changer la position des niveaux énergétiques fournirait une étude plus approfondie sur cette famille de matériaux. L'alternance de motifs squaraines avec d'autres unités hétéroaromatiques a permis l'obtention de copolymères semi-conducteurs avec de faibles valeurs de bande interdite. Les propriétés spectroscopiques dans ce cas semblent provenir principalement des motifs squaraines. Néanmoins, cette famille de matériaux pourrait être agrandie par l'alternance d'unités squaraines avec de nombreux autres motifs.

Les propriétés des polymères développés se sont révélées appropriées pour des applications en électronique organique. Cependant, des caractérisations plus complètes s'avèrent nécessaire, telles que la mesure de la mobilité des porteurs de charge. Même si ces matériaux ont tout d'abord été développés pour une application photovoltaïque, ils pourraient s'avérer d'un grand intérêt pour d'autres types de composants. Par exemple, leur photoluminescence présentant une grande intensité et étant répartie sur différentes zones du spectre visible selon le polymère, une application dans des dispositifs d'émission lumineuse est fortement envisageable.

Les polymères présentés dans la dernière partie de cette thèse ont été synthétisés via une étape de polymérisation sans catalyseur métallique. A cet avantage s'ajoute celui de n'obtenir que de l'eau comme sous-produit, pouvant être facilement éliminée du milieu réactionnel et du matériau final. Cependant, des métaux de transition sont tout de même présents dans certaines étapes de synthèse des monomères. Une perspective évidente de ce travail serait donc d'éliminer ces métaux de toutes les étapes de synthèses afin d'obtenir des polymères conjugués par voie de synthèse sans aucun métal de transition. Enfin, les problèmes de solubilité rencontrés pour les polyimines obtenues par

aryl-imino-de-oxo-bisubstitution pourraient être résolus par deux approches différentes.

Premièrement, les chaînes alkyles employées peuvent être remplacées par des chaînes plus longues et/ou plus encombrées. Deuxièmement, des substituants alkyles additionnels peuvent être ajoutés par quaternisation des atomes d'azote dans les liaisons imines. En combinant cette stratégie avec des substituants appropriés (portant des fonctions ioniques par exemple), cela pourrait même conduire à des matériaux solubles dans des solvants alcooliques et/ou dans l'eau, ce qui représente un pas en avant vers des procédés plus respectueux de l'environnement pour l'électronique organique.

Un des enjeux majeurs dans le domaine des polymères semi-conducteurs est l'obtention de faibles valeurs de bande interdite, ce qui est le cas des polysquaraines développés durant ce travail de thèse. En perspective, il est envisageable d'obtenir des matériaux avec des bandes interdites encore plus étroites en remplaçant l'acide squarique par de l'acide croconique. En effet, il a déjà été démontré que le remplacement des unités squaraines par des unités croconaines conduisait à un déplacement bathochromique de l'absorption optique.<sup>[14]</sup> De plus, les polycondensations sans catalyseurs métalliques décrites dans cette thèse pourraient aussi être employées.

L'obtention de polymères conjugués sans catalyseurs métalliques, plus respectueux de l'environnement et facile à manipuler reste une des principaux enjeux dans les années à venir afin d'accéder au marché de l'électronique flexible.

- [1] S. M. Sze, M. K. Lee, *Semiconductor Devices: Physics and Technology, 3rd Edition: Physics and Technology*, **2012**.
- [2] O. Madelung, *Semiconductors: Data Handbook*, Springer Verlag, **2004**.
- [3] C. K. Chiang, C. R. Fincher, Jr., Y. W. Park, A. J. Heeger, H. Shirakawa, E. J. Louis, S. C. Gau, A. G. MacDiarmid, *Physical Review Letters* **1977**, *39*, 1098-1101.
- [4] A. J. Heeger, N. S. Sariciftci, E. B. Namdas, *Semiconducting and Metallic Polymers*, OUP Oxford, **2010**.
- [5] M. Geoghegan, G. Hadziioannou, *Polymer Electronics*, OUP Oxford, **2013**.
- [6] A.-J. Attias, *Techniques de l'ingénieur Matériaux pour l'électronique et dispositifs associés* **2002**, base documentaire : TIB271DUO.
- [7] J. Roncali, *Chemical Reviews* **1997**, *97*, 173-206.
- [8] T. Ito, H. Shirakawa, S. Ikeda, *Journal of Polymer Science: Polymer Chemistry Edition* **1974**, *12*, 11-20.
- [9] B. Carsten, F. He, H. J. Son, T. Xu, L. Yu, *Chemical Reviews* **2011**, *111*, 1493-1528.
- [10] J. Sakamoto, M. Rehahn, G. Wegner, A. D. Schlüter, *Macromolecular Rapid Communications* **2009**, *30*, 653-687.
- [11] A. Iraqi, I. Wataru, *Chemistry of Materials* **2004**, *16*, 442-448.
- [12] A. Iraqi, I. Wataru, *Journal of Polymer Science Part A: Polymer Chemistry* **2004**, *42*, 6041-6051.
- [13] T. Kanbara, T. Yamamoto, *Chemistry Letters* **1993**, *22*, 419-422.
- [14] E. E. Havinga, W. ten Hoeve, H. Wynberg, *Synthetic Metals* **1993**, *55*, 299-306.